NIST

National Institute of Standards and Technology
Technology Administration, U.S. Department of Commerce

Thirteenth International Conference on Computerization of Welding

T. A. Siewert and W. G. Rippey, Editors

*T*he National Institute of Standards and Technology was established in 1988 by Congress to "assist industry in the development of technology . . . needed to improve product quality, to modernize manufacturing processes, to ensure product reliability . . . and to facilitate rapid commercialization . . . of products based on new scientific discoveries."

NIST, originally founded as the National Bureau of Standards in 1901, works to strengthen U.S. industry's competitiveness; advance science and engineering; and improve public health, safety, and the environment. One of the agency's basic functions is to develop, maintain, and retain custody of the national standards of measurement, and provide the means and methods for comparing standards used in science, engineering, manufacturing, commerce, industry, and education with the standards adopted or recognized by the Federal Government.

As an agency of the U.S. Commerce Department's Technology Administration, NIST conducts basic and applied research in the physical sciences and engineering, and develops measurement techniques, test methods, standards, and related services. The Institute does generic and precompetitive work on new and advanced technologies. NIST's research facilities are located at Gaithersburg, MD 20899, and at Boulder, CO 80303. Major technical operating units and their principal activities are listed below. For more information contact the Publications and Program Inquiries Desk, 301-975-3058.

Office of the Director
- National Quality Program
- International and Academic Affairs

Technology Services
- Standards Services
- Technology Partnerships
- Measurement Services
- Information Services

Advanced Technology Program
- Economic Assessment
- Information Technology and Applications
- Chemistry and Life Sciences
- Materials and Manufacturing Technology
- Electronics and Photonics Technology

Manufacturing Extension Partnership Program
- Regional Programs
- National Programs
- Program Development

Electronics and Electrical Engineering Laboratory
- Microelectronics
- Law Enforcement Standards
- Electricity
- Semiconductor Electronics
- Radio-Frequency Technology[1]
- Electromagnetic Technology[1]
- Optoelectronics[1]

Materials Science and Engineering Laboratory
- Intelligent Processing of Materials
- Ceramics
- Materials Reliability[1]
- Polymers
- Metallurgy
- NIST Center for Neutron Research

Chemical Science and Technology Laboratory
- Biotechnology
- Physical and Chemical Properties[2]
- Analytical Chemistry
- Process Measurements
- Surface and Microanalysis Science

Physics Laboratory
- Electron and Optical Physics
- Atomic Physics
- Optical Technology
- Ionizing Radiation
- Time and Frequency[1]
- Quantum Physics[1]

Manufacturing Engineering Laboratory
- Precision Engineering
- Automated Production Technology
- Intelligent Systems
- Fabrication Technology
- Manufacturing Systems Integration

Building and Fire Research Laboratory
- Applied Economics
- Structures
- Building Materials
- Building Environment
- Fire Safety Engineering
- Fire Science

Information Technology Laboratory
- Mathematical and Computational Sciences[2]
- Advanced Network Technologies
- Computer Security
- Information Access and User Interfaces
- High Performance Systems and Services
- Distributed Computing and Information Services
- Software Diagnostics and Conformance Testing
- Statistical Engineering

[1] At Boulder, CO 80303.
[2] Some elements at Boulder, CO.

NIST Special Publication 1008

Thirteenth International Conference on Computer Technology in Welding

Digest of a symposium sponsored by the
National Institute of Standards and Technology
in cooperation with the
American Welding Society and the Welding Institute

June 18, 2003
Orlando, Florida

Edited by
T. A. Siewert
W. G. Rippey

October 2003

CONTENTS

PREFACE

The Thirteenth International Conference on Computer Technology in Welding was held June 18, 2003 in Orlando, Florida, under the sponsorship of the American Welding Society, the National Institute of Standards and Technology (NIST), and The Welding Institute. These proceedings include all the manuscripts that were submitted (including viewgraphs)—twelve presentations grouped into sessions on modeling (general topics), modeling (weld pool and solidification), weld data flow, and computers and automation. Additional copies of this NIST Special Publication xxx are available from the National Technical Information Service (NTIS) or the Government Printing Office (GPO).

DISCLAIMER

Except where attributed to authors from the National Institute of Standards and Technology (NIST), the content of individual sections of this volume has neither been reviewed nor edited by the NIST staff. Therefore, NIST accepts no responsibility for comments or recommendations therein. The mention of trade names in this volume neither constitutes nor implies any endorsement or recommendation by the NIST.

Modeling—General Topics

THE DEVELOPMENT OF AN IN-PROCESS MONITORING SOLUTION FOR INERTIA FRICTION WELDING: AN INVESTIGATION INTO FEATURE DESCRIPTORS

*D.A. Hartman, V.R. Davé, and M.J. Cola[†]

ABSTRACT

The development of a novel sensing method coupled with a pattern recognition system is presented as a non-destructive evaluation (NDE) technique for inertia friction welding. The complex nature of solid-state welding processes, and, in particular, inertia friction welding, prevents a system from incorporating a simple model (e.g., upset) to separate acceptable from unacceptable welds when subtle process variations occur. This work presents the application of an array of non-contact, acoustic emission sensors for determining bond integrity. The sensor data is explored through a variety of feature descriptors (RMS, energy, attack and decay, and power spectrum) and, in some cases, fused with the machine data (speed, pressure, and upset) in an attempt to develop a robust, in-situ NDE technique. The results are presented for bar-to-bar inertia friction welding of copper to stainless steel which exhibits only marginal weldability and, therefore, is ideally suited for validating the capabilities of this new sensing technique.

INTRODUCTION

Although friction welding is a relatively robust process, highly performance-critical or man-rated joints require additional scrutiny. Examples of such critical friction welds abound in aerospace applications, e.g., shafts, discs, hubs, fan and helicopter blades, and rotors. In such environments, the total number of parts made is generally low. Therefore, destructive evaluation is a very costly proposition, not to mention that commercially available post-process, non-destructive evaluation (NDE) techniques are not able to detect all of the fault conditions of possible concern. Hence, an in-process approach is invaluable in precision, small lot manufacturing of mission- or performance-critical hardware.

For large lot manufacturing environments, the total number of parts can reach upward of tens to hundreds per hour. Environments such as these perform routine destructive evaluation (commonly referred to as "book-ending") to ensure that the process is performing under control. Unfortunately, this method of inspection is not always indicative of the integrity of bonds made before (or after) the part that is currently under scrutiny. Furthermore, once a flaw is detected by destructive evaluation all parts produced previously must be rejected (or reworked) regardless of quality. This method of quality inspection reduces productivity and increases

waste and cost while never guaranteeing that each and every bond is adequate. An in-process approach can alleviate this burden by providing a consistent, thorough, and real-time response to part quality and, thereby, leaving only suspect parts for further post-process investigation by traditional destructive or non-destructive methods.

This paper presents the development of an in-process monitoring solution for inertia friction welding (IFRW). An Experimental Setup Section briefly describes the experimental approach. A Process Description Section presents the in-process data that was collected. An overview of the four feature descriptors that were used to explore the process data is presented in the Feature Analysis Section. A Results and Discussion Section highlights the relevant results of this work. Finally, a Conclusions Section summarizes our findings and lists the benefits of employing an in-process monitoring solution for large- and small-scale manufacturing environments.

EXPERIMENTAL SETUP

The focus in this preliminary investigation was to search for and identify features within the acoustic energy and/or machine data that are indicative of bond quality. Bar-to-bar inertia friction welding of 1-inch diameter, oxygen-free, high-conductivity copper bar to 0.5-inch diameter, annealed Type 304L stainless steel was used in this proof-of-concept study. This material combination exhibits only marginal weldability and, therefore, was ideally suited for validating the capabilities of this new sensing technique. All welding was conducted using a MTI Model 90B inertia friction welding system. The welding parameter selection was based upon work by Bell, et al. (Ref. 1) but altered slightly to accommodate differences in available inertial mass.

Prior to welding, all copper specimens were machined and stored for five weeks at ambient temperature and pressure. In order to remove surface oxidation that might have developed during storage, selected copper specimens were machined immediately before welding while bathed in isopropyl alcohol. Others were welded as is. In all cases, the stainless steel was rotated during the weld cycle while the copper remained fixed.

A non-contact array of microphones surrounds the weld joint and collects the rapid release of energy (i.e., sound pressure) due to the mechanical, thermal, and metallurgical phenomenon occurring during the weld cycle. The acoustic transducers used in this research are off-the-shelf electret condenser microphones that were sampled at 40 kHz per channel. The welding system provided process data (speed, pressure, and upset) that was sampled at 100 Hz per channel.

A semi-quantitative evaluation of each joint was performed using unguided bend testing. As-welded, full-size specimens were tested. Image analysis techniques were used to determine the percent of bonded area after fracturing each specimen. A presentation of the experimental setup and the sensor can be found in Ref. 2.

PROCESS DESCRIPTION

The process description for this work was captured with machine process data (speed, pressure, and upset) and acoustic energy[1]. Representative plots for speed, pressure, upset, and acoustic energy are illustrated in

---

[1] A curious feature within all of the Cu-SS acoustic signatures is the presence of a second burst of acoustic energy soon after the initial weld burst. This burst also coincides with a sharp drop in the speed to zero. One plausible explanation for this phenomenon

Figure 1. This data represents the process inputs for an in-process monitoring system, while the process output (i.e., quality metric) is bond integrity.

(a)

(b)

(c)

(d)
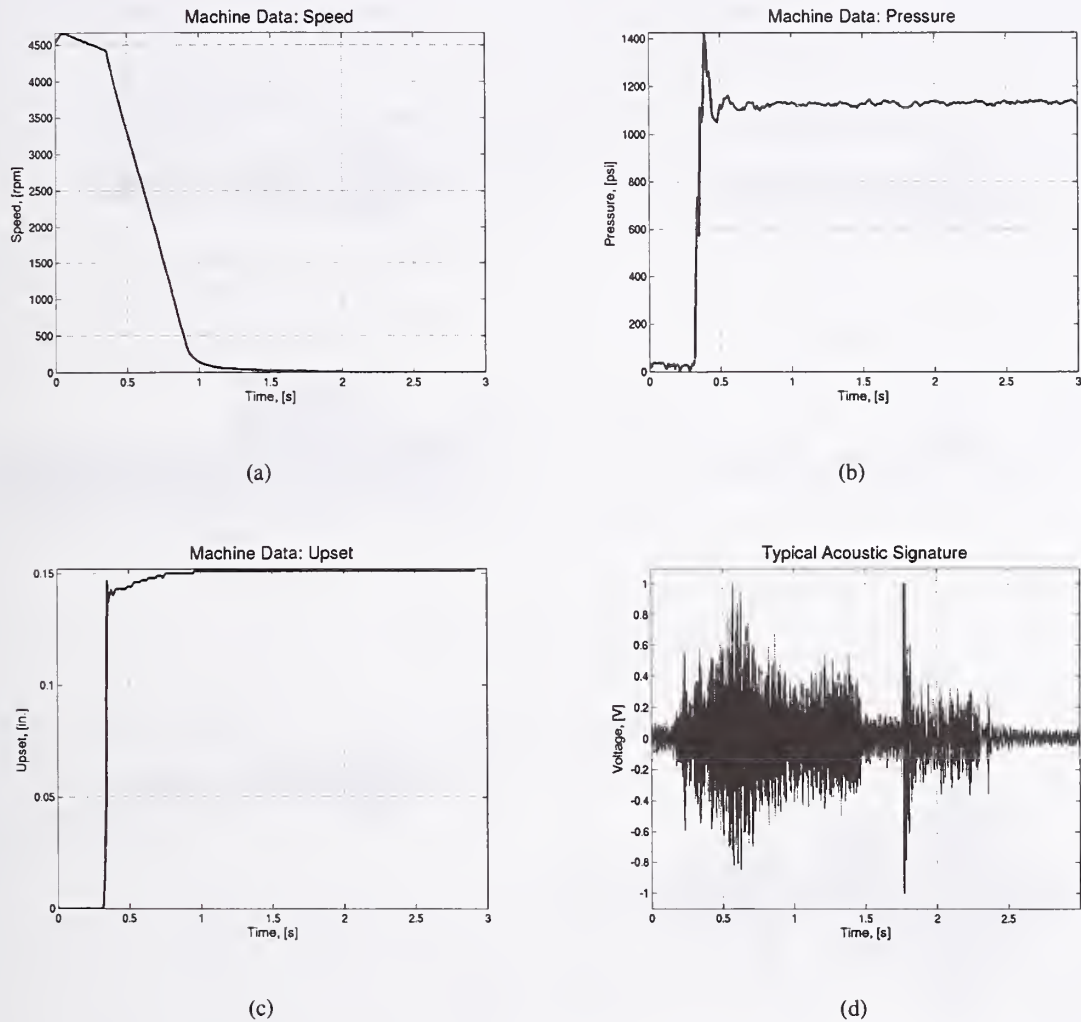
Figure 1: Representative plots for machine data and acoustic energy.

FEATURE ANALYSIS

Feature analysis involves implementing signal processing and data analysis techniques that explore and, potentially, improve upon the "raw" data. The implementation of a specific feature analysis technique is called a feature descriptor. Oftentimes, the raw data is in a format that is not conducive for direct input into a classifier and, therefore, requires manipulation in order to reduce and/or enhance the data for classification purposes.

---

is that as the weld material cools, its effective rheological behavior rapidly changes, and at a point the material reverts from a viscoplastic behavior to a largely elastic behavior. This change could occur over a very short time, and thereby result in a sudden "seizing" behavior. When this happens, an impulse load is effectively applied to the joint causing it to ring, and the acoustic sensor is able to discern this ringing

Ideally, the implementation of a feature descriptor makes the decision making process of the classifier trivial. The task of feature analysis is normally a domain-dependent operation. In addition to using the raw data in a normalized format, the following feature descriptors were investigated: root mean square (RMS), energy, attack and decay, and power spectrum. Each of these will be addressed separately in the following sections.

(a)

(b)

(c)

(d)
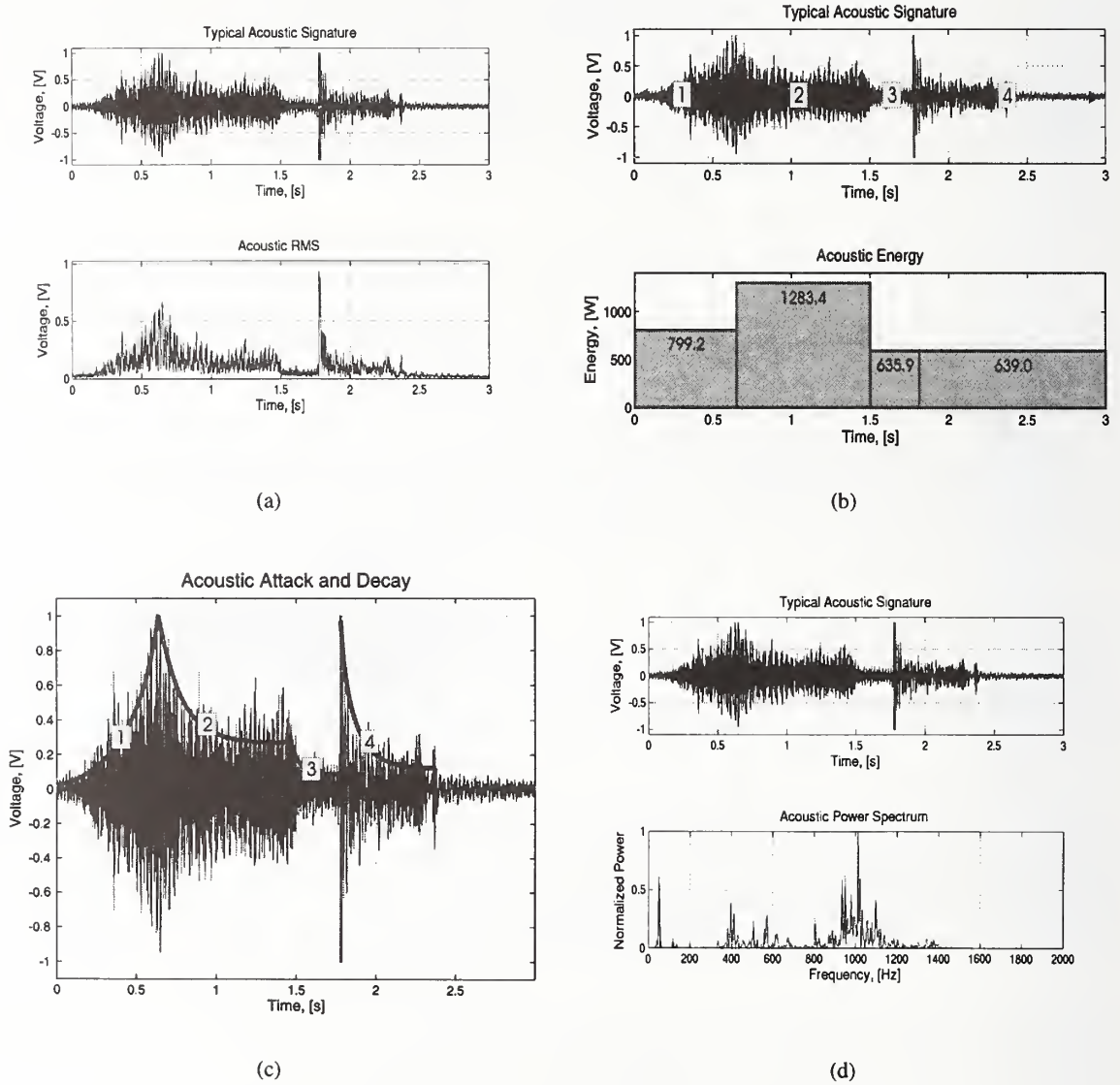
Figure 2: Four feature descriptors are investigated in this work.

RMS

The root mean square value is one way of describing an AC waveform. A true RMS measurement relates the heating potential of an applied voltage. The RMS gives the effective value of an AC voltage or current signal by (1) squaring the instantaneous values, (2) calculating the mean, and then (3) taking the square root. The following equation calculates the RMS value of an instantaneous current or voltage signal, $f(t)$:

$$RMS(f(t)) = \sqrt{\left| \frac{1}{T} \int_t^{t+T} f(t)^2 \right|}, \tag{1}$$

where $T = 1/f$ and $f = fundamental\ frequency$. A pure AC signal swings about a zero voltage (or current) axis, going positive one moment and negative the next. Consequently, its average value over a complete cycle is zero. The RMS value does not average out to zero, however, and is, therefore, essentially the AC equivalent of DC voltage or current. Figure 2(a) illustrates the RMS for a representative acoustic energy waveform.

Energy

The energy of a signal, $f(t)$, is defined as

$$E(f(t)) \equiv \sum_{t=-\infty}^{\infty} \left| f(t)^2 \right| . \tag{2}$$

The energy of a discrete-time signal, $x(n)$, over a finite interval, $-N \leq n \leq N$, is defined as

$$E(x(n)) = \sum_{n=-N}^{N} \left| x(n)^2 \right| . \tag{3}$$

Figure 2(b) illustrates the energy calculation for four segments of a representative acoustic energy waveform.

Attack and Decay

The attack and decay feature descriptors are commonly applied in audio processing of voice and musical instruments (Refs. 3, 4). Attack and decay phases are described by fitting a linear or non-linear function to a set of data. Attack descriptors are used for describing regions of increasing sound intensity, while, conversely, decay descriptors are used for describing regions of decreasing sound intensity. Similar to the energy descriptor, an important consequence of using attack and decay descriptors is in their ability to richly define a signal in an extremely compressed manner.

In this work, the attack and decay feature descriptors were fit to both machine and acoustic energy data using an exponential function of the form:

$$f(t) = ce^{kt} . \tag{4}$$

Figure 2(c) illustrates one attack and three decay descriptors for four segments of a representative acoustic energy waveform.

Power Spectrum

The power spectrum is accomplished using a discrete Fourier transform (DFT). The DFT "transforms" an ordered sequence of data samples from the time domain into the frequency domain. Spectral information

about the signal can be represented explicitly. In certain problem domains, the spectral information can prove to be extremely revealing, e.g., when attempting to describe physical phenomenon that exhibit periodicity.

A moving-window DFT was performed on the AE data using the fast Fourier transform (FFT) algorithm. A step size of 250 data points was used to move through the time-domain data without overlap. A representative power spectrum is illustrated in Figure 2(d).

RESULTS AND DISCUSSION

The experimental matrix consisted of 24 welds. Although the experimental matrix was designed with only one variable in mind, i.e., surface preparation of the copper, three different quality welds were generated: *acceptable*: bonded area is approximately 100%, *conditional*: bonded area is less than 100% but greater than 5%, and *unacceptable*: bonded area is less than 5%. Table 1 summarizes the bend test results.

Weld Number	Surface Condition Before Welding	Bond Quality	Bonded Area (%)
1 - 12	Freshly Machined	Acceptable	100.0
13	Freshly Machined	Conditional	80.0
14	Freshly Machined	Conditional	70.0
15	Freshly Machined	Conditional	69.0
16	Freshly Machined	Conditional	67.0
17	Freshly Machined	Conditional	54.0
18	Freshly Machined	Conditional	48.0
19	Freshly Machined	Conditional	26.0
20 - 24	Not Machined	Unacceptable	0.0

Table 1: Bend test results.

A Probabilistic Neural Network (PNN) was used as the classifier in this work[2]. The training/testing method was motivated out of a limited size of the available data set. Commonly referred to as the single holdout method, the training/testing method holds out one data point from the n-sized data set for testing while the remaining $n-1$ data points in the data set are used for training. This procedure is repeated until all of the data points in the data set have been tested independently. Classification accuracy is calculated based on the sum of the correctly classified data points minus the sum of the incorrectly classified data points divided by n.

Table 2 tabulates some of the more noteworthy process data combinations and feature descriptors that were investigated. Tests 4 through 7 employed a data-level sensor fusion operation on the normalized machine data, while tests 11 through 14 and 21 through 23 employed feature-level sensor fusion operations on the machine data and on the acoustic energy and machine data, respectively.

Among the machine data, speed provided the most accurate classification results, which agrees well with Bell, et al.'s (Ref. 1) findings, i.e., any minor contamination at the bond plane prevents a metallurgical bond from occurring which is manifested in the speed curve. Furthermore, the decreasing accuracy between acceptable versus unacceptable and acceptable versus conditional demonstrates the extreme subtleness that bond plane contamination can have on bond quality for this particular material combination. The authors

---

[2]For a thorough presentation of Probabilistic Neural Networks see Ref. 5

8

Pattern Classification Results

Test	Process Data	Feature Descriptor	Accuracy, [% correct]		
			Acceptable Unacceptable	Acceptable Conditional	Acceptable Unacceptable Conditional
1.	Speed	Normalize	82	74	63
2.	Pressure	Normalize	59	58	42
3.	Upset	Normalize	59	74	63
4.	Speed, Pressure	Normalize	76	63	54
5.	Speed, Upset	Normalize	59	68	58
6.	Pressure, Upset	Normalize	59	63	54
7.	Speed, Pressure, Upset	Normalize	59	63	54
8.	Speed	Attack and Decay	71	63	50
9.	Pressure	Attack and Decay	65	68	50
10.	Upset	Attack and Decay	47	68	50
11.	Speed, Pressure	Attack and Decay	65	68	54
12.	Speed, Upset	Attack and Decay	47	68	50
13.	Pressure, Upset	Attack and Decay	59	63	46
14.	Speed, Pressure, Upset	Attack and Decay	59	63	46
15.	Acoustic Energy	RMS	71	47	46
16.	Acoustic Energy	Energy (1 segment)	76	58	54
17.	Acoustic Energy	Energy (4 segments)	94	31	41
18.	Acoustic Energy	Attack and Decay	88	63	54
19.	Acoustic Energy	Attack and Decay, Energy	94	52	50
20.	Acoustic Energy	Power Spectrum	100	100	54
21.	Acoustic Energy, Speed	Attack and Decay	82	68	71
22.	Acoustic Energy, Pressure	Attack and Decay	71	68	63
23.	Acoustic Energy, Upset	Attack and Decay	72	68	63

Table 2: Pattern classification results for different combinations of process data and feature descriptors.

expect, however, that the classification accuracies (in all three categories) would improve with additional training patterns.

Perfect classification accuracy was found to occur only during the acoustic energy power spectrum feature descriptor (test 20). Upon further investigation, the authors found a unique characteristic ringing for both an acceptable and conditional part. This ringing occurs during the second burst of acoustic energy (i.e., when speed reaches 0 rpm)[3]. The existence of this phenomenon is readily discernible in the power spectrum. Consequently, bond integrity classification of acceptable versus unacceptable and conditional versus unacceptable[4] bonds becomes trivial – which is the ultimate goal of a feature descriptor.

The implementation of an in-process monitoring system does not, however, need to be limited to the use of a single data combination and feature descriptor. The PNN classifier's computational efficiency and

---

[3]This phenomenon is analogous to the mechanism employed in a resonant inspection system: the acoustic response of a part is monitored after being impacted by a hammer with a known and repeatable force.

[4]The classification results for conditional versus unacceptable is not presented in Table 2.

framework (i.e., its ability to not only provide a decision but also estimate the probability and reliability of a classification) enables it to be implemented on multiple data sets and feature descriptors. The output of each classifier (decision, probability, and reliability) can then be input into a decision-making module that employs, for example, a voting or "winner takes all" template.

Furthermore, feature descriptors and data combinations that do not yield 100% classification accuracy should not preclude their implementation in an in-process monitoring solution. In particular, an in-process monitoring solution can provide additional feedback about the process, such as, fault classification. Although the power spectrum is feature rich in indicating existence of a bad (or good) bond, it fails to reveal the reason why. In-process data can potentially yield relevant process information, in the form of fault diagnostics, when an unacceptable bond is made. For IFRW, speed, for example, is an indicator of surface contamination or joint misalignment. Consequently, the functionality of an in-process monitoring solution can provide both quality indicators and fault diagnostics.

CONCLUSIONS

A bond quality classification system was developed using a novel, non-contact, acoustic emission sensing technique. Various feature detectors were investigated to correlate the in-process data to bond integrity. The system provides a (near) real-time response with minimal hardware requirements.

The following benefits can be achieved by using an in-process monitoring solution for both small- and large-lot manufacturing environments:

- *Fast*: provides a real-time response immediately after welding is complete,

- *Inexpensive*: minimal hardware requirements are necessary,

- *Robust*: is capable of mapping complex or ill-defined multidimensional input/output systems and is tolerant of noisy data,

- *Consistent*: sensing and interpretation are performed without operator intervention and, therefore, ensures an accurate, repeatable, and reproducible system,

- *Thorough*: examination is performed for each weld, rather than randomly to ensure joint integrity,

- *Efficient*: only suspect welds are examined further using an "inspect for cause" methodology, and

- *Revealing*: in addition to providing quality feedback, an in-process monitoring system can potentially expose the cause for failure and, hence, provide fault diagnostic capabilities.

References

[1] R. A. Bell, J. C. Lippold, and D. R. Adolphson. Evaluation of copper-stainless steel inertia friction welds. *Welding Journal*, 63(11):325s–332s, November 1984.

[2] D.A. Hartman, M.J. Cola, V.R. Davé, N.G. Dozhier, and R.W. Carpenter. Nondestructive, in-process inspection of friction welding: An investigation into a new sensing technique. In H.B. Smartt, J.A. Johnson, and S.A. David, editors, *Trends in Welding Research, Proceedings of the 6th International Conference*, Callaway Gardens, Georgia, USA, April 15–18, 2002. ASM International.

[3] P. Herrera, X. Amatriain, E. Batlle, and X. Serra. Towards instrument segmentation for music content description: A critical review of instrument classification techniques. In *International Symposium on Music Information Retrieval*, 2000.

[4] P. Herrera, A. Yeterian, and F. Gouyon. Automatic classification of drum sounds: a comparison of feature selection methods and classification techniques. In *International Conference on Music and Artificial Intelligence*, Edinburgh, United Kingdom, 2002.

[5] D.F. Specht. Probabilistic neural networks. *Neural Networks*, 3:109–118, 1990.

The Development of an In-Process Monitoring Solution for Inertia Friction Welding: An Investigation into Feature Descriptors

D.A. Hartman, V.R. Davé, M.J Cola
Nuclear Materials and Technology
Los Alamos National Laboratory

13th International Conference on Computer Technology in Welding
June 18, 2003
Grosvenor Resort
Walt Disney World Resort
Orlando, Florida, USA

· Los Alamos
NATIONAL LABORATORY

12

Problem Statement

Both small- and large-lot manufacturing environments need in-process quality assurance:

- **Small-lot** *(high precision, performance-critical or man-rated)*:

  - *Number of parts made is low*

  - *Destructive evaluation is very costly*

  - *Non-destructive evaluation techniques are not able to detect all of the possible fault conditions*

- **Large-lot** *(low(er) precision, high volume)*:

  - *Number of parts made is high*

  - *Destructive evaluation (bookend'ing) is inconsistent*

  - *Non-destructive evaluation techniques are not able to detect all of the possible fault conditions*

Los Alamos
NATIONAL LABORATORY

NMT-10: Manufacturing and Process Science and Technology

D.A. Hartman

Problem Statement, cont.

- Collecting data is not in-process monitoring

- Data instills a false sense of security

Los Alamos
NATIONAL LABORATORY

NMT-10: Manufacturing and Process Science and Technology

D.A. Hartman

14

Problem Statement, cont: Fusion Welding

- Examples: GTA, EB, LB

- Typical approach to in-process monitoring:

  - Quantifies the heat source:

    - GTA: Voltage and Current

    - EB: Beam Profile (Faraday Cup)

    - LB: Beam Profile

  - Neglects the fundamental key in-process parameter!

    - Energy transfer: Heat source-to-material interaction

15

Inertia Friction Welding: The Process

One piece set in motion

Pieces are brought together under pressure

Heated and deformed material expelled from interface

Final weld exhibiting flash

The current industry approach maintains absolute upset within a predetermined ±3σ envelope.

Los Alamos
NATIONAL LABORATORY

NMT-10: Manufacturing and Process Science and Technology

D.A. Hartman

16

Inertia Friction Welding: The Process

DIRECT WELD PARAMETERS

- Surface appearance, i.e., flash formation
- Upset
- Heat and deformation affected zone
- Cooling rate
- Strength and ductility
- Internal discontinuities
- Metallurgical structure

MATERIAL PARAMETERS

Thermal conductivity
Thermal expansion
Hardness and strength
Oxidation resistance
Plastic temperature range
Forging temperature range
Forging temperature
Metallurgical properties

INFLUENTIAL PROCESS VARIATIONS

Joint variation
Surface condition

INDIRECT WELD PARAMETERS

- Inertial mass
- Rotational speed
- Axial force
- Dwell time

D.A. Hartman

Los Alamos
NATIONAL LABORATORY

NMT-10: Manufacturing and Process Science and Technology

17

NNSA

Research Objective

Investigate the development of a in-process monitoring system for bond integrity during inertia friction welding.

Los Alamos
NATIONAL LABORATORY

NMT-10: Manufacturing and Process Science and Technology

D.A. Hartman

18

Inertia Friction Welding: Sensor

- Acoustic emission sensing ring:

  - Free standing Aluminum ring.

  - Capable of holding up to 12 acoustic transducers (microphones).

  - Non-contact.

- Collects the rapid release of energy (in the form of sound pressure) due to the mechanical, thermal, and metallurgical phenomena occurring during friction welding.

- The acoustic transducers used in this research are off-the-shelf electret condenser microphones (approx. $0.99 each).

Los Alamos
NATIONAL LABORATORY

NMT-10: Manufacturing and Process Science and Technology

D.A. Hartman

Inertia Friction Welding: Machine and Sensor

Los Alamos
NATIONAL LABORATORY

NMT-10: Manufacturing and Process Science and Technology

D.A. Hartman

Inertia Friction Welding: Sensor

Magnetic Base Indicator Holder

3/8" Post

Segmented Collet

Sensor Ring

Segmented Flywheel
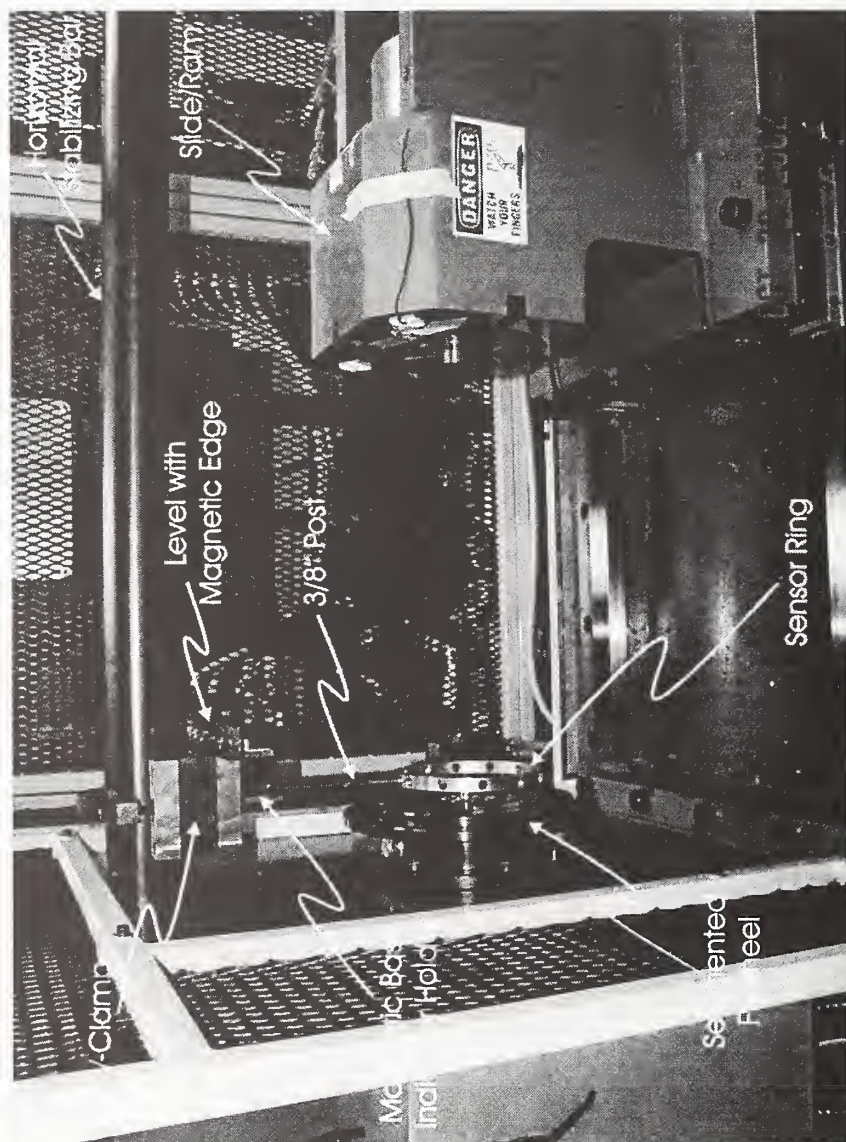
Microphone Mounts (0.1875" diameter)
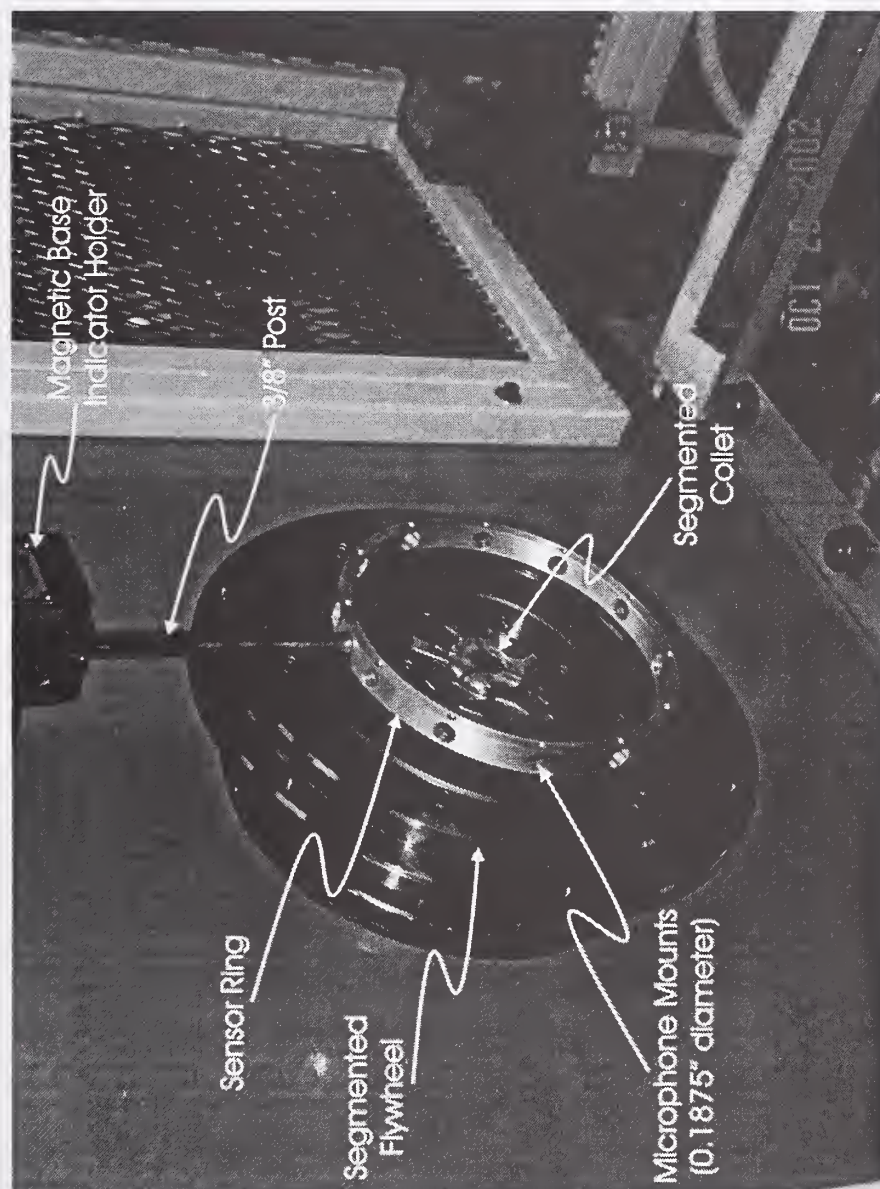
Experimental Objective

- Problem:

  - Cu-SS exhibits only marginal weldability.

  - Surface contamination (e.g., oxidation or other forms of contamination) prevents a metallurgical bond from being formed.

- In-Process Monitoring Objective:

  - Detect material contamination by identifying features within the in-process data: machine and acoustic energy.

Los Alamos
NATIONAL LABORATORY

NMT-10: Manufacturing and Process Science and Technology

D.A. Hartman

22

Experimental Approach

- Materials
  - OFHC Cu: 1.0 inch dia. bar
  - Type 304L: 0.5 in. dia. Bar with 3° taper
- Conditions
  - Freshly machined
  - Machined and exposed to atmosphere for 4-5 weeks
  - Surfaces contaminated with fingerprints
- Bond Quality Tests
  - Unguided bend tests
- Characterization
  - Optical microscopy
  - Image analysis

- Equipment & Parameters
  - MTI Model 90B IFR System
    - 4500 rpm (589 sfpm)
    - 1092 psi (7100 lb_f)
    - 1.52 lb_m-ft^2
    - 0.100 in. prebond gap
    - One diameter of stickout
  - Microphones
    - Frequency response: 0 – 16 kHz
    - Relatively flat response over its entire range
  - Data acquisition
    - Sampling rate: 40 kHz
    - Amplified and low-pass filtered @ 20 kHz

D.A. Hartman

Los Alamos
NATIONAL LABORATORY

NMT-10: Manufacturing and Process Science and Technology

Experimental Approach, cont.

Generate an experimental matrix with only one variable:

Surface preparation ⇒ <u>bond quality</u>

NMT-10: Manufacturing and Process Science and Technology

D.A. Hartman

Post-Process Analysis: Mechanical Properties

- Bend tests were performed as a semi-quantitative determination of bond quality.

- Image analysis of the fracture surfaces provided a reasonable approximation of the percent of interface area bonded.

- Specimens having acceptable bond quality exhibited ductile tearing without any lack of bonding over the majority of the interface.

- All of the specimens that were welded as-is exhibited a lack of bonding over the majority of the interface.

D.A. Hartman

Los Alamos
NATIONAL LABORATORY

NMT-10: Manufacturing and Process Science and Technology

Bend Test Results

Weld #	Surface Condition	Bond Quality	Bonded Area, (%)
1 – 12	Freshly machined	Acceptable	100
13	Freshly machined	Conditional	80
14	Freshly machined	Conditional	70
15	Freshly machined	Conditional	69
16	Freshly machined	Conditional	67
17	Freshly machined	Conditional	54
18	Freshly machined	Conditional	48
19	Freshly machined	Conditional	26
20 – 24	Not machined	Unacceptable	0

NMT-10: Manufacturing and Process Science and Technology

D.A. Hartman
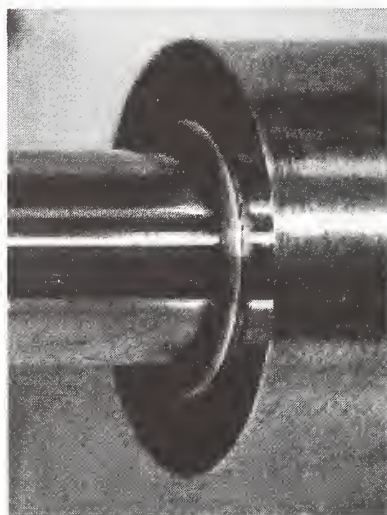
Los Alamos
NATIONAL LABORATORY
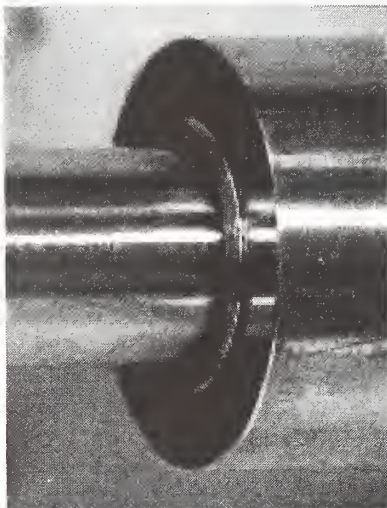
Bond Quality

- Three bond quality classes were created in the experimental matrix:
  - *Acceptable*: approximately 100% bonded area
  - *Unacceptable*: approximately no bonded area
  - *Conditional*: everything in between
- Acceptable and Conditional welds: freshly machined copper surface prior to welding.
- Unacceptable welds: welded as-is, i.e., machined copper surface that was exposed to the atmosphere for 4-5 weeks.

Los Alamos
NATIONAL LABORATORY
NMT-10: Manufacturing and Process Science and Technology

D.A. Hartman

Bond Quality, cont.

Acceptable

Conditional

Unacceptable

NMT-10: Manufacturing and Process Science and Technology
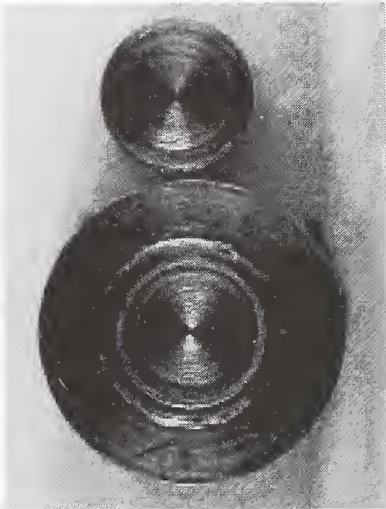
D.A. Hartman
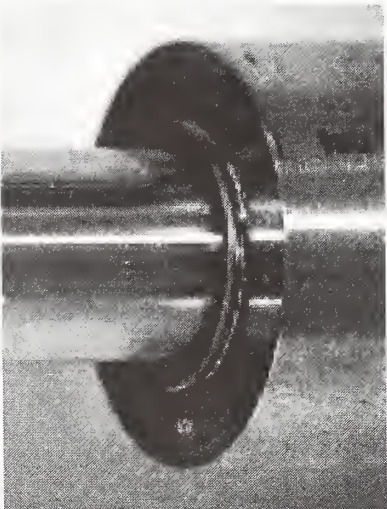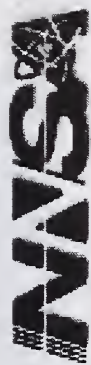
Pattern Classification: Goal

Goal:

- Identify features within the in-process data that can be correlated to bond integrity.

Los Alamos
NATIONAL LABORATORY

NMT-10: Manufacturing and Process Science and Technology

D.A. Hartman

Pattern Classification: Modules

Process Description
_____
Object Data: number and combination of microphones, machine data.

Classifier Design
_____
PNN: sigma

Feature Analysis
_____
Preprocessing: scaling, smoothing, normalizing, etc.
Extraction: transforms, spectra, correlation, etc.

NMT-10: Manufacturing and Process Science and Technology

D.A. Hartman

Los Alamos
NATIONAL LABORATORY

30
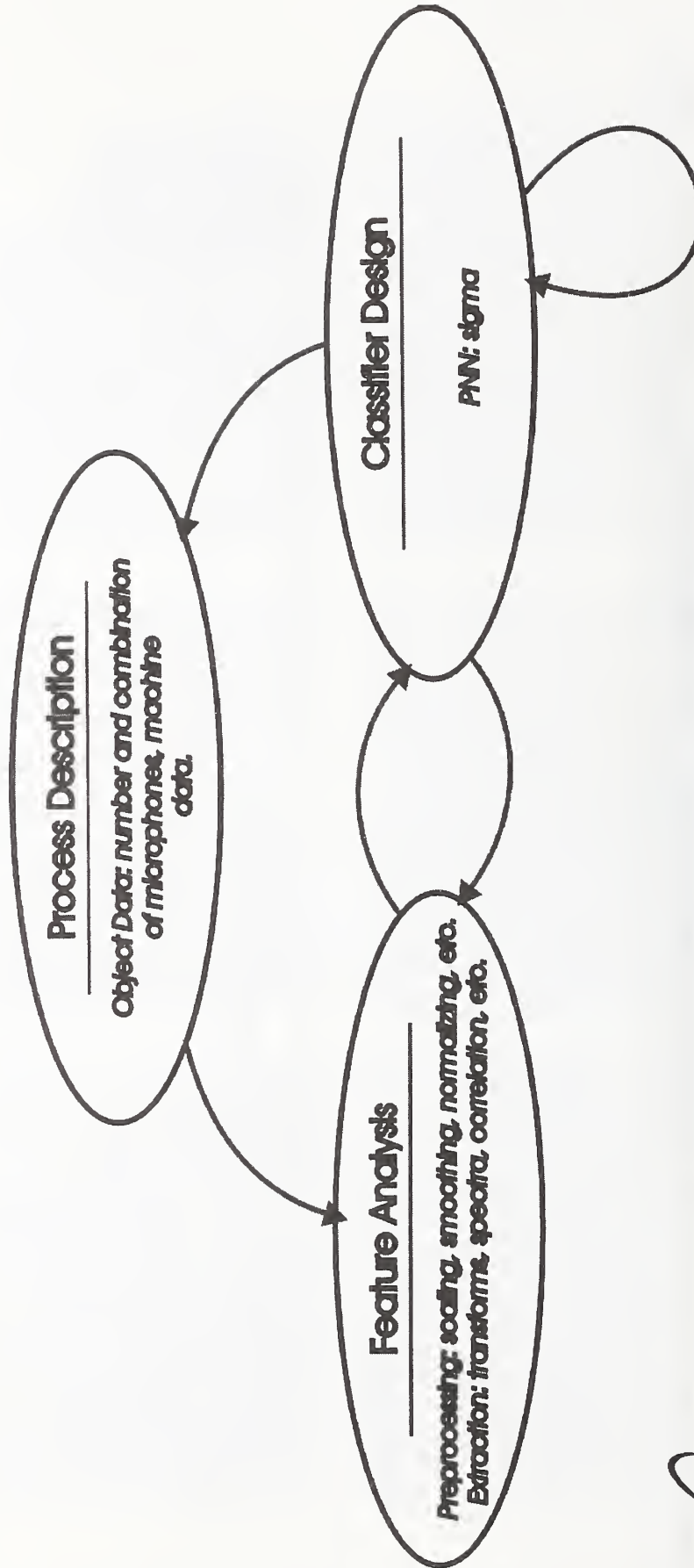
Pattern Classification: Modules, cont.

- **Process description:**

  - **Machine data: speed, pressure, and upset (100 Hz)**

  - **Sensor data: acoustic energy, (40 kHz)**

- **Feature Analysis:**

  - **Normalize, RMS, Energy, Attack and Decay, and Power Spectrum**

- **Classifier:**

  - **Probabilistic Neural Network**

Los Alamos
NATIONAL LABORATORY
NMT-10: Manufacturing and Process Science and Technology

D.A. Hartman

31

Process Description: Speed

Machine Data: Speed

NMT-10: Manufacturing and Process Science and Technology

D.A. Hartman

32
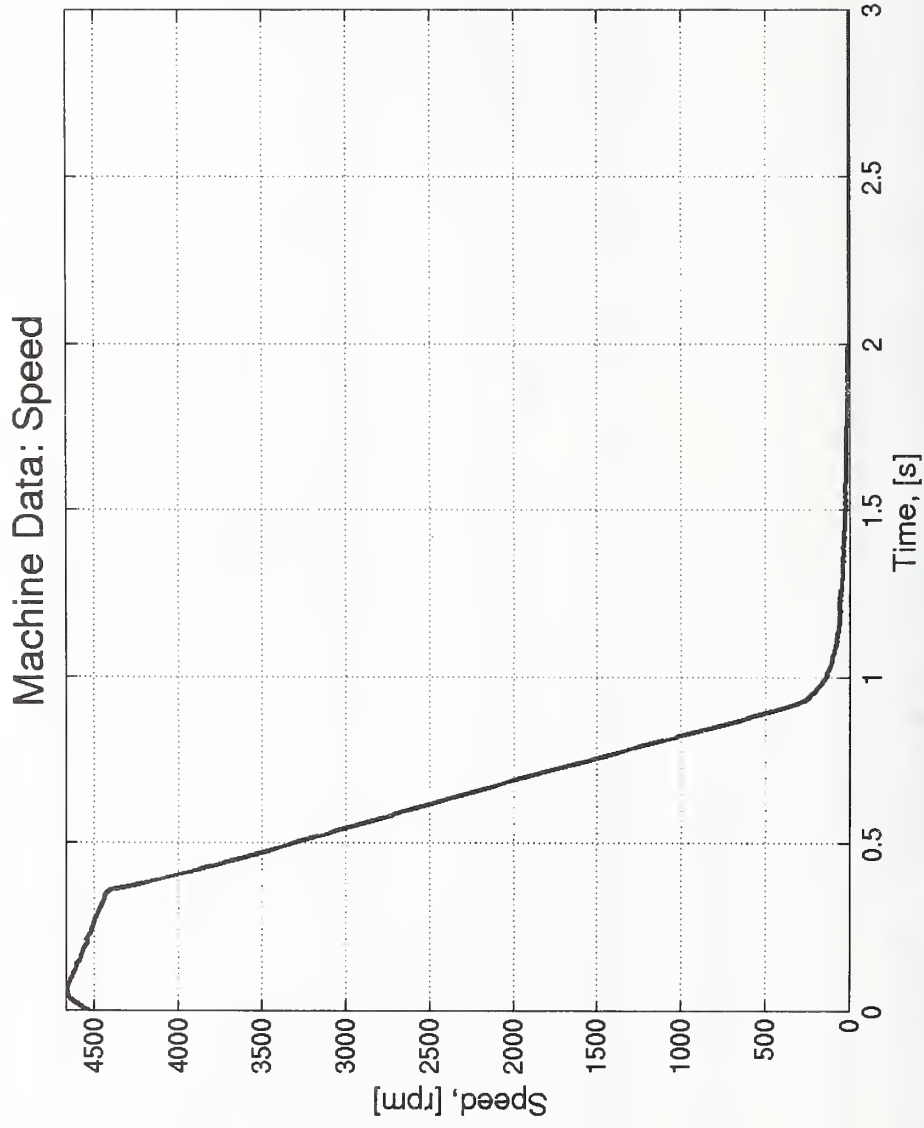
Process Description: Pressure

Machine Data: Pressure

NMT-10: Manufacturing and Process Science and Technology

D.A. Hartman

Process Description: Upset

Machine Data: Upset

NMT-10: Manufacturing and Process Science and Technology
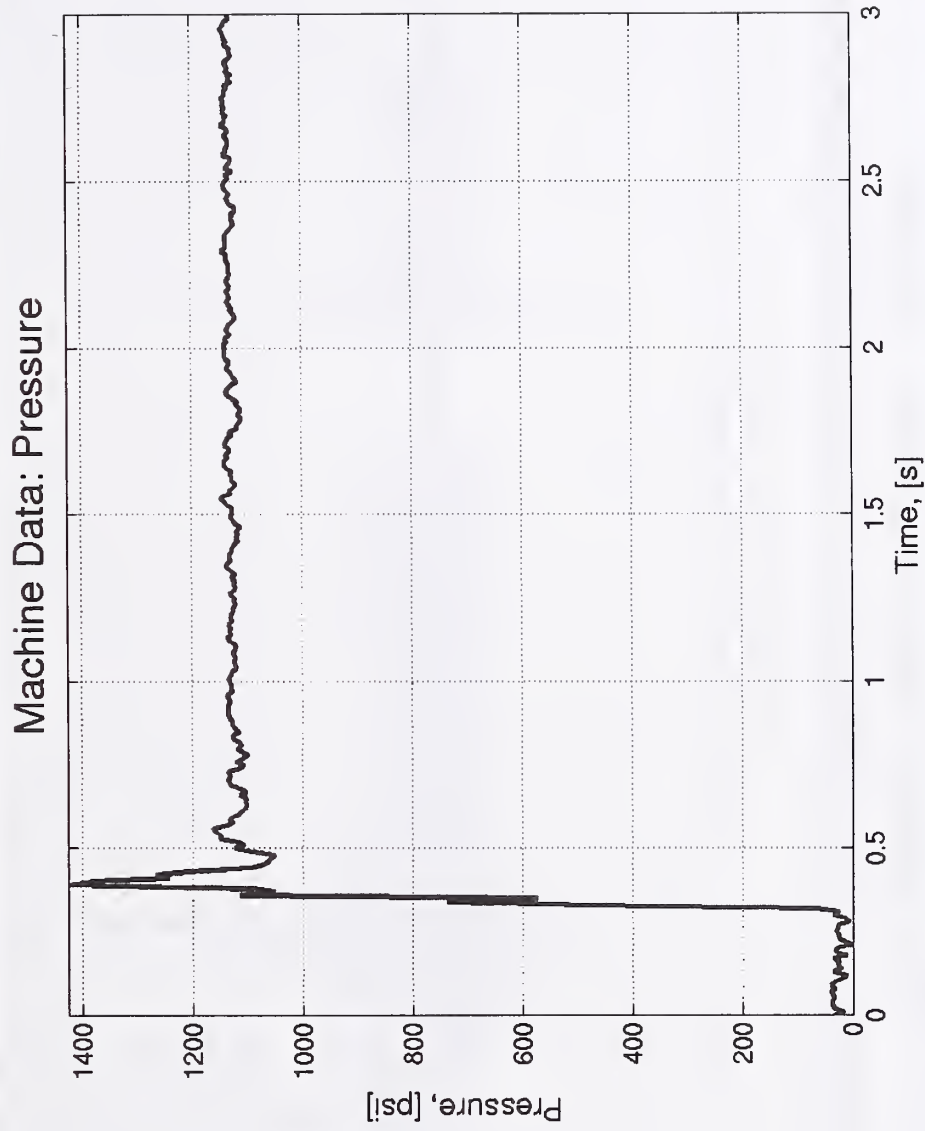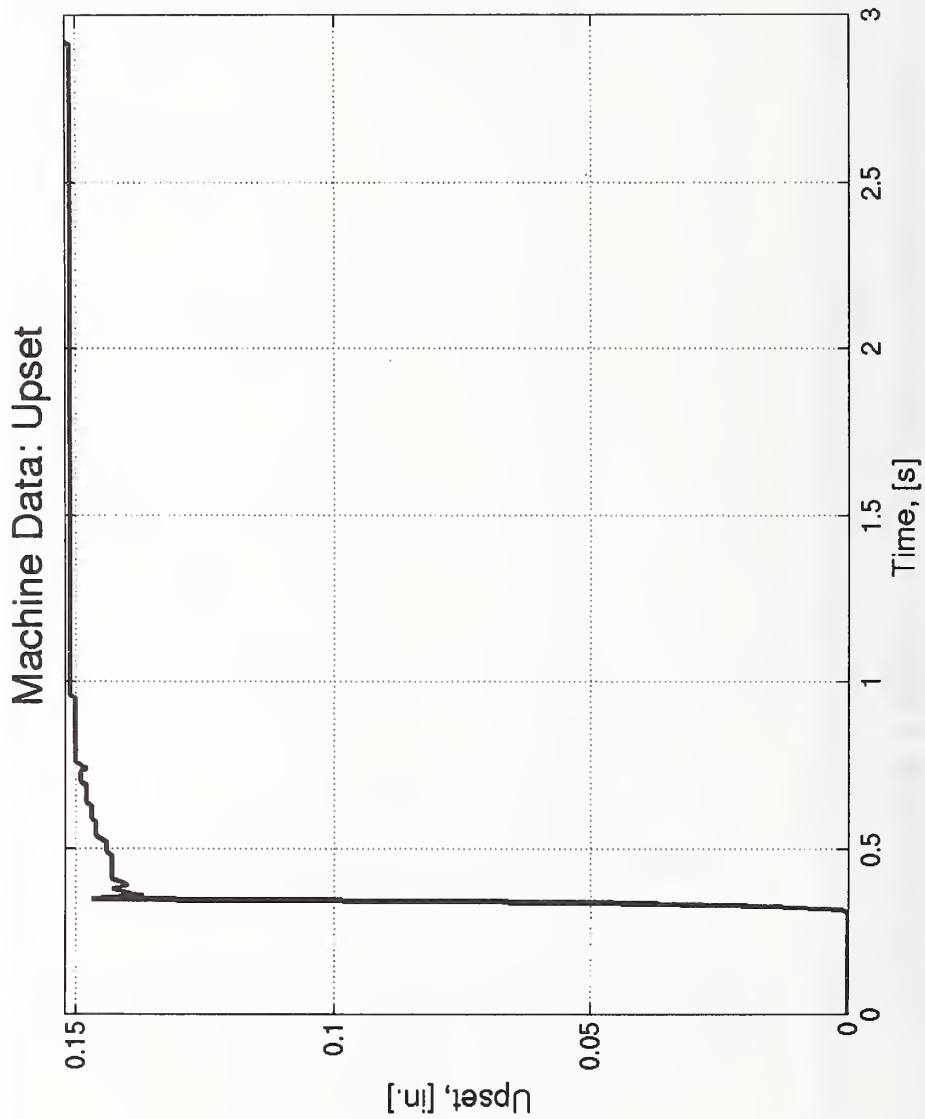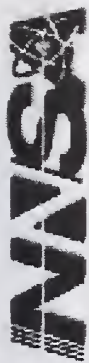
D.A. Hartman

Process Description: Acoustic Energy

Los Alamos
NATIONAL LABORATORY
NMT-10: Manufacturing and Process Science and Technology
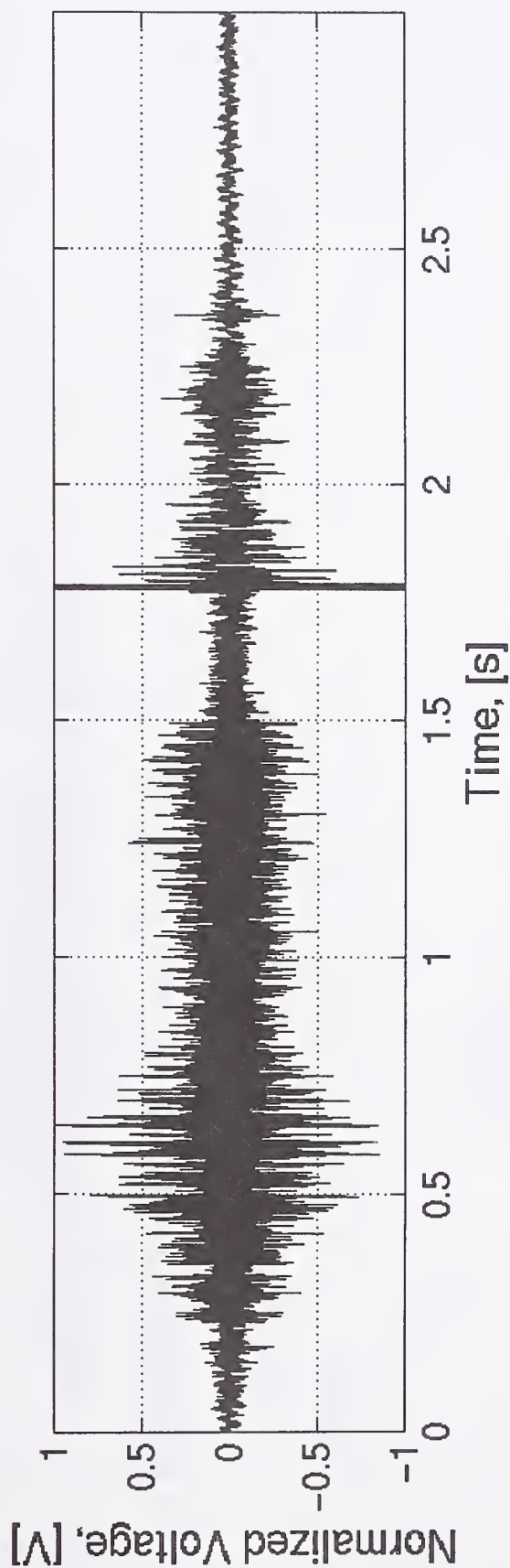
D.A. Hartman

Feature Analysis: Goal

- Goal:
  - Explore and, potentially, improve upon the raw data.
- Ultimate goal:
  - Make the job of the classifier trivial.

Los Alamos
NATIONAL LABORATORY
NMT-10: Manufacturing and Process Science and Technology

D.A. Hartman

Feature Analysis: RMS

Typical Acoustic Signature

Acoustic RMS

D.A. Hartman

NMT-10: Manufacturing and Process Science and Technology
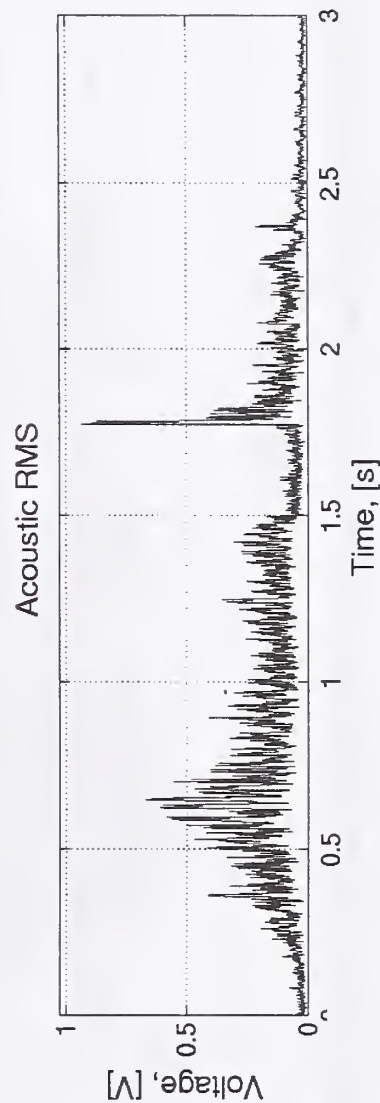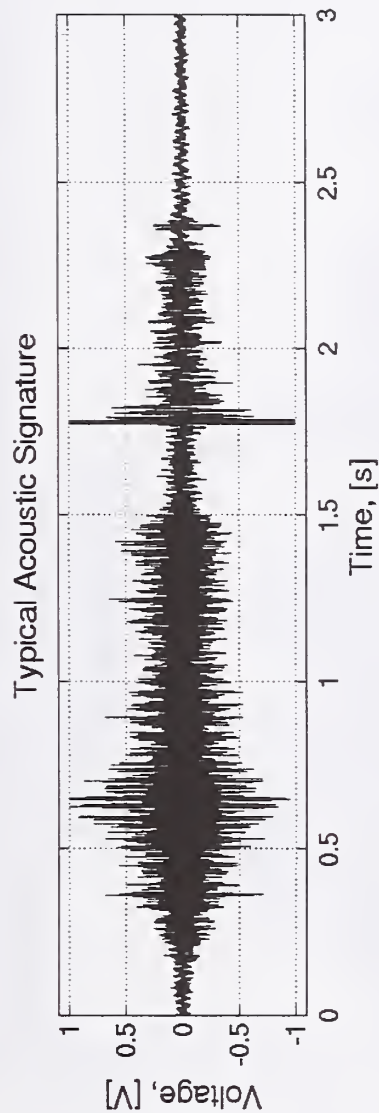
Feature Analysis: Energy

Typical Acoustic Signature

Acoustic Energy
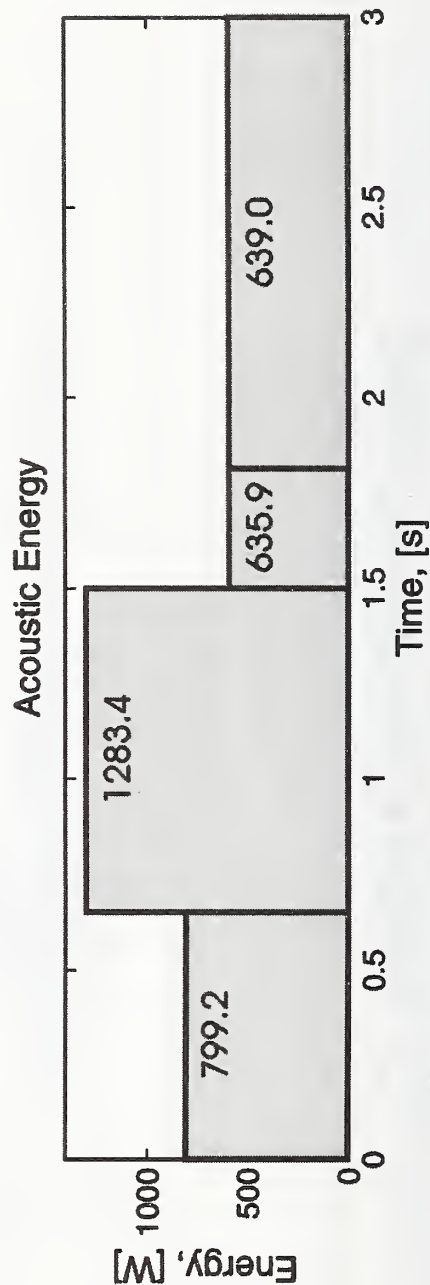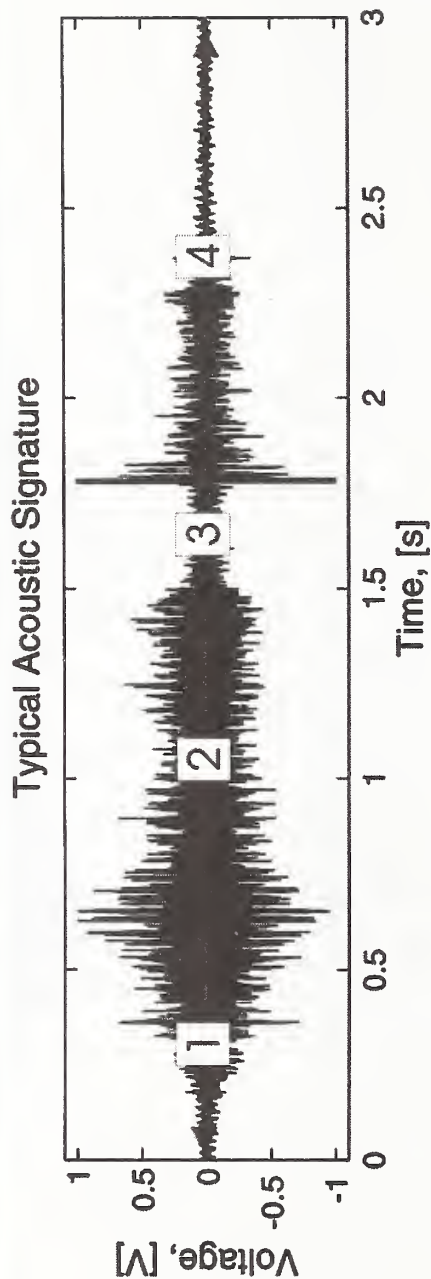
Feature Analysis: Attack and Decay

Acoustic Attack and Decay

NMT-10: Manufacturing and Process Science and Technology

D.A. Hartman
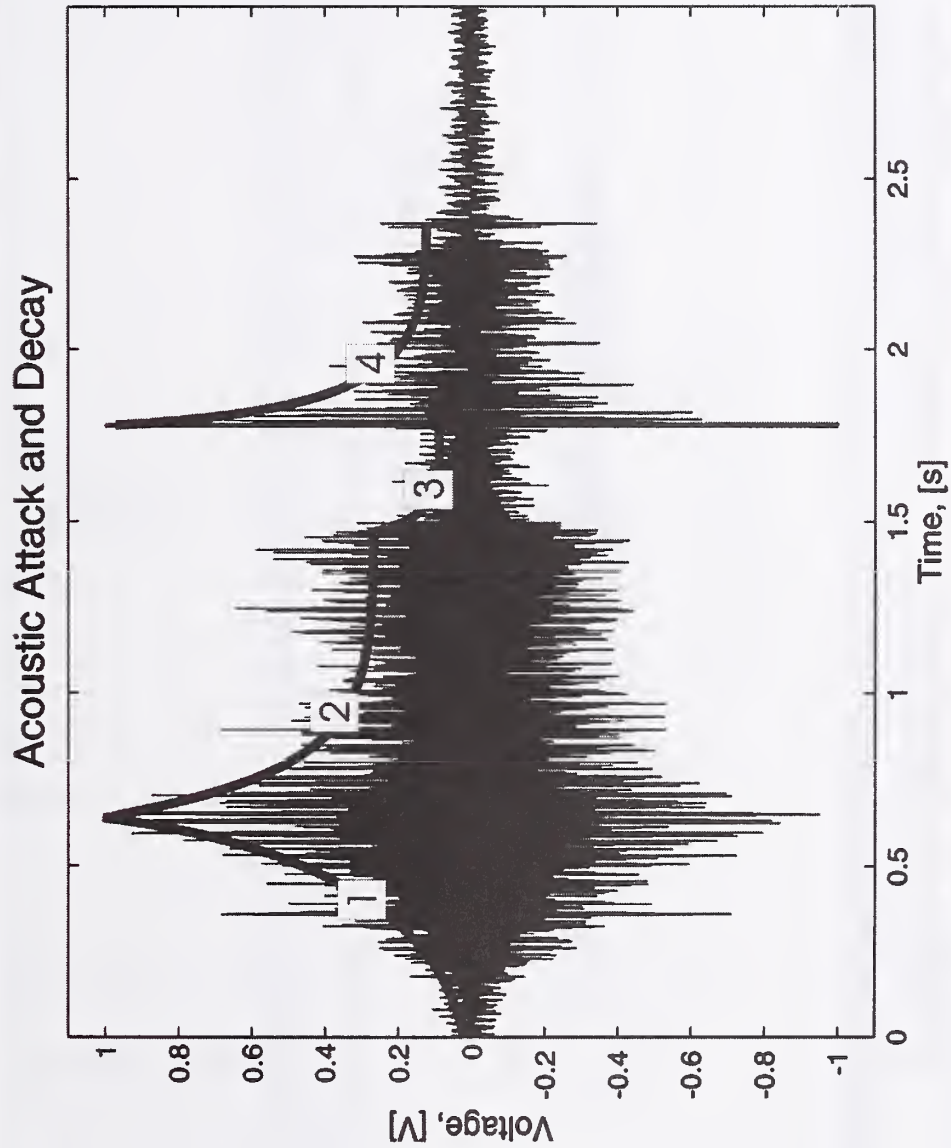
Feature Analysis: Power Spectrum

Typical Acoustic Signature

Acoustic Power Spectrum

NMT-10: Manufacturing and Process Science and Technology

D.A. Hartman
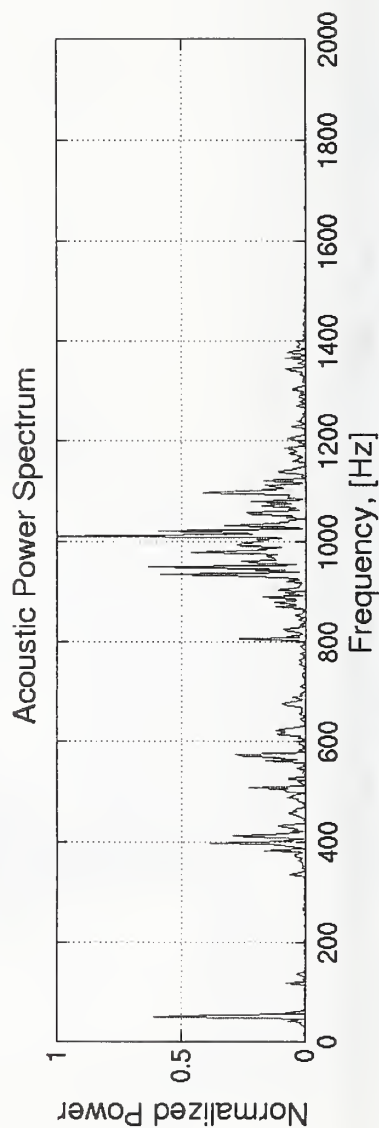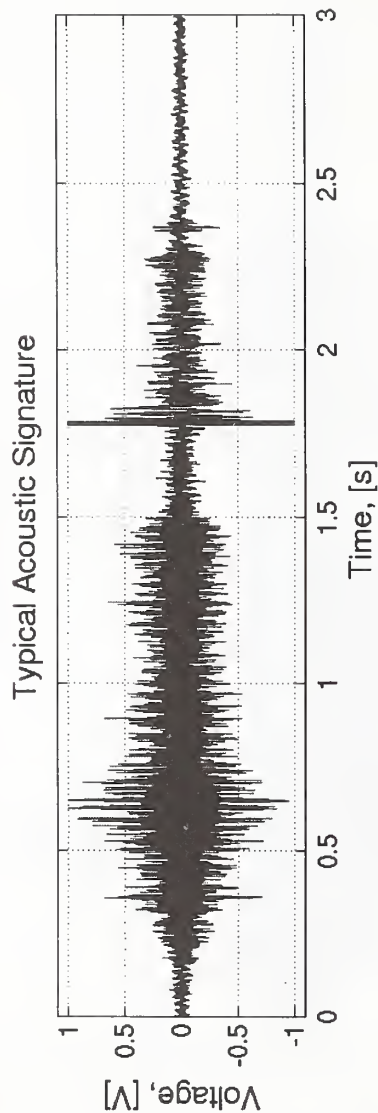
Classifier: PNN

A probabilistic neural network is a feedforward implementation of a Bayesian classifiers that provides a framework for solving pattern classification problems.

Los Alamos
NATIONAL LABORATORY

NMT-10: Manufacturing and Process Science and Technology

D.A. Hartman

Classifier: PNN, cont
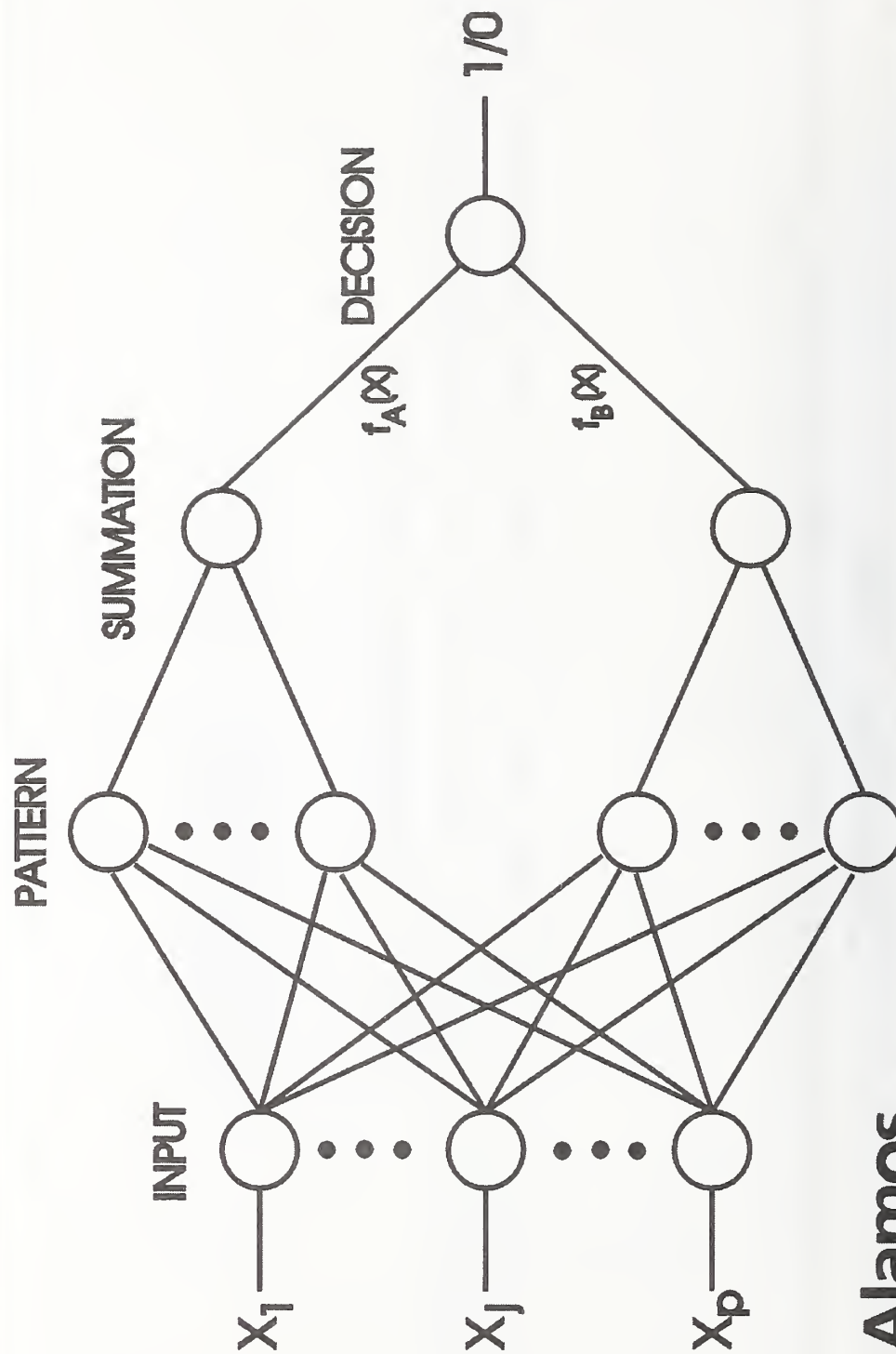
Classifier: PNN, cont

- Advantages over other neural network implementations:

  - Can begin classifying after having just one training pattern from each category.

  - Orders of magnitude faster to train than a traditional back propagation neural network.

  - Can be shown to asymptotically approach Bayes' optimal decision surface without the possibility of getting stuck in a local minima.

  - Conducive to enabling a human to interpret and understand how the network works.

Los Alamos
NATIONAL LABORATORY

NMT-10: Manufacturing and Process Science and Technology

D.A. Hartman

Classifier: PNN, cont

A PNN is therefore ideal for exploring data sets in which the structure is ill-defined and that contains both deterministic and random signals.

Classification Results: Machine Data

Test	Process Data	Feature Descriptor	Acceptable Unacceptable	Acceptable Conditional	Acceptable Conditional Unacceptable
1	Speed	Normalize	82	74	63
2	Pressure	Normalize	59	58	42
3	Upset	Normalize	59	74	63
4	Speed, Pressure	Normalize	76	63	54
5	Speed, Upset	Normalize	59	68	58
6	Pressure, Upset	Normalize	59	63	54
7	Speed, Pressure, Upset	Normalize	59	63	54

Classification Results: Machine Data, cont.

Test	Process Data	Feature Descriptor	Acceptable Unacceptable	Acceptable Conditional	Acceptable Conditional Unacceptable
8	Speed	Attack & Decay	71	63	50
9	Pressure	Attack & Decay	65	68	50
10	Upset	Attack & Decay	47	68	50
11	Speed, Pressure	Attack & Decay	65	68	54
12	Speed, Upset	Attack & Decay	47	68	50
13	Pressure, Upset	Attack & Decay	59	63	46
14	Speed, Pressure, Upset	Attack & Decay	59	63	46

NMT-10: Manufacturing and Process Science and Technology   D.A. Hartman

Classification Results: Acoustic Energy

Test	Process Data	Feature Descriptor	Acceptable Unacceptable	Acceptable Conditional	Acceptable Conditional Unacceptable
15	AE	RMS	71	47	46
16	AE	Energy (1 seg)	76	58	54
17	AE	Energy (4 segs)	94	31	41
18	AE	Attack & Decay	88	63	54
19	AE	Attack & Decay, Energy	94	52	50
20	AE	Power Spectrum	100	100	54

Classification Results: Acoustic Energy, cont.

Test	Process Data	Feature Descriptor	Acceptable Unacceptable	Acceptable Conditional	Acceptable Conditional Unacceptable
21	AE, Speed	Attack & Decay	82	68	71
22	AE, Pressure	Attack & Decay	71	68	63
23	AE, Upset	Attack & Decay	72	68	63

Los Alamos
NATIONAL LABORATORY

NMT-10: Manufacturing and Process Science and Technology

D.A. Hartman

In-Process Data: Acoustic Energy & Speed

D.A. Hartman

NMT-10: Manufacturing and Process Science and Technology
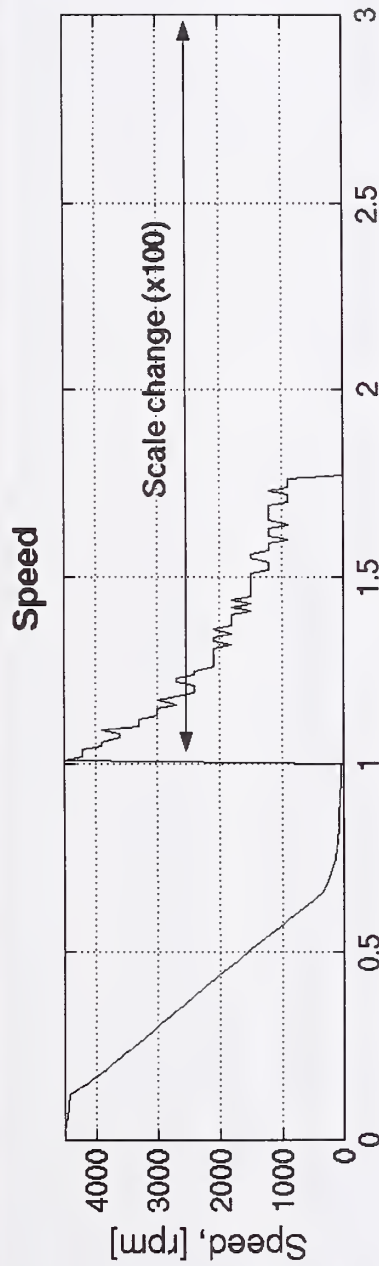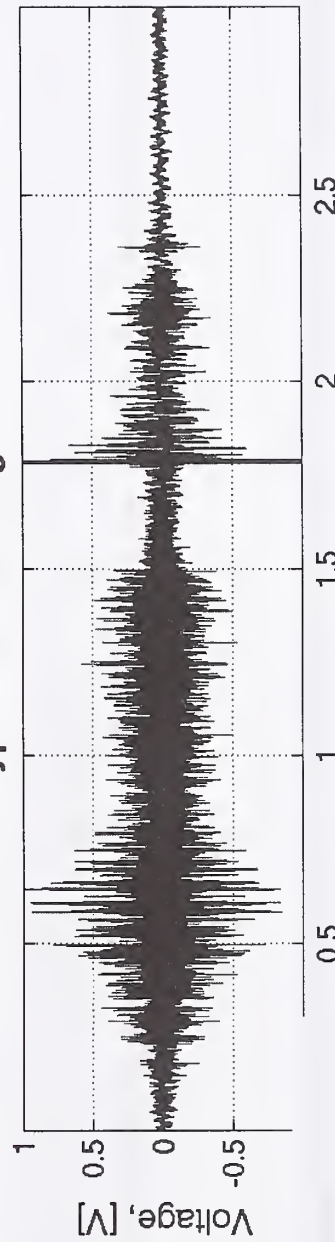
Conclusions

- *A classification system was developed with a new acoustic emission sensing technique.*

- *The classification system is capable of detecting subtle bond-plane contamination conditions.*

- *It exploits the capabilities of a neural network to interpret multidimensional and ill-defined data.*

NMT-10: Manufacturing and Process Science and Technology

D.A. Hartman

50
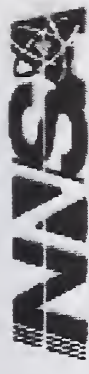
Successful Implementation

The successful implementation of an in-process monitoring system requires:

- *Thorough (sufficient?) understanding of the process*

- *Identification of the key variables*

- *Appropriate sensing mechanism*

- *Data analysis techniques that can identify features within the data that can be correlated to quality*

Los Alamos
NATIONAL LABORATORY

NMT-10: Manufacturing and Process Science and Technology

D.A. Hartman

51

Benefits

- *Fast*: Provides a real-time response immediately after welding is complete.

- *Inexpensive*: No additional hardware requirements are necessary.

- *Robust*: Is capable of mapping complex or ill-defined multidimensional input/output systems and is tolerant of noisy data commonly found on production floors.

- *Consistent*: Sensing and interpretation is performed without operator intervention and, therefore, ensures an accurate, repeatable, and reproducible system.

- *Thorough*: Examination is performed for each weld, rather than randomly, to ensure joint integrity.

- *Efficient*: Only suspect welds are examined further using an "inspect for cause" methodology, which, thereby ensures nuclear safety and promotes weapon system reliability

NMT-10: Manufacturing and Process Science and Technology

D.A. Hartman

52

NUMERICAL SIMULATION OF RESISTANCE SPOT WELDING PROCESS USING FEA TECHNIQUE

C. Srikunwong[*,**] ,T. Dupuy[*] ,and Y. Bienvenu[**]

ABSTRACT

2-D axisymmetric finite element models incorporating electrical-thermal and thermal-mechanical coupling procedures were developed for resistance spot welding (RSW) process simulation. A commercial finite element code, namely SYSWELD®, was utilized for these simulation purposes. The coupling procedures can provide a more realistic and efficient computational approach accounting for the variation of contact size; particularly for the application of curved-face electrodes producing a spot weld. The temperature dependency characteristics and properties of both sheets and electrodes were also taken into account throughout the study. The welding schedules based on practical aspects of similar two- as well as three-sheet assemblies were considered for the entire of process. Not only the utilization of pulsed direct current but also that of pulsed alternating current was utilized in order to efficiently achieve the industrial protocol. The experimental study was centered on nugget formation. The validation for the nugget development was determined in the case of pulsed direct current welding.

The impact of pulsed alternating current welding combining supplementary post-heating pulses on the nugget size as well as on the thermal history was investigated. It was concluded that both heating and cooling rates depend strongly on the position of weld. The results of electrical-thermal analysis were discussed in view of the thermal history during welding, with particular regard for different types of welding current used.

INTRODUCTION

Resistance spot welding (RSW) is widely utilized as a joining technique for automobile structure due to flexibility, robustness and high-speed of process combining with very high quality joints at very low cost. Not only heavy gauge two-sheet assemblies are joined by this technique but also stack-up sheet assemblies can often be encountered in the application. In some cases of heavy gauge two-sheet joining, the use of a common continuous current signal is sometimes not efficient to construct the desired weldability lobe. The pulsed welding approach then becomes an other choice to achieve this purpose. The pulsed welding current based schedule is sometimes recommended for heavy gauge and stack-up assembly cases associated with some welding signal modification in order to improve weldability and mechanical properties of spot weld. The pulse current used can be medium frequency direct or alternating current pulse. Other adapted current signal such as down sloping, quenching or post-heating can be also introduced to a required welding current signal. These modifications become a common convenient technique for the improvement of weld mechanical-metallurgical properties in high strength steel joining (Ref. 1). The use of pulsed welding has many advantages in heavy gauge sheet joining including the stability of nugget development characteristics and the reduction of electrode wear.

* CRDM, Sollac Atlantique, ARCELOR Group, BP 2508, 59381, Dunkirk, France
** Ecole des Mines de Paris, BP 87, Evry Cedex, 91003, France

The recent development in finite element analysis for RSW numerical simulation is well documented in the literature (Refs. 2 and 3) showing that there is a significant change in the contact radii between electrode-to-sheet and sheet-to-sheet interfaces during welding stage. This has significative impacts on thermal history, nugget formation and thermal stresses in the assembly. Therefore, it is vital to implement a coupling procedure between electrical-thermal and thermal-mechanical modules in order to capture this physical interaction and produce a more realistic predictive model.
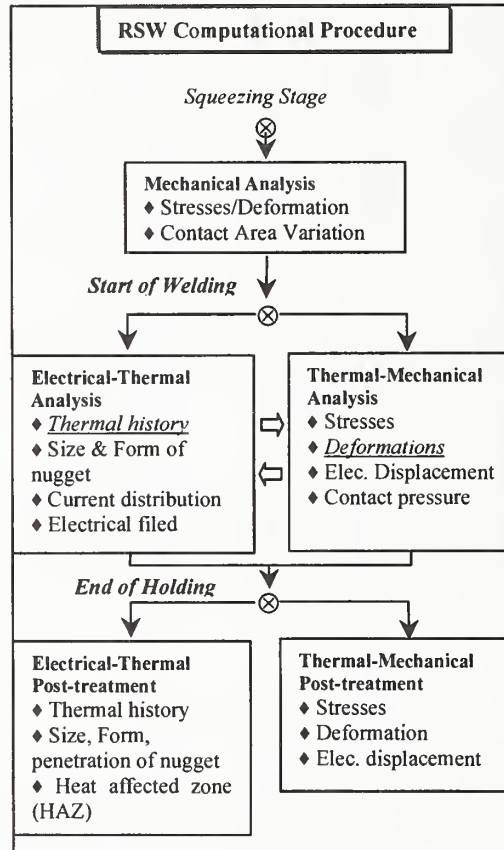

Figure 1: Schematic illustration of computational procedure

The aim of this study is to obtain a better understanding of the influence of process parameters for heavy gauge sheet joining with the use of pulsed welding current. The features of the coupling procedures can be described by loop sequential computational procedures of the nodal temperatures transferred from the electrical-thermal analysis to the thermo-mechanical analysis in order to compute the thermal stresses and assembly distortions. On the other hand, the stress distributions associated with assembly deformation are then transferred back to the next electro-thermal computation step in order to up-date the variation of the contact size and pressure. These successive sequential loops are cumulated until the end of RSW process. The computational procedure employed in this study is illustrated in fig. 1.

FORMULATION FOR MODELING

Structure Modeling

A representative assembly of electrode and sheet utilized for analysis as shown in fig. 2 illustrates a half axisymmetric finite element model for electrode and sheet assembly, which is considered for both electrical-thermal and thermal-mechanical analyses. 2-D axisymmetric models of two- and three-sheet joining incorporated with the curved face electrode of 6mm and 8mm.-diameter are constructed. Both electrical-thermal and mechanical contact elements are specially treated at electrode-to-sheet and sheet-to-sheet interfaces.
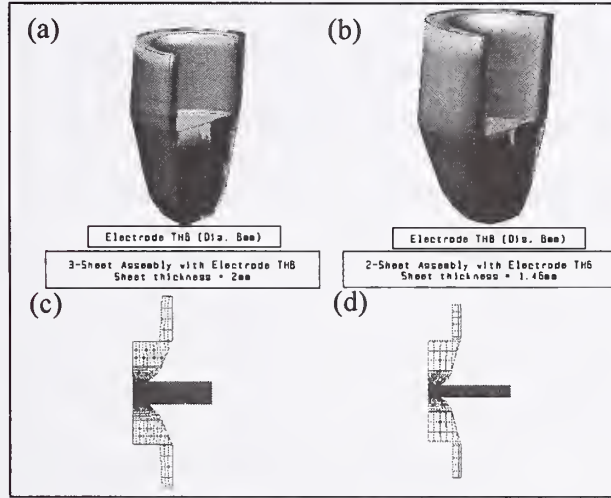

Figure 2: Illustration of structure mesh models used in analysis
Figure 2a: Curved-face electrode of 6mm-dia; Figure 2b: Curved-face electrode of 8mm-dia
Figure 2c: Three-sheet assembly mesh model; Figure 2d: Two-sheet assembly mesh model

Electrical-Thermal Modeling

RSW process is a resistance welding process governed by Joule heating effect with a concentration of the heat generation at the interface between two solid bodies in contact while passing the current. This heat further propagates into these bodies by conduction heat transfer mode associated with the imposed thermal boundary conditions. Electrical-thermal governing system equations are presented in (1) and (2):

$$\rho \frac{\partial H}{\partial t} - div(\lambda.\mathbf{grad}T) - \mathbf{grad}V.\sigma.\mathbf{grad}V - Q = 0 \qquad (1)$$

$$div(\sigma.\mathbf{grad}V) = 0 \qquad (2)$$

Where T, V are the temperature and the scalar electrical potential, respectively. ρ, λ and σ represent the density, the thermal conductivity and the electrical conductivity of the medium. The temperature dependency characteristics can be taken into account in these equations. H is the enthalpy also with a temperature dependency. The full coupling between electrical and thermal phenomena can be governed by the term $\mathbf{grad}V.\sigma.\mathbf{grad}V$ in the heat equation. The modeled alternating current signal used in the analysis is shown in fig. 3a.

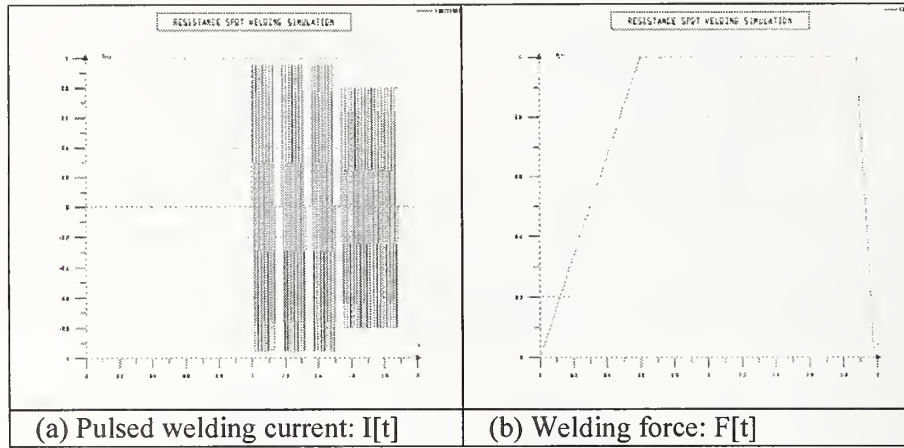| (a) Pulsed welding current: I[t] | (b) Welding force: F[t] |

Figure 3: Modeled welding signals used in analysis

<u>Thermal-Mechanical Modeling</u>

The electrode force as illustrated in fig. 3b is modeled from the welding force signal. The mechanical boundary conditions (Ref. 4) are the electrode force applied at the top surface of the upper electrode by assuming a uniform pressure distribution across the annular end and the vertical nodal displacement of annular end of the lower electrode, which is constrained similar manner to that of practical weld. The elasto–plastic Von-Mises criterion without deformation rate dependency is defined for sheet characteristics. The non-linearity due to temperature dependency of sheet properties and contact characteristics including transient computational approach are considered for this study. The three governing equations, namely, the compatibility condition, the constitutive relation, and the equilibrium equation in cylindrical co-ordinate are discussed elsewhere (Ref.5).

EXPERIMENTAL PROCEDURE

Two sheet grades of ARCELOR, a Transformation Induced Plasticity (TRIP) grade and a non-coated drawing quality Low Carbon Steel (LCS) sheet are utilized in this study. Properties of both sheets are given in Refs 6 and 7. The metallurgical examination is conducted only for the low carbon steel sheet joining.

Table 1: Welding schedules utilized in the study

Welding conditions		Current: [kA/Cycles] Force
Elec. dia. (mm)	Configuration	
1) 8	2sheets:(LCS) 2mm-thick	11.2-DC/4(6+2) 400 daN
2) 6	2sheets:(LCS) 2mm-thick	8.97-DC/4(6+2) 400 daN
3) 8	3sheets:(LCS) 2mm-thick	10.6-DC/4(6+2) 450 daN
4) 6	2sheets:(TRIP) 1.46mm-thick	7.80-AC/3(7+2)+6.5×17 500 daN

Welding schedules in table 1 indicate the utilization of pulsed welding current. In the case of TRIP steel sheet joining with electrode face diameter of 6mm., alternating current with a magnitude of 7,80 kA is applied for 3 pulses, each pulse has 7 cycles of welding plus 2 cycles of current shut-off. Furthermore, the post-heating current is then applied for 17 cycles with a magnitude of 6.5 kA. The aim of post-heating current application is to achieve the good quality of residual metallurgical phases and minimize the weld fracture of HSS sheet joining. The as-received sheets are cut to 50×50-mm coupons. Electrode conditioning prior to welding is performed for 50 welding points with bare sheet. The trial welding tests are then conducted in order to determine the expulsion limit. These trial welding conditions are based on the French Industrial Standard (Ref.8), which is considered as welding schedule guideline. The welding schedules, just below the expulsion limit, are used for three welding coupons and for each pulse in order to examine the formation of nugget relating to configurations. The no-expulsion welding of each pulse can be verified from the force and the displacement signal monitoring on the LABVIEW® window. The effective current magnitude is obtained from the MIYASHI® current signal recorder. Nugget development kinetics can be further examined by sectioning the spot after each interrupted pulse. The polished axial sections of spot welded samples are etched with picric acid to determine the fusion line or the nugget contour. This etchant is suitable for the examination of the fusion zone of low carbon steel spot welds. Quantitative macro-photographic measurements are made for the nugget size.

EXPERIMENTAL RESULTS AND DISCUSSION

Influence of Process Characteristics on Nugget Formation

Nugget development kinetics for two and three LCS sheet joining of 2mm-thick at the end of each pulse is shown in fig. 4. As expected, both the height and the diameter of the nugget increase at the end of the first two pulses. During the third and the fourth pulse, the nugget expands more in diameter than in height. The indentation on the sheet surfaces and the sheet separation can also be observed. The influence of electrode face diameter on nugget formation is demonstrated by comparing case 1 and 2. It is revealed that the increase of electrode diameter face leads to the increase in magnitude of welding current by around 2.2kA if the electrode face diameter of 8 mm is used instead of 6 mm. This is due to the enlargement of contact size reducing the concentration of current flux at faying surface. The utilization of smaller electrode face diameter results in remarkable indentation onto sheet surfaces at the end of welding. Concerning the nugget formation kinetics in the case of two-sheet joining, the occurrence of nugget at faying surface is already observed at the end of the first pulse.

In the case 3, instead of initiating at center of three-sheet assembly, the hot zone originates in superior and inferior regions at the end of the first pulse but the nugget does not start forming yet. For the latter pulses, nugget penetration and development also show a trend similar to that of two-sheet assembly case. The dissymmetry in the upper and the lower nugget diameters can be found before the saturation of nugget diameter at the end of the fourth pulse. However, both symmetrical or dissymmetrical nugget development can be observed for three-sheet joining case. The sheet edge separation between faying surfaces is slightly different. The decrease in current magnitude for the three-sheet assembly comparing to that of two-sheet joining can be explained by the increase of bulk electrical resistance with the increase in number of sheets.
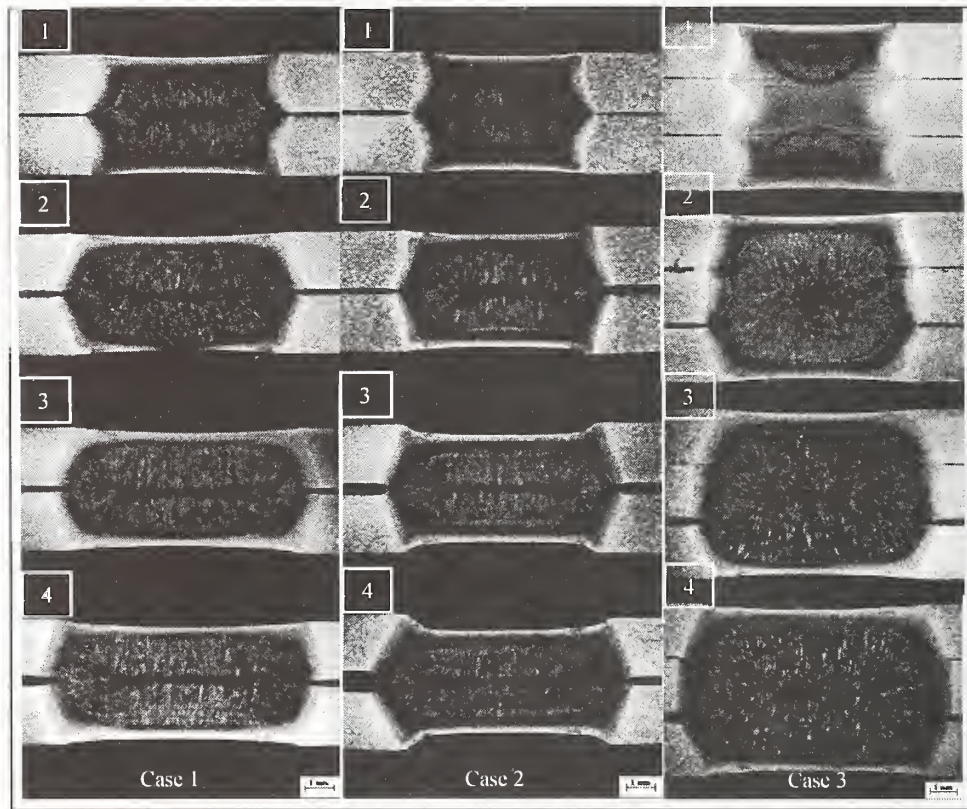
Figure 4: Illustration of nugget formation of two- and three-sheet assembly at the end of each pulse (Number of pulse is indicated on the macro-photograph and see also table 1 for the case study)

COMPUTATIONAL RESULTS AND DISCUSSION

Influence of Process Characteristics on Thermal History

For two-sheet joining case, the temperature history at different positions demonstrates the same dynamic response to the type of welding current used. The drop in temperature during current shut-off can be obviously observed on temperature evolution and markedly seen for the positions located in the nugget region as illustrated in fig.5a. The instantaneous significant increase in heating rate is found during the first pulse, particularly at the beginning. In contrast to the heating rate of weld center for two-sheet joining, there is no significant change in heating rate during the first two pulses for three-sheet joining as shown in fig 5b. An insignificant variation is seen for weld center thermal history during the current shut-off between the first and the second pulses.

For both two- and three-sheet joining cases, There is no variation in thermal history for the positions located far away from the nugget and the HAZ, i.e. r=8mm., during the weld stage. Unfortunately for the sheet joining with RSW technique, it is not easy to attain the same value of the maximum temperature in order to compare the thermal histories. This is due to the difference in the inherent welding parameters and the configuration used.
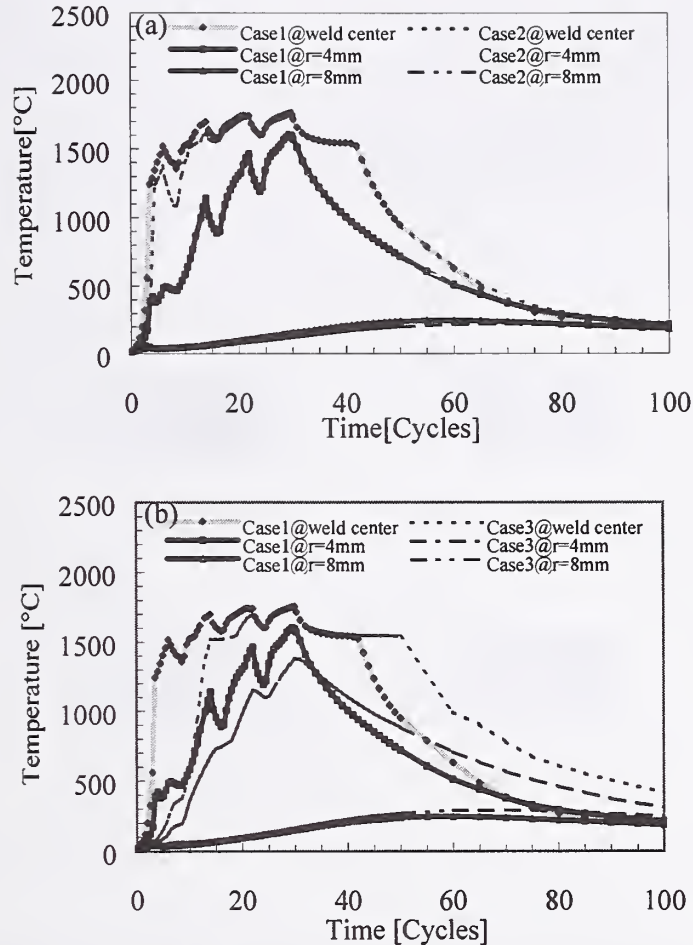
Figure 5: Influence of process characteristics on thermal history considering at the upper limit of weldability lobe

Figure 5a: Influence of electrode face diameter resulting in welding current adaptation and consequently on thermal history

Figure 5b: Thermal history in two- and three-sheet joining cases

Influence of Post-heating Current on Weld Geometries

The nugget geometries and sizes at the end of each pulse in the case of TRIP steel joining are illustrated in fig. 6. It is obvious that the nugget develops until the end of pulsed welding. The peak temperature at the weld center is found at the end of the last or the third pulse. After that, there is no significant evolution of heating rate during the post-heating stage. It is shown that there is no further development in nugget size during the application of post-heating current and this is contrast to metallurgical phase evolution in the HAZ during this supplementary stage. Let us examine a node located inside the nugget and near the fusion line, i.e. node at y=1,168mm as shown in fig. 7b. The maximum temperature of this node is about 1535°C at the end of the welding process.

The temperature drop can be also observed during the current shut-off. The thermal history of this node increases again during the post-heating stage but with a lower heating rate than that experienced in the assembly during welding. The maximum temperature of this node reaches

about 1354°C at the end of post-heating stage. This reveals that the simulated nugget size at the end of post-heating will be smaller than that obtained at the end of welding. It is worth noting that the appearance of maximum nugget height and diameter is an irreversible phenomenon and only takes place at the end of welding. Therefore, this discussion can be supported by the occurrence of maximum nugget diameter at the end of welding stage with the examination of thermal history. Fig. 6d shows the simulation result of the smaller size of nugget diameter at the end of post-heating stage than that predicted at the end of welding as illustrated in fig. 6c.
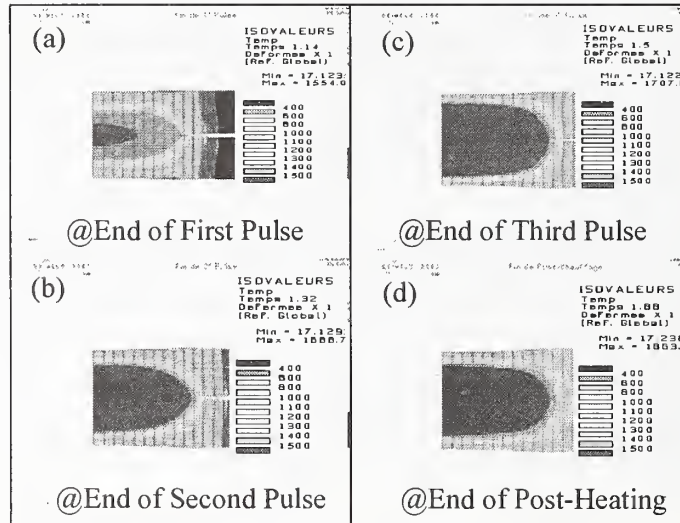

Figure 6: Predicted nugget development kinetics using post-heating current: case4

It is obvious that more important heating rates can be found for the nodes located along the axis than for the nodes located along the radius. However, the temperature history considered at the position located outside and near the HAZ zone, at the position (r = 4,50mm) as shown in fig.7, is increased even during the current shut-off. For the positions located sufficiently far away from the weld center (r=5.10 mm), the drop in their thermal histories cannot be observed and the temperature increases continuously during current shut-off and post-heating stage.

The simulation results reveal that the number of pulses and the magnitude of post-heating current should be prudently selected while practically examining the mechanical and metallurgical properties of weld.
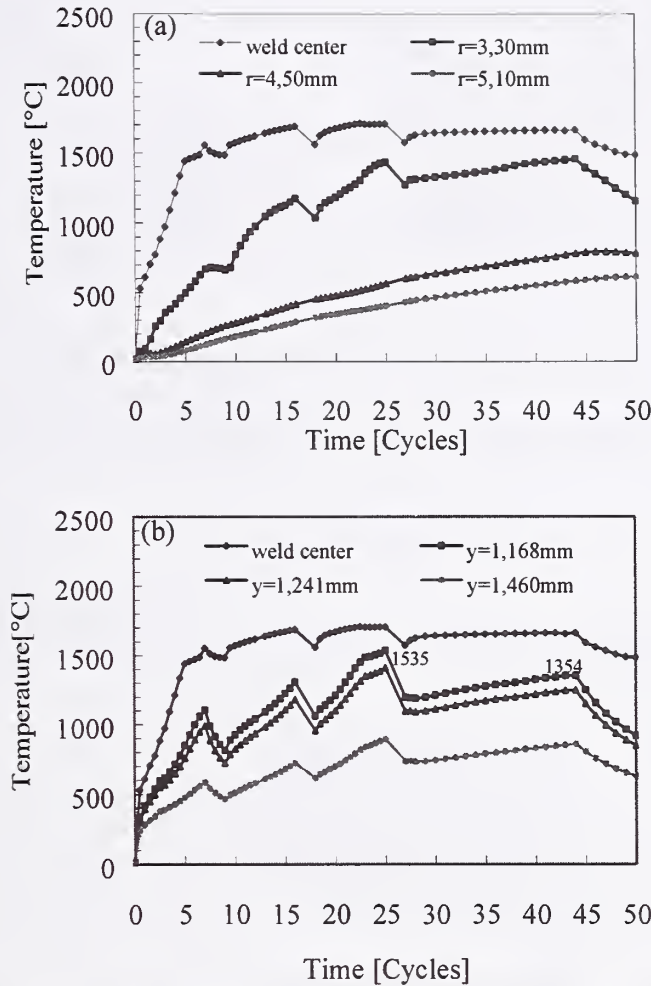
Figure 7: Influence of post-heating current on nugget size at the end of welding: case4
Figure 7a: Average thermal history at different radial position
Figure 7b: Average thermal history at different axial position

Residual Stresses in Assembly

The slide-line mechanical contact element without friction is defined at sheet-to-sheet and electrode-to-sheet interfaces throughout the computation. This contact condition however may not be a very realistic approach for the appearance of nugget at faying surface. In fact, when the nugget starts forming, the faying surface is joined by the molten mold. Therefore, the contact condition associating with the occurrence of nugget should be the sticking contact condition. The novel mechanical contact approach is under development with the modification of mechanical boundary conditions at the different stage of process.
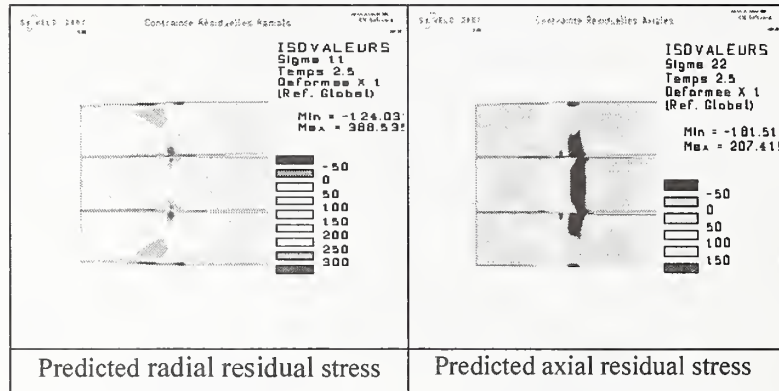The residual stresses for three-sheet joining case are shown in fig.8.

| Predicted radial residual stress | Predicted axial residual stress |

Figure 8: Predicted residual stresses in assembly at the end of process: case 3

EXPERIMENTAL VALIDATION

For three-sheet joining case, the validation is carried out for the quantitative measurement of nugget diameter appearing at the interfaces between the upper-to-middle and the middle-to-lower sheets, namely $D_{upper@exp}$ and $D_{lower@exp}$ respectively.
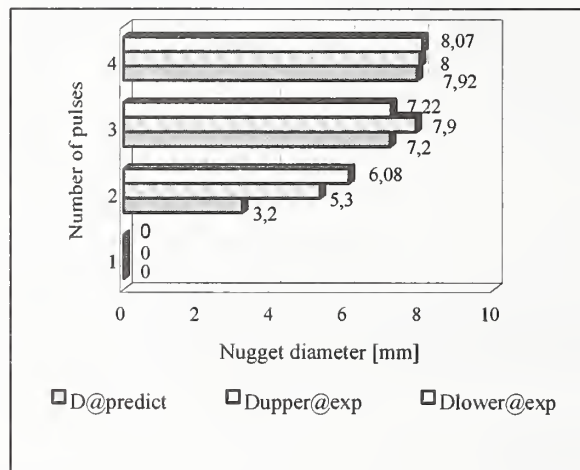

Figure 9: Validation of nugget diameter for three-sheet joining: case 3

Note that the nugget diameters increase significantly during the first two pulses and saturate for the latter stages. Both predicted and measured nugget growth kinetics exhibit similar trend for long welding time. The validation shows a quantitative agreement in nugget diameters at the end of welding, which are of 8mm corresponding to the diameter of electrode face used. However, it is found that there is a discrepancy between the measured and the predicted nugget diameter size, particularly at the end of the second pulse. The measured nugget diameters for the upper-to-middle and the middle-to-lower interfaces are around 5.30 and 6.08mm, respectively. While the simulated nugget diameter sizes are found in an order of 3.2mm and show the effect of planar symmetry as depicted in fig. 9. This discrepancy may be due to the inappropriate electro-thermal contact values at faying surface, particularly for the temperature extending from ambient temperature to 200-400°C. It is understood that the

faying surface contact resistance diminishes rapidly with temperature (Ref. 9) and plays a significant role on the nugget development. These electrical contact resistances also depend strongly on the surface condition of sheet, the welding force and the temperature.

CONCLUSIONS

A finite element analysis based predictive model incorporating an electrical-thermal and thermal-mechanical coupling procedure was applied to study the heavy gauge sheet joining by the RSW technique. This model provides a better understanding of the effects of welding parameters on the nugget development kinetics and on the thermal characteristics in the assembly with the use of pulsed welding current schedules.

The main conclusions of this study are:

1) It is experimentally found that the use of the larger electrode diameter leads to an increase in the magnitude of welding current due to a better distribution of current flux and reduces the indentation of electrode face onto the sheets. Concerning three-sheet welding configuration, it well demonstrates the significance of the total bulk electrical resistance of sheet at elevated temperature with the decrease in welding current magnitude. The nugget development exhibits similar trend for long welding time.

2) The simulation results show the difference in thermal history experienced in the assembly between two- and three-sheet joining while respecting the upper limit in the weldability lobe before the occurrence of expulsion. The drop in thermal history due to current shut-off can be seen on the temperature evolution for both cases and more markedly in the two-sheet joining case. The thermal history depends strongly on the position in the assembly. For position located sufficiently far away from the nugget and the HAZ regions, there is no impact of current shut-off on the thermal history.

3) It is demonstrated that the appropriate selection of the magnitude and the number of post-heating pulses has no effect on the final nugget size obtained at the end of welding. However, the temperature history is slightly increased during the post-heating stage for every position in the assembly.

4) The validation result shows a good agreement for the final nugget size at the end of welding in the case of three-sheet joining. But the discrepancy in nugget diameter size development can be observed during the first two pulses before the saturation of nugget. This may be due to the inappropriate values of electrical contact resistances introduced at faying surface. Electrical contact resistance determination will be further conducted in order to evaluate the contact characteristics.

ACKNOWLEDGEMENTS

REFERENCES

1.   Peterson, W. May 15-17 2002. Methods to minimize the occurrence of interfacial fractures in HSS spot welds. <u>Sheet metal welding conference X.</u> Stering Heights, MI.

2.   Khan, J.A.; Xu, L.; and Chao, Y.J. 1999. Prediction of nugget development during resistance spot welding using coupled thermal-electrical-mechanical model. <u>Science and technology of welding and joining.</u> Vol. 4, No.4: 201 to 207.

3.   Sun, X.; and Dong, P. Aug. 2000. Analysis of aluminum resistance spot welding processes using coupled finite element procedures. <u>Welding research supplement</u>: 215-s to 221-s.

4.   Srikunwong, C.; Dupuy, T.; and Bienvenu, Y. Nov., 2001. A decoupled electrical-thermal and mechanical model for resistance spot welding. 15th <u>annual conference of mechanical engineering network of Thailand.</u> Bangkok, Thailand. Vol.2: 76 to 84.

5.   Murakawa, H.; Kimura, F.; and Ueda, Y. 1997. Weldability analysis of spot welding on aluminium using FEM. <u>Mathematical modeling of weld phenomena 3</u>: 944 to 966.

6.   Thiéblemont, E. 1992. <u>Modèlisation du soudage par points</u>. Ph.D. dissertation. L'Institut National Polytechnique de Lorraine. (in French)

7.   Bobadilla, M.; Niederleander, M.; Nuss, C.; Perrin, G.; and Selaries, J. Juin 1994. <u>Données thermiques pour différentes familles d'acier.</u> Rapport interne IRSID, Groupe Usinor. (in French)

8.   Caractérisation de la soudabilité par résistance par point de produits plats revêtus ou non, Déc. 1994, <u>Normalisation française A87-001</u>. (in French)

9.   Vogler, M.; and Sheppard, S. June 1993. Electrical contact resistance under high loads and elevated temperatures. <u>Welding research supplement</u>: 231-s to 238-s.

THE FINITE ELEMENT MODELING OF RESISTANCE SPOT WELDING

A. V. Gohil [*], S. M. Patel [#]

ABSTRACT

Resistance spot welding process is the most significant joining process in the automobile industry due to its high speed and suitability for automation. One of the recent demands in the automobile industry is to reduce the vehicle weight so as to improve the fuel efficiency and to meet this requirement, aluminium alloys is being considered as an important alternative for auto-body material. The vehicle corrosion problem can also be squarely dealt with. However, unlike resistance spot welding of steel, joining of aluminium through the same process has met with serious difficulties, because of faster deterioration of electrodes. High electrical and thermal conductivity, high shrinkage during solidification and the presence of natural oxide coating are some of the features that make spot welding process of aluminium alloys markedly different. At a very high temperature aluminium chemically reacts with copper alloy (electrode material). Subsequently random chipping-off of material from the electrode faces takes place and it results in electrode wear. Further, the electrode life reduces drastically when spot welding aluminium alloys. In terms of weldability, this is an extreme negative point since weldability for automobile use is greatly dictated by electrode tip life.

Since the process is very fast, important information, such as transient distribution of current density and temperature, are difficult to obtain from the experimental methods. Thus, it is aimed at the present work to develop an integrated computer simulation model for analyzing resistance spot welding process of aluminum alloys by finite element method. Several calculations have been carried out for different welding current, weld time and electrode force and for different surface conditions of aluminium sheets. Non-linear, temperature-dependent, thermo-physical material properties have been considered. It is interestingly observed that in most cases the nugget diameter is formed well within 0.02~0.04sec and further flow of welding current simply increases the electrode face heating. Also, the initial surface condition influences the nugget formation phenomenon to a great extent. Various other conclusions have been arrived at as a part of this study.

INTRODUCTION

Resistance spot welding process is the most significant joining process in the automobile industry due to its high speed and suitability for automation and thus, any new development of this welding process is closely influenced by the demand of this industry. The need to reduce vehicle weight, improve fuel economy, and reduce exhaust emission has led to increased use of light weight materials such as aluminium alloys. However, many technical issues have to be solved before the use of aluminium becomes commonplace in high-volume production. Unlike

[*] Department of Production Engineering, Shantilal Shah Engineering College, Bhavnagar, India
[#] Department of Production Engineering, Shantilal Shah Engineering College, Bhavnagar, India

resistance spot welding of steel, joining of aluminium through the same process has met with serious difficulties. Aluminium is a very good electrical conductor with a bulk resistivity one third that of steel. Joule heating is proportional to resistance for a given current. It is understandable that a significant increase in welding current will be required to join aluminium, compared to an equivalent gauge of steel sheet. Further, aluminium has a high thermal conductivity and the localized heat generated by the welding current will be will be conducted away rapidly. It is therefore necessary to use short weld times. Aluminium alloys posses a surface oxide layer that varies depending on the prior thermal and mechanical processing. The oxide has a high resistivity band high melting point, around three times greater than pure aluminium. Therefore, spot welding of aluminium alloys has become an important research area in the last couple of years both in the academic as well as industrial research laboratories.

The electrical resistance spot welding process for joining two materials at their common interface is a complicated interaction of electrical, thermal, mechanical, metallurgical and surface phenomena. In this process, electrodes press against two or more steel sheet and high amperage current is passed through the sheet-electrode system. Because of the electrical contact resistance, heat will be generated at electrode / work piece interfaces and faying surface. The heat at the faying face melts the work pieces to form a nugget. To prevent melting at the electrode / work piece interface, water is circulated in the cooling chamber of the electrode.

The current carrying zone in the sheet is determined by the region over which electrodes touches the sheet and this, in turn depends on the electrode force and consequent plastic flow at sheet-electrode interface. The complete phenomenon is thus, an electro - thermal problem which is also influenced by plastic flow in the sheet. Coupled with this are various types of nonlinearities present in the system. For example, thermal conductivity and bulk electrical resistivity vary with the temperature. Besides, the interface resistance along sheet – sheet interface and sheet – electrode interface varies with various parameters in a very uncertain manner. Hence, a finite element code for simulating the spot welding process which includes all those features mentioned above is developed in the present work for modeling resistance spot welding process of aluminium alloys.

PREVIOUS INVISTIGATIONS

Since the physics of the process is so complicated, it is quite understandable that very little was published in the open literature on the finite element modeling which covers these many aspects. In 1984, Nied [3] had reported a two-dimensional simulation model for analysing resistance spot welding process of uncoated steel using commercial FEM package ANSYS. A coupled thermo-electrical and thermo-mechanical analysis has been tried. However, the contact resistance along the sheet-to-sheet and sheet-to-electrode interfaces was neglected. Gould [4] reported a one-dimensional numerical model to calculate weld nugget development during spot welding of uncoated steel. However, the model being one-dimensional, failed to account for the radial heat loss into the surrounding sheet. Cho [5] had reported a two-dimensional, finite difference method based heat transfer model for resistance spot welding process. It has been concluded from the publications cited above that the resistance spot weldability of aluminium alloys is not yet fully explored although there is now tremendous demand of the these materials to be used in the automobile industry. The purpose of this present work is to develop finite element based

66

numerical model which also consists a nonlinear thermo – mechanical coupling to provide a more realistic simulation of the resistance spot welding process of aluminium alloys.

FINITE ELEMENT MODEL

Geometric Modeling

Considering a typical arrangement for resistance spot welding of two pieces of aluminium sheets, the geometric representation of two identical electrodes simplifies the geometry of two – dimensional axisymmetric model. Fig. 1 shows the finite element mesh structure used for the modeling purpose. The mesh structure consists of 358 nodes and 297 elements. The element mesh size at the end of the electrode and for the work piece is sufficiently refined to account for thermal gradients in that region. A coarser mesh is considered in the upper region of the electrode where the gradients are shallower because of heat conduction to the water – cooling channel. Only one quadrant of the complete geometry has been analyzed considering the axial symmetry of the sheet-electrode system in spot welding process.

Heat Transfer Analysis

Heat transfer in resistance spot welding process involves convective heat transfer as well as heat conduction in bulk of the sheet-electrode system. The transient heat flow in resistance spot welding process has been modeled as a case of axisymmetric heat conduction problem.

$$\frac{1}{r}\frac{\partial}{\partial r}\left(r K \frac{\partial T}{\partial r} \right) + \frac{1}{r}\frac{\partial}{\partial z}\left(r K \frac{\partial T}{\partial z} \right) + \dot{Q} = s c \frac{\partial T}{\partial t} \tag{1}$$

where s, c and K are density, specific heat and thermal conductivity respectively. All the material

properties are considered to be temperature dependent. The term $\dot{Q}$ refers to the rate of internal heat generation per unit volume.

Electrical Field Analysis

The current density distribution in the sheet-electrode geometry (in two-dimensional cylindrical coordinate system) can be represented by the following relationship,

$$\frac{1}{r}\frac{\partial}{\partial r}\left(r \frac{1}{\rho} \frac{\partial J}{\partial r} \right) + \frac{1}{r}\frac{\partial}{\partial z}\left(r \frac{1}{\rho} \frac{\partial J}{\partial z} \right) = 0 \tag{2}$$

where, ρ is the electrical resistivity and $\mathbf{J}$ is the current density vector. The electrical resistivity is considered temperature dependent in the present work.

Internal Heat Generation

The internal heat generation at every point in the sheet-electrode geometry is calculated by the following relationship,

$$\dot{Q} = \rho J^2 \tag{3}$$

67

Internal Heat Generation

The finite element discretisation of the complete sheet-electrode geometry has been carried out using four-noded ring type isoparamtric, solid element with rectangular cross-section. Within an element, temperature (T) can be expressed as,

$$\{T\} = [N_i \; ..... \; N_l] \{T^e\} \tag{4}$$

where, N_i, ... N_l are the shape functions (based on nodal co-ordinates of the element) of the element. The transient heat conduction equation (eq.1) is first discretised and the discretised equation can be stated as,

$$[H]\{T\} + [S]\frac{\partial}{\partial t} + \{F\} = 0 \tag{5}$$

where $[H]$ is the thermal conductivity matrix, $[S]$ is the thermal capacity matrix and $\{F\}$ is the load vector due to internal heat generation. Equation (6) is further discretised in time domain following Galerkin's Principle. The solution of electrical analysis represents the elemental current density distribution throughout the sheet-electrode geometry. These results are then used to calculate the internal heat generation in each element and subsequently the heat transfer equation is solved to obtain the nodal temperature distribution in the complete geometry. The total weld time has been divided into a number of small time steps. Within each time step, the electrical field analysis is carried out first to obtain the elemental current density and the heat transfer analysis is done next considering the internal heat generation.

RESULTS AND DISCUSSIONS

A Simulation model has been developed and extensive numerical calculations were carried out to find out the nugget diameter, penetration, etc. for resistance spot welding of aluminium alloy sheets using the FEM Software ANSYS. Fig. 1 shows the geometry used for the modeling purpose. Only one quadrant of the complete geometry has been analyzed considering the axial symmetry of the sheet-electrode system in spot welding process.

The sheet thickness used for the present analysis is 0.8mm and the temperature dependent material properties for aluminium and copper electrode are shown in Fig.2 – 5. The sample temperature distributions in the sheet-electrode system for welding current of 45 KA at different instant of times are shown in Fig.6. It can be observed that the temperature isotherms are more concentrated along the faying surface and the maximum temperature occurs along the sheet-to-sheet contact zone only. The time histories of the highest temperature experienced by the sheet-electrode system at two different welding currents (35 KA and 45 KA) are plotted in Fig.7. The development of nugget diameter with time for two different weld currents (40 KA & 45 KA) for the same material is shown by the Fig.-8. It is observed that the nugget development process is complete within 0.06 sec and with further increase in time no more radial growth occurs. It has been observed in Fig.9 that within 0.02 sec., the maximum temperature generated is above the liquidus temperature of the sheet and with further increase in time there is no more rise in

maximum temperature. This occurs presumably as the faying surface resistance decreases and heat generation becomes more heavily dependent on bulk resistivity and further due to the higher conductivity of aluminium alloy heat dissipation becomes more with longer weld time. It has been shown by the Fig.9 that the current density is not uniform throughout the sheet-electrode geometry and hence hosts the importance of the electrical field analysis in case of resistance spot welding process.

CONCLUSION

A comprehensive simulation model using FEM for the analysis of resistance spot welding process has been developed. It has been observed that the finite element modeling of the resistance spot welding process can provide good simulation, if the model includes the electro-thermal mechanical interaction and good temperature – dependent material properties. The results presented herein indicate that there is another alternative: the use of a realistic analytic model. This finite element model so developed can calculate most of the resistance spot welding responses in terms of nugget diameter, depth of penetration, the extent of heat affected zone, rate of heating and cooling, electrode face heating etc. Finally this FEM model will certainly help in optimizing process parameters combinations in any industrial application of resistance spot welding process. The authors are also intending to perform real time experiments so as to validate the theoretical results with in-house experimental data since such data are scarcely available in the literature.

REFERENCES

1. Johnson, K. I. 1976. Aluminium in vehicle bodies, Metal Construction & British Welding Journal 8(9): 392 to 395.
2. Ostgard, E. 1980. Spot welding of aluminium as delivered, Metal Construction 12 (2): 78 to 86.
3. Nied, H. A. 1984. The finite element modeling of the resistance spot welding process. Welding Journal 63(4): 123 to 132.
4. Gould, J. E. 1987. An examination of nugget development during spot welding using both experimental and analytical techniques. Welding Journal 66(1): 1 to 10
5. Cho, H. S. 1989. Study of the thermal behavior in resistance spot welding. Welding Journal 68(6): 236 to 244.
6. Brown, D. J. 1995. Computer simulation of resistance spot welding in aluminium. Welding Journal 74(10): 339 to 344
7. Brown, D. J. 1995. Computer simulation of resistance spot welding in aluminium. Welding Journal 74(12): 417 to 422.
8. Murakawa, H.; Kimura, H.; and Ueda, Y. 1995. Weldability analysis of spot welding on aluminium using FEM. Transaction of JWRI. 24: 101 to 111.
9. De. A.; Dorn. L.; and Gohil. A. V. 2001. Numerical Modeling of Resistance spot welding of aluminium alloys. Proc. International Conf. on Advances in Welding and Cutting Technology. Eds. The Indian Institute of Welding.
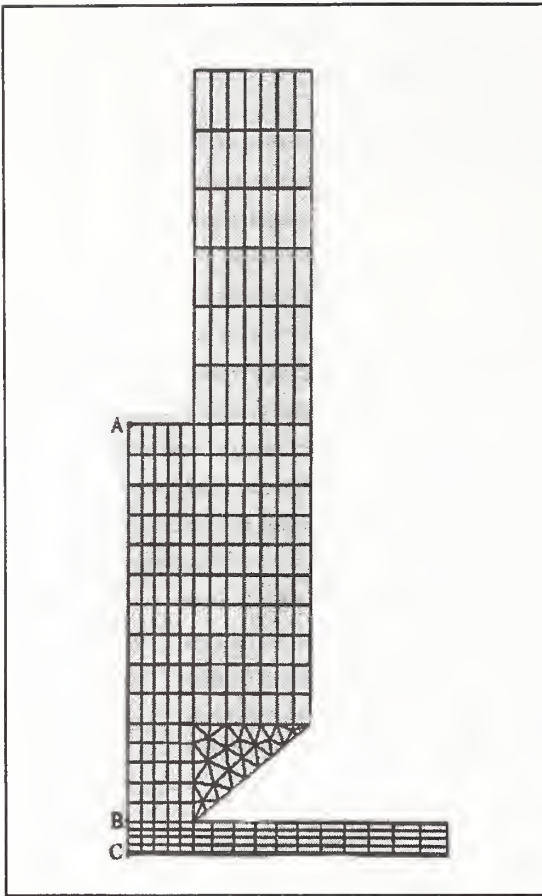
Fig. 1. Finite Element Model for equal
sheet thickness

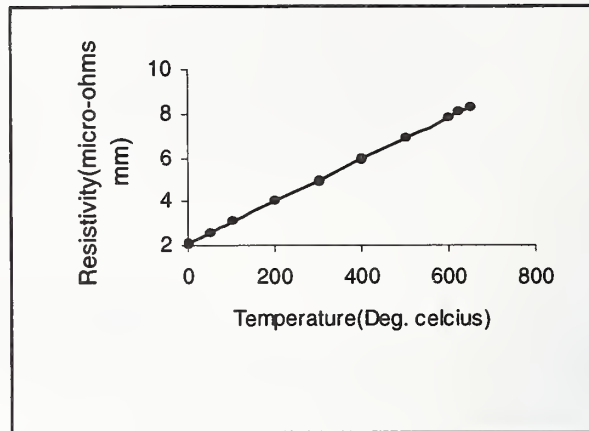Fig. 2 Temperature dependent resistivity
of copper
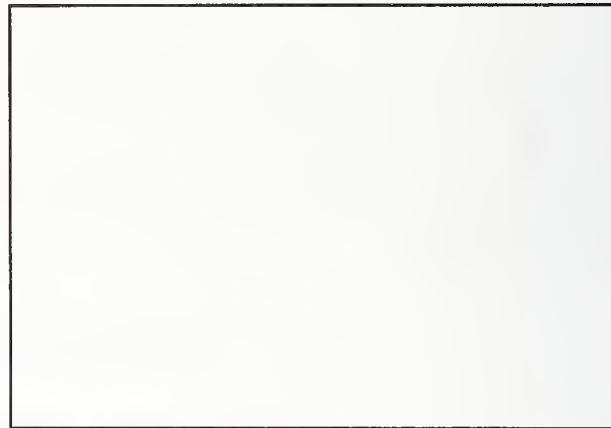
Fig. 3 Temperature dependent resistivity
heat of aluminium
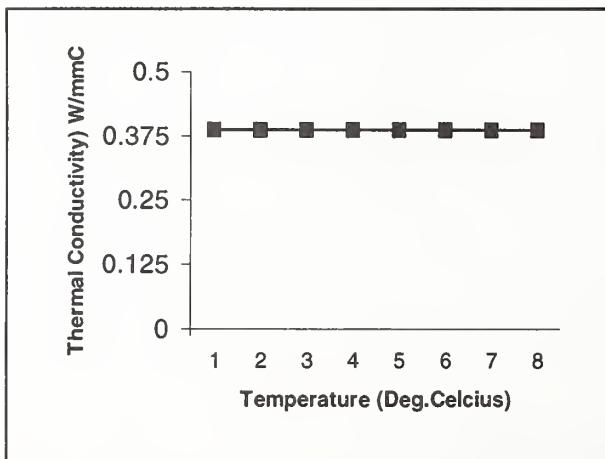
Fig. 4 Temperature dependent thermal
conductivity of copper
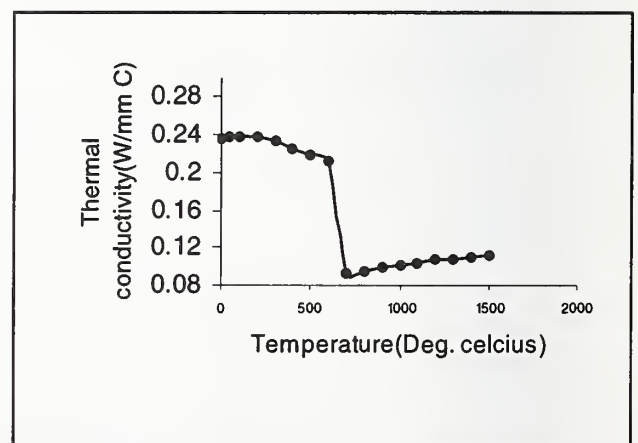
Fig. 5 Temperature dependent thermal
conductivity of aluminium
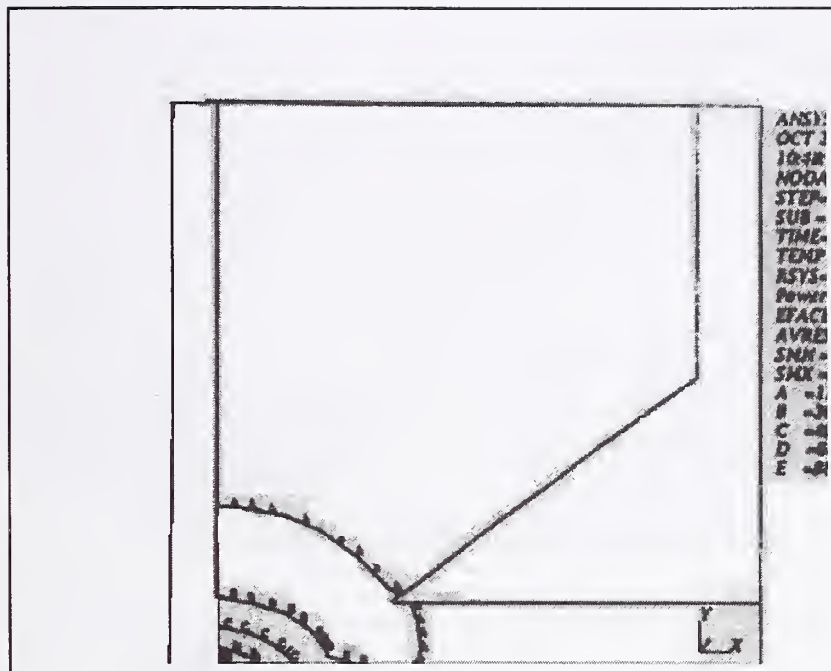
Fig. 6(i) Temperature Distribution as Resistive heating progress (after 0.2 sec)
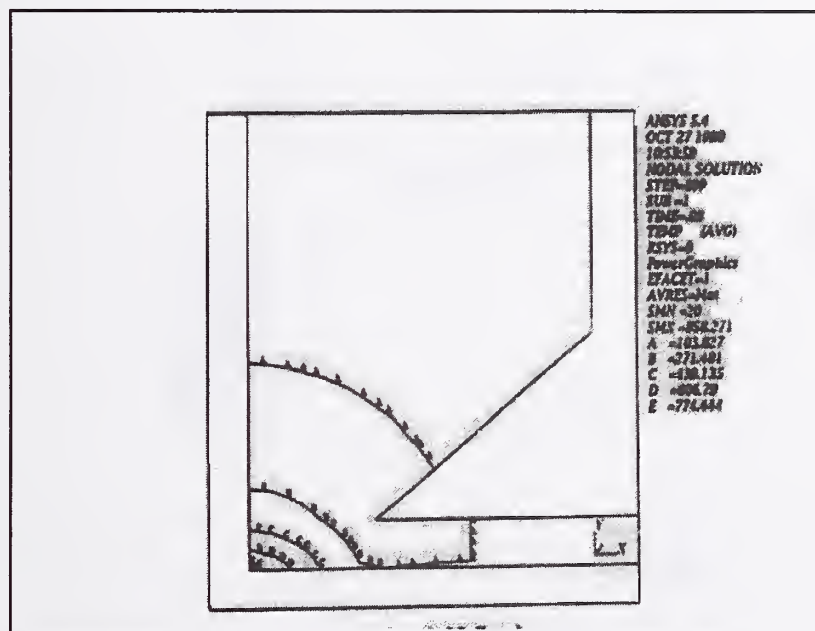
Fig. 6(ii) Temperature Distribution as Resistive heating progress (after 0.8 sec)
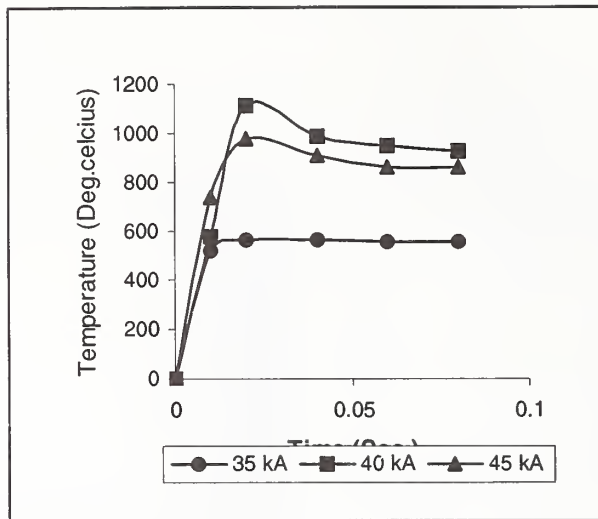
Fig. 7 Maximum temperature generated
at different instant of time (sec)
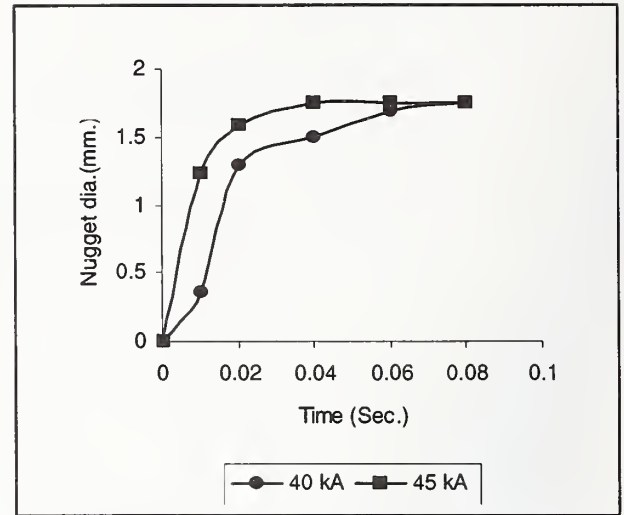
Fig.8 Nugget development at different
instant of time (sec.)

(After 0.04 Sec.)

(After 0.08 Sec.)
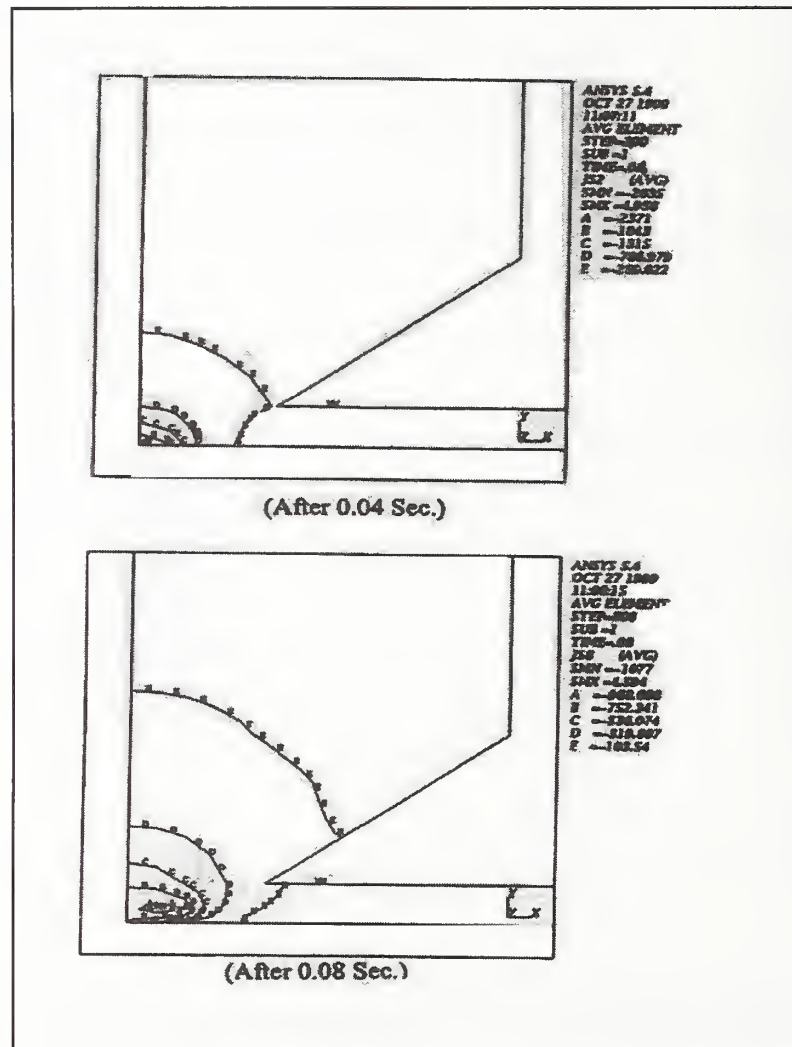
Fig. 9 Current Density Distribution as Resistive heating progress
(For sheet thickness 0.8 mm and current I = 45 kA)

Weld Pool and Solidification

THE POSSIBILITIES OF THE APPLICATION OF AN EXPERT SYSTEM IN THE MANUFACTURING OF RESISTANCE SPOT WELDED RAILWAY VEHICLE STRUCTURES

I. Borhy[*], B. Palotás[#]

ABSTRACT

The satisfaction of heightened quality requirements for railway carriage bodies as complex engineering structures are only possible by way of a comprehensive controlling of the entire design and manufacturing process and the close cooperation of all experts taking part in the process. In the design phase several different points of view need to be taken into consideration and weighed in order to satisfy the various demands for the vehicle structure, which often even contradict each other. In view of the complexity of the task to be solved, the development of an expert system to be used in the area of resistance spot welding procedures is fully justified. In our paper we are discussing the topical questions of the development of expert systems assisting the design and manufacturing of spot welded vehicle structures with optimum characteristics.

KEYWORDS

Case-based expert system, Resistance spot welding, Railway vehicles, Weld quality requirements, Finite Element Model, Genetic Algorithm

INTRODUCTION

The market value (success) of a product is basically determined by how competitive it is. Competitiveness, in turn, is primarily a function of the costs associated with the product throughout its entire life cycle, i.e. from its design and manufacturing, through its operation and maintenance to decommissioning. In the design and manufacturing phase, several different points of view need to be taken into consideration and weighed in order to satisfy the customer's various demands and expectations for the product, which often even contradict each other. The achievement of an optimal result taking into account these various different requirements is a difficult task, since in addition to the demands of strength, reliability, aesthetic considerations, etc., attention must also be paid so that the product can be manufactured and inspected to specifications. An indispensable means of attaining these objectives is a close cooperation between the design engineer, the technologist and the experts carrying out the inspections both in the phase of product design and the manufacturing technology design. At the same time,

---

[*] Expert, TÜV Rheinland InterCert Ltd., Paulay Ede u. 52., Budapest H-1061, iborhy@hu.tuv.com

[#] Associate Professor, Budapest University of Technology and Economics, Department of Mechanical Technology and Material Science, Bertalan Lajos u. 7., Budapest H-1111, palotasb@eik.bme.hu

competitiveness also presupposes a reduction of the time devoted to the design phase. In view of the complexity of the task at hand, the short time frames available, and the increased expectations towards the experts participating in the project (thorough theoretical knowledge combined with extensive practical experience), the use of expert systems in the design process for the achievement of the objectives set forth is well justified.

The Department of Mechanical Technology and Material Science of the Budapest University of Technology and Economics (BMGE) has been conducting significant research projects for over a decade in the area of computer-aided design of welding processes [1, 2, 3, 4]. Connecting to this research, our project aims to promote the development of an expert system to be used in the area of resistance spot welding procedures. I this paper we intend to discuss some of the most recent results of research carried out in this field.

RESISTANCE SPOT WELDING PROCEDURES
IN THE MANUFACTURING OF RAILROAD STRUCTURES

The chassises and bodies of both road and railway vehicles are built on the basis of the principle lightweight construction [5]. Vehicle structures demand designs that are rigid enough and can withstand fatigue loading, but at the same time have the smallest weight possible. The most common manufacturing method for such vehicle structures is resistance spot welding, because of the various advantages (efficiency, the availability of mechanization, uniform weld quality, etc.). The questions of inspections related to the design and manufacturing of these vehicle structures is a very current issue these days.

This is primarily the case because this industrial sector is characterized by large series, where the questions of economic efficiency come to the foreground to a greater extent. The above objectives can only be attained by increasing the quality and reliability of the vehicle structures, while at the same time reducing the design, manufacturing, operation and maintenance costs. Competitive market conditions, therefore, demand a constant development of the materials used, the design, the manufacturing and the control of production, as well as the application of the most advanced design and manufacturing methods. Without such development success on the market - maintaining and strengthening the market position by gaining further customers - cannot be achieved. With regard to the fact that vehicle manufacturing industry is one of the driving forces of global economy, continuous development is justified.

This is secondly the high quality standards set for the vehicles and various components can only be ensured by controlling the entire manufacturing process from design and the selection of materials to manufacturing and subsequent checking. This justifies the creation of strict regulations regarding the design, manufacturing and checking of vehicle structures, which includes the increasing of the reliability of welded joints. The increasing demands for product safety also justify continuous development.

On the basis of the above it is reasonable to place the customer's expectations in the focus, to analyze and quantify them (i.e. convert them into index numbers), thereby endeavoring to design a structure with the most optimal parameters. In other words, the satisfaction of the customer's expectations may be best ensured by solving an optimization task, which places quality in the focus. Such a quality-centered optimization task justifies the development of expert systems for use in resistance spot welding procedures. The application of an expert system can provide, among other things, the following benefits:

- help achieve the strict quality (reliability) requirements set for vehicle structures;
- facilitate the control of the entire design and manufacturing process (from design and the selection of materials to manufacturing and subsequent checking); and
- increase the reliability of welded joints.

SCIENTIFIC PRELIMINARIES

The literature of methods, optimization procedures and expert systems used in the design of vehicle structures in very extensive [6, 7, 8]. It cannot be our objective in the confines of the present paper to describe in detail the theoretical background of optimization procedures and expert systems, and so we will only briefly refer to some of the preliminaries.

The ultimate objective of several decades of research is intelligent problem solving. An expert system is a computer-based problem solving system that provides assistance in the analysis and solving of highly complicated and complex problems by evoking the problem solving procedures used by human experts [9]. The intelligence of the system is best manifested in its ability to adapt to new circumstances, which is closely related to the use of experiences acquired earlier [10].

The problem solving method of expert systems is basically determined by the form in which knowledge is represented. *Case-based design* implements a system whereby the elements of earlier designs are re-used in the design process. A complex design problem can thus be solved in shorter time by appropriately modifying the results of a similar, but already solved problem.

Keeping in mind the complexity of the topic, in our paper we wish to discuss some topical questions of the development of an expert system assisting in the design and manufacturing of spot welded vehicle structures. The practical applicability of the development results are demonstrated through the example of updating of vehicle structures in the plant of Bombardier Transportation in Dunakeszi, Hungary. We intend to demonstrate how the experiences gathered in the design and manufacturing were utilized in the development of the expert system. We intend to show how the special welding technological requirements are used in the design and manufacturing of the side walls. We intend to show what measures had to be taken and what questions had to be answered in order for these requirements to be taken into consideration as early as the design process and what preparations need to be taken during the design of the technology and the actual production, so that the welded joints would satisfy the quality requirements set forth.

DESIGN REQUIREMENTS

Bombardier Transportation was commissioned to build, rebuild and/or modernize various types of railway passenger wagons in its Dunakeszi plant. Among other projects, the updating of 136 pieces of Bhv-type suburban passenger wagons at the orders of the Hungarian State Railways (MÁV) and 79 pieces of second-class passenger wagons at the orders of the Greek Railway Company (OSE) can be highlighted (Figures 1. and 2.). The objectives of these projects included the improvement of the quality of rail transportation, the increase of passenger comfort, and the raising of the technical quality of the aged vehicle fleet.

Figure 1.: Modernized, Bhv-type, suburban railroad passenger railway carriage

Figure 2.: A second-class passenger wagon at the orders of the Greek Railway Company

In view of the loads on the structure, the geometric configuration of the vehicle, the material quality and typical thickness of the side plates and the framework, as well as the minimum expected lifetime, we strove to find the optimum structure satisfying the customer's requirements in the design of the spot welded side walls. For this purpose, we have:

- analyzed and quantified the customer's requirements, and defined the limit values for each parameter (Table 1.);
- prepared a finite-element model of the closed frame;
- examined the stresses and deformations arising in the closed frame as a result of the loads;
- performed examinations in order to define optimum weld distribution (geometric position and weld distance).

No.	Requirement	Index number	Limit value	Index number in optimal case:
1.	Strength adequacy of spot welds	Load on spot welds [kN]	Shear/breaking strength characteristic of spot welds [kN]	decreases
2.	Aesthetic requirement: deformation for entire vehicle structure	Extent of deformation [mm]	Maximum deformation allowed by standard	decreases
3.	Production cycle time	Number of spot welds	-	decreases
4.	Extent of weld's utilization	Utilization factor	100%	increases

Table 1.: Customer's requirements and quality indexes

THE FINITE ELEMENT MODEL

The finite element analyses were carried out with the application of the MSC.Nastran/Patran v. 70.5 software package. The loads that the vehicle structure is exposed to were determined in accordance with the customer's requirements, on the basis of the MSZ EN 12663:2000 standard and the provisions of UIC 566. In the course of the finite element modeling, we examined the stresses and deformations resulting from normal operation and extraordinary loads as defined by the standard (Figure 3.). A detailed review of the examinations performed is contained in [11, 12].

Figure 3.: Stresses and distortions in the carriage body

Figure 4. shows the finite element model of the spot welded joints of the side wall windows and corner frames. On the basis of earlier operation experiences we can state that the lifetime of the vehicle structure is significantly determined by the behavior of the environment of the side wall windows and corner frames under stress loads. Deterioration processes starting from the environment of the side wall windows and corner frames have a fundamental effect on the lifetime of the vehicle structure; therefore, special attention had to be paid to the design of appropriate connections in this area. The forces affecting the individual welded joints with a given density of welds is shown in Figure 5.

Figure 4.: The finite element model of the side wall windows and corner frames with resistance spot welds
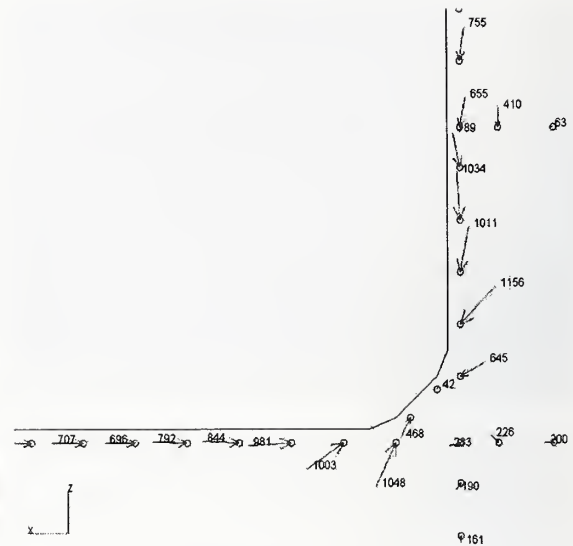
Figure 5.: The loads on the spot welds

The weld quality requirements and the testing instructions were determined with the results of the finite element modeling in mind. The results derived from the modeling were checked in the series of measures taken on a completed carriage body made possible by the Institute of Development and Experiments of MÁV Rt. Upon the evaluation the examinations we could conclude that the spot welded joints made with the standard characteristics satisfy the expected loads affecting the carriage body.

THE CASE-BASED DESIGN SYSTEM

The experiences gained in the design problems were utilized in the development of the expert system assisting in the design and manufacturing of spot welded vehicle structures with optimum characteristics. The focus of our research was the various methods of knowledge representation and inference that can be used in the expert systems. Figure 6. shows the diagram of a case-based expert system developed for the designing of a spot welded vehicle side wall.

Figure 6: Block diagram of a case-based design system

In the development of the system, we were looking for solutions to the following problems:

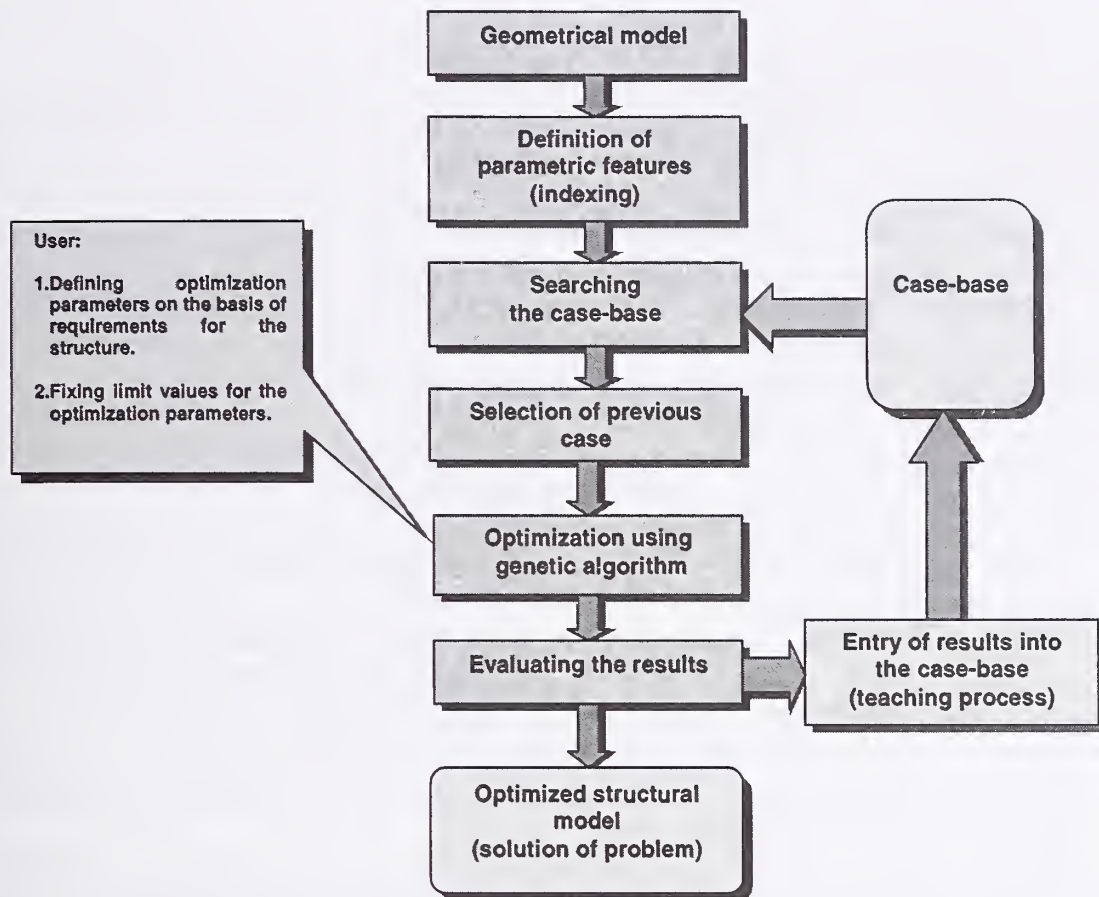- A parametric system was developed for the definition of the characteristic features of unique individual cases, i.e. for the coding of the cases;
- For the determination of similarities between individual cases, examinations were carried out in order to introduce index numbers for similarities;
- Studies were made for the modification (adaptation) of a similar design selected from the case-base. A genetic algorithm was used for the performance of the optimization process.

The results of the study provide sufficient basis for the achievement of the objectives set forth in the introduction, and they also facilitate the further development of the model and its additional industrial application. The experiences gained in the course of the development of the case-based expert system also point out the directions of future research, since in the case of a weld made with given parameters it becomes possible to define deformations and residual stresses. These two characteristics are extremely important from the point of view of the production railway vehicle parts, because the former affects the usability of the part, while the latter reflects the effect of the given part on the whole structure; and furthermore.

SUMMARY

The paper discusses the possibilities of using expert systems in the design and manufacturing of railway vehicle structures with resistance spot welds. After the demonstration of the importance of the topic, the necessity of developing and improving expert systems that can be used in the area of resistance welding procedures is emphasized. The application of welding technology requirements to design and manufacturing is shown through a concrete example. We have presented an outline and the characteristic features of a case-based expert system developed for the design of spot welded vehicle side walls, and references have been made to a possible method of implementing knowledge representation and inference methods.

REFERENCES

1. Brenner, A.; Palotás, B. 1989. Computer Aided Welding. BME Mérnöktovábbképző Intézet. Budapest.
2. Borhy, I. 1999. Actual Considerations on Modelling of Resistance Welding Procedures. Proceedings of microCAD '99 International Computer Science Conference, Section H (Mechanical Technologies). p.: 25-30. University of Miskolc.
3. Palotás, B. 2001. Finite Element Modeling on Welding Processes and Welding Phenomena. Proceedings of 11th International Conference on Computer Technology in Welding. p.: 297-305. Colombus (Ohio).
4. Palotás, B. 2002. Modelling of Pressure Welding Processes by Methods of Mechanical Forming. Proceedings of 3rd Conference on Mechanical Engineering. p.: 229-233. Springer-Verlag. Budapest.
5. Sostarics, Gy. 1991. Railway Vehicles. Tankönyvkiadó. Budapest.
6. Pahl, G.; Beitz, W. 1993. Konstruktionslehre (Methoden und Anwendung). Springer-Verlag. Berlin.
7. Jármai, K.; Iványi, M. 2001. Gazdaságos fémszerkezetek analízise és méretezése. Műegyetem kiadó. Budapest.
8. Radaj, D. 2001. Integrated Finite Element Analysis of Welding Residual Stress and Distortion. Proceeding of 6th International Seminar on the Numerical Analysis of Weldability. p.: 469-487. Graz University of Technology.
9. Ignizio, J. P. 1991. Introduction to Expert Systems. McGraw-Hill. New-York.
10. Savory, S. E. 1990. Expert Systems for the Professional. Ellis Hoewood. New-York.
11. Borhy, I.; Schwartz, I. 2002. Practical application of FEM in the technology design of resistance spot welding in railway production. Proceeding of 3rd Conference on Mechanical Engineering. p.: 479-484. Springer Verlag. Budapest.
12. Borhy, I.; Kovács, L. 2003. Application of FEM in the production of welded railway vehicle parts. Proceeding of International Conference on Metal Structures. University of Miskolc.

NUMERICAL SIMULATION SYSTEM OF DEVELOPMENT OF ULTRA-NARROW GAP GMAW PROCESS

T.Nakamura[*] , K.Hiraoka[*]

ABSTRACT

An Ultra Narrow Gap GMA welding (UNGW) process with less than 5mm gap width has been developed in which the arc occurring at wire tip is forcibly oscillated over the groove wall in the thickness direction. To control the wire tip position, the low-frequency pulse current is used.

An UNGW process simulation system which is based on analysis of non-steady state wire melting under low-frequency pulse arc welding conditions has been proposed to obtain defect free joints and find out adaptive welding conditions. In this simulation system, the equivalent electric circuit of arc welding and many factors on welding phenomena are conceded such as the digging action by arc force, motion of molten pool, equivalent heat input in wire tip, super heat of droplets, arc current-voltage characteristics and so on.

This simulation system makes it possible to find out appropriate welding conditions for UNGW which is characterized by many pulse parameters that correlate in a complex manner.

KEYWORDS

GMA welding, Ultra-narrow gap, Numerical simulation, Non-steady state, and adaptive welding condition

INTRODUCTION

New type steel with various properties have recently been developed, and using these materials, high quality and efficient welding methods that maintain the properties of the materials is expected (Ref. 1). To reduce deterioration of joint properties by welding heat and welding deformation, small heat input welding method is effective, however high efficient welding is difficult for this welding process.

Narrow gap welding has been developed as a highly efficient and small heat input welding method (Ref. 2). The smaller groove width is more effective to small heat input welding and higher efficiency welding, however good welding is impossible with a groove width less than 5 mm. Because the arc is so unstable that the arc pole irregularly traverses up and down the groove wall, and welding defects such as lack of fusion are formed. To obtain good joint by prevention of unstable arc, mechanical weaving method in the direction of the groove width is used (Ref. 2). However, since the welding speed is limited if mechanical weaving is used, the high welding efficiency, which is the advantage of narrow gap welding, cannot be sufficiently obtained.

We developed ultra-narrow gap welding (UNGW), in which stable and high efficiency welding is possible in the groove with a width narrowed until mechanical weaving in the direction of the groove width becomes unnecessary(Ref. 3,4).The welding of the I-type joint with a groove width less than 5 mm is achieved by oscillating the arc pole over the groove wall in the thickness direction using low frequency pulse current less than 10 Hz.

[*]National Institute for   Materials Science,1-2-1,Sengen,Tsukuba,Ibaraki,JAPAN

To obtain both melting of the root area and concave surface beads, the choice of the amplitude and position of oscillation over the groove wall in the thickness direction is important. To obtain the appropriate conditions for oscillation in UNGW, it is necessary to determine many control parameters such as the pulse peak current, pulse base current, pulse peak duration, pulse base duration, frequency of pulse current and wire feed rate. Furthermore, arc behavior in the groove strongly affect the molten pool behavior rand the oscillation of the wire tip over the groove wall in the thickness direction. However, it will be impractical to determine appropriate parameters by experiments, because a tremendously large number of experiments are necessary. Therefore, GMA welding process simulation is useful to investigate optimum welding conditions and numerical models for GMA welding has been studied (Ref. 5-8).

In this study, we propose a numerical simulation system using a model of ultra-narrow gap GMA welding. In the model of ultra-narrow gap GMA welding, non-steady wire melting behavior, molten pool and arc behavior in the groove and GMA welding electric circuit were considered. The appropriate conditions of UNGW with many parameters were studied using the numerical simulation system.

NUMERICAL SIMULATION MODEL FOR UNGW

Non-Steady wire melting model for UNGW process

As the arc generating point (wire tip) is oscillated over the groove wall in the thickness direction by using low frequency pulse current less than 10 Hz, the wire melting behavior is in non-steady state (Ref. 9,10). Numerical simulation of non-steady state of wire melting behavior is performed in the equivalent electric circuit of GMA welding shown in Fig. 1.

The temperature distribution of wire is expressed the following one-dimensional heat conduction equation on the fixed coordinate system.

$$\frac{\partial U}{\partial t} + v_f \cdot \frac{\partial U}{\partial X} = \frac{\lambda}{C \cdot \gamma} \cdot \frac{\partial^2 U}{\partial X^2} + \frac{\rho_S}{C \cdot \gamma} \cdot \left(\frac{I}{S}\right)^2 \quad (1),$$

where $U(X, t)$ is the temperature(K) at time t(s) and position X (mm), and λ, γ, C, ρ_s and S are the thermal conductivity of the wire (J/mm·s·K), density(g/mm^3), specific heat (J/g·K), electrical resistivity(Ω·mm),and cross-sectional area of wire(mm^2), respectively. The extended wire is divided shown in Fig. 2. The equation (1) is converted into the moving coordinate system expressed as $Z=X-v_f \times t$,following equation is obtained.

$$\frac{\partial T}{\partial t} = \frac{\lambda}{C \cdot \gamma} \cdot \frac{\partial^2 T}{\partial Z^2} + \frac{\rho_S}{C \cdot \gamma} \cdot \left(\frac{I}{S}\right)^2 \quad (2),$$

Figure 1: Equivalent electric circuit in UNGW system

where $T(Z, t)$ is temperature(K) at time t (s) and position Z (mm). The temperature-dependence is considered in λ, γ and C.

84

A new element is added in front of the contact tip every Δt(s), and the origin of the moving coordinate system is set in front of a new element. The relationship between Δt and ΔZ is expressed as $\Delta Z = v_f \times \Delta t$.

The increment time of heat conduction is defined as δt(s), and the calculation is performed $K_n = \Delta t / \delta t$ times during Δt until a new element is added. To obtain a stable convergent solution, it is necessary that δt(s) and ΔZ satisfy the following equation (Ref. 11).

$$\frac{\lambda_{max}}{(C \cdot \gamma)_{min}} \times \frac{\delta t}{\Delta Z^2} \leq \frac{1}{2} \qquad (3)$$

The experimental ranges of this study are as follows : v_f = 100 -250 mm/s; Δt = 10^{-3} -10^{-4} s; ΔZ = 0.01-0.25 mm ; δt = 10^{-7}- 10^{-8} s (Ref. 9,10).

Arc heat input $q_a = I \times \Phi$ (Ref. 12) is provided to the wire tip element, where I is current (A) and Φ is equivalent anode melting potential (V). Correlations between Φ and superheat temperature of droplets ΔT (K) expressed as function of I are applied (Ref. 9,10). Assuming that ΔT is 500K in CO_2 welding of 1.2mm wire, Φ is expressed as the following equation .

Figure 2: One dimensional non-steady heat conduction model

$$\Phi = 6.8 + 0.0016 \times I \qquad (4)$$

Elements which become $T_M + \Delta T$ are immediately removed from the wire tip as a droplet ,where T_M is melting temperature (K).

Arc length in groove

It is assumed that the arc occurs at the minimal geometric distance between the wire tip and groove wall, which is $W_G/2$ (mm), or the minimal geometric distance between the wire tip and the surface of the molten pool just under the wire, which is L_{bottom} (mm). The arc length L_a (mm) is $W_G/2$ at $W_G/2 \leq L_{bottom}$, and $L_a = L_{bottom}$ at $W_G/2 > L_{bottom}$.

Molten metal behavior in groove

The molten pool depression by arc force is discussed. We assumed that the surface of molten pool just under the wire tip is depressed to the position of hydrostatic potential of molten metal H_g (mm) which is balanced with arc force F. In this study, arc force is related to hydrostatic potential of molten metal (HPMM), and the following experimental equation is used (Ref. 13).

$$H_g = 9.7 \times 10^{-5} \times I^2 - 1.3 \times 10^{-10} \times I^4 \qquad (5)$$

The molten metal can not response because of the viscosity and surface tension of molten metal, when the arc force changed by the low frequency pulse current. Therefore, transient responses of molten metal are discussed. The depression depth Y (mm) is defined as the distance between the surface of weld metal in the groove and the surface of the molten pool just under the wire. The temporal changes of Y is expressed by a dashpot with the viscous damping
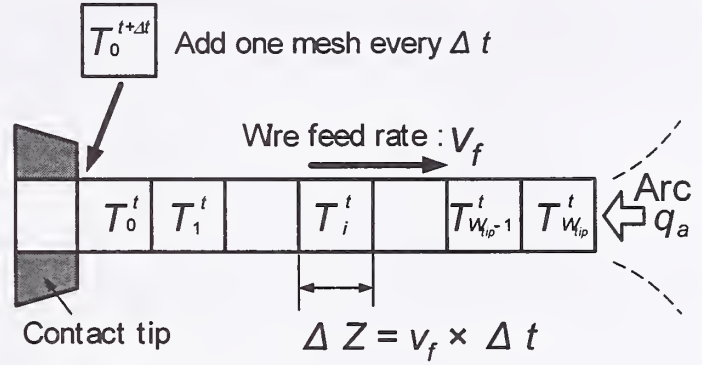
85

coefficient c, spring force with the spring constant k and external force F shown in Fig. 3 (Ref. 14). As the viscosity of molten metal suppresses its movement as the resistance, the viscosity works as same as the dashpot when external force is added. Since the HPMM increases corresponding to the concavity of molten metal, the force balancing with the HPMM is assumed to be in proportion to the concavity (displacement), and replaced by spring force with the spring constant k. The relation of displacement Y of (A) shown in Fig. 3 is expressed following equation.
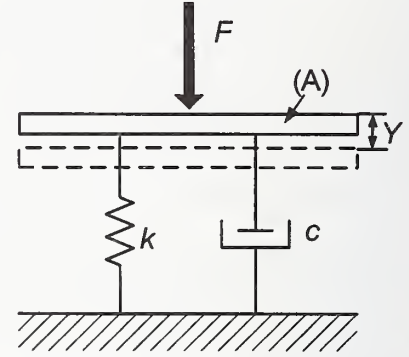
$$c\frac{dY}{dt} + kY = F \qquad (6)$$

When the arc occurs between the wire tip and the surface of the molten pool, we assumed that arc force f acts on the surface of the molten pool just under the wire tip independent of wire tip position, and this arc force is F, and the HPMM is H_g. In equation (6), the time constant c/k is regarded as τ (s), The arc force is replaced by the HPMM, the following equation is obtained.

$$H_g = \tau\frac{dY}{dt} + Y \qquad (7)$$

When arc occurs between the wire tip and the groove wall, we assumed that the arc force acting on the molten pool is regarded as f $=\alpha F$, and the HPMM is αH_g (α, constant).The following equation is obtained.

$$\alpha H_g = \tau\frac{dY}{dt} + Y \qquad (8)$$

To estimate τ and α, the behavior of the molten pool just under the wire in the narrow groove is observed by a high-speed video camera (Fig. 4). The time $t_{sp}\geq0$(s) of swelling of the surface of the molten pool from the groove bottom is 0.17-0.19s (Fig. 4 (c)

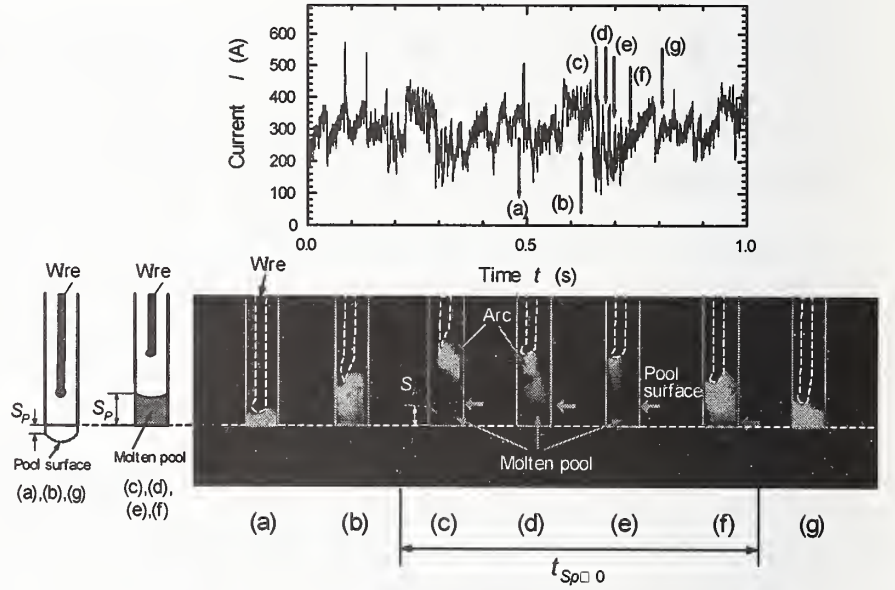Figure 3: Equivalent mechanical system

Figure 4: Measured results of motion of molten pool surface just under wire tip

(a) $\{S_p\}$max
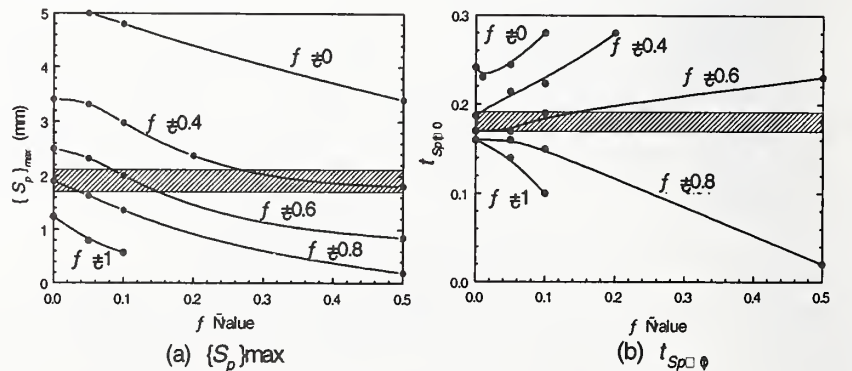
(b) $t_{Sp\square\varphi}$

Figure 5: Determination of τ value and α value

86

□(f)), and the maximal swelling of the surface of the molten pool $\{S_p\}_{max}$ (mm) was 1.7-2.1 mm.

Combinations of α and τ are determined so that $\{S_p\}_{max}$ is included in the hatched area in Fig. 5(a). For example, combinations of $\tau<0.05$ at $\alpha=0.8$, $0.08<\tau<0.14$ at $\alpha=0.6$ and $0.28<\tau$ at $\alpha=0.4$ are agreed with measurements. The combination of α and τ determined from Fig. 5(b) in the same manner is $\tau<0.16$ at $0.8>\alpha>0.4$. To satisfy the measurement of both $\{S_p\}_{max}$ and $t_{sp}\geq 0$ simultaneously, α is about 0.6, and the τ is about 0.1.

SIMULATION SYSTEM FOR UNGW

Procedure of numerical simulation system

Figure 6 shows flowchart of numerical simulation on the behavior of the melting wire tip and molten pool. In part A, input of welding conditions, welding speed v(mm/s), wire diameter d(mm), wire feed rate v_f (mm/s), distance between contact tip and groove bottom L_T(mm), groove gap width W_G(mm) and setting of the pulse conditions are performed. Initial conditions, current I_0(A), extension L_0(mm) and wire temperature T_0 (K) are inputted.

In part B, the one-dimensional non-steady heat conduction FDM analysis of wire extension is performed. ΔZ, Δt, δt and K_n are set. The Φ is determined from equation (4). The arc heat $I\times\Phi$ is added at the tip element. The calculations of the heat conduction are performed K_n times during Δt. Wire tip elements with temperature higher than $T_M + \Delta T$(K) are deleted as droplet. The extension $L_{t+\Delta t}$(mm), temperature $T_i^{t+\delta t}$, melting rate v_m(mm/s) and voltage drop of extension V_L(V) are determined at the time $t+\Delta t$.

In part C, the molten pool position just under wire tip is determined. The position of the molten pool surface just under wire tip is determined from the hydrostatic potential of molten metal H_g and depression depth Y.

In part D, the arc length and arc voltage V_a(V) are determined. The distance between the molten pool surface just under wire tip and the wire tip and the
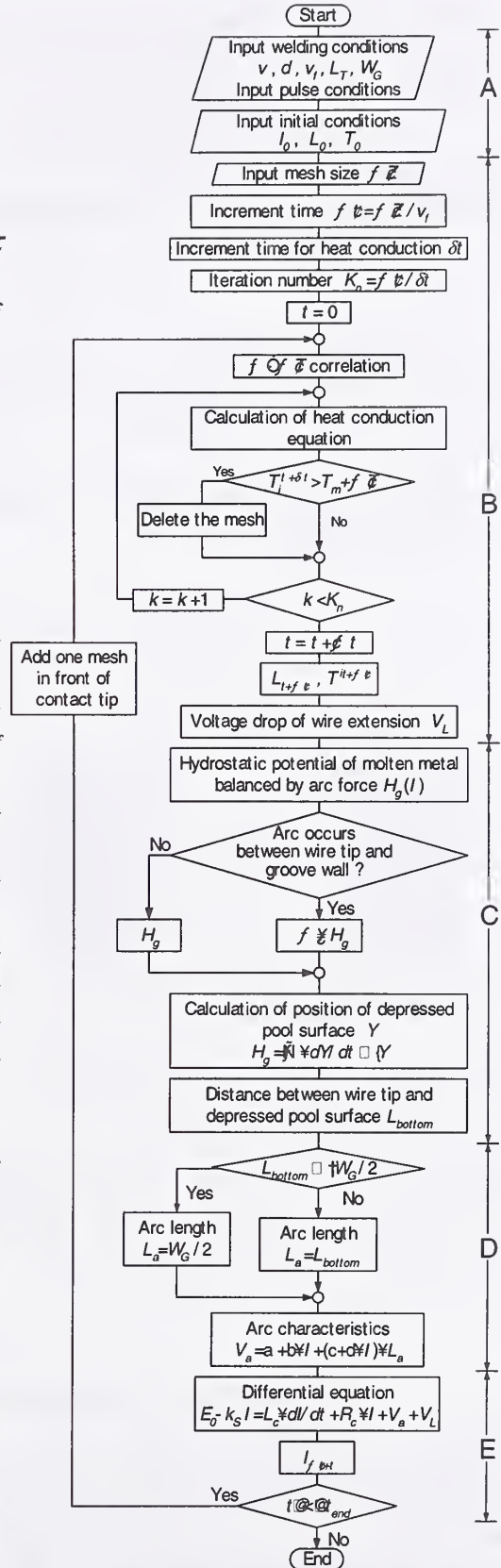

Figure6: Flowchart of simulation system for UNGW

minimal distance between the wire tip and groove wall are compared, and the shorter one is regarded as the arc length L_a. The arc voltage is determined from the following properties of CO_2 arc(Ref. 15).

$$V_a = 21.0 + 0.011 \cdot I + (2.6 + 0.0052 \cdot I) \times L_a \qquad (9),$$

where wire diameter is 1.2mm .

In part E, current $I_{t+\Delta t}$ at $t+\Delta t$ (s) is determined by following equation.

$$E_0 - K_S \cdot I_t = L_C \times \frac{I_{t+\Delta t} - I_t}{\Delta t} + R_C \cdot I_t + V_a + V_L \qquad (10),$$

where E_0 and K_s are the non-load voltage (V) of the constant voltage power source and the slope of the external characteristics (V/A), respectively. The inductance and resistance of the circuit are 0.3 mH and 0.025 Ω, respectively.

Numerical simulation and the experimental results in UNGW

Simulation results of I-type joints with a groove width of 5 mm are compared with experimental results. The position of the wire tip in the groove are examined by a high speed video camera system (2250 flames/s). The current and voltage at moments corresponding to the images obtained by this camera system are indicated in Fig. 7 using thin lines. Numerical simulations are performed under the same welding conditions. Current, voltage, wire tip position and pool surface position are indicated in Fig. 7 using thick lines.

Qualitatively, simulation results of current wave patterns, voltage wave patterns and the wire tip position are agreed with the experimental results. The lowest position of the molten pool surface by the simulation was 2.1 mm, and the penetration depth at root was 3.0 mm. These simulated values agreed with the results of experiments. These results indicate that the wire tip position in the ultra-narrow groove, current, voltage and the molten pool position can be simulated.
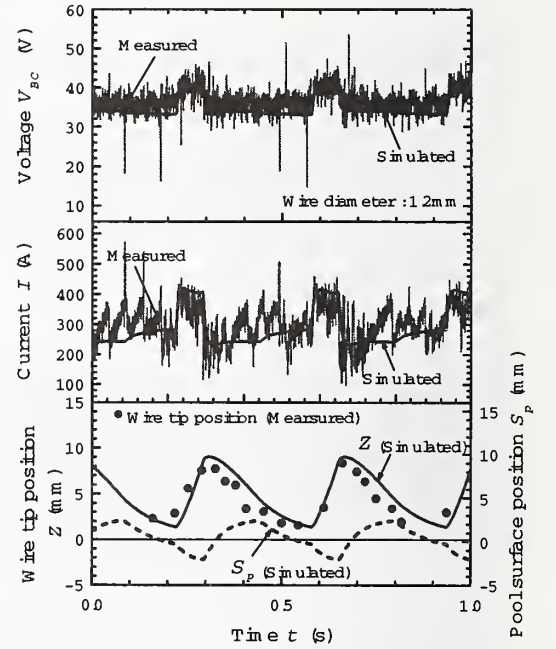
Figure 7: Comparison between simulation and experimental results
(t_P=0.07s,t_b=0.28s,
V_P=45V,V_b=39V
v_f=171mm/s,v=7.5mm/s,

SEARCH FOR APPROPRIATE PULSE CONDITONS OF UNGW

Oscillation ranges and position of the wire tip are simulated to obtain appropriate welding conditions. Criterions to melt root area and to form the concave bead surface in the ultra-narrow gap are determined as follows□
(1) To melt the root area, the lower limit Z_{min} of the wire tip oscillation should be set below the root surface ($Z_{min} \leq 0$).

(2) To obtain the concave bead surface, the upper limit Z_{max} of the wire tip oscillation should be set at top of the weld metal (throat thickness) H_T ($Z_{max} = H_T$).

The no load voltage V_P during the peak period is searched under the following pulse condition□ no loaf voltage of during the base period $V_b = 37$ V, the pulse frequency is 2.8 Hz, pulse peak duration t_P : pulse base duration $t_b = 1 : 4$.

The simulation results of Z_{min} , Z_{max} and H_T are shown in Fig. 8. Criterions ,which is $Z_{min} \leq 0$, $Z_{max} = H_T$ are satisfied in the hatched area.

The ultra-narrow gap GMA welding with a groove width of 5 mm is performed at $V_P = 44$ V and $V_P = 41$V. Figure 9 shows the simulated results of Z_{min} and Z_{max} and cross section of experimental joins. As the penetration shape is thin and long at $V_P = 44$V, the arc heat is distributed effectively in the upper and lower groove areas. Z_{min} locates near the root face and Z_{max} locates near the bead surface, these results indicate that criterions are satisfied by this appropriate pulse condition. The position of the maximal penetration width is center of penetration shape at $V_P = 41$V. As Z_{max} locates lower that in Fig. 9(b), it is considered that wire tip is oscillated around the groove bottom.

These results obtained in the above simulation are the example of the appropriate conditions. There are many appropriate conditions among combinations of other pulse conditions.

The GMA welding process numerical simulation is useful because quantitative evaluation is possible to examine the range of appropriate conditions for UNGW, in which many welding condition parameters and factors are related. Appropriate welding conditions can be efficiently obtained according to changes in the pulse frequency, the relative ratio of the peak to base periods and wire feed rat by this simulation system.
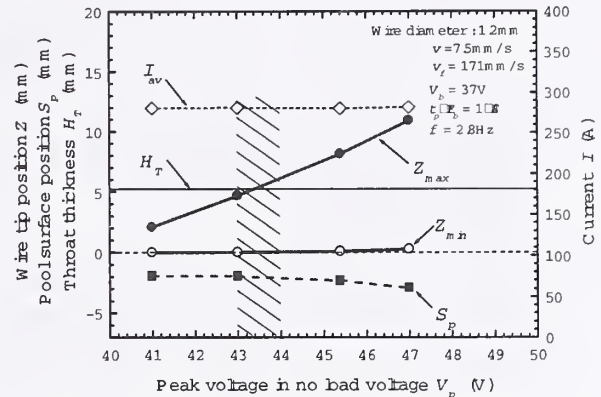
Figure 8: Effect of setting peak voltage V_P on wire melting behavior

(a) $V_P = 41$V (b) $V_P = 44$V
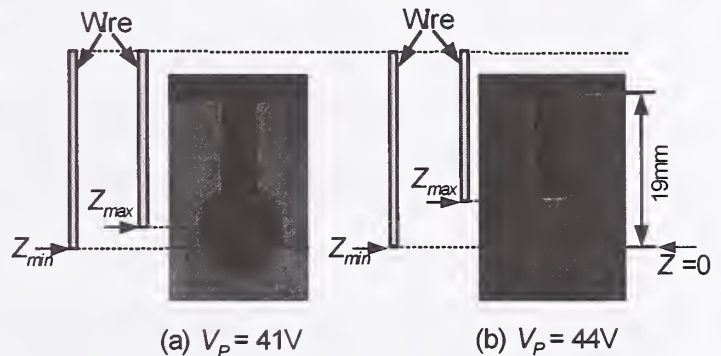
Figure 9: Experimental results under welding conditions shown in Figure 8

CONCLUSION

(1)We developed a GMA welding process numerical simulation system considered non-steady wire melting behavior, the temporal changes of molten pool depression by arc force, characteristics of the arc current-voltage, equivalent arc heat input at the wire tip and the welding electric source circuit.

(2) In ultra-narrow gap GMA welding with a groove width of 5 mm, the oscillation behavior of the wire tip induced by low frequency pulse current was measured, and it was indicated from the

measured results that numerical simulation was possible.

(3) It was indicated that welding conditions to obtain melting in the ultra-narrow groove bottom and formation of the concave bead surface could be searched using this numerical simulation system, and the usefulness of this system was demonstrated by ultra-narrow gap GMA welding. This simulation system makes it possible to find out adaptive welding conditions for UNGW which is characterized by many pulse parameters that correlate in a complex manner.

REFERENCES

1. Shiga,C. 2000. Systematic approach to solution of welding problems in STX21 project: aiming for remarkable advances in welded joints. Science and Technology of Welding and Joining 5(6): 356-364.
2. Malin,V.Y. 1987.Monograph on narrow -gap welding technology. WRC Bulletin 323
3. Nakamura,T. and Hiraoka,K. 2001. Ultranarrow GMAW Process with newly developed wire melting control system. Science and Technology of Welding and Joining 60(2):355-362.
4. Nakamura,T. and Hiraoka,K. 1999. Development of Ultra-Narrow Gap Welding Process by Numerical Simulation. Proc. 9th Int. Conf. on Computer technology in welding, Eds. T.Siewert and C.Pollock:201-210.American Welding Society.
5. Bingul,Z.;Cook,G.E. and Strauss,A.M. 2001.Dynamic model for electrode melting rate in gas metal arc welding process. Science and Technology of Welding and Joining 6(1): 41-50.
6. Yamamoto,T.;Ohji,T.;Miyasaka,Y. and Tsuji,Y. 2002.Mathematical modeling of metal active gas arc welding. Science and Technology of Welding and Joining 7(4): 260-264.
7. Xiaolin,Y.;Ping,S.;Shengsun,H. and Zhen,L. 2002.A numerical model of wire melting rate in CO_2 gas-shielded welding. Materials and Design 23(8): 501-504.
8. Trasov,N,M.;Gorlov,A,K. and Lashko,S.N. 2002.Numerical modeling of the process of formation of a molten metal drop at the tip of a consumable electrode. The Paton Welding Journal. 6: 21-24.
9. Nakamura,T. and Hiraoka,K. 2002. Wire Melting Behavior by Non-Steady Heat Conduction Numerical Analysis in Gas Metal Arc Welding. Quarterly Journal of the Japan Welding Society 20,(1): 53-62 (in Japanease).
10. Nakamura,T. and Hiraoka,K. 2001. Wire Melting Behavior by Unsteady Heat Conduction Numerical Analysis in GMA Welding. IIW Doc.212-1004-01
11. Katayama,K.; Hattori,K.; Okada,M.; and Kotake,I. 1972. Numerical analyses of unsteady thermal conduction for depending on temperature of material properties. Tran. JSME. 38(307): 574-580. (in Japanese)
12. Lancaster,J. E. ,Ed. 1984.The Physics of Welding: Oxford: Pergamon Press.
13. Nakamura,T. and Hiraoka,K. 2001.Charactersistcs of Bead Formation Phenomena in Narrower Gap Welding and Proposed of New Welding Process at Ultra-Narrow Gap Joint, Quarterly Journal of the Japan Welding Society 19,(1): 44-53 (in Japanease).
14. Maruo,H.;Hirata,Y;Kusano,T and Okano,I. 1985. Measurement of weld Pool Oscillation in Pulse TIG Welding, Quarterly Journal of the Japan Welding Society 3,(1): 457-464 (in Japanease).
15. Nakamura,T. and Hiraoka,K. 2002. GMA Welding Process with Periodically Controlling Shielding Gas Composition, Quarterly Journal of the Japan Welding Society 20,(1): 237-245 (in Japanease).

DIMENSIONAL DISTORTION OF T-JOINTS USING ALUMINUM 6063-T52 EXTRUSION MATERIAL IN MIG WELDING

R. Koganti, Zaluzec. M, Velez. J, Karas. C, Joaquin. A, and A. Caliskan

ABSTRACT

The development of manufacturing processes for joining and assembling of lightweight aluminum vehicles requires detailed process capability studies as well as dimensional variation analysis studies to ensure process controls are in place. These manufacturing processes not only have to provide cycle time viability but also need to maintain or surpass product safety and quality. T-Nodes joint designs are an integral of aluminum architectures based on hybrid designs, i.e those fabricated from mixed aluminum products consisting of castings, stampings and extrusions. The purpose of this study was to find optimum parameters for minimum distortion for the welding of 6063-T52 T-Nodes. The welding factors considered were locators (4-way and 2-way pins verses net surfaces), the welding equiment process factors (power input, pulse frequency, gas flow rate, torch angle and arc intensity), the use of simultaneous welding, and welding sequence order. A partial factorial design of experiment (DOE) was conducted to understand the effects of these factors on T-node joint distortions. A total of 14 points were considered for dimensional distortion measurements. Results showed power (heat) input is the only statiscally significant factor on joint distortion. Locators type as well as welding sequence and simultaneous welding also had a measurable affect on part deviation during welding.

KEYWORDS

INTRODUCTION

Ford Motor Company is investigating various lightweight materials for high mileage performance and also safety of occupants during collision. Aluminum is one of the chosen materials for the structural development work for high mileage as well as crashworthiness. Aluminum structures have many advantages in automotive applications due to its lightweight and energy management performance in crash applications. Various automotive manufacturers are currently using aluminum in structural applications. The Plymouth Prowler, Audi A8, Audi A2, Ferrari's 360 Modena, Panoz's Esperante, Ford's - Th!nk Neighbor, and Honda's NSX and Insight, are just a few of aluminum intensive vehicles currently in production.

Although unitized steel body architectures represent the most common body structure, aluminum architectures can come in a variety of designs including unitized body, space frame and hybrid body architectures. Stamped and extruded (straight and hydroformed) components

are finding more applications in unitized body architectures as automotive engineers find cost saving associated with applying these types of aluminum products. Hybrid architectures consist of a combination of aluminum products including stampings, extrusions (straight and hydroformed) and castings. Joining and assembling these components is often challenging task since most of the automotive and joining infrastructure is based on spot welded steel assemblies. In the case of aluminum, a multitude of joining methods can be applied to join extrusions, stampings, and castings. Commonly used techniques include riveting, Metal Inert Gas (MIG) welding, laser welding and adhesive bonding. In addition, hybrid laser/MIG welding, magnetic pulse welding, and friction stir welding are future enabling technologies in aluminum joining processes for hybrid architectures. The Ford's Scientific Research Laboratory (SRL) is currently investigating the joining and assembly of hybrid aluminum body architectures using MIG welding as the primary joining process. One of the chosen architecture for development purposes consists of stampings, castings and straight and bent extrusions as shown in Figure 1 and the joint configurations are shown in Figure 2. One of the main attributes in any body architecture is dimensional management of Body-In-White (BIW) assemblies. Prior to weld the full structure, it was necessary to understand the weld process effects on a lab scale level and ultimately optimum process factors can be selected for minimum structural distortions. This study is mainly focused on a T-Node joint (shown in Figure 3) for economical purposes and ultimately the information was used for the final front end assembly.
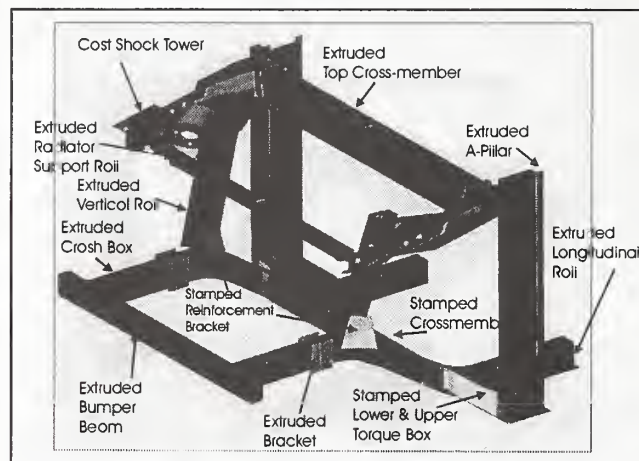

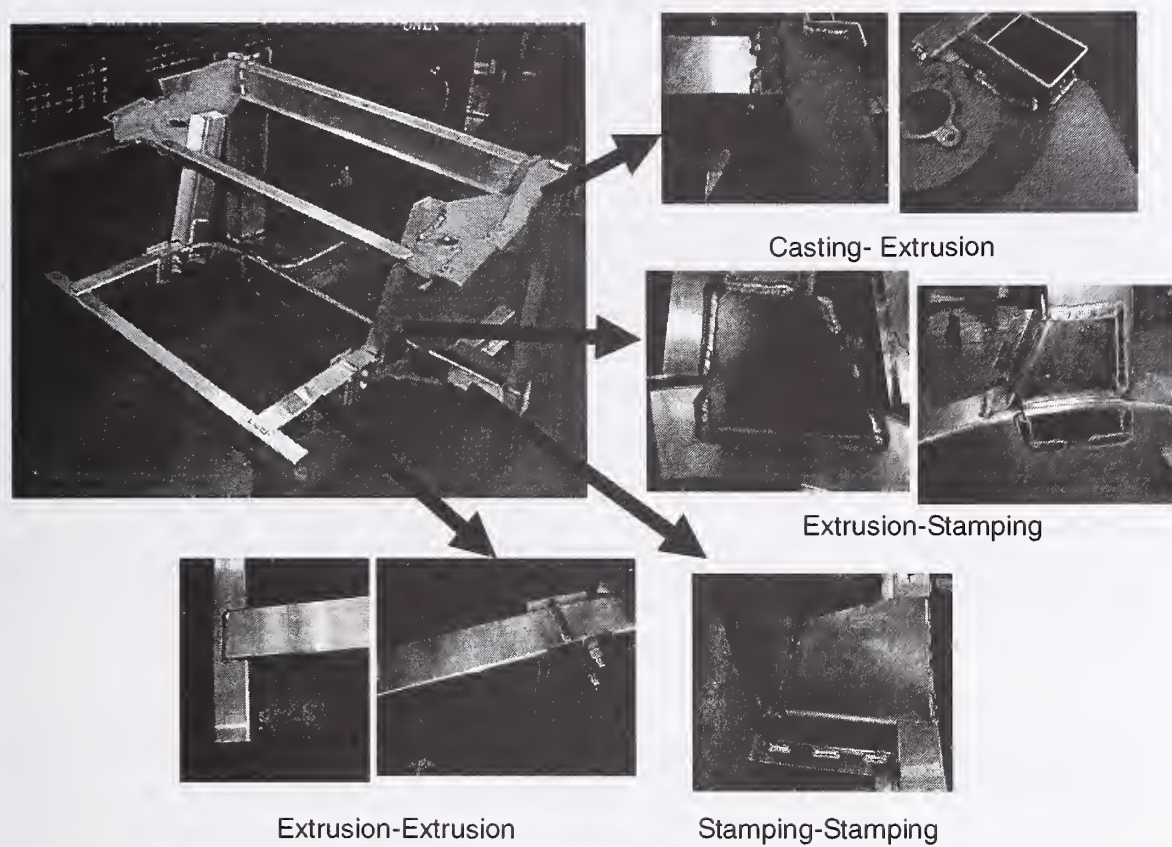Figure 1: Hybrid aluminum front end assembly

Casting- Extrusion

Extrusion-Stamping

Extrusion-Extrusion   Stamping-Stamping

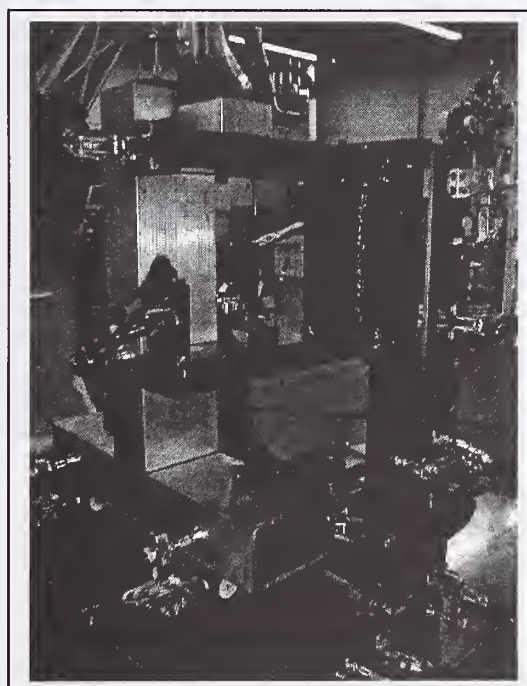Figure 2: Hybrid aluminum front end module joint configurations

Figure 3: T-Node configuration

WELDING DEVELOPMENT WORK

In order to understand the weld parameters influence on joint properties, initially several experiments were conducted to optimize the MIG welding parameters on single lap joint properties. In MIG welding besides the joint strength, the other important attribute is distortion of the aluminum structures due to the welding.

Initial screening experiments were conducted on lap coupons to identify the welding equipment process factor ranges with an acceptable weld quality (weld strength and weld penetration). The welding equipment used for the coupons as well as T-Nodes experiments is an OTC/Daihen CPD-350 welding system and DR-4000 pulse power supply (Figure 4). Based on screening experiments, the ranges for voltage, current, torch speed, gas flow rate, pulse frequency were selected. Since, torch speed, voltage, current and wire feed rate are inter-dependent, all these factors are lumped as one factor i.e., power input (also called as heat input). Moreover, with the Daihen equipment, wire feed rate can't be changed due to the fact that voltage and current set the wire feed rate automatically. Initial studies were focused on optimization of welding parameters for various alloy combinations (5754, 6063 and A356) for joint strength. From the single lap coupon DOE study, it was concluded that power input and gas flow rate are statistically significant on lap shear load.

This study was developed to identify the influence of locators strategy, equipment parameters, number of welding robots, and welding sequence on joints dimensional variation in the welding of aluminum 6063-T52 T-Nodes (Figure 3).
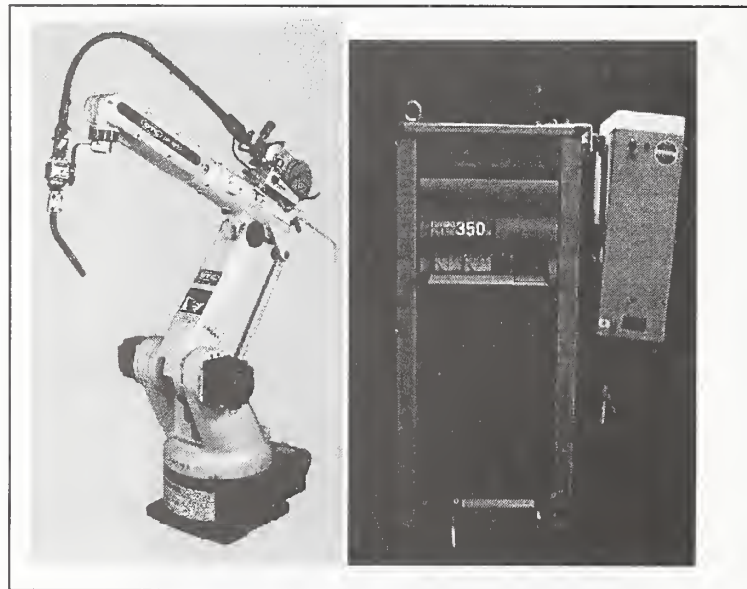

Figure 4: OTC/Diahen welding equipment

EXPERIMENT

The objective of the experiment was to understand the welding parameters influence on T-Node dimensional distortions. The welding equipment process factors selected for this DOE were power input (torch speed, voltage current, and wire feed as one factor), pulse frequency, gas flow rate, torch angle, and arc intensity. The extreme levels of power input, pulse frequency, gas flow, torch angle, and arc intensity are shown in Table 1. Argon gas (@99.9%), commonly used for aluminum MIG welding [1], was used as the shielding gas. The filler wire selected was a 1.2 mm diameter Al-4047 filler wire. Other factors maintained constant throughout the experiment were lead push angle (20°), weld length (75mm), and wire stick out (15mm).

These experiments were conducted for the following strategies for the minimum distortions of the T-Nodes:
- i)   MIG welding factors on dimensional distortions due to locator strategy
    - a. Both vertical and horizontal extrusions are constrained on net pads
    - b. Both vertical and horizontal extrusions are constrained using 4 way and 2 way locator pins
- ii)   Synchronous welding (1 robot verses 2 robots)
- iii)   Weld sequences (normal versus reverse order) using one robot

A partial factorial DOE was conducted consisting of eight experimental runs as shown in the experimental matrix in Table 2. A total of eighty T-Nodes (10 samples of each experimental run) were welded and fourteen point locations (Figure 5 – Points 2-15) measured on each one three times: (1) after-welding clamped, (2) after-welding unclamped, and finally (3) at freestanding. The last forty of these eighty T-Nodes were also measured before welding to understand the variability of components as well as the fixture. Forty T-Nodes were positioned for welding with pins and the other forty with surface pads. Five additional T-Nodes were welded at low input settings for simultaneous welding analysis and another five at high input settings for welding sequence (normal versus reverse) analysis.

Table 1. DOE-T2 process factors matrix

Factor	Low Level	High Level	Unit
Torch Speed	635	1270	mm/min
Corresponding Voltage/Current	21.5/150	25.3/220	Volts/Amperes
Pulse Frequency	10	30	Hz
Gas flow rate	0.71	1.27	CubicMt/hr
Torch Angle	45	50	Degrees
Arc Intensity	Normal	Soft	N/A

Table 2. Experimental matrix

Run #	Power Input	Pulse Frequency	Gas Flow Rate	Torch Angle	Arc Intensity
1	*-1*	*-1*	*-1*	*-1*	*-1*
2	*-1*	*-1*	*1*	*1*	*1*
3	*1*	*1*	*-1*	*-1*	*1*
4	*1*	*1*	*1*	*1*	*-1*
5	*-1*	*1*	*-1*	*1*	*-1*
6	*-1*	*1*	*1*	*-1*	*1*
7	*1*	*-1*	*-1*	*1*	*1*
8	*1*	*-1*	*1*	*-1*	*-1*

Note: -1 and 1 are low and high levels of the factor settings as referred in table 1.

Figure 5. Measurement point (# 2 -15) locations
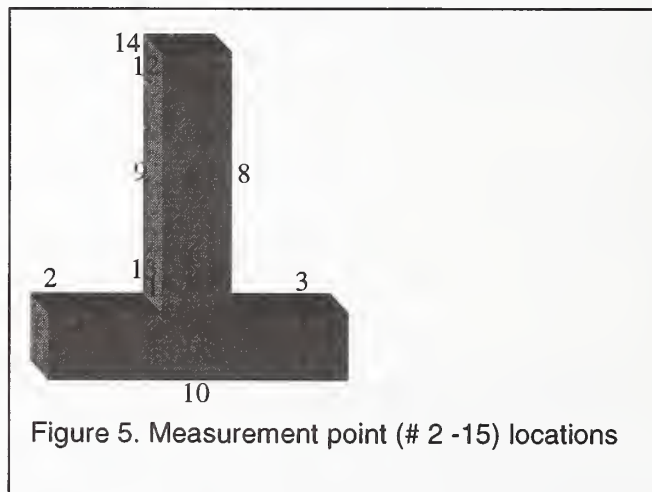
DATA RESULTS

A total of ninety T-Nodes (for all the strategies mentioned above) were welded for dimensional variation analysis. The first forty samples were measured at three different conditions (after-welding clamped, after-welding unclamped and at freestanding) at fourteen selected measurement point locations. Thereafter, the remaining fifty included one additional measurement before welding for parts and fixture induced variation accountability.

A comparison of "before weld" measurements and their respective nominal showed that the deviation induced by the combination of the parts dimensional variation and the fixture variation was not significant (Figure 6). Additionally, there was no significant difference between the clamping condition, unclamped condition, and freestanding condition measurements (Figure 7). Therefore freestanding was compared to nominal for dimensional variation study purposes.

Figure 6. Before weld to nominal variation (mm)

Figure 7. After weld clamped, unclamped and freestanding averages and standard deviations of measurements (mm)
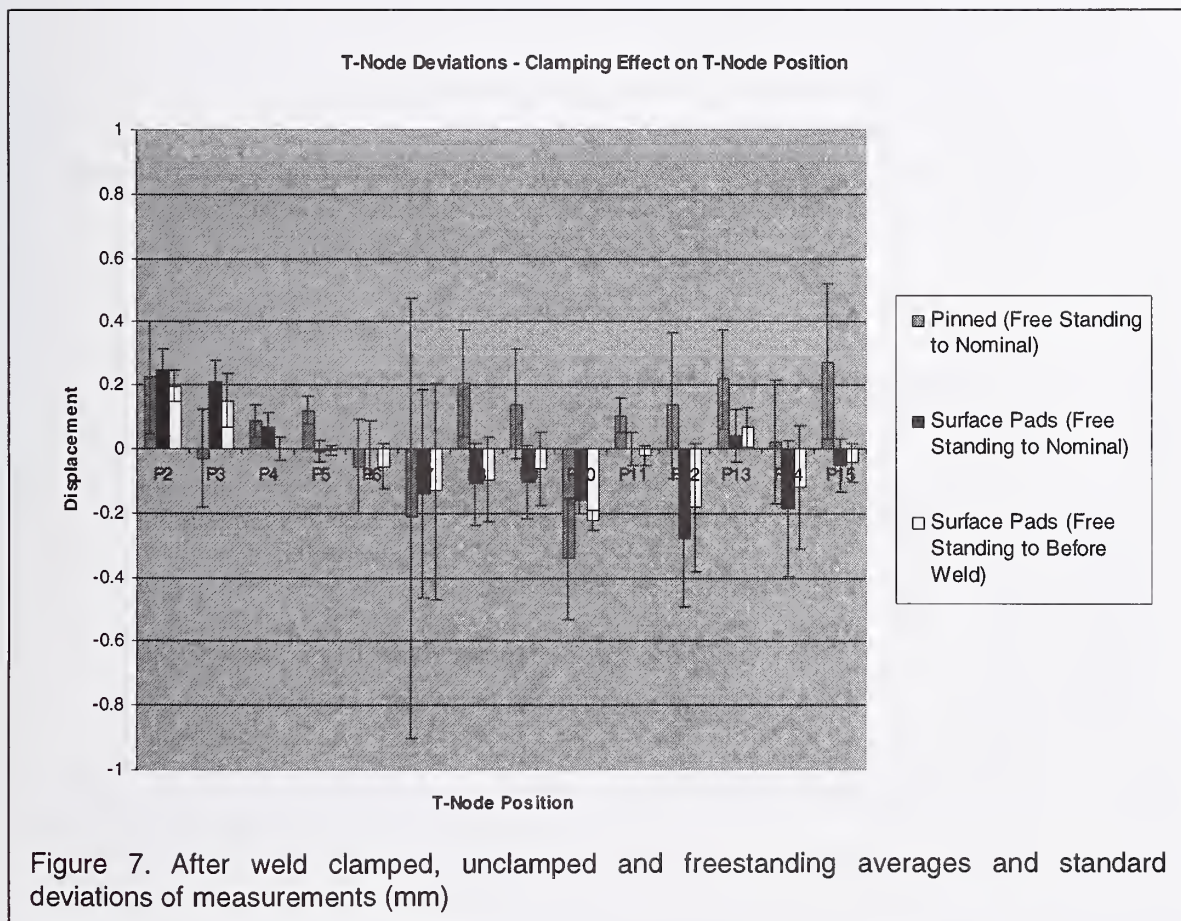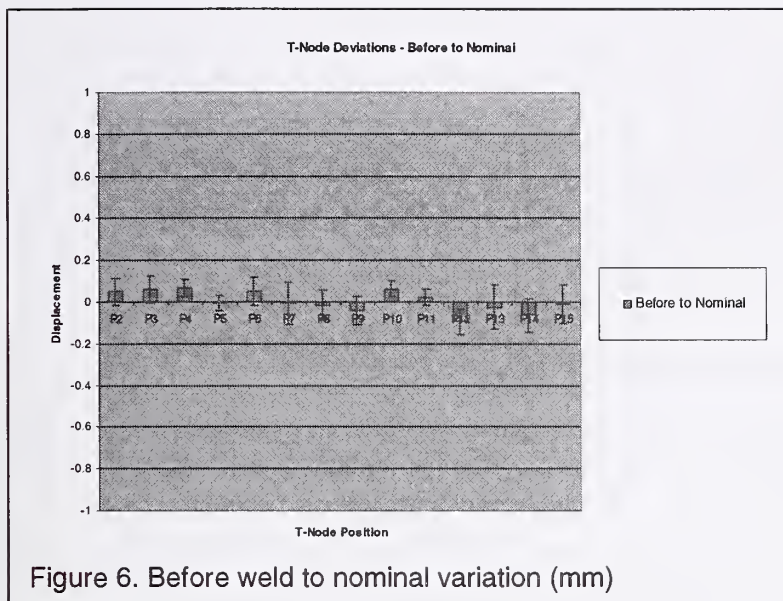
Power input was the only input value that showed significance on distortion. Typical assumptions on welding power input and its effect on distortion is that the more heat input during the welding process, the more distortion will occur thus more measured deviation. Although high and low settings of power input referred to 5.57kW and 3.23kW respectively, the high setting of power input induced less heat distortion than the low setting because of its higher travel speed (Figure 8). In this study the interrelation between the torch speed and power at high and low settings are 50 ipm and 5.57 kw (at high setting), 25 ipm and 3.23 kW (at low setting). The influence of the other process factors on the dimensional variation of the T-Nodes during welding remained less of a significant factor.

Influence of Locator Strategy on Dimensional Deviations

Power input shows a significant effect on when the parts are constrained by 4-way and 2-wau locator pins. High power input exhibited lower distortion and vice versa. The reason for power input contributes distortion is the horizontal and vertical members are free to slide (against the friction between the net pads and components) due to coefficient of thermal expansion. Higher power input (higher torch speed) resulted in lower distortion (Figure 8); this is favorable for reducing the cycle times in high production volumes.

Experiment results indicated that dimensional deviation was higher when extruded parts are located by 4-way and 2-way pins (movement restraints) compared to surface pads (Figures 9 and 10). In addition, the standard deviation of the measurements was significantly higher for those T-Nodes positioned by pin locators (Figure 10). The fact that the heat of fusion welding caused aluminum expansion within the aluminum extrusion and shrinkage around the weld joint, followed by a slow cool accounts for the variations in measurement variation when the part is restricted by pin locators.

Figure 8. Welding equipment input values effect on T-Node deviations (mm) for surface pad locators
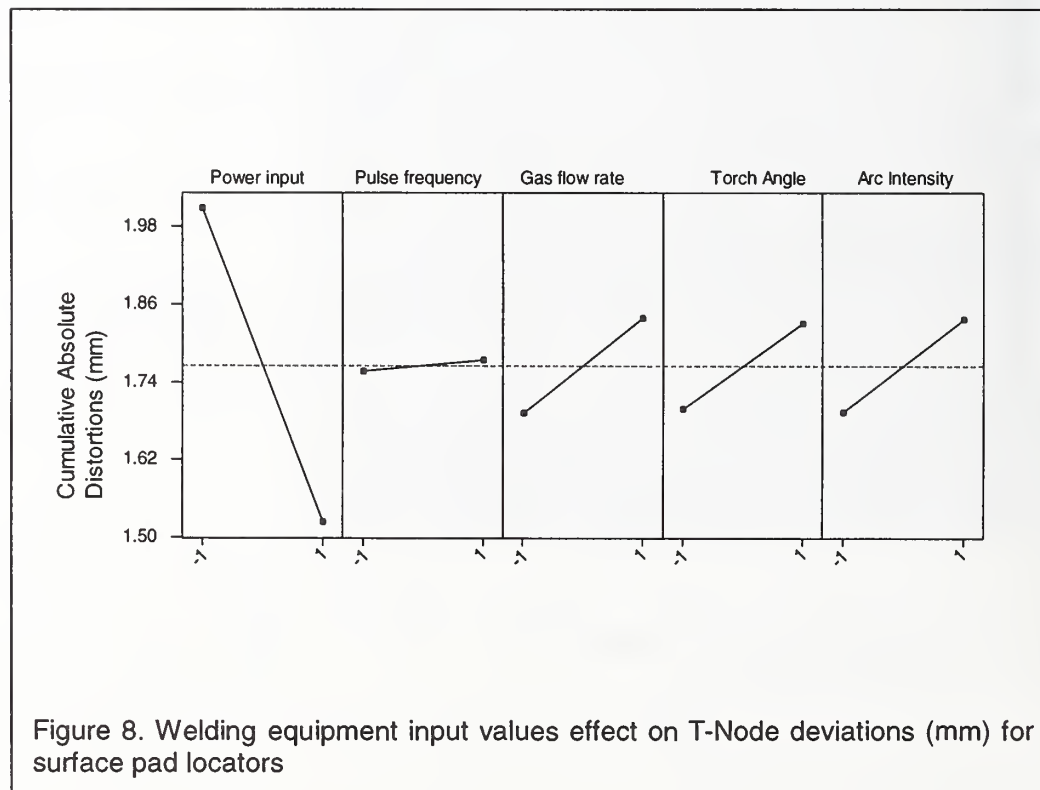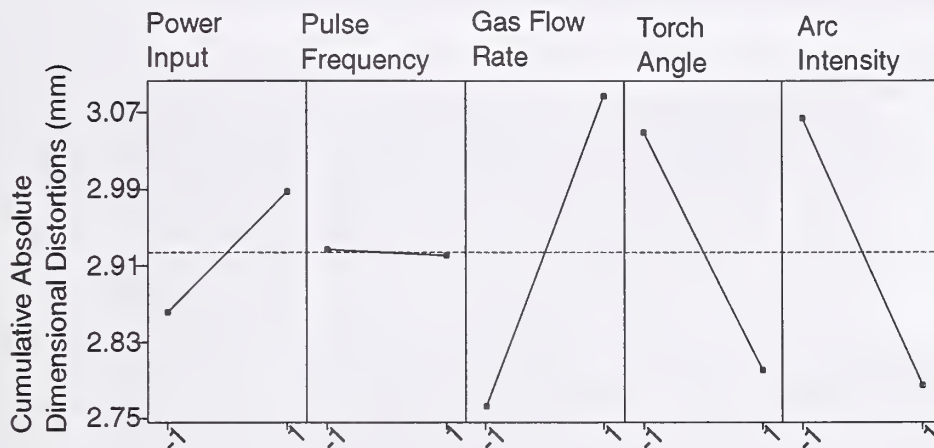
Figure 9. Welding equipment input values effect on T-Node deviations (mm) for pin locators (4-way and 2-way locators)
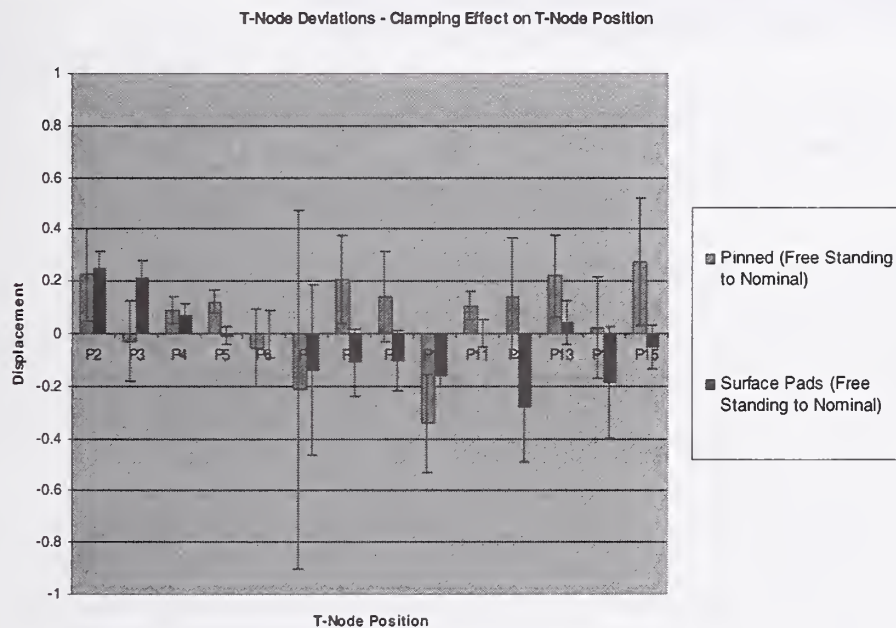
Figure 10. Pinned surface vs. surface pads clamping averages and standard deviations of measurements (mm)

Single Versus Simultaneous Welding Effects on Dimensional Deviations

Single and simultaneous (dual torch) welding averages and standard deviations of the measurements were comparable for most of their sample points; however, one of the measurement points (point #7) showed a very significant difference between single and simultaneous welding. The dimensional deviations in single vs. simultaneous welding are shown in figure 11.
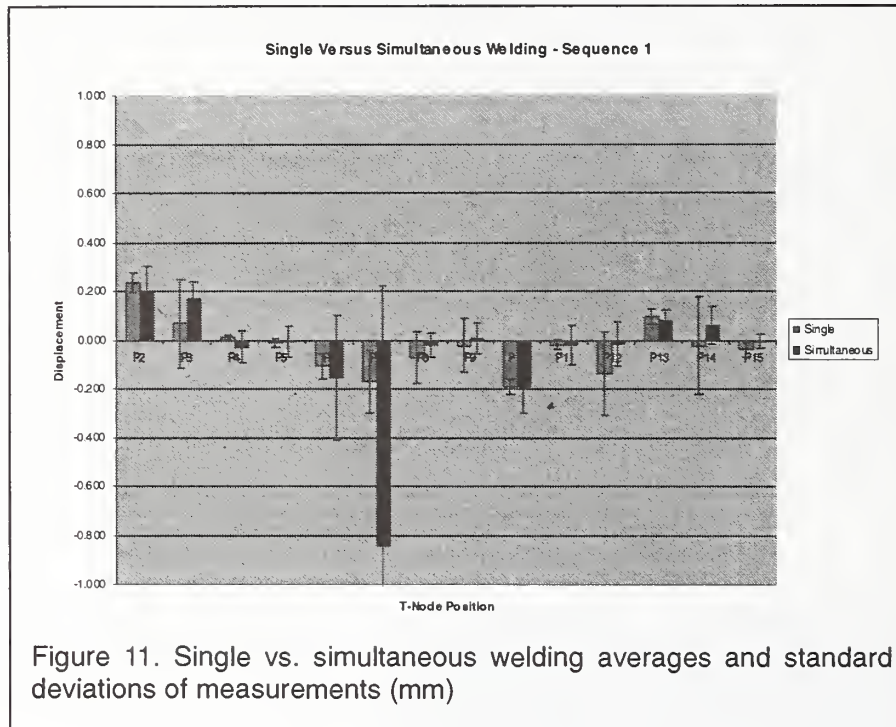
Figure 11. Single vs. simultaneous welding averages and standard deviations of measurements (mm)

Welding Order Effects on Dimensional Deviations

Welding order was reversed (using only one robot) in order to study the effects of changing the welding direction and sequence order to look for significant effects. On the other hand, the direction of the deviation kept unchanged and the standard deviations of the measurements remained similar (Figure 12).

Figure 12. Normal vs. reversed order averages and standard deviations of measurements (mm)
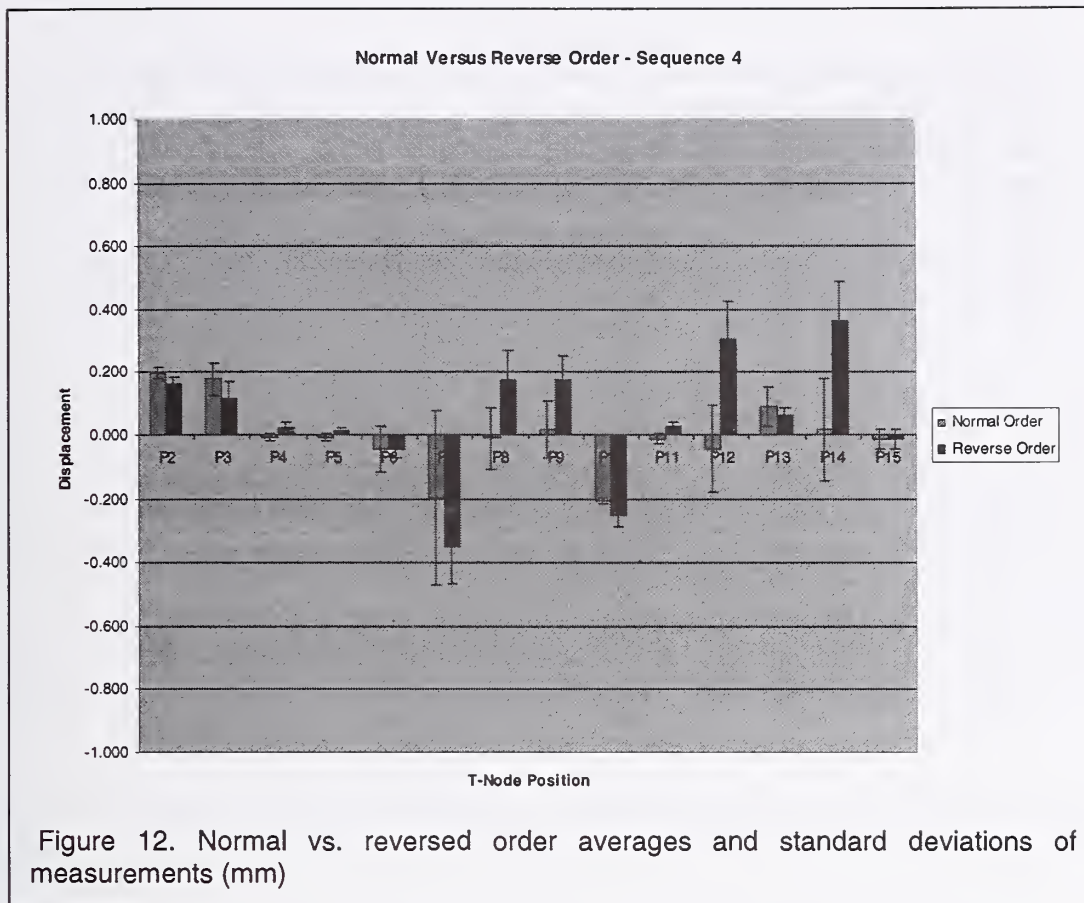
SUMMARY AND CONCLUSIONS

- The purpose of this study was to identify the influence of clamping devices, equipment parameters, number of welding robots, and sequence factors on 6063-T52 T-Node joint distortions.
- Surface pads resulted to provide a significantly lower part deviation and lower standard deviation than pin locators.
- Besides decreasing cycle time, high power input settings for surface pads locator strategy contributed to a lower part deviation than low power input settings.
- Welding order influenced magnitude of deviation, yet the direction of the deviation remained unchanged for the two weld orders studied.
- Dimensional distortion was more likely to occur in the direction opposite to part restraints (pins or surface pads).

RECOMMENDATIONS

Further study should concentrate on clamp pressure and clamping area effects on T-Node deviation, different combinations of simultaneous sequences and several additional welding order combinations (24 possible combinations).

101

REFERENCES

1. Juvinall, Robert; Marshek, Kurt. Fundamentals of machine component design. USA: John Wiley & Sons, Inc., 1991, Second Edition
2. Douglas C. Montgomery. Design and analysis of experiments. USA: John Wiely & Sons, Inc.
3. Ashby, Michael; Jones, David. Engineering Materials 2 – An introduction to microstructures, processing and design, U.K.: Pergamon Press, 1986, First Edition.

Fractional Factorial Technique to Predict Welding Current in Gas Metal Arc Welding

Masood Aghakhani

Abstract

During research on Gas Metal Arc Welding (GMAW) of aluminum, it was observed that the welding current was affected by any change in wire feed rate, arc voltage, nozzle-to-plate distance, torch angle, and welding speed. To determine accurately the welding current for any set of these parameters, a mathematical model has been presented. The model was developed using a two-level fractional factorial design and its adequacy was tested by the analysis of variance technique. The estimated and observed values of the welding current have been shown on a scatter diagram and the interaction effects of different parameters involved have been presented in graphical forms. These results can be utilized for determining accurately the heat input into the workpiece from which reliable predictions can be made about the mechanical and the metallurgical properties of welded joints.

Keywords: *Fractional Factorial Technique*; *Welding Current*; *Gas Metal Arc Welding; and Aluminum*.

Introduction

Gas Metal Arc (GMA) also known as Metal Inert Gas (MIG) is the most often used welding process for welding aluminum and it's alloys (Ref. 1). In MIG welding, the wire electrode used is thin (0.5-1.6 mm diameter) and consequently the wire feed speed is high. To achieve self-adjustment of arc at high-speed rates, it is essential to use power sources with flat or nearly flat V-I (volt-ampere) characteristics. For welding with such a power source, the wire feed rate has been given by Halmoy (Ref. 2) by the following equation:

$$W = \alpha I + \frac{\beta l I^2}{a}$$

Where
W = wire feed rate
I = welding current
l = electrode stick-out
a = area of cross section of the wire
α = constant of proportionality for anode or cathode heating
β = constant of proportionality for electrical resistance heating

----
Masood Aghakhani, Assistant Professor in Production Engineering (Welding Technology), College of Engineering, University of Razi, Kermanshah-67149, Iran.
E-Mail: aghakhani@razi.ac.ir & aghakhanim@yahoo.com

It is reported that for aluminum $\alpha = 0.75$ mm/A-sec and β is negligible (Ref. 3), thus reducing Halmoy's equation for GMAW of aluminum to:

$$W = \alpha I$$

or, in other words, the welding current (I) is directly proportional to the wire feed rate (W). However, during prolonged investigations on GMAW of aluminum, it was observed that the welding current (I) was not only affected by the changes made in wire feed rate (W), but arc voltage (V), nozzle-to-plate distance (N), torch angle (θ), and welding speed (S) also affected the welding current accordingly. Welding current affects the metal transfer (pinch effect $\alpha\ I^2$) and the amount of heat input into the weld pool and consequently it affects the bead shape as well as the metallurgical and mechanical properties. To avoid any serious effects on the analysis of results of erroneous assumption that the welding current is only proportional directly to wire feed rate, it was found imperative to determine accurately the welding current as affected by different welding parameters.

This paper reports the development of a mathematical model, based on practical observations, made during gas metal arc welding of aluminum to estimate accurately the welding current as affected by welding parameters.

Plan of Investigation

To achieve the desired aim, the planning for investigations were carried out in the following steps:
1. Selection of a mathematical model;
2. Design of experiments;
3. Selection of useful limits of the welding parameters viz.; wire feed rate (W), arc voltage (V), nozzle-to-plate distance (N), torch angle (θ) and welding speed (S);
4. Developing a design matrix;
5. Conducting experiments as per designed matrix;
6. Estimation of the coefficients of the equation;
8. Checking the adequacy of the model;
9. Testing the significance of the regression coefficients and arriving at the final form of the mathematical model;
10. Presenting the estimated and observed data on a scatter diagram;
11. Presenting the significant interactions between different parameters in graphical form;
12. Analysis of results; and
13. Conclusions.

Selection of the Mathematical Model

It was observed from the preliminary experiments that the welding current (*I*) was affected by wire feed rate, arc voltage, nozzle-to-plate distance, torch angle, and welding speed within the limits employed for the study. Under these conditions, the response function could be expressed as
$$I = f(W, V, N, \theta, S)$$

Assuming a linear relationship and taking into account all possible two-factor interactions, it could be written as:

$$I = b_0 + b_1 W + b_2 V + b_3 N + b_4 \theta + b_5 S + b_6 WV + b_7 WN + b_8 W\theta + b_9 WS + b_{10} VN$$
$$+ b_{11} V\theta + b_{12} VS + b_{13} N\theta + b_{14} NS + b_{15} \theta S$$

Where I is the estimated welding current and $b_1, b_2, \ldots, b_{15}$ are the coefficients of the polynomial to be determined.

Design of Experiments

The design of experiment, that is, the decision to use different values of different parameters for conducting a particular experiment was based on the fractional factorial design, which is a standard statistical tool to investigate the effects of a number of parameters on the required response. In addition, interactions between two or more parameters can be evaluated, which is not possible with the conventional experimental approach since in that approach all parameters other than being studied are held constant.

For calculating the main and interaction effects of five variables W, V, N, θ, S at two levels, a half fractional factorial design was selected. This design gave $2^{5-1} = 16$ weld runs to fit an equation and was sufficient for the evaluation of coefficients.

Selection of Useful Limits of Welding Parameters

On the basis of preliminary experiments conducted using 1.6 mm diameter wire with argon shielding, it was found that for proper bead configurations the wire feed rate, arc voltage, nozzle-to-plate distance, torch angle, and welding speed were required to be kept between 6.1 m/min and 7.6 m/min, 24 V to 29 V, 15 mm to 20 mm, 80 deg to 100 deg and 25 cm/min to 40 cm/min respectively. These limits were adhered to throughout the investigations reported here.

For the ease of recording and processing of the observed data, upper and lower levels of welding parameters were coded as + 1 and -1, respectively by using the following relationship:

$$Coded\ Value = \frac{Natural\ Value - Average\ Value}{Variation\ Interval}$$

Two levels of welding parameters, their levels, units, and coded values are given in Table 1.

Table 1-Welding parameters and their limits.

Parameter	Unit	Symbol	Coded Value Low (-1)	Coded Value High (+1)
Wire Feed Rate	m/min	W	6.1	7.6
Arc Voltage	volts	V	24.0	29.0
Nozzle-to-Plate Distance	mm	N	15.0	20.0
Torch Angle	deg	θ	80.0	100.0
Welding Speed	cm/min	S	25.0	40.0

Design Matrix

The design matrix evolved to conduct sixteen experiments is given in Table 2 and is based on the method suggested elsewhere (Refs. 4, 5).

Table 2-2^{5-1}Design Matrix

S. #	W	V	N	θ	S (-WVNθ)
1	+	+	+	+	-
2	-	+	+	+	+
3	+	-	+	+	+
4	-	-	+	+	-
5	+	+	-	+	+
6	-	+	-	+	-
7	+	-	-	+	-
8	-	-	-	+	+
9	+	+	+	-	+
10	-	+	+	-	-
11	+	-	+	-	-
12	-	-	+	-	+
13	+	+	-	-	-
14	-	+	-	-	+
15	+	-	-	-	+
16	-	-	-	-	-

Experimentation

Employing a mechanized welding system, experiments were conducted as per the conditions set in the design matrix of Table 2. Welding current observations were made by making weld runs of 25 cm length on 13 mm thick plates of aluminum. The power source used was a three-phase transformer cum full-wave rectifier unit having a flat V-I (volt-ampere) characteristics with a current capacity of 425 A at 60% duty cycle and an infinitely variable OCV (open circuit voltage) of 12-48 V in two ranges. A 1.6 mm diameter NG-6 filler wire (Al-5%Mg) with argon as shielding gas at a flow rate of 30 l/mm was used.

Sixteen weld runs were made using the conditions set in the design matrix but to avoid any systematic error in experimentation, the sets of conditions were chosen at random. The recorded values of welding current (*I*) for two sets of experiments are given in Table 3.

Table 3-Recorded values of welding current

S.#	Trial No.	W	V	N	θ	S	Welding Current I_1	I_2
1	1	+	+	+	+	-	260	270
2	2	-	+	+	+	+	240	240
3	3	+	-	+	+	+	260	260
4	4	-	-	+	+	-	220	220
5	9	+	+	+	-	+	280	290
6	10	-	+	+	-	-	245	245
7	11	+	-	+	-	-	270	270
8	12	-	-	+	-	+	240	240
9	13	+	+	-	-	-	290	290
10	14	-	+	-	-	+	240	240
11	15	+	-	-	-	+	280	280
12	16	-	-	-	-	-	240	240
13	5	+	+	-	+	+	290	290
14	6	-	+	-	+	-	240	250
15	7	+	-	-	+	-	260	260
16	8	-	-	-	+	+	245	245

Evaluation of Coefficients of the Model

To determine the regression coefficients of the selected model, following formula (Ref. 4, 5) based on the method of least squares was used:

$$b_j = \frac{\sum_{i=1}^{N} X_{ji} Y_i}{N}, j = 0, 1, 2, \ldots, k$$

where:
X ji   = value of a factor or interaction in coded form.
Yi   = average value of the response parameter, that is, the welding current in this case
N   = number of the observations.
k   = number of the coefficients of the model.

A matrix designed to apply this formula to calculate different coefficients is given in Table 4.

Table 4-Design matrix to calculate different coefficients

S.#	Trial No.	b_0	b_1	b_2	b_3	b_4	b_5	b_6	b_7	b_8	b_9	b_{10}	b_{11}	b_{12}	b_{13}	b_{14}	b_{15}	Y_{avg}
1	1	+	+	+	+	+	-	+	+	+	-	+	+	-	+	-	-	265
2	2	+	-	+	+	+	+	-	-	-	-	+	+	+	+	+	+	240
3	3	+	+	-	+	+	+	-	+	+	+	-	-	-	+	+	+	260
4	4	+	-	-	+	+	-	+	-	-	+	-	-	+	+	-	-	220
5	9	+	+	+	+	-	+	+	+	-	+	+	-	+	-	+	-	285
6	10	+	-	+	+	-	-	-	-	+	+	+	-	-	-	-	+	245
7	11	+	+	-	+	-	-	-	+	-	-	-	+	+	-	-	-	270
8	12	+	-	-	+	-	+	+	-	+	-	-	+	-	-	+	-	240
9	13	+	+	+	-	-	-	+	-	-	-	-	-	-	+	+	+	290
10	14	+	-	+	-	-	+	-	+	+	-	-	-	+	+	-	-	240
11	15	+	+	-	-	-	+	-	-	-	+	+	+	-	+	-	-	280
12	16	+	-	-	-	-	-	+	+	+	+	+	+	+	+	+	+	240
13	5	+	+	+	-	+	+	+	- ,	+	+	-	+	+	-	-	+	290
14	6	+	-	+	-	+	-	-	+	-	+	-	+	-	-	+	-	245
15	7	+	+	-	-	+	-	-	-	+	-	+	-	+	-	+	-	260
16	8	+	-	-	-	+	+	+	+	-	-	+	-	-	-	-	+	245

The estimated coefficients of the variables and their interactions computed using the above relationship are given in Table 5.

Table 5-Coefficients of the model

b_0	b_1 W	b_2 V	b_3 N	b_4 θ	b_5 S	b_6 WV	b_7 WN	b_8 Wθ	b_9 WS
257.2	17.8	5.3	-4.1	-4.1	2.8	2.2	-0.9	-2.2	0.9

b_{10} VN	b_{11} Vθ	b_{12} VS	b_{13} Nθ	b_{14} NS	b_{15} θS
0.3	1.6	-1.6	-2.8	0.3	2.8

Using these coefficients, the complete model, in coded form, can be expressed as follows:

$$I = 257.2 + 17.8W + 5.3V - 4.1N - 4.1\theta + 2.8S + 2.2WV - 0.9WN - 2.2W\theta$$
$$+ 0.9WS + 0.3VN + 1.6V\theta - 1.6VS - 2.8N\theta + 0.3NS + 2.8\theta S$$

Checking the Adequacy of the Model

The adequacy of the model was determined by the analysis of variance technique. The regression coefficients were determined by the method of least squares, from which the F-ratio

for the polynomial was found. The F-ratio of the model was compared with the corresponding F-ratio from the standard tables and it was found that the model was adequate within 95% level of confidence, thus justifying the use of assumed polynomial. Details of analysis of variance are given in Table 6.

Table 6-Details of analysis of variance

Response	Degrees of Freedom for	Variance of Response	Standard Deviation of Coefficients	Variance of Adequacy	`F' Ratio Model	`F' Ratio Table	Adequacy of Model
	S_y^2 S_a^2	S_y^2	$S_{bj} = \sqrt{\dfrac{S_y^2}{d_f}}$	S_a^2	$F_m = \dfrac{S_a^2}{S_y^2}$	at (10,16,0.05)	Whether $F_m < F_t$
Welding Current	16 10	9.375	0.765	7.50	0.80	2.49	Yes

Checking the Significance of the Coefficients of the Model

To eliminate the statistical insignificant terms of the model, if any, it is essential to check the significance of each of the coefficient and to do that Student's `t'-test was employed. It was found that the coefficients of all the main effects and WV, Wθ, Nθ, and θS interactions were significant. The rest of the coefficients could be dropped conveniently. Thus the final model with only the statistically significant coefficients in the coded form is given as:

$$I = 257.2 + 17.8W + 5.3V - 4.0N - 4.0\theta + 2.8S + 2.2WV - 2.2W\theta - 2.8N\theta + 2.8\theta S$$

Results

A large number of observations were taken under different sets of parameters within the limits investigated and the corresponding estimated values of welding current were determined from the model. The observed and the estimated values were then represented in a graphical form as a scatter diagram shown in Fig. 1.

The significant interactions viz. WV, Wθ, Nθ and θS as deduced from the model are shown in Figs. 2-5.

Analysis of Results

Fig. 1 shows that the estimated and the observed values of the welding current are scattered close to 45° lines, passing though the origin, indicating an almost perfect fit of the developed empirical model. Furthermore, the analysis of results show that the increase in the levels of W, V, and S resulted in the corresponding increase in welding current whereas, the increase in the levels of N, and θ proved to be otherwise.

109

Effect of Wire Feed Rate (W)

Wire feed rate is the most important parameter affecting the welding current. An increase in welding current from 6.1 to 7.6 m/min resulted in the increase in welding current by a magnitude of 34.36 amperes. This increase in welding current with the increase in wire feed rate is to keep the wire feed rate and burn off rate in equilibrium.

Effect of Arc Voltage (V)

The second largest increase in welding current is caused by arc voltage by a magnitude of 10.6 amperes when it is varied from 24 to 29 volts. The increase in welding current with the increase in arc voltage indicates the rising characteristics of the welding arc.

Effect of Nozzle-to-Plate Distance (N)

The welding current decreased by approximately eight amperes with the increase in nozzle-to-plate distance from 15 to 20 mm. This is due to the fact that as the value of 'N' is increased, the arc length also increases momentarily thereby increasing the arc voltage but the same is restored to its original value due to the self-adjustment of the welding arc. This increases the stick-out and hence the amount of I^2R heating. Increase in the preheating of the stick-out reduces the welding current slightly so that the equilibrium between wire feed rate and the burn off rate is maintained.

Effect of Electrode/Torch Angle (θ)

The increase in the torch angle from 80° to 100° resulted in the decrease of welding current by approximately 8 amperes. The reason for this could be explained due to the fact that as the electrode angle increases the effective arc length increases, and hence a decrease in welding current is observed.

Effect of Welding Speed (S)

The increase in welding speed from 25 to 40 cm/min resulted in the increase in welding current by approximately 6 amperes. This could be due to the fact that at low welding speed the arc is very close to the deposited metal and since the melting point of the filler wire is quite low, the current required to maintain the burn off rate equilibrium, is less and when the welding speed is increased, the heat content of the arc is reduced and hence to maintain the burn off rate equilibrium, the welding current requirement increases.

Effect of Interactions

Fig. 2 shows that welding current increased with the increase in wire feed rate. The increase in welding current was 6 and 12 amperes for low and high values of wire feed rate when, arc voltage was varied from 24 to 29 volts. This shows that the interaction of W&V is highly significant at higher levels.

Fig. 3 shows that welding current increased with the change in the torch angle from 80° to 100°, backhand to forehand. The increase in the welding current was just 3 amperes compared to 12 amperes for low and high values of wire feed rate.

Fig. 4 shows that welding current decreased with the change in torch angle from backhand to forehand position. Effect of torch angle on welding current at low levels of wire feed

rate is quite insignificant compared to the variation of 14 amperes at the high level of nozzle-to-plate distance.

Fig. 5 shows that welding current decreased with the increase in torch angle from 80° to 100°. There is no effect of welding speed on the welding current at low level of torch angle however; it became quite significant at the high level of torch angle. The figure also shows that there is hardly any effect of torch angle of 80° on welding current. The welding current decreased by 12 amperes at 40 cm/min & forehand angle of 100°.

Conclusions

1. In GMAW, the welding current is affected not only by the wire feed rate but also by the arc voltage, the nozzle-to-plate distance, the electrode/torch angle and the welding speed.
2. An empirical model was developed to estimate the welding current by correlating these parameters for GMAW of aluminum.
3. At low wire feed rates, the effect of arc voltage on welding current was negligible. However, it increased enormously at higher feed rates.
4. Increase in nozzle-to-plate distance resulted in the decrease in welding current possibly due to the increase in arc length.
5. The increase in arc voltage resulted in the increase in welding current indicating a rising volt-ampere characteristic of the welding arc.
6. The increase in electrode/torch angle resulted in the decrease in welding current.
7. The increase in welding speed resulted in the increase in welding current.

Acknowledgement

References

1. Walser, H.; and Zehnder, M. 1981. Practical and technological aspects of inert gas welding of aluminum and its alloys. Colloquium on Aluminum and Its Alloys. Porto (Portugal): IIW, Paper I-8.
2. Halmoy, E. 1979. Wire melting rate, droplet temperature and effective anode melting potential. Proc. of International Conference on Arc Physics and Weld Pool Behavior-- Paper 44. Welding Institute, London, pp. 241-249.
3. Trindade, H. 1982. M.Sc. thesis. School of Industrial Science, Cranfield, Cranfield Institute of Technology.
4. Adler, Yu.P.; Markova, E.V.; and Granovsky, Yu.P. 1975. The design of experiments to find optimal conditions, Moscow: Mir Publishers.
5. Box, G. E. P.; Hunter, W.G.; and Hunter J. S. 1978. Statistics for experimenters: An introduction to design data analysis and model building, New York: John Wiley & Sons.
6. Montgomery, D.C. 1991. Design and analysis of experiments, Third Edition, New York: John Wiley & Sons.

Weld Data Flow

CONTROL OF GMA BUTT JOINT WELDING BASED ON NEURAL NETWORKS

K. H. Christensen[*], T. Sørensen[*]

ABSTRACT

This paper presents results from an experimentally based research on Gas Metal Arc Welding (GMAW), controlled by the artificial neural network (ANN) technology. A system has been developed for modeling and online adjustment of welding parameters, appropriate to guarantee a high degree of quality in the challenging field of butt joint welding with full penetration under stochastically changing boundary conditions, e.g. major gap width variations. GMAW experiments performed on mild-steel plates (3 mm of thickness), show that high quality welds with uniform back-bead geometry are achievable for gap width variations from 0.5 mm to 2.3 mm - scanned 10 mm in front of the electrode location. In this research, the mapping from joint geometry and reference weld quality to significant welding parameters, has been based on a static multi-layer feed-forward network. The Levenberg-Marquardt algorithm, for non-linear least square error minimization, has been used with the back-propagation algorithm for training the network, while a Bayesian regularization technique has been successfully applied for minimizing the risk of inexpedient over-training.

KEYWORDS

GMA welding, butt joint welding with full penetration, open-loop weld geometry control, neural network modeling, Marquardt algorithm, and Bayesian regularization.

INTRODUCTION

Gas Metal Arc Welding (GMAW) is - due to its considerable flexibility, productivity and weld quality - the most prevalent arc welding process in industry; but unfortunately also one of the most complex processes. Basically, the GMAW process involves conductive, convective, radiative heat and metal transfer, phase transformations among many unknown disturbances. Accordingly, the GMAW process is a time varying, non-linear, coupled, multi-variable process whose highly complex physics, is not fully comprehended neither qualitatively nor quantitatively. Selecting appropriate welding parameters to get a given weld quality (i.e. weld geometry), is clearly a non-trivial task. Furthermore, even minor changes in system dependent parameters, e.g. joint geometry, heat conduction, etc., from given reference values necessitate a continuous adjustment of significant welding parameters, such as welding speed, current, voltage etc. to facilitate a sufficient quality and shape of a desired weld. Therefore, to handle such situations in a reasonable way it is appropriate to obtain a mathematical model that correlate welding process pa-

[*] Department of Mechanical Engineering, Technical University of Denmark, DK-2800 Kgs. Lyngby, Denmark

rameters to weld quality - or vice versa; but obviously, it seems to be a challenging issue in the field of arc welding automation.

During the past decades, intense research into the area of mathematical modeling of the complex arc welding processes has been made to increase the understanding of the effects of the arc welding process parameters on the weld quality. This extended work includes theoretical studies based on heat transfer and fluid flow theory etc. as well as empirical methods based on knowledge collected from specific weld task experiments. However, the many years of work has proven that the development of exact and reliable models based on the fundamental physical laws are extremely complicated if not impossible, and even the most promising models are typically unsuitable for real-time control purposes. Even though empirical models inherently have many drawbacks, such as sensitivity on geometry and material properties, and much more, they tend to have some advantages in the area of arc welding automation. Classic regression analysis was applied to welding geometry research in the late half of the 80'ties (Ref. 1), while the first step towards the application of artificial neural network (ANN) was reported a few years later (Ref. 2). In this, ANN was used to determine the relationship between significant welding parameters and characteristic weld bead dimensions for gas tungsten arc welding.

Since the publication of (Ref. 2), a diversity of papers, typically addressing optimization and control, have been published underlining the quality of ANN, as a generic tool with a high degree of flexibility for modeling and control of a great variety of arc welding processes on different kind of joint geometries, materials, etc. (Ref. 3-8). Some of the publications, e.g. (Ref. 7-8) show that artificial neural networks are indisputable alternatives to classic regression analysis.

Still, research on modeling and control of real-life welding based on ANN techniques are limited and more contributions are needed. Therefore, in this paper research on the ANN based modeling and control of the GMAW process, is presented. A model based control system has been developed, that continuously compensate for gap width variations in butt joint welding with full penetration by selection and maintenance of the equipment parameters necessary to achieve a user specified reference back-bead geometry, which is naturally a considerable factor to the final weld quality.

After a short introduction of ANN, the paper proceeds with a description of the general considerations concerning the welding experiments that have been carried out. Next, the results from these experiments are presented and discussed together with the applied control strategy, and finally a conclusion on the work is drawn.

THE MODELING TECHNIQUE: ARTIFICIAL NEURAL NETWORK (ANN)

Due to their theoretical ability to approximate arbitrary non-linear mappings, ANN's are typically applied when appropriate analytical models are unknown or extremely complex. In mathematical terms, an ANN can be characterized as a highly complex, non-linear mapping function, which in a given domain transforms input to output. Although an ANN model may be very complex, the basic mathematics is relatively simple. Modeling with ANN is empirical modeling, and thus a sample database covering the entire problem domain must be available, similar to conventional regression analysis. When presented with inputs inside this domain, but not appearing in the training data, a suitably trained network will have the ability to generalize well.

The static multi-layer feed-forward network with biases and at least one sigmoid layer is widely recognized for the capability of approximating any function with a finite number of discontinui-

ties (i.e. non-linear, coupled, and multivariable systems such as e.g. the GMAW process addressed here). In the context of this paper, a feed-forward network of this type, shown in Figure 1, is applied.
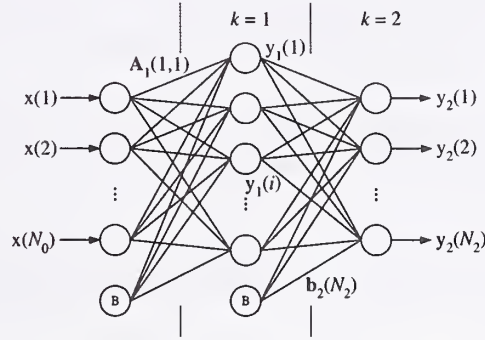

Figure 1: Two-layer feed-forward network, performing the mapping $\mathbf{y}_2 = \mathbf{F}(\mathbf{x}) : \mathfrak{R}_0 \rightarrow \mathfrak{R}_2$.

The mapping from input to output can be expressed as follows:

$$\mathbf{y}_0 = \mathbf{x}$$
$$\mathbf{y}_k = \mathbf{f}_k(\mathbf{A}_k \mathbf{y}_{k-1} + \mathbf{b}_k) \quad \text{for } k = 1, 2, ..., n$$

where $\mathbf{x}$ ($N_0 \times 1$) is an input vector, while $\mathbf{y}_k$ ($N_k \times 1$) is an output vector from the k'th layer. The sigmoid-function is applied as transfer function: $\mathbf{f}_k(\mathbf{s}) = (1+\exp(-\mathbf{s}))^{-1}$ ($N_k \times 1$). $\mathbf{A}_k$ is a weight matrix of dimension $N_k \times N_{k-1}$, $\mathbf{b}_k$ is a bias weight column vector of length N_k, and n is the number of layers.

In this paper the Levenberg-Marquardt algorithm for non-linear least squares (a standard numerical optimization technique) is used with the back-propagation algorithm for training the feed-forward neural network. In (Ref. 9), it has been shown that the Levenberg-Marquardt algorithm is much more efficient than other known algorithms, when the network contains less than a few hundred weights, which is the case in this paper.

Minimizing the risk of inexpedient over-training by use of a so-called regularization technique (Ref. 10), is more important than guaranteeing a fast rate of convergence. Instead of minimizing the sum of squared errors, $F = E_D$, which is the traditional approach for network training, the objective of this technique is to minimize a performance function with the following structure (for training based on a set of weld data of size m containing: $\{\mathbf{x},\mathbf{t}\}_{(1)}, \{\mathbf{x},\mathbf{t}\}_{(2)}, ..., \{\mathbf{x},\mathbf{t}\}_{(m)}$):

$$F = \beta E_D + \alpha E_W \quad \text{with } E_D = \sum_{i=1}^{m} (\mathbf{t}_{(i)} - \mathbf{y}_n^{(i)})^T (\mathbf{t}_{(i)} - \mathbf{y}_n^{(i)})$$

As shown in (Ref. 10), this modification of the performance function - the addition of the term E_W, representing the sum of squares of the network weights - will improve network generalization, so that any modestly oversized network will have the ability to sufficiently represent the true underlying function. The basic idea of the method, which consistently produces networks with good generalization abilities, is that the true underlying function is assumed to have a limited degree of smoothness, for which reason this method constrains the size of the network weights. The optimal setting of the regularization parameters, α and β, is based on the Bayesian

117

theory, and so this technique is referred to as Bayesian regularization. Furthermore, it is assumed that the experimental data are infected by Gaussian noise, and finally, it should also be noted that input and output, in this paper, are scaled similar to (Ref. 2):

$$p_n = \frac{0.9-0.1}{p_{\max}-p_{\min}}(p - p_{\min}) + 0.1$$

where $p_{\max}$ and $p_{\min}$ are maximum and minimum, respectively, of the physical data parameter p, and p_n is the scaled parameter applied to the network.

GENERAL CONSIDERATIONS CONCERNING THE WELDING EXPERIMENTS

The developed system is based on an ANN model, which facilitates the mapping from some characteristic features describing the weld quality and joint geometry to some significant welding equipment parameters. For that reason, it is assumed that a correlation between the characteristic features, shown in Figure 2, and significant welding parameters (welding speed, voltage, and wire feed speed) emerge during welding, by. which it is possible to design and train an ANN model that estimate feasible welding parameters. Furthermore, it is to be noted that the control system design is based on the static characteristics of the welding process.
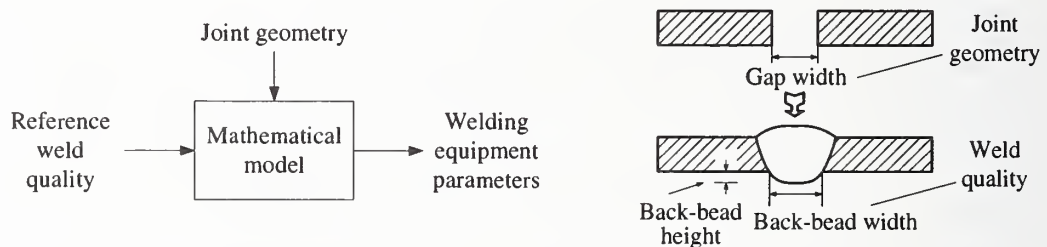
Figure 2: The process model maps weld quality and joint geometry into welding parameters.

To perform the described experimental validation, a PC-based welding system has been established, consisting of a welding machine, a two-axis table system, and a laser vision system, which is applied for real-time seam tracking and online gap width measurement. The joint geometry is scanned 10 mm in front of the welding torch. A schematic diagram of the system is shown in Figure 3, while technical specifications relevant for the experiments are given in Table 1.
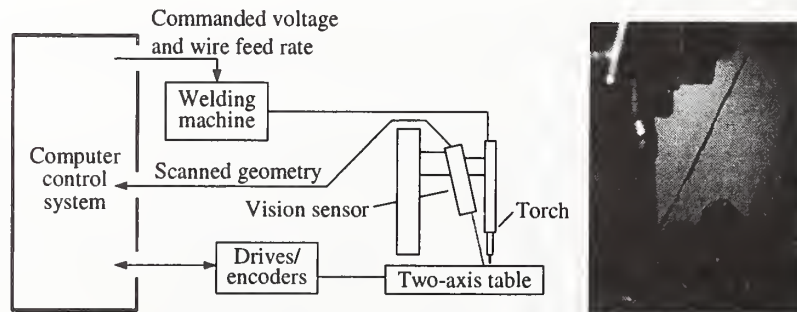

Figure 3: Structural diagram of the experimental system.

Joint type	Butt weld (without backing)
Plate material	Mild steel (S235)
Plate thickness	3 mm
Plate dimensions (LxW)	330×50 mm
Power supply	Constant voltage machine
Wire type	EN440 – G3Si1
Wire diameter	$\varnothing$1.2 mm
Shielding gas	Mixture: 92 % Ar and 8 % CO_2
Gas flow rate	15 l/min
CTWD	10 mm
Welding torch orientation	Horizontal (PA) with a travel angle of 90 degrees

Table 1: Technical specifications for the experiments conducted (CTWD: Contact Tip to Work-piece Distance).

OPEN-LOOP CONTROL STRATEGY

The experimental investigation of the applicability of ANN in an open-loop control strategy contains two steps: (1) To verify that the proposed ANN model based on static weld data in fact can fit the characteristics of the weld task in a suitable way. (2) To examine the applicability of the static ANN process model in an open-loop control system controlling a dynamic process.

Input parameters

Back-bead height Back-bead width Gap width	Neural network	Welding speed Wire feed speed Voltage

Output parameters
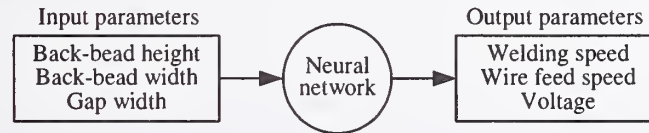
Figure 4: The developed process model applied to an open loop control system.

According to (1) the applicability of the developed process model (Figure 4), in terms of precision and robustness, has been demonstrated. A series of GMAW experiments has been conducted to obtain the decisive knowledge about how the significant welding parameters affect the back-bead geometry, given different joint geometries. Consequently, a total of 39 quality welds have been made, and the welding parameters have been selected within the domain of useable parameters, when parts to be welded are fixed to produce given constant gap widths within a prescribed interval. During the welding process, the gap width is scanned 10 mm in front of the welding torch following the centerline of the gap, while the back-bead width and height have been measured afterwards. The relatively few experiments have been carried out in an unsystematically way for gap widths within the interval of 0.0-2.3 mm (Table 2), and the main objective of the experiments has been to maintain homogenous back-bead geometries, as shown in Figure 5.

Obviously, different sets of welding parameters for a given gap width can produce identical back-bead geometries. Therefore, for later use of the weld data it is crucial to perform these preliminary experiments with a certain degree of attention to the aim of this original research.

Weld No.	Wire feed speed [m/min]	Voltage [V]	Welding speed [mm/min]	Gap width [mm]	Back-bead width [mm]	Back-bead height [mm]
8	3.8	19.0	325	1.00	3.70	1.00
16	5.0	21.0	375	0.40	2.80	0.60
25	2.8	18.0	310	2.00	3.70	0.85
26	3.0	18.0	350	1.60	2.80	0.40
Min	2.8	18.0	300	0.00	1.50	0.25
Max	5.8	22.0	375	2.30	5.10	2.70

Table 2: Four out of 39 experiments are shown with the boundary limits of each parameter. The considerable variation of the gap width obviously implies major changes in wire feed speed and voltage.
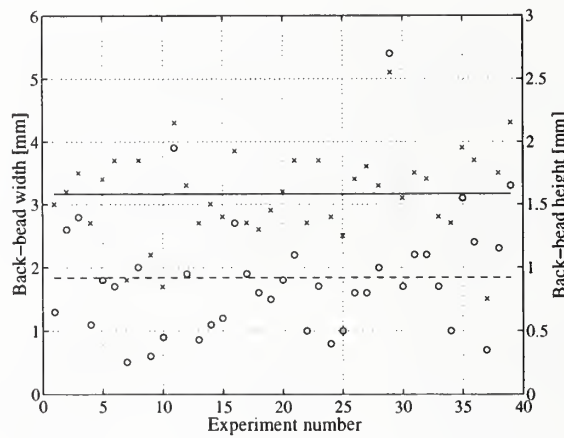
Figure 5: The $\times$'s indicate the back-bead width, for which the solid line represent the mean value ($<w_b>$ = 3.17 mm), while the o's and dotted line represent the back-bead height ($<h_b>$ = 0.92 mm).

Based on these experimentally obtained weld data, a static multi-layer feed-forward network has been trained by supervised learning. The trained network manages the mapping shown in Figure 4. The selection of feasible design parameters of the neural network, such as the number of hidden layers, the number of nodes in each layer, type of activation function etc., rely on the specific modeling task. In this study, a two-layer network with a hidden layer containing three neurons and an output layer containing three neurons as well - according to the number of outputs - has been selected. All neurons contain the sigmoid transfer function. Data sets from 33 of these experiments have been used for network training, while the remaining 6 data sets have been used for testing the generalization capabilities of the trained network.

The Bayesian regularization technique (Ref. 10) introduces γ, a so-called effective number of parameters, which is a measure of the number of parameters (weights) in the neural network that are effectively used in reducing the error function. In the network training $\gamma = 19.52$, which is much less than the 24 weights that appears in the chosen network. Accordingly, the neural network applied seems to be large enough to properly represent the true function.

The performance evaluation of the trained network has been based on a traditional error analysis applied to the training and test data sets, respectively. Table 3 shows the absolute mean errors for the welding parameters, and on the basis of these results the trained network seems to generalize

well. Furthermore, to investigate the network performance in further detail, a linear regression analysis between the network response and the corresponding measured data sets has been performed. The result of this analysis is shown in Figure 6, and it appears that the wire feed speed and voltage correlate well, while the welding speed does it barely as well. However, it is notable that especially the wire feed speed has a great influence on the penetration, and consequently, it is very important that this particular welding parameter is well correlated. Since the wire feed speed varies between 2.8-5.8 m/min, while the welding speed only varies 300-375 mm/min, it is concluded that the influence of the welding speed is much less that the effect of the wire feed speed in this series of experiments.

	Wire feed speed [m/min]	Voltage [V]	Welding speed [mm/min]
Training data	0.20	0.32	12.37
Verification data	0.35	0.41	12.36

Table 3: The prediction accuracy of the trained ANN is shown by the absolute mean errors for the welding parameters. It seems as if the ANN identifies the underlying trends rather than just memorizes the input/output relations of the experimental data sets.
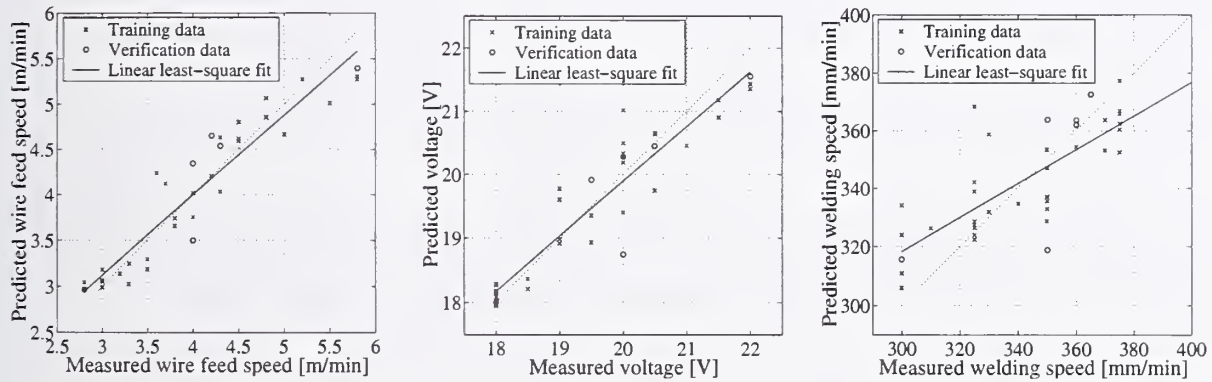
Figure 6: Predicted versus measured welding parameters for the complete data set. For wire feed speed, voltage, and welding speed, the correlation coefficients are 0.95, 0.94, and 0.77, respectively.

Simulations of control performance were conducted with the trained network, and according to Figure 5, the desired back-bead geometry were set as $h_b = 0.75$ mm and $w_b = 3.0$ mm. In Figure 7 and 8 results from a simulation with significant gap width variations along the joint - from 0.5 mm to 2.3 mm - are shown. From the photograph shown in Figure 7, it is seen how the front-bead geometry varies due to the continuous adjustment of welding parameters. As expected, the front-bead geometry became larger when the gap width became smaller and vice versa. From Figure 8, it follows that a uniform back-bead has been obtained, even though minor local variations of the height, as well as of the width, appear along the weld. The mean values of the back-bead height and width are 0.76 mm and 3.19 mm, respectively, and in general, it is concluded that quality welds, fully competitive with skilled manual welding, are achievable.
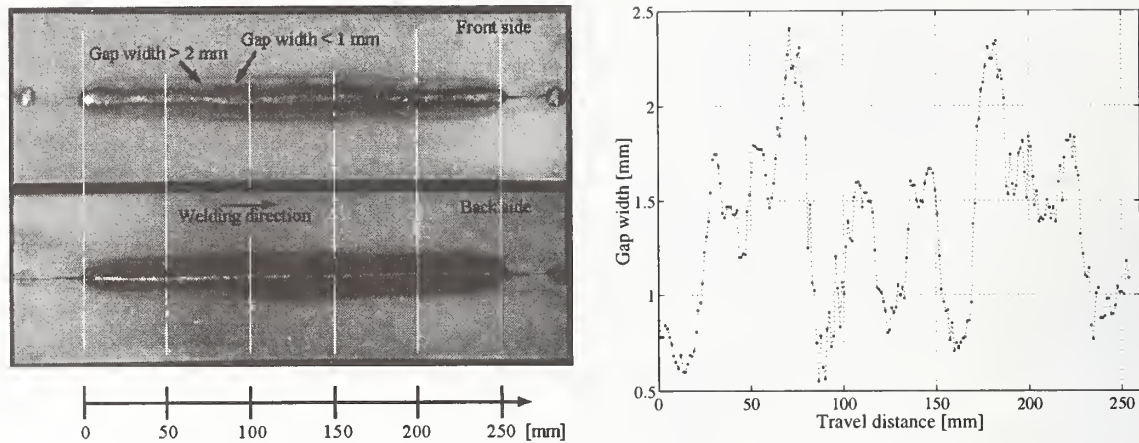
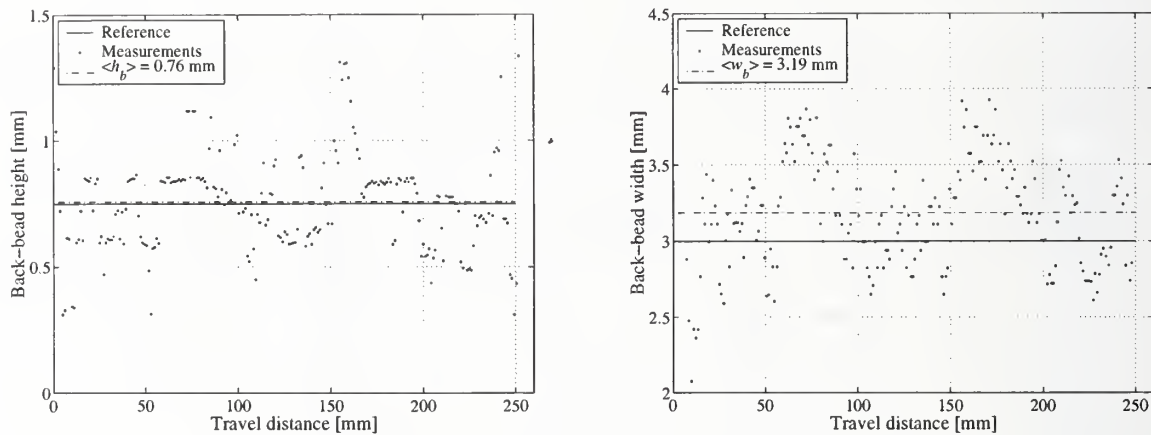Figure 7: A test weld and its measured gap width variation.

Figure 8: Back-bead height and width according to the simulation shown in Figure 7.

CONCLUSION

Physical experiments have shown that the weld bead geometry is extremely sensitive to gap width variations in GMA butt joint welding with full penetration, and consequently, a continuous adjustment of welding parameters is essential for the realization of a uniform back-bead geometry. An open-loop control strategy, based on neural network technology, was experimentally investigated and applied successfully to this particular weld task.

In fact, a series of laboratory based experiments shows, that it is possible to apply static data to train an ANN to obtain a model of the GMAW process, and that the model is feasible for high quality, open-loop butt joint welding with full penetration of 3 mm plates with variations in the gap width from 0.5 to 2.3 mm.

Unfortunately, the weld quality has proven to be quite sensitive to changes in welding conditions (not only the gap width), and since it is expensive, impractical, and often impossible to sustain constant welding conditions in an industrial environment, the open-loop control strategy is typically too vulnerable to be applied in such disturbing surroundings. For that reason future work will be focused on development of a closed-loop control system based on online monitoring and control of the weld quality.

122

REFERENCES

1. Raveendra, J., Parmar, R.S.: Mathematical models to predict weld bead geometry for flux cored arc welding, Metal Construction, Vol. 19 Issue 1, pp. 31R-35R, 1987.
2. Andersen, K., Cook, G.E., Karsai, G., and Ramaswamy, K.: Artificial Neural Networks Applied to Arc Welding Process Modeling and Control, IEEE Transactions on Industry Applications, Vol. 26 No. 5, pp. 824-830, 1990.
3. Lim, T.G., Cho, H.S.: Estimation of weld pool sizes in GMA welding process using neural networks, Proceedings of the Institution of Mechanical Engineers, Part I (Journal of Systems and Control Engineering), Vol. 207 Issue 1, pp. 15-26, 1993.
4. Chan, B., Pacey, J., and Bibby, M.: Modelling Gas Metal Arc Weld Geometry Using Artificial Neural Network Technology, Canadian Metallurgical Quarterly, Vol. 38 No. 1, pp. 43-51, 1999.
5. Chen, S.B., Lou, Y.J., Wu, L., and Zhao, D.B.: Intelligent Methodology for Sensing, Modeling and Control of Pulsed GTAW: Part 1 - Bead-on-Plate Welding, Welding Journal – Including Welding Research Supplement, Vol. 79 Issue 6, pp. 151s-163s, 2000.
6. Chen, S.B., Zhao, D.B., Wu, L., and Lou, Y.J.: Intelligent Methodology for Sensing, Modeling and Control of Pulsed GTAW: Part 2 - Butt Joint Welding, Welding Journal - Including Welding Research Supplement, Vol. 79 Issue 6, pp. 164s-174s, 2000.
7. Di, L., Chandel, R.S., Srikanthan, T.: Static Modeling of GMAW Process Using Artificial Neural Networks, Materials and Manufacturing Processes, Vol. 14 No. 1, pp. 13-36, 1999.
8. Lee, J., Um, K.: A comparison in a back-bead prediction of gas metal arc welding using multiple regression analysis and artificial neural network, Optics and Lasers in Engineering, Vol. 34 Issue3, pp. 149-158, 2000.
9. Hagan, M.T., and Menhaj, M.B.: Training Feedforward Networks with the Marquardt Algorithm, IEEE Transactions on Neural Networks, Vol. 5 No. 6, pp. 989-993, 1994.
10. Dan Foresee, F., and Hagan, M.T.: Gauss-Newton Approximation to Bayesian Learning, 1997 IEEE International Conference on Neural Networks, Vol. 3, pp. 1930-1935, 1997.

ARC WELDING PROCESS SIGNATURE VISUALIZATION AND ANALYSIS

C. Hsu[*]

ABSTRACT

Arc voltage-current population (histogram) density two dimensional color plots are generated for various arc welding processes, including CV spray, CV short-circuiting, pulsed MIG, AC submerged arc, tubular electrodes, Surface Tension Transfer® (STT®), and stick electrode in pipe welding.

Actual voltage and current signals are recorded at a sufficiently high sampling rate (50 KHz or higher). Each voltage-current data pair, or data in combination with its first order derivates (e.g. dv/dt, di/dt) is digitized to a pixel location on a raster image area. The occurrences of data pairs at each location are accumulated for a fixed weld time. Color models (e.g. RGB) are used to represent the histogram depth, based on normalized density, from "warm to cold", as a signature of each welding process. Attractors in the short region and the arc region are identified, and the transition between regions, such as between short and arc, is animated and analyzed statistically. Applications such as welding process stability and welding procedure optimization, derived from digital image processing techniques, are illustrated.

KEYWORDS

Arc Monitor, quality monitor, weld quality assurance, arc stability, stubbing, GMAW, GMAW-P, GMAW-S, SAW, SMAW, FCAW, STT, AC, CV, MIG, MAG, data acquisition, SPC, histogram, statistics, pulse welding, pipe welding, short circuiting, dip transfer, spatter, droplet transfer, digital signal processing, digital image processing

INTRODUCTION

Weld quality assurance is becoming an important consideration in manufacturing industry. Many process variations in production, such as poor part fit-up, arc blow, poor grounding or voltage sense connection, multiple arc interference, disturbed gas shielding, poor wire feeding, etc. can yield weld defects. A returned assembly from an automaker to its first tier supplier incriminates not only the welding process but also the quality inspection process. Therefore there is a growing demand for weld quality monitors, preferably based on simple signals, such as arc voltage and current, wire speed and gas flow rate.

Techniques using statistical process control (SPC) tools such as data trending, tolerance chart and sequential analysis are discussed by Cook et al. [1]. Statistical algorithms were developed by Quinn et al. in CV arc welding that flag out defective welds by comparison with a baseline of

[*] Engineering Manager, The David C. Lincoln Research and Development Center, The Lincoln Electric Company, 22801 St. Clair Avenue, Cleveland, Ohio 44117

defect-free welds [2]. Power spectral density of arc signals is used to predict contact tip wear [3] and porosity and burn-through [4]. Fast Fourier Transform of the current waveform is used to determine stability of short-circuiting metal transfer [5].

The goal of a weld monitor is obviously to catch *all* faults determined by an application's acceptance criteria without *any* false alarms. Common faults in manufacturing are burn-through, weld too cold or too small, porosity, undercut, wire stub sticking out of the weld, insufficient weld length, weld off joint, and weld simply missing. The foundation of an effective statistical weld monitor comprises of 1) all faulty welds will be accompanied by significant arc signal disturbances above the noise level; 2) an arc signal departing from the statistical norm will necessarily produce unacceptable weld faults. These are presumptions in the absolute sense. In practice it is a leap of faith from arc signal behavior to weld quality.

One commercial system based on statistical methods called ARCAgent™ from Impact Engineering is applied in semi-automatic applications [6] and another called ADM IV™ from Computer Weld Technology is used in hard automation and robotic applications. Fanuc's Data Monitor option integrated in its R-J3 controller tracks statistics of up to 6 arc signals at 250 Hz maximum rate and reports error conditions, using Data Monitor Schedule to set upper, lower and time limits. These systems work well to identify gross weld defects in simple CV spray process. However, they have limitations arising from relatively low sampling rates (e.g. 10-1000 Hz) and may not be effective in pulse welding, short-circuiting welding or STT welding. The arc waveforms are commanded at a few hundred Hz with large swings in amplitude, which make it difficult to identify statistical anomalies. In many automotive applications, the welds may last one second or less, and 1 KHz sampling only captures 1,000 data points where a good fraction is spent in arc strike, run-in, crater fill and arc end transients.

One approach is to use the power source itself as both waveform generator and waveform monitor in synergic pulse welding and STT welding. This has the advantage of *a priori* knowledge of time segmented commanded signals [7]. For example, the background time and background current can be monitored and compared to programmed settings, when the power source is adjusting background time and current to adapt for stickout changes at a specific synergic wire speed. Fluctuation of background current or time would be indicative of process instability. Externally extracting peak current or monitoring average current would not be as useful or effective when the power source uses a fixed peak current at a given wire speed. The welder manufacturer can predetermine fault thresholds as part of the waveform development effort, to be adjusted for a given application if necessary.

Barborak and Conrardy used histograms of current, voltage, power and conductance to detect stickout, gas, and wire speed disruptions in short-circuiting welding [8]. Cross-plots, or scatter diagrams of voltage and current produce a graphical view of the short-circuiting process. Simpson applied chaos theory and drew his cross-plot on an adaptive scale to improve resolution in regions of interest, using arc voltage and an "artificial current" derived from the weighted time history of arc voltage [9]. A plot is generated every second with a 8 KHz sampling rate for online stability computation and fault detection, commercially known as WeldPrint™.

This paper introduces a 2D color artificial image to represent a histogram of arc signals, using arc voltage, arc current and their time derivatives, to display and analyze the stability of many arc welding processes.

DATA ACQUISITION AND ANALYSIS SOFTWARE

Equipment

Arc current and voltage are acquired using a high-speed data acquisition device with channel-to-channel isolation, 14-bit measurement resolution, and 250 KHz aggregated sampling rate. Most of the data is collected at 50 KHz - 75 KHz per channel. Current is measured by an AEMC MR561 current probe. The data acquisition box streams data to the laptop hard disk through a USB connection. All instruments are NIST traceable.

Arc Caliper

Arc Caliper is a software program developed at the Lincoln Electric Company to analyze high-speed data acquisition files producing arc signal and wire feeding statistics, timing and synchronization statistics, arc start behavior, burn-back and arc ending characteristics. Optionally a 2nd order Butterworth low pass digital filter with 3dB cutoff set at 2500 Hz can be engaged. Ad hoc algorithms are developed to represent or estimate arc stability, spatter, heat input, fume, operating voltage etc. for welder, feeder, robot and consumable evaluation. It is written in Java for portability to non-Windows platforms such as PDA or mobile phone as part of an online user interface or as an embedded web page residing in the power source or robot, and for ease of factory networking.

One output of Arc Caliper is the so called voltage-current population density plot. Each voltage-current data pair is saved to a pixel location on a raster image area. The occurrence of data pairs at each location is accumulated for the entire weld (e.g. 20 seconds of welding). Color models (e.g. RGB or HSB) are used to represent the histogram depth, based on normalized density, from "warm to cold", as a signature of the welding process. The signals can be played back (animated) to reveal the dynamic behavior of a measured process and the results can be exported as a spreadsheet.

APPLICATIONS IN ARC WELDING PROCESSES

CV Spray transfer process

A stable CV spray process above the transition current is simply one blob in the VI density plot. The weld is done at about 22.5V and 365A using S-6 wire on an inverter. A sequence of white, yellow, red, pink, and blue is used to represent the decreasing levels of normalized frequency of digitized voltage-current pairs, or histogram density. Most of the data falls within the "hot zone" where the zone width corresponds to inverter ripple and the blue fringes may be explained by the

voltage disturbances from "incipient" shorts when a droplet is stretched and may briefly kiss the puddle surface before being detached.
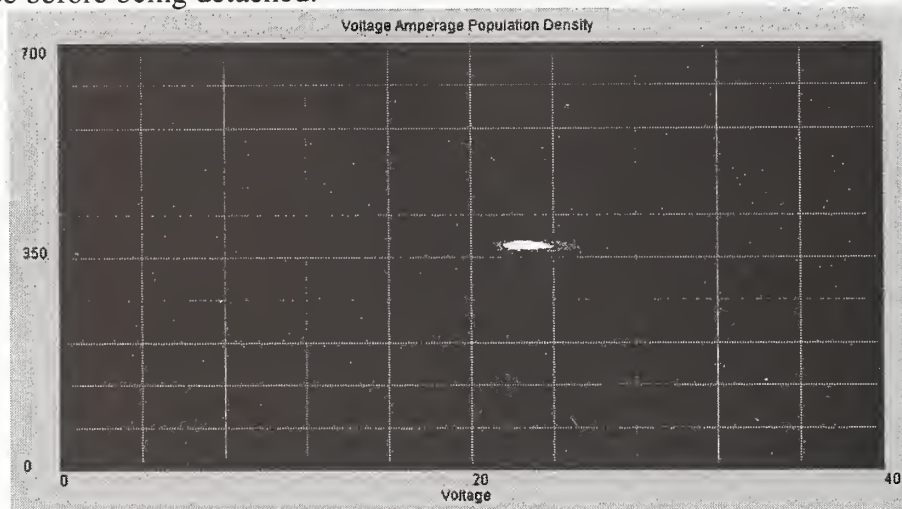

Figure 1: CV spray VI density plot from PowerWave 455, L-56 electrode, 90% Ar+10% CO_2
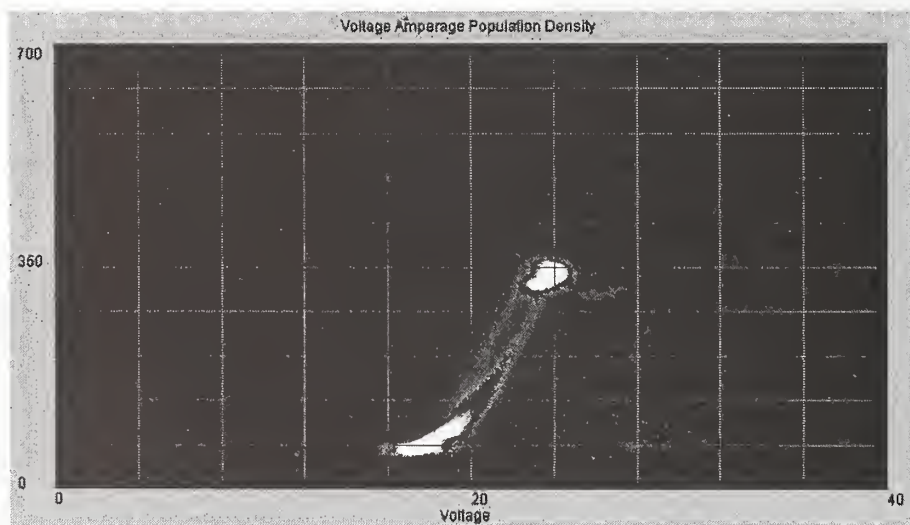
Pulsed spray process

Figure 2: Pulsed spray transfer VI density plot from PowerWave 455, L-50 electrode, and 90% Ar+10% CO_2

Two distinctive "attractors" or hot zones appear in pulsed spray transfer process, corresponding to the high peak current and low background current and their transition behavior. Both zones are above 12V implying that a plasma is always present.

CV short-circuiting process

A typical CV short-circuiting process (see Figure 3) also has two zones, one at low voltage or in a short, and the other at high voltage 15-21V. During the short the current is slowly ramped up,

applying pinch force to the liquid bridge, until it breaks into an arc, at which instant it snaps into the arc zone.
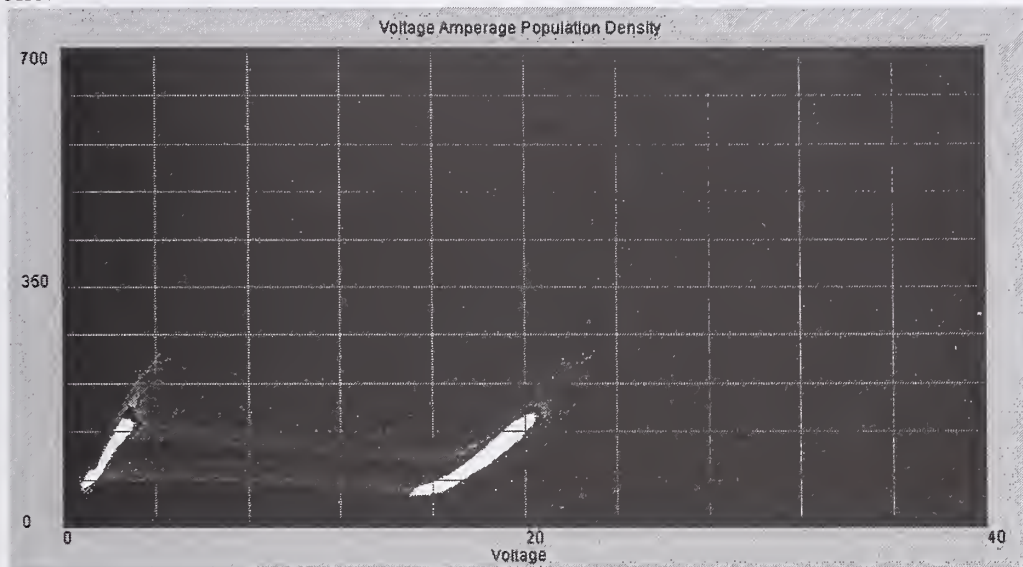
Figure 3: CV short-circuiting VI density plot from PowerMIG 300, L-50 electrode, 90% Ar+10% CO_2

STT controlled short-circuiting transfer process
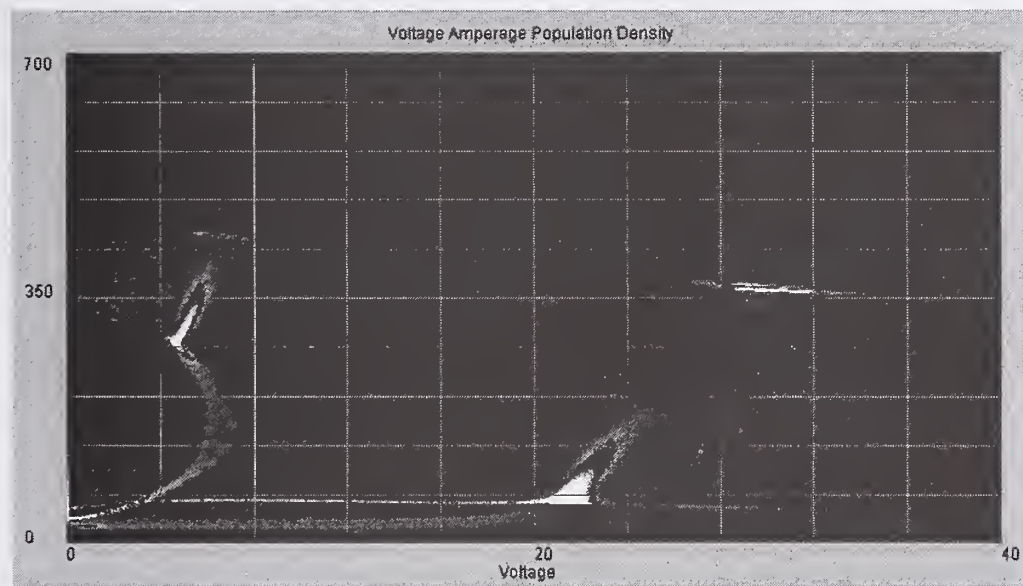
Figure 4: STT VI density plot from STT II, AutoWeld electrode, 75% Ar+25% CO_2

The low spatter STT process has four hot zones in Figure 4. A background current of 70 amps maintains the arc and contributes to plate heating at the right bottom corner. After the electrode initially shorts to the weld pool, it jumps to the low voltage-low current zone to ensure a solid short. Pinch current is then applied following the S-shaped curve to the top left zone. Molten metal is squeezed down and the derivative of voltage (dV/dt) is monitored. When the liquid bridge is about to break, dV/dt increases sharply and power source reacts by driving the process back to the low voltage-low current zone. Immediately following the arc establishment, it

129

swings up to the high current-high voltage zone on the top right corner, to produce plasma force pushing down the weld pool. Finally it returns to the background zone and stays there until it shorts again.

AC submerged arc process
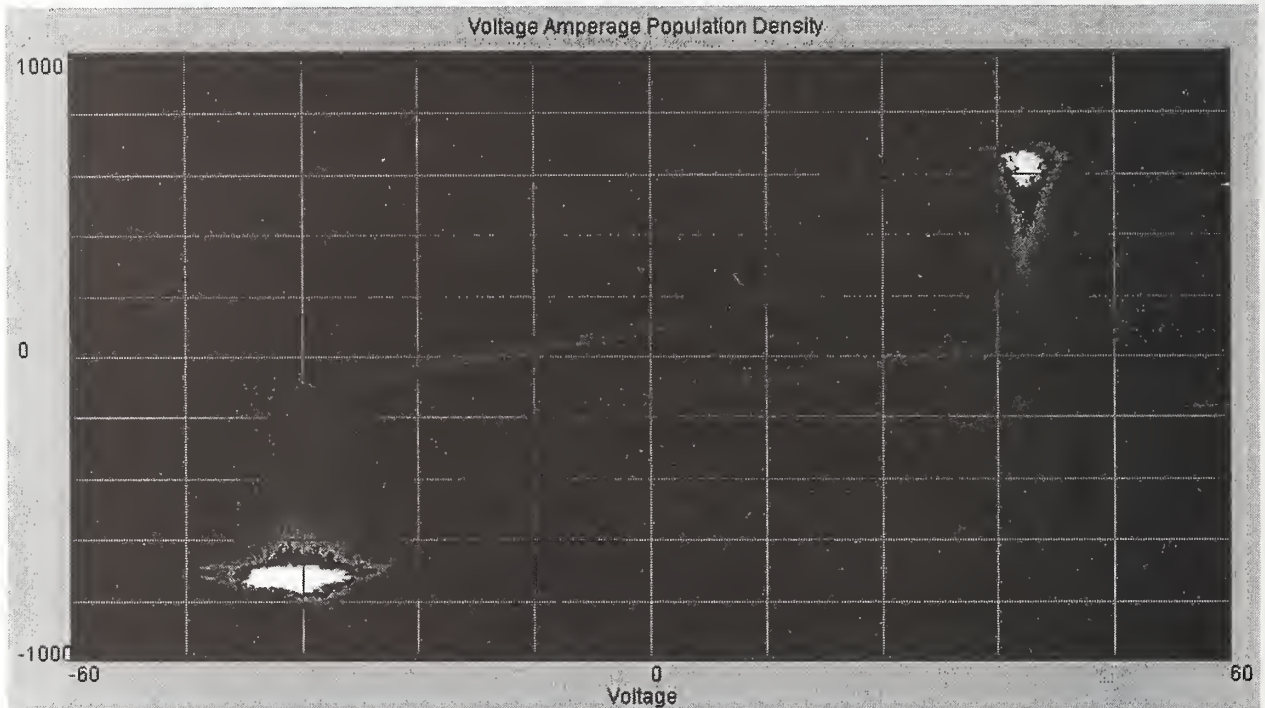
Figure 5: AC sub-arc VI density plot from PowerWave AC/DC with L-60 electrode and 860 flux

The AC submerged arc process circulates between a DC positive zone and a DC negative zone in a loop. One advantage of inverter based, computer controlled AC sub-arc equipment is exhibited in the transition between the two zones. The current is being reduced gradually so that zero-crossing occurs at low current in order to reduce stress applied to the power electronics. It also shows that the zero-crossing occurs rapidly with a large voltage swing from the center tap choke design that prevents arc outages.

CC process with stick electrode

Pipe welding using E6010 electrode on an electronically controlled engine welder is shown in Figure 6. The main hot zone is characterized by a constant current with voltage ranging from 18-34V. The stick electrode is being whipped back and forth, and shorting does occur as shown in the left hot zone. Transition dynamics in the VI plot from the shorting zone and arc zone are essential for puddle fluidity control in all position pipe welding.
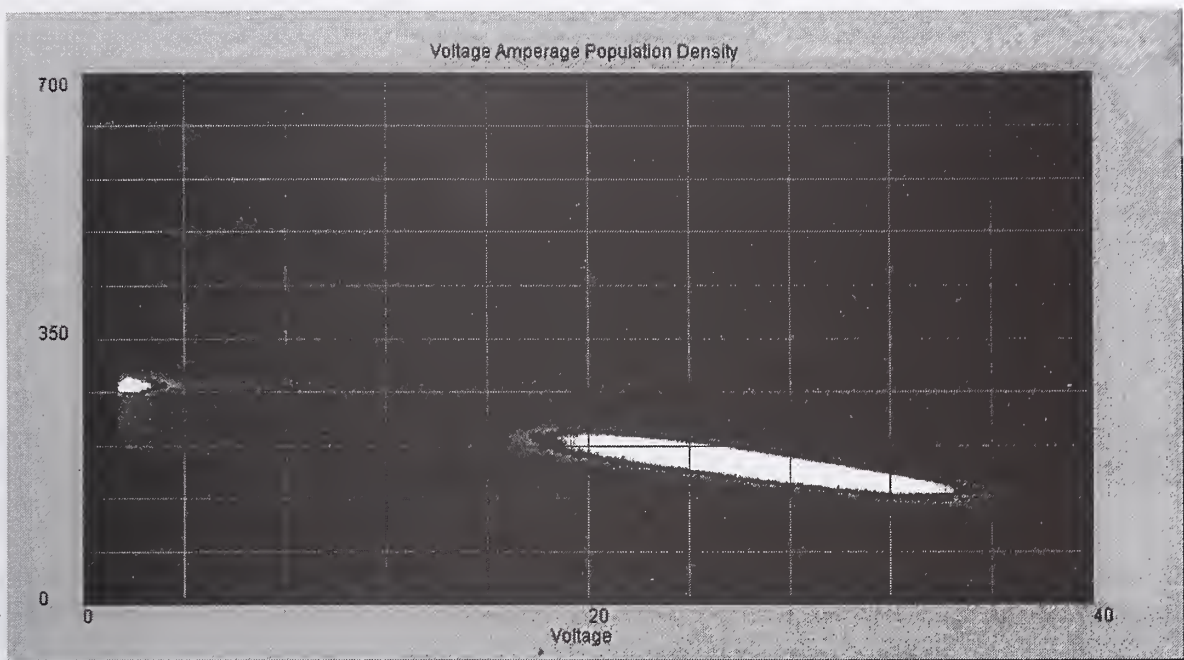
Figure 6: CC process VI density plot from Ranger 305G, Fleetweld® 5P+ electrode
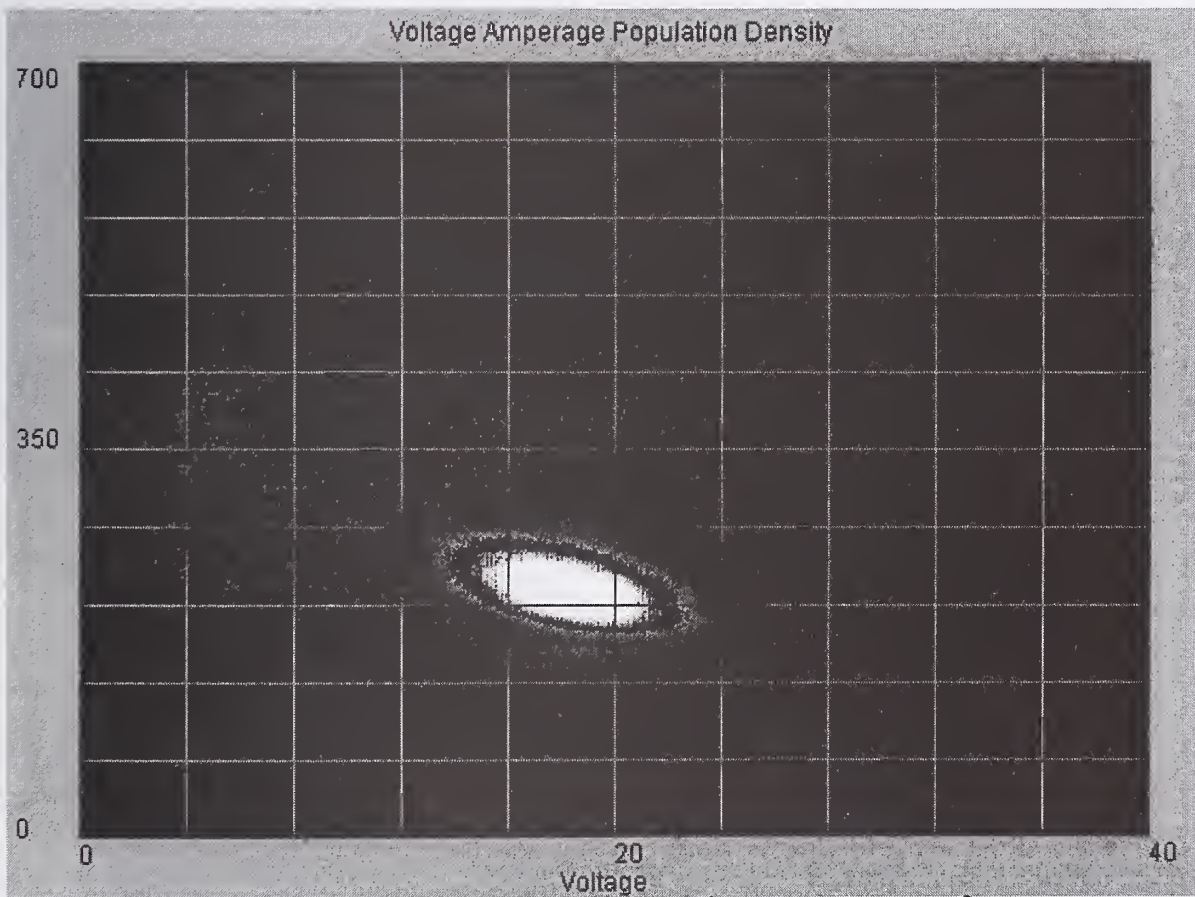
Globular transfer process

Figure 7: Globular transfer VI density plot from Invertec® V350, Innershield® electrode, no gas

Globular transfer is exhibited in an example of pipe cap pass welding by an inverter V350 and self-shielded flux cored electrode shown in Figure 7. The process stays mostly in the arc region above 13V building up a large droplet hanging at the bottom of the electrode, and occasionally it shorts briefly to transfer the molten ball to the puddle and returns to the arc region. The size and shape of the hot zone and its blue fringes usually indicate the equipment's ability to hold a constant arc length.

Advanced cross-plots
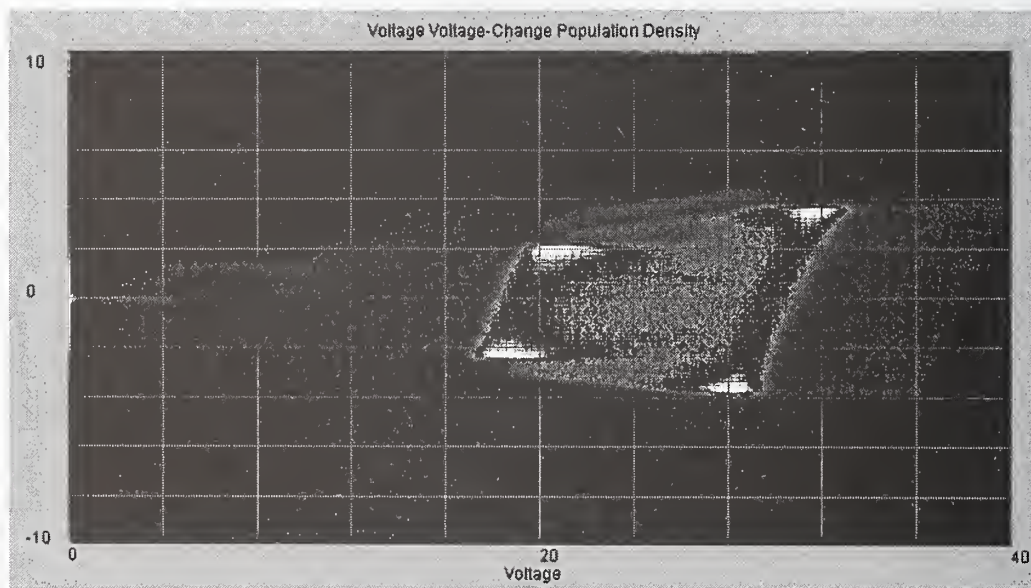
Figure 8: Pulsed spray transfer V-dV density plot from PowerWave 455, L-50 electrode, and 90% Ar+10% CO_2
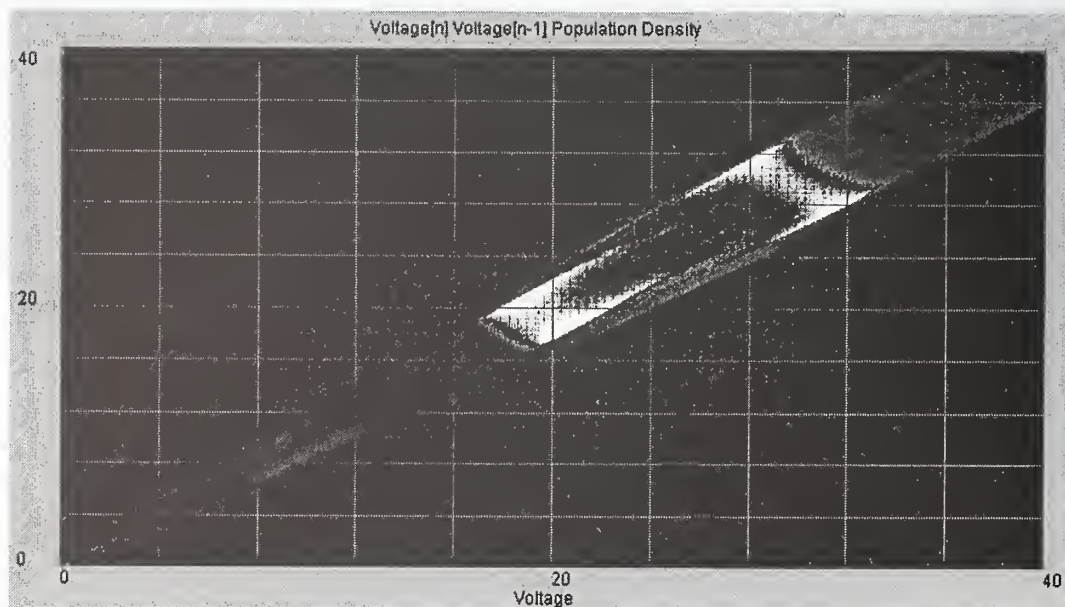
Figure 9: Pulsed spray transfer V(n) vs. V(n-1) density plot from PowerWave 455, L-50 electrode, and 90% Ar+10% CO_2

Figure 8 illustrates pulse welding in a voltage vs. time derivative of voltage image. Time derivate of voltage is useful in prediction of short-to-arc transition and droplet detachment. Figure 9 illustrates the same process in voltage vs. its immediate past. Comparing a signal to its past history can serve as a predictor of change. Figure 10 illustrates the same process in current vs. time triggered at 150A down-slope, where the fluctuation of the waveform including shorting response is clearly visible. Other graphs such as voltage-time graph, cyclical current period vs. voltage period can also provide insight into the arc welding process. Arc power, arc impedance and their time derivatives can also be used for plotting. In general, an arc signal passing through a digital filter with any transfer function, with IIR or FIR implementation in the Z domain, can be used as one axis or both axes in the plot. Digital image processing techniques can be applied to extract weld quality and arc stability. Unstable process tends to have an "out-of-focus" VI plot without high frequencies in its power spectrum. Segmentation, template matching and statistical pattern recognition can be used to distinguish a defective weld from an acceptable weld.

Figure 10: Pulsed spray transfer arc voltage vs. time density plot from PowerWave 455, L-50 electrode, and 90% Ar+10% CO_2

This paper is intended to provide an overview of using a voltage-current population density plot to characterize each arc welding process. Concepts for using this technique in analyzing process stability, power source and consumable dynamic performance characterization, procedure optimization, waveform development, weld defect identification, and fume and spatter estimation are evident but not explored in detail.

133

CONCLUSION

Voltage-current cross-plot histogram population densities of many arc welding processes are presented, including CV spray, CV short-circuiting, STT, pulsed spray, CC stick, AC sub-arc and globular transfer with tubular electrode. Image analysis tools can be employed to measure arc welding process stability from artificial image created by arc signals directly, their time derivates, or digitally filtered arc signals.

ACKNOWLEGEMENT

REFERENCES

1. Cook, G.E. et al. 1997. Statistical Process Control Application to Weld Process. IEEE Transactions on Industry Applications. Vol. 33. No. 2.
2. Quinn, T.P. et al. 1999. Arc Sensing for Defects in Constant-Voltage Gas Metal Arc Welding. The Welding Journal. September 1999. 322s-328s.
3. Siewert et al. 1993. Sensing of Gas Metal Arc Welding Process Characteristics for Welding Process Control. United States Patent 5,221,825.
4. Crane, B.L.; Kilty, A.L.; Ludewig, H.W.; Jones, B.A. 2001. Method and apparatus for monitoring weld quality, United States Patent 6,184,491.
5. Lucas, W.; Tapp, J. 1998. Development of a PC based system for monitoring arc welding parameters. Research Report 88264.01/97/966.3. The Welding Institute.
6. Ivkovich, S.P., Noch, R.F. 2000. Automated Verification of Complex, Manually Welded Production Assemblies. Gas Metal Arc Welding for the 21st Century Proceedings
7. Hsu, C. 2002. Monitor for Electric Arc Welder. United States Patent 6,441,342.
8. Barborak, D.; Conrardy, C. 1998. Monitoring of Weld Quality During Thin-Sheet GMA Welding. Cooperative Research Program Summary Report SR9806. Edison Welding Institute
9. Simpson, S.W. 2001. Weld Quality Measurement. United States Patent 6,288,364.

NETWORK COMMUNICATIONS FOR WELD CELL INTEGRATION—
STATUS OF STANDARDS DEVELOPMENT

W.G. Rippey**

ABSTRACT

Network technology is being used more and more to replace direct-wired links to integrate equipment components of automated and semi-automated welding systems. The standardization of device-level network technology, and the gradual appearance of network capable welding devices, means that users and integrators are facing the challenge of using networks for the first time, or of choosing one among multiple kinds of networks. A survey of network technologies currently being used for welding products is presented. Two formal welding standards efforts, one by the American Welding Society (AWS) A9 Committee and one by the Open DeviceNet Vendor Association (ODVA), are described. An effort by the Robotics Industries Association (RIA) in sponsoring general purpose network standards for robots is described. Examples of non-standard uses of device-level networks in welding products are given.

The AWS A9 committee can gather experts to express the needs of vendors, integrators, and users, and if appropriate develop standards that will reduce the number of diverging choices to be made.

This paper should be useful to users and integrators of weld cells to evaluate the different network technologies available for implementing welding systems. It may also help device developers make decisions about which technology to adopt, or it may suggest new welding areas where networks can be employed. The goal of standards efforts is to make a common communications solution available for new products and new systems, allowing vendors to provide compatible component products to integrate. Standards can also ease the burden of system developers who currently spend significant effort designing custom protocols or point-to-point interfaces.

KEYWORDS

CAN bus, A9.4, Ethernet, networks, high level protocol, weld cell integration, robotic welding, automatic welding, standards

INTRODUCTION

Networks are being used in many industries. Go to any network web site (Ref. 1-9) and see their "applications". You won't see welding. But there are welding products that use network technology and their numbers will probably increase.

What is network technology? One view is of the physical interfacing connections. To integrate products of different vendors, current methods use the connectors like those in Figure 1. Use of networks would use a single type of connector and cable on all devices. Each networked device has its own input/output circuitry for processing a transducer signal, and embedded software to participate in the network protocol. Instead of using one wire per control signal conveyed, a network uses a digital message with parameters that are configured in software. What is the

---

benefit from using networks? The main benefit is easy connection of a wide variety of devices for real-time control. Wouldn't it be efficient to easily cable together a robot, power source, and a laser vision system with a single connector and cable style and then configure some software parameters to have them work together to weld ship joints?   And networks make possible the exporting of data from within cells and devices for use by computer controllers and/or human monitors, and even internet processes.
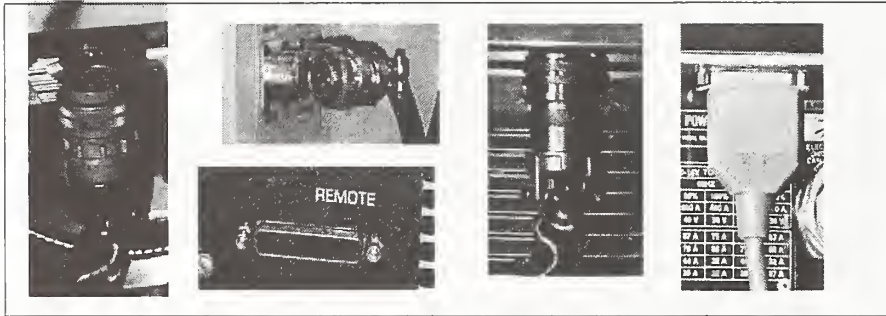

Figure 1. Multiple connector and cable types found in a welding cell.

Weld Cell Integration – the Technology is Changing

Figure 2 shows the point-to-point connections, typical of a non-networked weld cell. The legacy of point-to-point connection can be represented by an AWS standard, *Guide for Components of Robotic and Automatic Welding Installations, D16.2-2001.*   It describes a 37 pin cable and connector that connects a cell or robot controller to a power source. Each wire conveys binary interlock or 0-10 volt analog signals to and from the power source.
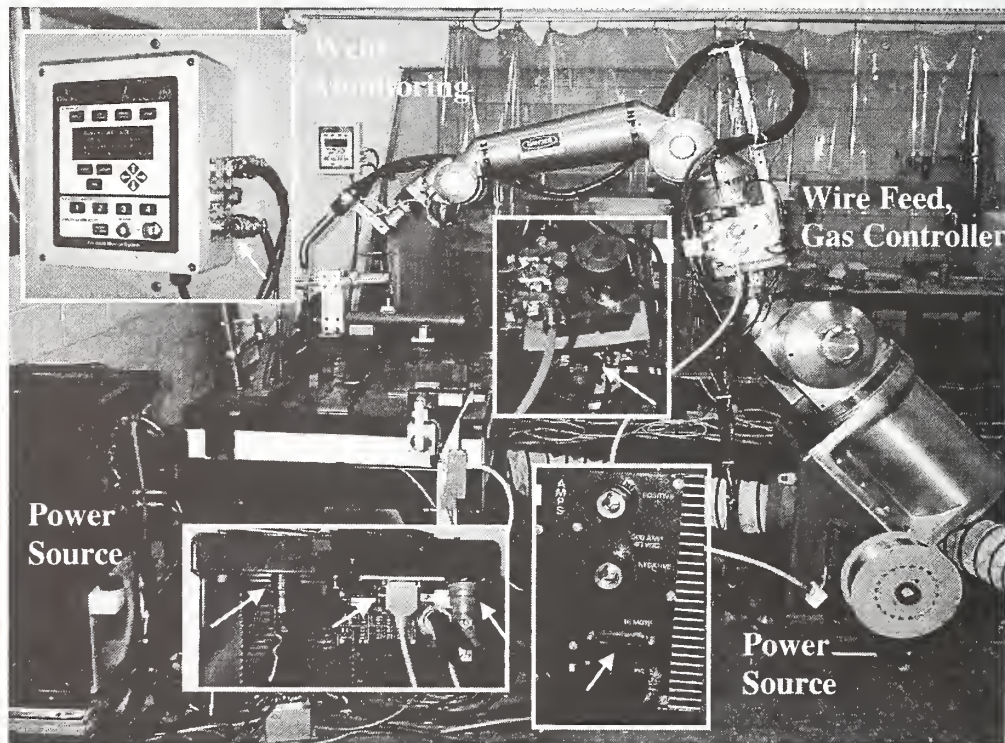
Non-standard interfaces

Figure 2. Opportunities for network connections in a weld cell.

Development of Networks in Other Industries

Several industries are moving forward with comprehensive formal standards for their applications. Table 1 shows a few of them. Their approaches take a broad look at the communications needs for multiple devices that work in integrated units.

INDUSTRY	STANDARD
Semiconductor manufacturing	SEMI E4, E5, 54-0997, IPC 2500
Motor vehicle control	SAE J1939, J1708 (heavy equipment), LIN
Building HVAC and control and monitoring	BACnet, LonTalk (EIA 709.1)
General purpose interface to robots	RIA R15.04 Committee Drafts
Packaging	Leverages device standards of e.g. CAN, Profibus, Ethernet/IP, DeviceNet
Process Instrumentation	HART

Table 1. Comprehensive Industry Standards

Some standards have narrower scope and define standards for specific devices. Examples are shown in Table 2. These efforts define the characteristics of individual devices within the framework of an established general-purpose network specification.

APPLICATION	NETWORK
Bar code readers	CAN based, Profibus, Ethernet, …
Weaving machines, extruder downstream devices, asphalt paver, diesel locomotives	CANOpen
Lab devices, water treatment	Profibus, Profinet
Coal Mining	Australian project using Ethernet/IP
Components of petrochemical, refining control	Foundation Fieldbus
Pneumatic vales, AC/DC drives	SDS, DeviceNet, Profibus
General purpose devices: Analog IO, binary IO, motion control, valves, photo sensors, proximity sensors, temperature, pressure, limit switches, motor drives	Most field buses

Table 2. Standard Application-Specific Devices

Most industries use generic component-level specifications defined in device-level standards. These specifications define standard interfaces to binary and analog input/output (I/O), proximity switches, limit switches, photo sensors and encoders.

How much is welding control like other applications? Can current networks meet the requirements of welding? Table 3 shows analogies between current standard network devices and welding devices. Many simpler welding devices fit well with models used in other industries. The more complex devices will need welding-specific models but still fit the performance guidelines of existing networks well. The most challenging welding application for networks is the coupling of torch positioners (including robots) with adaptive control processes like thru-arc tracking, or with real-time vision sensors that "see" weld joints and report

parameters as the torch is moving. The devices involved are fairly complex, with rich data sets needed for configuration and control. Data rates must meet the needs of torch positioning to produce good welds while adapting to changing sensor parameters.

Welding Component	Standardized Network Device
Clamp, wire snipper	Binary actuator
Part positioner	Motion controller
Switches, optical and proximity sensors	Switches, optical and proximity sensors
Power source	Analogous to position/motion controller
Robot or cell controller	PLC or cell controller
Sensor driven torch positioning system	Coordinated multi-axis motion control

Table 3. Standard general purpose networked devices and similar welding components

WELDING CELL ARCHITECTURE

Opportunities for Networks Inside Welding Cells

The interfaces shown as lines in Figure 3 can be implemented using network technology. Additional devices could include safety sensors, clamps, wire snippers and manual switches. The power source could be a controller for some of the devices, or a robot or PLC could be used. The primary issue for standardization is, are there useful generalizations of each device type that can be used as a standard device profile so that products from different manufacturers will respond the same to network messages, and perform the same functionality.   An important vendor concern about standards is that they must also accommodate use of unique device features.

Issues for Welding Component Developers and Integrators

At this time there are very few commercial network-capable products, and no formal welding standards.   There is no network technology that dominates in number of available welding devices, and thus no obvious preference expressed by users.   Component developers and integrators must risk choosing a network technology with no guarantee of future availability of more devices.   In many cases they develop their own network capable devices instead of buying them, and in some cases invent new protocols. Regarding choice of network technology, in some cases where different networks have similar data rate and message properties, gateways can be used to translate messages back and forth. This can ease the integration effort. Some current standard network pairs can by linked by off the shelf gateway products.

There are few off-the-shelf welding devices that come network ready. Some companies develop their own interfaces and protocols because of this. An example is a maker of automated pipeline welding systems that uses basic Controller Area Network (CAN) bus technology with a proprietary high level protocol for their in-house developed components (Ref 11). Standards, and products that conform to them, could have reduced their integration effort. They got their system running with a simplified protocol while the standards situation is not well defined, but will have to develop their own compatible devices. Standards can help pursuade component vendors to implement network interfaces because conformant products are guaranteed to be compatible.   Developers within each industry are looking to implement the smallest set of

network choices to make their products attractive in the market, where there isn't and probably won't be a single dominant network technology.
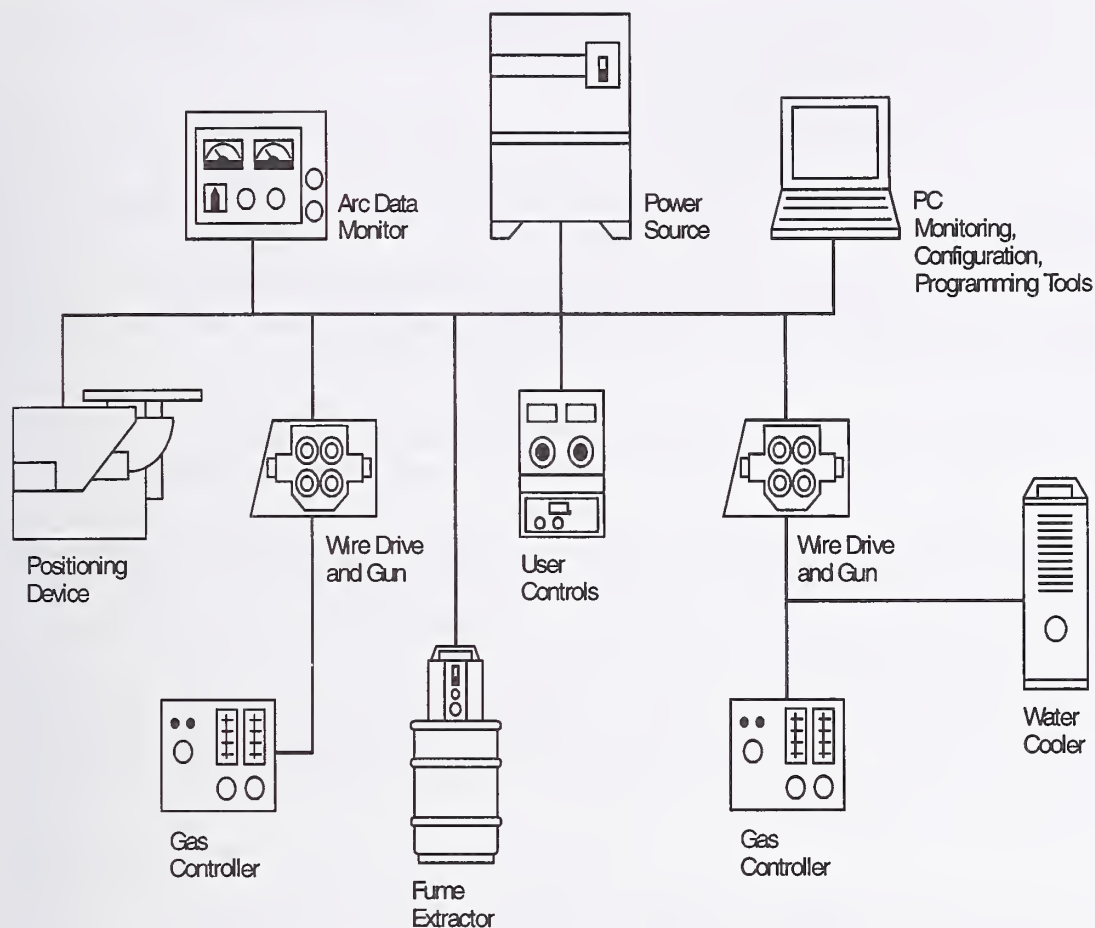
Figure 3. A sampling of welding components interconnected within an automated cell.

CURRENT COMMERCIAL NETWORK TECHNOLOGY FOR WELDING

There are three broad layers of network technology that are targets of standardization. The *Packet layer* defines cable, connectors, and electrical signals, and raw packets of data. The *High Level Protocol* (HLP) defines the formatting and meaning of packets and how they are routed, and general definitions of device and data types. The *Device layer* describes very specific application-dependent devices, their internal information, and their functionality in response to HLP messages.

Non-Standard Network Interfaces

Table 4 shows examples of welding products that implement network technology, but do not implement standard, formal public specifications. The packet layer and HLP used are usually formal standards, but the device layer is defined by vendor specifications.

PRODUCT	NETWORK TECHNOLOGY
Wrist interface, resistance welding controller, resistance weld monitoring, welding robot (for IO), power source	DeviceNet, InterBus
Resistance welding controller	Profibus, ControlNet
Power source	CANOpen, Ethernet with proprietary protocol
Pneumatic valves, AC/DC drives	SDS
Automated pipeline welding system (Ref 11)	CAN bus with proprietary protocol
Wire feed, gas controller, power source	CAN Bus with proprietary protocol

Table 4. Examples of welding products with non-standard interfaces

CURRENT FORMAL WELDING STANDARDS EFFORTS

There is one formal public standard for welding devices that encompasses the device layer. The InterBus-S *Weld-COM-Profile C0 Welding Controllers* [Ref 5] specifies 16 bits of command data and 16 bits of status data. The remainder of the 4 byte interface is allocated to manufacturer data. This narrow scope interface may not support modern power sources. There are two projects underway to develop complete interoperable public specifications, by the American Welding Society (AWS) and the Open DeviceNet Vendor Association (ODVA). Both techniques use the CAN bus and protocol for conveying messages, but they differ in their scope and the details of their application level protocols. Both techniques use 5 wire cables that include 2 wires for DC power. There are also variations in physical cable specifications and the electrical characteristics of signals.

The American Welding Society develops public standards for a wide variety of welding products and processes. The resulting standards are called "American Standards" because the development procedures are proscribed and monitored by American National Standards Institute (ANSI). Participants in AWS standards activities can be any interested and qualified person. The AWS project, *A9.4 Specification for Data Structures and Protocols for the Exchange of Intra-cell Welding Information,* specifies a device-level network for integrating welding components such as power source, wire feeder, gas controller and positioner. Figure 3 comes from the A9.4 document. A9.4 uses the standard CAN specification (ISO 11898) for the bus access arbitration and message encoding. A9.4 defines services implemented using network messages, and ways to define the devices that use the network. It also specifies the descriptions of welding devices in terms of attributes and services that can be accessed. A9.4 is an ongoing project and should be published in 2004. AWS also has a committee on Robotics, called D16, which could sponsor robot-related specifications.

ODVA is a controls and networks industry vendor organization (Ref 5). It sponsors the DeviceNet and Ethernet/IP specifications for networks. Participants must be members of ODVA. The DeviceNet specification contains several general purpose devices, with provision for Special Interest Groups (SIGs) to develop further refinements of device profiles for specific applications. The Arc Welding SIG is working on a DeviceNet profile and IO addressing scheme for an arc welding power source. The network view of the power source includes status of lower level devices but no control of them. The interface would be used by a robot controller

or cell PLC to configure welding parameters, command arc on/off, purge gas, and to assess status like voltage and current, arc-started and faults. The scope of this spec is "looking into" the power source from supervisory control. The A9.4 scope covers the interfaces to devices typically "seen" by the embedded real-time controller of a power source or PLC. A network configuration using both specifications would be a DeviceNet interface conveying commands to the integrated power source, possibly from a robot controller, and the internal controller of the power source connected to the wire feeder and gas controller using A9.4.

A standards effort that could affect welding systems is the Robotics Industries Association (RIA) R15.04 Communication and Information Committee (Ref 12). RIA is a North American trade group formed to serve the robotics industry. R15.04 is working on general purpose interfaces to robot controllers, using Ethernet, for functions including controller boot up, configuration, file transfer, status reporting. The committee has begun by choosing among the wide list of current services and defining standard data sets for robots, rather than developing new communications protocols. The effort will eventually address real-time control issues. The specification could eventually apply to welding robotics.

What Organizations Would Sponsor Formal Welding Network Standards?
Specifications for welding devices could remain as informal vendor-developed or corporate versions that could be quite useful to users and integrators of welding systems. However formal standards can produce greater market effect and lead to wider adoption of networks in welding. The most common candidate technologies come from industry associations that represent network technology segments or specific industries. The A9.4 document is an exception to this trend, and AWS, as an American national standards organization, is the sponsor of the standard. AWS standards are eligible for International Organization for Standardization (ISO) consideration, but no plans are yet made for A9.4.

Industry association specifications are often adopted by national, regional (e.g. European), or international organizations. The most likely protocols for welding devices are: DeviceNet, Ethernet/IP, ControlNet, Profibus, CANOpen and ModBus. DeviceNet (EN 50325-2:2000), CANOpen (EN 50325-4:2002) and parts of Profibus have been adopted by the European organization CENELEC (Ref 8), and by International Electrotechnical Commission (IEC). It could be expected that welding device specifications would also follow this route. CENELEC's network committee would be Technical Body CLC/TC 65CX (Fieldbus). From their mission statement: "CENELEC, the European Committee for Electrotechnical Standardization, was created in 1973. CENELEC is a non-profit technical organization set up under Belgian law and composed of the National Electrotechnical Committees of 20 European countries. CENELEC's mission is to prepare voluntary electrotechnical standards that help develop the Single European Market/European Economic Area for electrical and electronic goods and services by removing barriers to trade, creating new markets and cutting compliance costs."

The IEC is an international organization that works with CENELEC and ISO to jointly develop documents. IEC prepares and publishes international standards for all electrical, electronic and related technologies. The IEC group that would develop welding network specs would be TC65 (Industrial Measurement and Control), SC 65C (Digital Communications) or SC 65B (Devices). The ISO branch is TC 184 (Industrial Automation Systems)/SC5 (Communications and Architecture).

SUMMARY

Network capable products are used in manufacturing, process control, and transportation industries extensively. Network implementations for control seem to be yielding the advertised benefits of easier integration, ability to convey data outside of cell limits, more reliable operation than point-to-point, and possible wider marketing opportunities for smaller equipment vendors. A few networked products for welding are available: some use proprietary protocols and some leverage public standard networks, complemented by vendor-defined device profiles. It is likely that the welding industry could benefit from more extensive use of networks for device control, with standards helping to guide component vendors and system integrators in narrowing the choice of network to use among the wide variety available.

There are currently two formal network standards efforts for welding specific devices. There are more non-formal public and proprietary implementations, which may make their way to the formal public standards arenas. AWS supports the "A9.4" effort and can serve as a forum for interested users, vendors and integrators to work together.

REFERENCES

1. ARCnet Trade Association, http://www.arcnet.com.
2. ASHRAE SSPC 135, sponsor of BACnet. http://www.bacnet.org.
3. CANOpen, http://www.canopen.org.
4. Foundation Fieldbus, http://www.fieldbus.org.
5. InterBus, http://www.interbusclub.com/en/doku/index.html.
6. Modbus, http://www.modbus.org.
7. Open DeviceNet Vendor Association (ODVA), sponsor of ControlNet and Ethernet/IP – http://www.odva.org.
8. Profibus, http://www.profibus.org
9. Smart Distributed System (SDS), http://content.honeywell.com/sensing/prodinfo/sds/.
10. European Committee for Electrotechnical Standardization (CENELEC), http://www.cenelec.org.
11. IPC website for semiconductor manufacturing specifications, http://www.ipc.org/html/fsstandards.htm, and http://www.gencam.org.
12. "Men and Machines Set New U.S. Pipeline Productivity, Quality Record". *Welding Design and Fabrication Monthly*, Nov. 2002, Penton Media Publisher. Article available at http://www.appliedwelding.com/arcs_in_action/arc1su02.html.
13. NIST/RIA Open Architecture Workshop, http://www.isd.mel.nist.gov/projects/openarch. RIA R15.04 Chairman Jeff Fryman, (734) 994-6088, jfryman@robotics.org, http//:roboticsonline.com.
14. Sink, Perry, "A Comprehensive Guide to Industrial Networks", June 2001, *Sensors Magazine*, http://www.sensorsmag.com/articles/0601/28/index.htm
15. AWS A9.4, working draft 8. *Specification for Data Structures and Protocols for the Exchange of Intra-cell Welding Information.*
16. Balfour, Chris, Smith, Jeremy, "Controller Area Network (CAN) Applied to Welding Systems", Proceedings of Welding Technology Institute of Australia, 50th Annual Conference, Melbourne, Australia, August 2002.

Commercial equipment and materials are identified in order to describe certain procedures. Such identification is not intended to imply recommendation or endorsement by the National Institute of Standards and Technology, nor is it intended to imply that the materials or equipment identified are necessarily the best available for the purpose.

Network Communications for Weld Cell Integration

## *Status of Standards Development*

Bill Rippey

NIST

william.rippey@nist.gov

Network Standards for Welding Capsule

- Use of networks for manufacturing is increasing, including for welding

- Approaches vary; *proprietary, ad-hoc, standard's* formal public welding standards that exist are under development

- Benefits enhance efficiency and effectiveness of connecting welding manufacturing components

Outline

- Welding as an Application for Networks

- Network Concepts

- Welding Standards Efforts

- Summary

Automation, semi-automatic welding
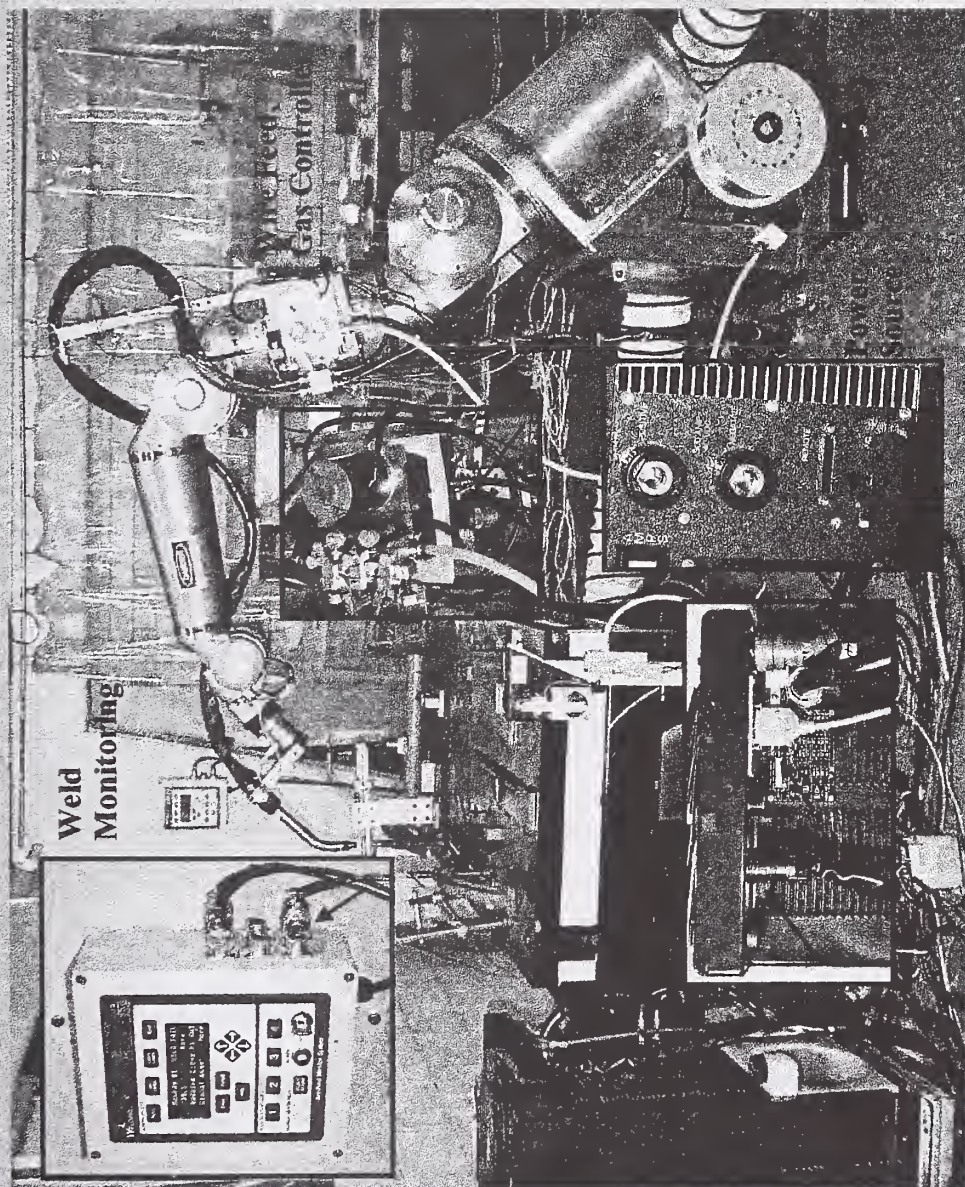
Benefits

- Simplify cabling
- Easier integration
- Multi-vendor choices

147

AWS D16.2-94

Interface, controller<->welding equipment

IWES Cmd (0-10v)

Current Cmd (0-10v)

Weld Voltage (0-10v)

Arc On Signal

Gas On Signal

Arc Failure Input

Trig Wire Forward

AVC Isolation Control Enable

AVC Isolation Control Enable

Contact Tip to Work Open

AWS D16.2 Connector A, Pins

Controller to Welding Machine
June 1995
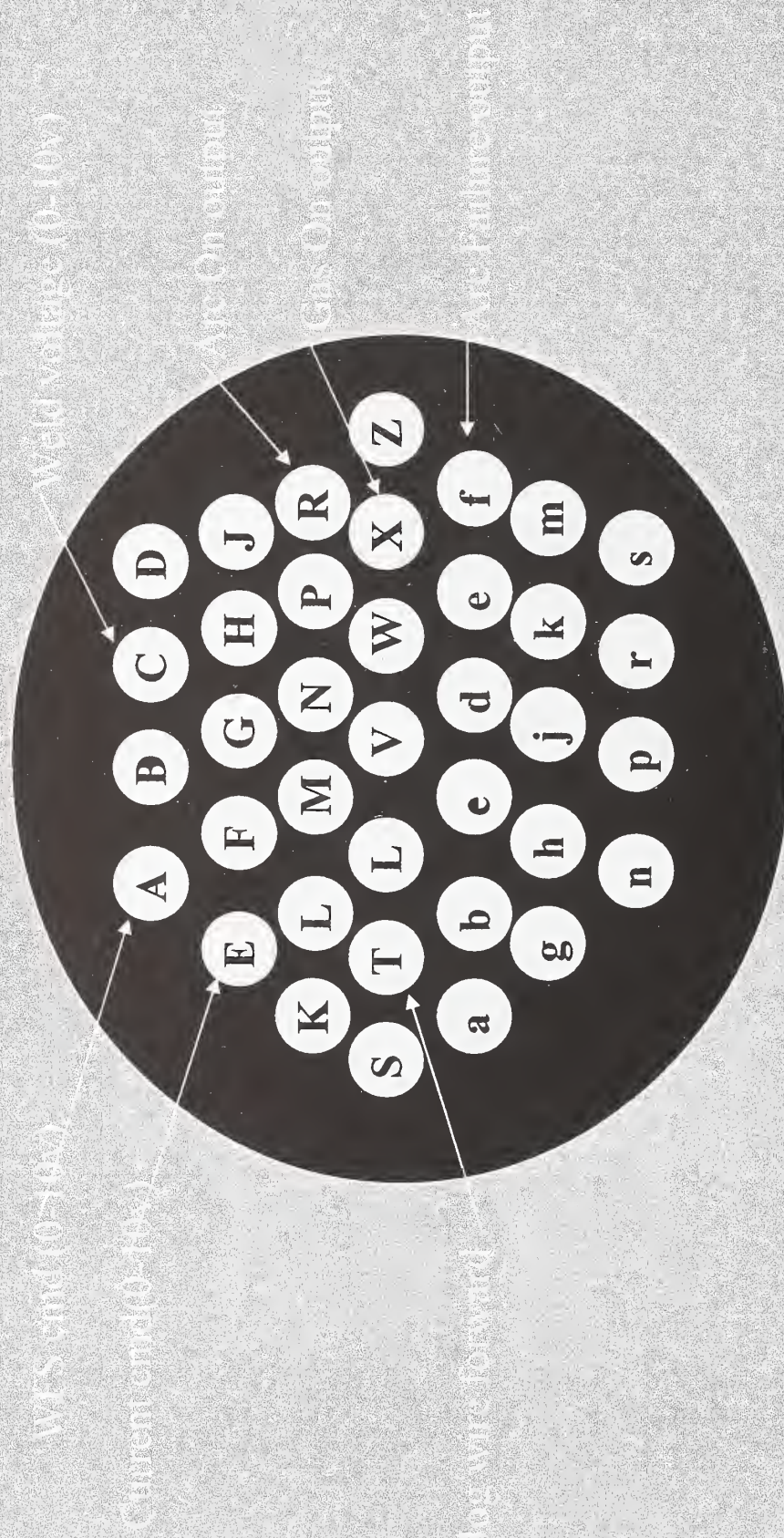
Factory Communications Architecture

Factory Control
And
Monitoring

Controllers

Devices

Internet
Server

Weld
Monitor

Power
source

Robot
or
PLC

Positioner

Gas
Controller

Power
source
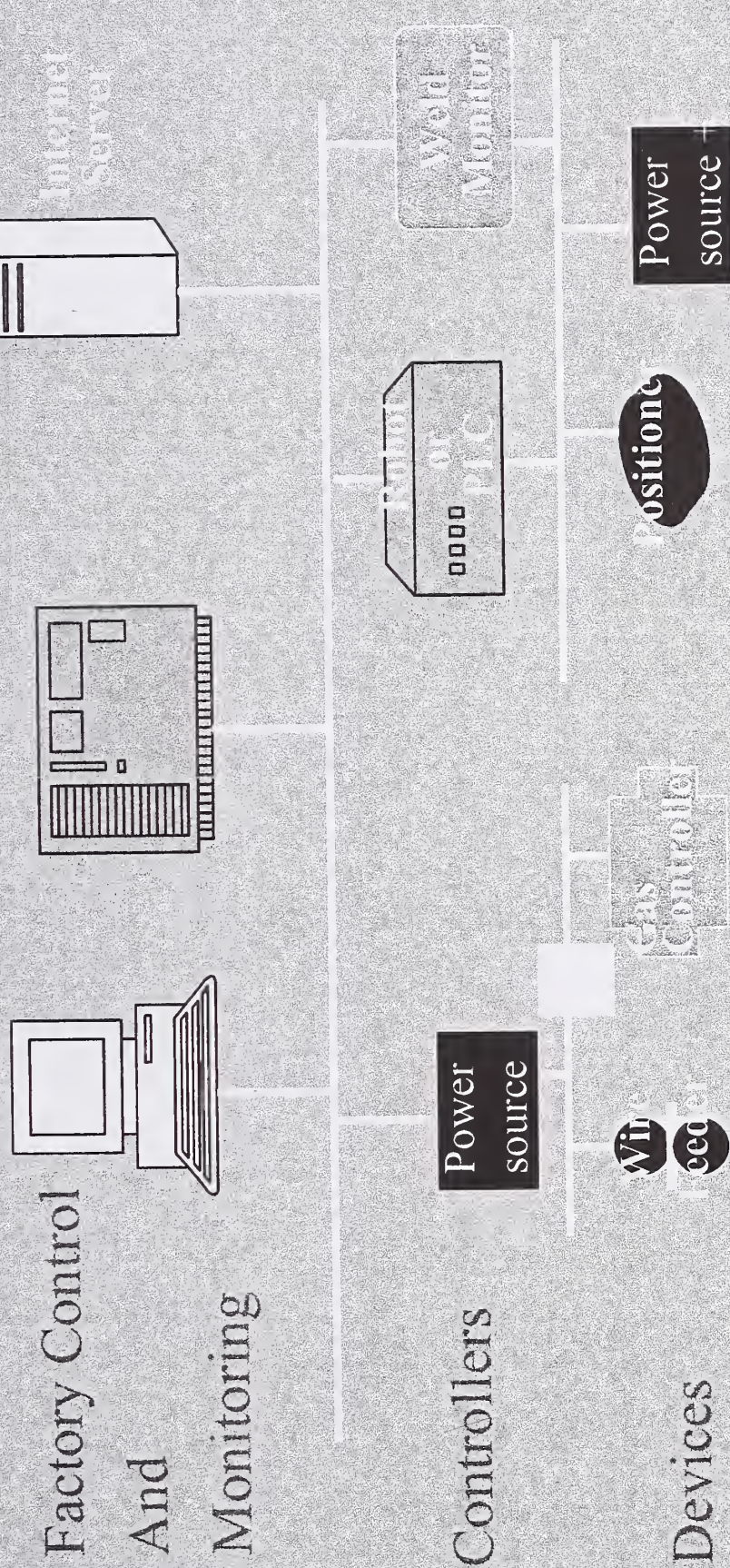
Wire
Feeder

Network Concepts

- Network Structure (layers)
  - *Proprietary implementations*
  - *Ad hoc standard implementations*
  - *Formal Standards*

Wire Drive Object

#	Name	Description	Units
512	Motor command	Motor ON/OFF	BOOLEAN
513	Set Wire Feed Speed	WFS	mm/min
514	Motor Direction	Wire direction	BOOLEAN
527	Cold Inch feed rate	WFS for cold inche	mm/min
528	Cold Inch Command	No current wire feed	BOOLEAN
.....		...	

Device Specific - device models, description of functional interactions

e.g. wire feeder, I/O module, power source

High Level Protocol - packet formatting, routing, message meaning, services

e.g. DeviceNet, Ethernet/IP, Profibus

Physical - medium, medium access, connections, plus raw packets

e.g. CANbus, Ethernet

Proprietary Networks

Device Specific - device models, description of functional interactions

High Level Protocol - packet formatting, routing, message meaning, services

Physical - connections, media access, plus raw packets

Standard

e.g. wire order, I/O table, power state

e.g. DeviceNet, ControlNet, Ethernet/IP, Profibus
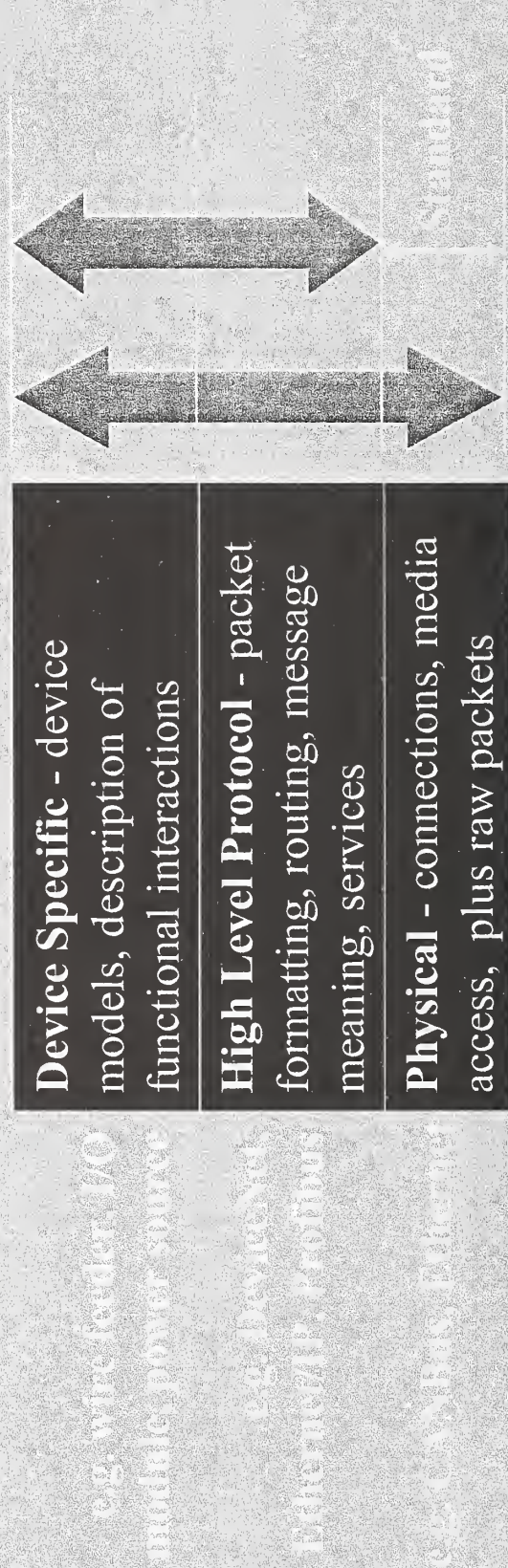
e.g. CAN bus, Ethernet

Proprietary Network Examples

- AMET cell integration using CAN bus

- CRC-Evans Automated pipeline welding system

153

Ad-Hoc Standard Networks
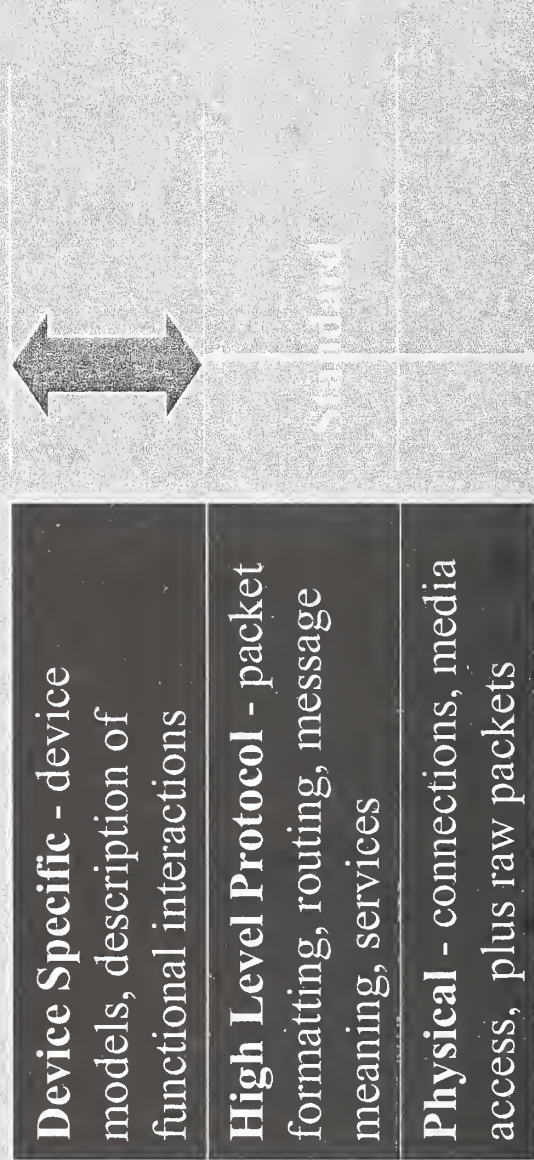
Device Specific - device models, description of functional interactions

High Level Protocol - packet formatting, routing, message meaning, services

Physical - connections, media access, plus raw packets

Ad-hoc Network Products

- Resistance welding controllers -> DeviceNet, Profibus, ControlNet
- Robotic quick change interface -> DeviceNet
- Power source with Profibus, Ethernet/IP, Modbus, CANopen, SDS, Interbus, LON, FTT
- Wrist interface, resistance welding controller, resistance weld monitoring, welding robot (for IO), power source -> DeviceNet, InterBus

Standard Specifications

Device Specific - device models, description of functional interactions

High Level Protocol - packet formatting, routing, message meaning

Physical - connections, media access, plus raw packets

AWS A9.4 Standard Project

A9.4 Scope

PC
Monitoring,
Configuration,
Programming Tools

Power Source

Arc Data Monitor

User Controls

Wire Drive and Gun

Wire Drive and Gun

Water Cooler

Gas Controller

Gas Controller

Fume Extractor

Positioning Device
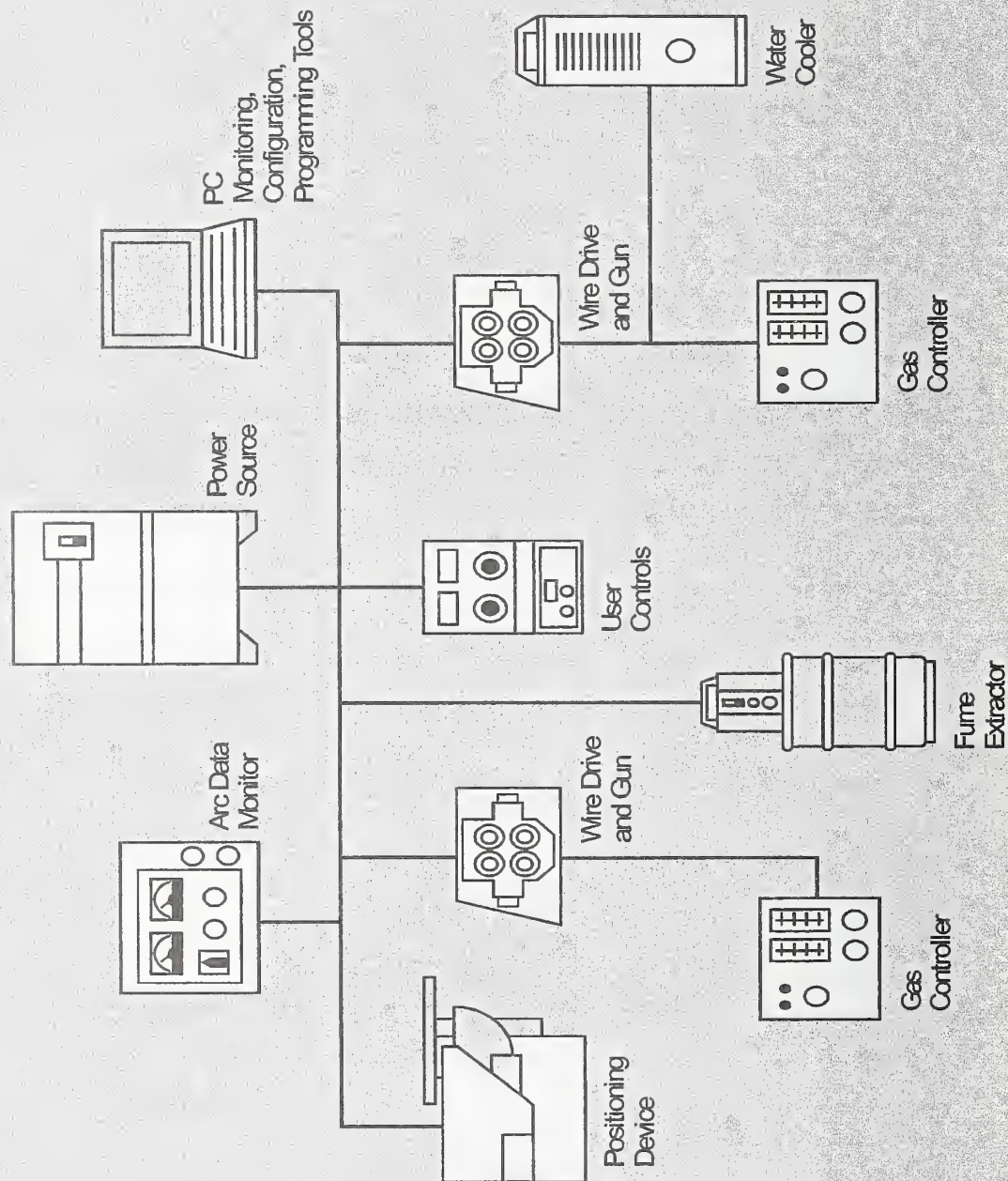
AWS A9.4 Project

Gas Controller Object

#	Name	Description	Value semantics	Req	Class	Type
512	Gas Command	Command input	0: OFF 1: ON	Y	Sequence controlled command	BOOLEAN
513	Total gas flow rate	Commanded rate	None	Y	reference	SINT2
514	Actual flow rate	Measured flow	None	N	signal	SINT2
521	Gas 1 command	Command	0:OFF 1: ON	N	Reference	BOOLEAN
521	Gas 2 command	Command	0:OFF 1: ON	N	Reference	BOOLEAN
532	Actual Gas 1 percentage	Measured percentage	None	N	Signal	UNIT2
533	Actual Gas 2 percentage	Measured percentage	None	N	Signal.	UNIT2

AWS A9.4 Project

Wire Drive Office

#	Name	Description	Value semantics	Req	Class	Type
512	Motor Command	Command input	0: OFF 1: ON	Y	Sequence controlled command	BOOL
513	Set WFS	Command	None	Y	Reference, Sequence controller	UINT2
514	Actual WFS	Measured WFS	None	N	Signal	UINT2
524	Positive polarity	Selects positive or negative electrode polarity	0: electrode neg 1: electrode pos	N	Configuration	BOOL
528	Cold inch command	Input to jog wire	None	Y	Command	BOOL

160

DeviceNet Arc Welding SIG

- Cell controller interface to power source
- Object model of integrated power source
  - Welding Object
  - Weld Schedule Object
- New services defined
  - Read Procedure Details
  - Weld Procedure Search
  - Read ArcLink Attribute
  - Write ArcLink Attribute

Computer Technology in Welding
June 2000

Welding Object Attributes (51)

- Welding Trigger, Workpoint
- Weld Mode, Gas Command
- Strike WFS, Restrike WFS, Arc Detect, Wire Touch
- Gas Fault, Wire Fault, Wire Stick
- .....
-

Weld Schedule Object

- Specifies 15 phases of a weld sequence

  - Idle, Setup, Gas Preflow, Strike, Start, Upslope, Weld1, Weld2, Downslope, Crater, Burnback, Gas Postflow, Restrike, Fault.

  - Each phase has many parameters that can be set.

German DVS CANOpen Project

- Cell controller interface to power source

- Progress interrupted by lawsuit over patent

- Players were SKS, Siemens, Schneider…

Leveraging IT Standards to Integrate Robots into Factories

- RIA R15.04 Communications and Information Committee
- Networking standards for robot controllers
- 3 wave approach
- Jeff Fryman, RIA, (734) 994-6088, jfryman@robotics.org http://roboticsonline.com

Acknowledgement: These slides come from Fred Proctor who is a member of R15.04

http://www.isd.mel.nist.gov/projects/openarch/

Wave I - Definition From January 2001 Meeting

- Expressed in RIA 15.04-TR.1 2003 Technical Report

- Key Points
  - FTP
  - TCP
  - IP
  - 802.3 10BaseT

Wave 1 Networking Standards:
Features and Functionality

Wave 1 Priority: Enable Basic UDC Capability

Spec	GM Robots Today	Wave I (Proposed)
	GRS-1	GRS-1 (Subset)
Application	FTP,DHCP,DNS	FTP
Transport	TCP	TCP
Network	IP, ARP	IP
Data Link	ANSI/IEEE 802.3	ANSI/IEEE 802.3
Physical	Cat 5 UTP	Cat 5 UTP
	10BaseT	10BaseT
	RJ 45	RJ 45 (Need Robust Connector?!)

RIA-NIST Open Architecture

Printed: 9/18/2003

Result - Successful Definition of Wave I Specification

Computer Technology in Welding
June 2003

166

Waves II and III Content, 2003

Wave II

- **Centralized Configuration**
- Remote address administration and determination, disaster recovery:
- Time synchronization (1 sec for File date/time)
  - DNS
  - BOOTP/DHCP Client
  - ARP
  - UDP/TFTP
  - NTP or others as appropriate

Wave III

- Network Management Capabilities
  - SNMP MIB-II
- Data Abstraction and Presentation
  - HTTP
  - HTML
  - XML
- Real Time Communication Over Ethernet
- Timing : Start after Wave II is agreed

Timing: 2003

SUMMARY

- Networks are pervasive in other industries, use in welding is increasing.

- There are a few formal standards developments, more "ad-hoc standard" and proprietary products.

- Benefits — easier integration, better capabilities?, possible opportunities for small vendors.

- Integrators and component vendors are looking to find which technology/technologies to implement.

- AWS supports the A9 formal standards effort.

End

- Bill Rippey
- 301-975-3417
- William.rippey@nist.gov
- Chairman of AWS A9 committee
- NIST

26

RIA 15.04 Chairman

- Jeff Fryman, RIA
- (734) 994-6088
- jfryman@robotics.org
- http://roboticsonline.com

Computers and Automation

A COMPUTER PROGRAM FOR CHOOSING WELDING PARAMETERS IN SPIRALLY WELDED PIPE PRODUCTION

Kahraman ŞİRİN, Mannesmann Pipe Company
Şule Y. ŞİRİN, University of Kocaeli
Erdinç KALUÇ, University of Kocaeli

Abstract: The main problem faced in the manufacturing of the pipe by SAW is the choosing of the process variables. Therefore, identification the effect of the process parameters and finding their limits are essential in order to get the required bead size and quality. Regarding with the pipe production, a computer program in Excel is developed to choose the welding parameters. This program is mainly based on the relation between welding parameters and weld bead size and quality.

Introduction: The principle of the spiral pipe production is simply the bending of the steel strip into cylindrical shape and ultimately welding edges together in two steps as inside and outside weld. The submerged arc welding (SAW) process is widely used for spirally welded pipe production. In this process, welding parameters namely welding current, arc voltage, weld speed, diameter of the wire, number of the electrodes, melt-off rates, edge joint design including bevel angle and root face, wire configuration and etc. are very effective on welding quality. All those parameters should be optimized to get satisfactorily weld quality. This computer program is developed to optimize welding parameters. The working steps of the program are given below in detail.

The working steps of the program:

After entering the diameter and wall thickness of the pipe to the program, it will be seen automatically permissible number of the electrodes, which can be used for inside weld. In spirally welded pipe production, there is only a very limited area to positioning the inner welding heads, when the diameter of the pipe is getting smaller. Therefore, the number of electrodes for inside weld should be limited in accordance with the diameter of the pipe.

Secondly, the program asks the required pipe production to define the main geometrical dimension of the weld. Penetration, width of the bead and height of the reinforcement are taken into consideration as main characteristics of weld by the program. Penetration, for both inside and outside weld, should be at least 60 per cent of wall thickness to provide good joint. Width of the bead should be as wide as to give enough surface area to the gases to leave easily to the weld pool.

As a third step of the program, the grade of the material is asked to give the lower and upper limits of the heat input. An increase in heat input could result in a wide heat affected zone (HAZ) with low impact strength. In spirally welded pipe production, high rates of welding speeds can be achieved by using multiple electrodes. In two-pass

SAW process, each pass (inside and outside weld) can be considered as one puddle even using multiple electrodes. Heat input for each pass could be calculated equation given below;

$$H_n = (f \sum_1^n I.E)/v$$

where, H_n is net heat input, I is welding current, E is arc voltage, v is welding speed, f is heat transfer efficiency and n is number of electrodes. Also, two-pass multi-electrode SAW process could be characterized by cooling time, which is around 50 seconds. Cooling time, between 800 to 500 °C, can be calculated by using Rosenthal's equations given below.

$$\Delta t_{8/5} = \frac{1}{4\pi c\lambda\rho}\eta 2 E^2 \frac{1}{d^2} F_2 \left(\frac{1}{500-T_0}\right)^2 - \left(\frac{1}{800-T_0}\right)^2$$

$$\Delta t_{8/5} = \frac{1}{2\pi\lambda}\eta\, EF_3 \left(\frac{1}{500-T_0} - \frac{1}{800-T_0}\right)$$

On the next step, user should define the joint preparation in conjunction with the wall thickness. Generally, Y or X type of joints could be used for thickness from 8 mm (see figure 1). The main purpose of joint preparation is to ensure required penetration. Here the main criteria are the angle of the bevel and the height of the root face. The bead width and depth ratio (W/D) should be between 1 and 4 to prevent hot cracking. Therefore, bevel angle should be bigger than 60°. This will also help not to having flux inclusions in the weld. The root face could be 60 per cent of wall thickness.

I type   Y type   X type
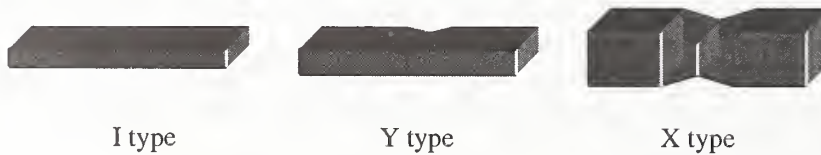
Figure 1. Type of joints

After definition of joint type, automatically the cross-sectional area of reinforcement and bevel are calculated in accordance with weld geometry design and type of joint. By this way, the cross-sectional area of the added filler metal in mm^2 is cleared. This is done for both inside and outside weld separately. After that, the program easily computes possible highest weld speed. As a last step of in this stage, the weld speed is chosen by the user according to permissible limits given by the computer.

174

Finally, the user should choose welding currents starting from the first head of the inside weld then second and third ones if necessary. Multiple arc welding usually consist of a DC(+) welding head on the lead arc followed by AC welding heads on trailing arcs. To define the current levels it is necessary to know the relation between current and wire melt-off rate. The below equations developed by *Chandel and Baya* could be used for predicting of the deposition rate of submerged arc welding process; where MR is melting rate in kg/h, I is welding current, L is the electrode extension and d is diameter of the wire.

$$MR_{DC(+)} = 0.010371.I + (2,2426 \times 10^{-6}.I^2.L)/d^2 - 0,462$$

$$MR_{DC(-)} = 0.016178.I + (2,087 \times 10^{-6}.I^2.L)/d^2 - 0,643$$

Measured wire feeding values, under various conditions, are plotted in Figure 2. It can be seen that actual values are closed to the theoretical values, originated from Chandel's equation (Table 1). There is around 5,5 % difference which is acceptable to make prediction about deposition rate.

Table 1. Comparison between actual and theoretical values about deposition rate.

#	Type of current	Current (A)	Wire diameter (mm)	Wire extension (mm)	Average feeding speed (m/min)	Calculated deposition rate (kg/hour)	Deposition rate acc. to Chandel (kg/hour)	(%)
1	AC	675	3,2	26	2,77	10,30	10,91	5,6
2	DC(+)	600	3,2	26	2,02	7,51	7,81	3,8
3	AC	460	3,2	28	1,87	6,94	6,81	1,9
4	DC(+)	750	4,0	26	1,59	9,26	9,37	1,2
5	DC(+)	550	4,0	26	1,05	6,09	6,34	3,9
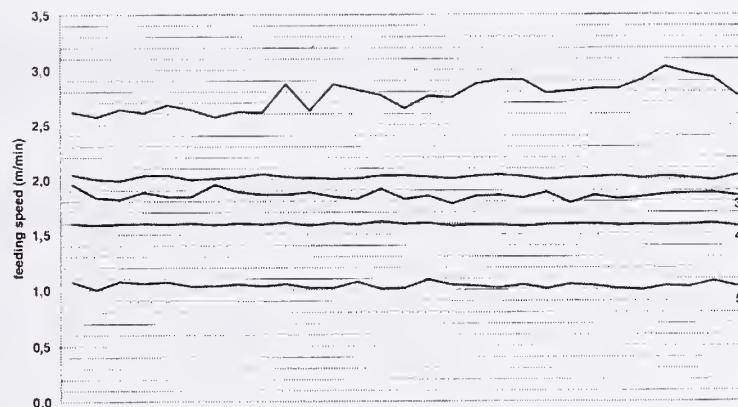
Figure 2. Wire feeding speed diagrams.

On the real work condition, another experiment is done to check the deposition rate. 1016 x 17,7 mm dimension pipe is produced under various conditions. The weld speed is changed while all the other electrical parameters, given in Table 2, kept constant. Geometrical dimensions are measured by taking samples from each step of the weld process. Then the real deposition rate is calculated (Table 3). Maximum 5,4 % difference is found in compare with the formula basis calculation. The sequence of the weld seam is given in Figure 3.

Table 2. Electrical parameters of 1016x17,7 mm dimension pipe.

	Inside weld			Outside weld		
	Current (A)	Voltage (V)	Wire diameter (mm)	Current (A)	Voltage (V)	Wire diameter (mm)
DC (+)	1100	30	4,0	1100	30	4,0
1. AC	850	30	3,2	750	30	3,2
2. AC	550	30	3,2			

Table 3. Electrical parameters of 17,7 mm wall thickness pipe

Weld speed (m/min)	Weld position	Cross sectional area of the added filler metal (mm²)	Cross sectional area of the reinforcement (mm²)	Cross sectional area of the weld bead (mm²)	Deposition rate (kg/hour)	Theoretical deposition rate for 26 mm wire extension (kg/hour)	%
1,80	Inside	48,22	23,51	145,52	40,10	28,47	4,2
	Outside	31,85	21,37	120,81	26,49	27,90	5,0
1,50	Inside	58,53	33,82	169,76	40,56	38,47	5,4
	Outside	39,89	29,41	153,11	27,64	27,90	1,0
1,20	Inside	72,46	47,75	195,63	40,17	38,47	4,4
	Outside	48,19	37,71	187,24	26,72	27,90	4,2
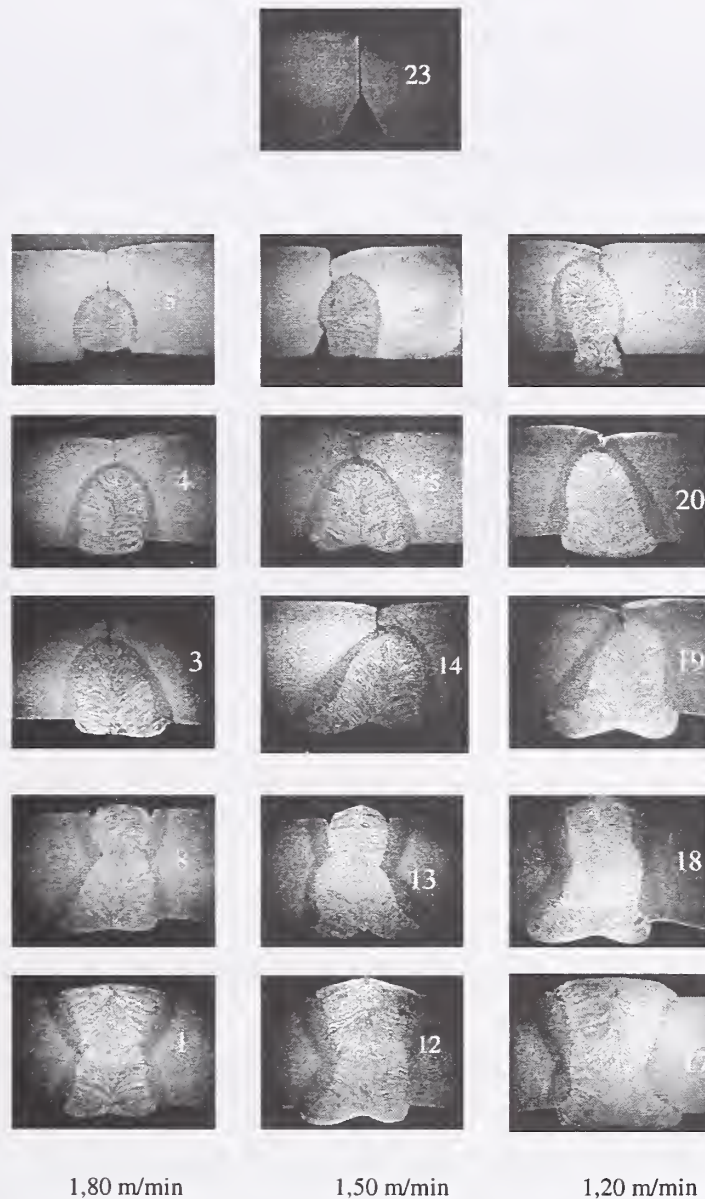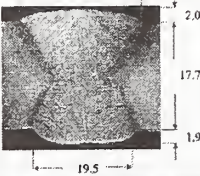
Figure 3. The sequence of the weld seam with the different weld speeds.
(Pipe dimension : 1016x17,7 mm Grade of the material : St 52)

After the choosing the welding current, the program automatically gives the diameter
of the wire, arc voltage, deposition rate, heat input applied to the material and cooling
rate. Also computer always checks the results and compare to the permissible values.
If the results are beyond the limits, immediately warning are sent o the user and also
blocked to the next stages of the program. A view of the program is given in Figure 4.

Figure 4. A view of the computer program.

| MANNESMANN BORU | | WELDING PARAMETERS | | 1016 x 17,7 mm |

Standart : TS 1997   Material : St 52   Y joint type   Inside weld   Outside weld

type of current	welding current (m/min) max 1,80	inside weld						outside weld						
		current (amp)	voltage (V)	wire diameter (mm)	wire extension (mm)	melting rate	heat input (J/mm)		current	voltage	wire diameter	wire extension (mm)	melting rate	heat input
DC +		1100	30	4,0	26	15,4			1100	30	4.0	20	14,3	
1.AC	1,80	850	30	3,2	28	15,0	2500		750	30	3,2	22	12,0	1850
2.AC		550	30	3,2	28	8,5								

References

- ASM Handbook, "Welding, Brazing and Soldering", Metals Handbook, vol.6, page 115-152, 1983

- Lincoln Electric Company, "The Procedure Handbook of Arc Welding", 13th Edition, Sec. 6, 1994.

- G.E.Linnert, "Welding Metallurgy" Fourth edition, vol.1, chapter 7, 1994.

- J.Tusek, "Mathematical Modeling of Melting Rate in Twin-Wire Welding", Journal of Materials Processing Technology 100, page: 250-256, 1999.

- R.S.Chandel, H.P.Seow, F.L.Cheong, "Effect of Increasing Deposition Rate on the Bead Geometry of Submerged Arc Welding", Journal of Materials Processing Technology 72, page: 124-128, 1996.

- M.Graf, K.Niederhoff, "Toughness Behavior of the Heat-Affected Zone (HAZ) in Double Submerged-Arc Welded Large-Diameter Pipe", Mannesmann Röhrenwerke.

- P.A.Peters, H.G.Frackmann, "The Manufacture of Spiral Welded Pipe with Integrating Quality Assurance" Mannesmann Röhrenwerke

METAL INERT GAS (MIG) WELDING PROCESS OPTIMIZATION FOR EXTRUDED (6063-T52) T-JOINT CONFIGURATION USING OTC/DIAHEN EQUIPMENT

R. Koganti, Zaluzec. M, Velez. J, Karas. C, Joaquin. A, Caliskan. A., and Wang. J.*

ABSTRACT

The prodcution of aluminum intensive vehicles requires the development of optimum manufacturing processes for the joining and assembling of lightweight architectures. These manufacturing processes not only have to provide cycle time viability but also need to maintain or surpass product safety and quality. T-joint configurations are an integral design used on front end structure structures, crash boxes, etc. used in hybrid aluminum vehicle architectures. The purpose of this study was to find optimum welding parameters for the welding of 6063-T52 aluminum materials in a T-Node configuration. The welding process factors considered were power input, pulse frequency, gas flow rate, torch angle, and arc intensity. A partial factorial design of experiment (DOE) was conducted to understand the effect of these factors on joint strength and weld geometry. All the welded T-Nodes were subjected to tensile, bending and shear testing as per the experimental matrix. Results showed power input as the most statiscally significant factor with an adverse effect on joint strength and weld geometry at high settings. In addition, a correlation between joint shear and tensile load to failure and weld throat was found. None of the MIG welding process factors showed any statistical significance on bending load to failure.

KEYWORDS

Metal Inert Gas Welding, Aluminum, Extrusion, Power Input, Pulse Frequency, Torch Angle, Gas Flow, Penetration, T-Nodes, Tensile Load, Shear Load, Bending, Heat Affected Zone, Depth of Penetration

---

INTRODUCTION

This study was developed to identify the influence of MIG welding process factors on weld strength and weld geometry on 6063-T52 extruded aluminum in a T-Node joint configuration (Figure 1). The welding system used in this experiment was an OTC/Daihen CPD-350 welding system (Figure 2) accompanied by a DR-4000 pulse power supply with a weld controller capable of handling a superimposed waveform ranging from 0-30Hz by the uses of a dual pulse wave controller. The ranges for power input (torch speed, voltage, current, wire feed); pulse frequency, gas flow rate, torch angle, and arc intensity were selected based on screening experiments of previous DOE's.

Post-weld analysis consisted of mechanical testing, weld geometry evaluation, and microhardness testing. Fifteen samples of each experimental run were subjected to tensile, shear and bending tests. One additional T-Node of each experimental run was used for metallographic evaluation and microhardness testing. Standard sectioning and mounting practices were used to prepare cross sections of the welds. Photomicrographs were obtained from mounted cross section samples. The same samples were used for weld geometry measurements (depth of penetration, throat, etc.) and for microhardness characterization. Weld geometry principal factors and microhardness were then correlated to input parameters and mechanical test results.

EXPERIMENT

The welding equipment process factors selected for this DOE were power input (torch speed, voltage current, wire feed), pulse frequency, gas flow rate, torch angle, and arc intensity. The extreme levels of power input, pulse frequency, gas flow, torch angle, and arc intensity are shown in Table-1. Argon gas (@99.9%), commonly used for aluminum MIG welding [1], was used as the shielding gas. The filler wire selected was a 1.2 mm diameter Al-4047 filler wire supplied by Alcotech. Other factors maintained constant throughout the experiment were lead push angle (20°), weld length (75mm), and wire stickout (15mm). A partial factorial DOE was conducted consisting of eight experimental runs as shown in the experimental matrix in Table 2 (Appendix).

The mechanical testing of the T-nodes was performed on the Tinus Olsen testing machine at The Automotive Safety Center. Fifteen samples of each experimental run were tested for joint load to failure under three different configurations: tensile, bending and shear loading. Specific geometry of the test specimen and the test loading conditions are shown in Figures 3-5. The crosshead speed was 10mm/min. For statistical analysis purposes, maximum joint load to failure was used.

Table 1. DOE-T1 Process factors matrix

Factor	Low Level	High Level	Unit
Torch Speed	635 (25)	1270 (50)	mm(in)/min
Corresponding Voltage/Current	21.5/150	25.3/220	Volts/Amperes
Pulse Frequency	10	30	Hz
Gas flow rate	0.71 (25)	1.27 (45)	m^3/hr (ft^3/hr)
Torch Angle	45	50	Degrees
Arc Intensity	Normal	Soft	N/A

DATA ANALYSIS

Joint Load to Failure

The typical failure mode was different for each test configuration (Figures 6-8). Under tensile loading, the failure occurred at both the welds and the heat affected zone. Under bending load, the majority of the failure occurred in the base alloy at the heat-affected zone while leaving the welds primarily intact after the test. Under shear load conditions, the failure occurred mostly in the weldment and at the interface of the weld and the heat-affected zone. Substrate/heat affected zone failure tended to give relative lower peak load as compared to weld/weld interface failure. Tensile, bending and shear data were used in the statistical analysis to evaluate factors influence on load to failure. The statistical significance of the welding factors was verified by an analysis of variance (ANOVA). The normal probability plots with a 90% confidence and main effect plots are shown in Figures 9-15.

The normal distribution plots showed that:

1. The interaction of power, torch angle, and arc intensity have 90% confidence statistical significance on joint load to failure under tensile loading.

2. No process parameters were statistically significant on joint load to failure under bending loading.

3. Power was the only factor with 90% confidence statistical significant on joint load to failure under shear loading.

The effects of the above mentioned welding factors on joint load to failure under tensile, bending and shear loading are shown in Figures 12-15. Power input had an adverse effect on joint load to failure under both tensile and shear loadings. The interaction of power input and torch angle suggested that the negative effect of high power input settings was even more pronounced at low

torch angle settings (Figure 15). Additionally, arc intensity showed a positive effect on joint load to failure under tensile loading.

WELD GEOMETRY

Transverse Weld Shape

One specimen of each experimental run was cross-sectioned into six segments. Two of those six segments consisted of cross-sections of the butt weld. The remaining four sections consisted of the cross-sections of the two transverse welds at one inch after the starting and one inch before the ending points of the weld (Figure 16).

Throat Length

The weld throat is defined as the area formed by the product of the weld length and the shorter distance from the intersection of the welded plates to (1) the straight line connecting the ends of the two legs formed or (2) to the weld bead surface, whichever is less [1]. Based on statistical data, power input was the only factor among the five considered that contributed to throat length. Power input at high settings tended to reduce the throat length by as much as 20% (3.36 to 2.72mm) - (Figures 17-18). Although throat area does not consider weld beads as part of its area, visual examination of the exterior of the specimens revealed concave beads for low arc intensity settings versus convex bead for high settings of the arc intensity.

Although in coupon configuration a direct correlation between throat length and joint load to failure was not attained, for T-Nodes, throat length was directly related to joint load to failure. Correlations of the averages of each experimental run and their corresponding joint loads to failure values under tensile and shear loading respectively were found with R-Square values of 51% and 82% (Figures 19-20).

Top and Bottom Penetration

Image Pro Plus software was used to measure the depth of weld penetration into the top and bottom aluminum substrates. The top and bottom penetration of the welds were measured by projecting perpendicular lines from the weld top and bottom legs respectively to the outermost point of penetration as shown in (Figure 21). Although power input, gas flow and arc intensity seemed to affect top penetration of the T-Nodes, they showed no statistical significance (Figure 22). On the other hand, bottom penetration increased as torch angle increased (Figures 23-24).

Although top and bottom penetration values described how susceptible the material was to melt under different input welding conditions, the shape of the resulting weld cannot be visualized by only knowing the magnitude of these values. In order to further describe the weld shape, top and bottom penetrations at the two specimens point of intersection was measured and correlated as a ratio to top and bottom maximum penetrations. The top ratio was referred to the ratio of the penetration at the point of intersection and the maximum penetration in the direction of the top (vertical) specimen, and the bottom ratio was referred to the ratio of the penetration at the point of intersection and the maximum penetration in the direction of the bottom (horizontal) specimen. Although power input did not show any input on top coupon penetration, it

contributed to a higher top ratio meaning that the weld shape maximum top penetration value tended to occur near the point of intersection of the two specimens (Figures 25-26). Conversely, bottom ratio decreased as power input increased (Figures 27-28).

T-Node Side and Measurement Position Relative to the Starting and Ending Points of the Weld

T-Node side and measurement position relative to the starting and ending points of the weld showed significance on the weld geometry. Although T-Node side position was not significant on weld throat, top section penetration was more pronounced at the first weld in the welding sequence (Figure 29). Also, measurements closer to the ending point of the welds showed more top penetration than those close to the starting points. On the other hand, bottom penetration showed a tendency to increase from starting to ending points and from first to second weld in the welding sequence (Figure 30).

Side and position showed minor effects on top ratio; however, T-Node side of the weld (first or second side of the welding sequence) affected the bottom penetration ratio in the way of an interaction with power input (Figure 31). For high power settings the ratio increased with side from first side to second side of the welding sequence, while for low power settings the effect was opposite, the ratio decreased from first to second weld.

HEAT AFFECTED ZONE

In order to understand the influence of weld factors on the heat affected zone (HAZ), one sample of each run was cross-sectioned for microhardness testing. A Leco Micro-hardness Tester MHT series 200 system was used to measure Vicker's hardness values. The measurements were taken at 1.0mm increments across the weld zone and base material with a 0.5kg load applied using a five second dwell time.

The graphs of the hardness data showed a hardness decrease from 60-65HV for the base material to 40-45HV at the HAZ as shown in (Figure 32). This pattern was present in every weld examined; however, the length of the HAZ was higher and the hardness values lower at low power settings, settings for which, in actual fact, weld strength resulted to be higher (Figure 33). This loss in hardness across a HAZ is typical in most heat treated materials subject to fusion welding. The data obtained from the aluminum materials used in this study is typical of that obtained in other heat treatable aluminum alloys subjected to MIG welding.

SUMMARY AND CONCLUSIONS

- This study was developed to identify the influence of MIG welding process factors on weld strength and weld geometry on 6063-T52 extruded aluminum in T-Node configuration.

- The welding equipment process factors selected were power input (torch speed, voltage current, wire feed), pulse frequency, gas flow rate, torch angle, and arc intensity.

- Post-weld analysis consisted of mechanical testing (tensile, bending, and shear loading), weld geometry evaluation, and microhardness testing.

- Power input had an adverse effect on joint load to failure under both tensile and shear loadings. The negative effect of high power input settings was even more pronounced at low torch angle settings. On the other hand, arc intensity showed a positive effect on joint load to failure under tensile loading.

- Power input at higher settings tended to reduce the throat length by as much as 20% (3.36 to 2.72mm).

- Correlations of the throat averages of each experimental run and their corresponding joint loads to failure under tensile and shear loading respectively with R-Square values of 51% and 82% were found.

- Torch angle at higher settings showed increase in bottom penetration.

- Power input at higher settings set the outermost top penetration line close to the specimen horizontal leg while setting the deepest bottom penetration away from the vertical leg formed by the specimen intersection.

- Top section penetration was more pronounced at the first weld in the welding sequence and measurements closer to the ending point of the welds showed more top penetration than those close to the starting points. On the other hand, bottom penetration showed a tendency to increase from starting to ending points and from first to second weld in the welding sequence.

- The graphs of the hardness data showed a hardness decrease from 60-65HV for the base material to 40-45HV at the HAZ.

- The length of the HAZ was higher and the hardness values lower at low power settings, for which weld strength resulted higher.

REFERENCES

1. Juvinall, Robert; Marshek, Kurt. Fundamentals of Machine Component Design. USA: John Wiley & Sons, Inc., 1991, Second Edition, pp. 415-416.

2. Riley, William; Sturges, Leroy; Morris, Don. Mechanics of Materials. USA: John Wiley & Sons, Inc., 1999, Fifth Edition, pp. 221-223.

3. Beer, Ferdinand; Johnston, Russell. Mechanics of Materials. USA: McGraw-Hill-Inc, 1992, Second Edition, pp. 233-235.

4. Douglas C. Montgomery. Design and Analysis of Experiments. USA: John Wiely & Sons, Inc.

5. Ashby, Michael; Jones, David. Engineering Materials 2 – An Introduction to Microstructures, Processing and Design. U.K.: Pergamon Press, 1986, First Edition, pp. 85, 126-127.

6. OTC/Daihen Doc. CPDP-599, p.19.

APPENDIX

Figure 1. T-Node configuration
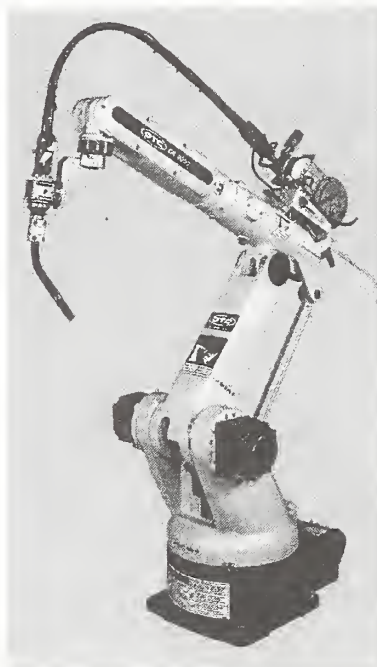
Figure 2. OTC/Daihen robot welding equipment

Two holes (opposite each other) need to be drilled on the sample to mount the top plate before each test. The clamp has drill guide bushings. The top clamp will be bolted to the sample then located to the platen and fastened.
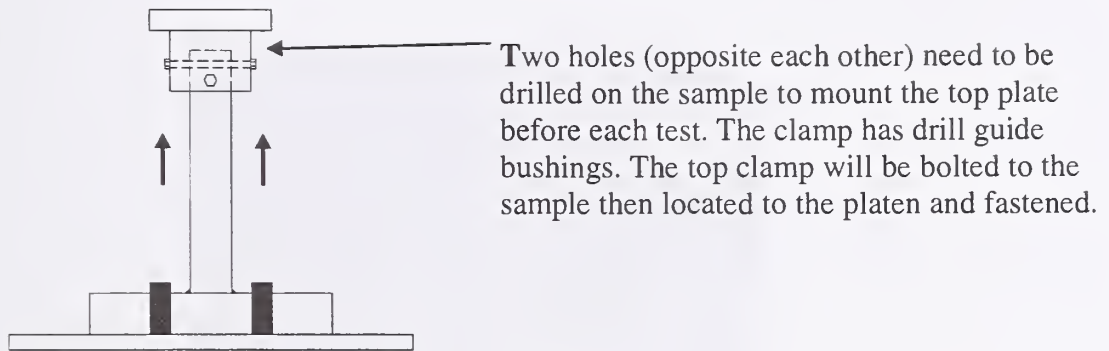
Figure 3. Tensile Test Configuration

200 mm from weld

A solid mandrel insert to avoid bending of the extension. The mandrel stops within 1 inch of the weld.

ation

A solid mandrel inside the extrusion which stops at the inner edge of the collar.

4 inch wide collar to prevent bending during shear test.
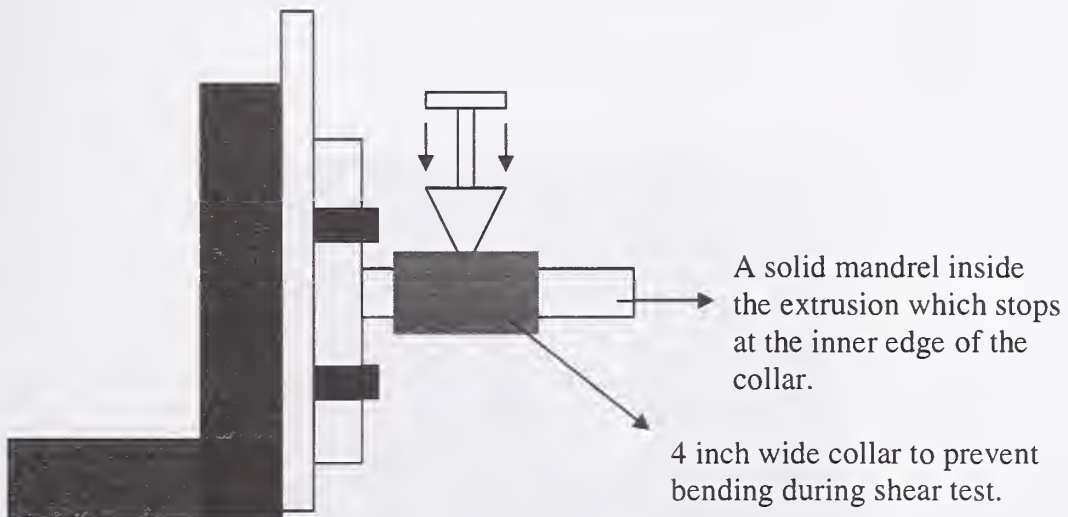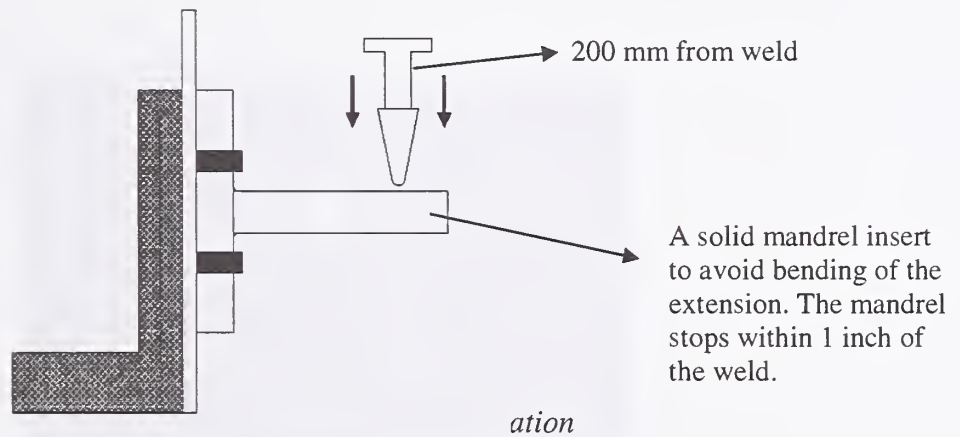
Figure 5. Shear Test Configuration

Figure 6. Failure mode of tensile test specimen
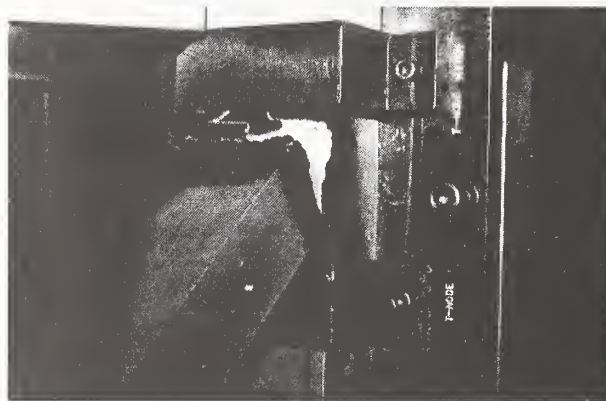
Figure 7. Failure mode of bending test specimen

Figure 8. Failure mode of shear test specimen

Normal Probability Plot of the Standardized Effects
(response is Tensile, Alpha = .10)
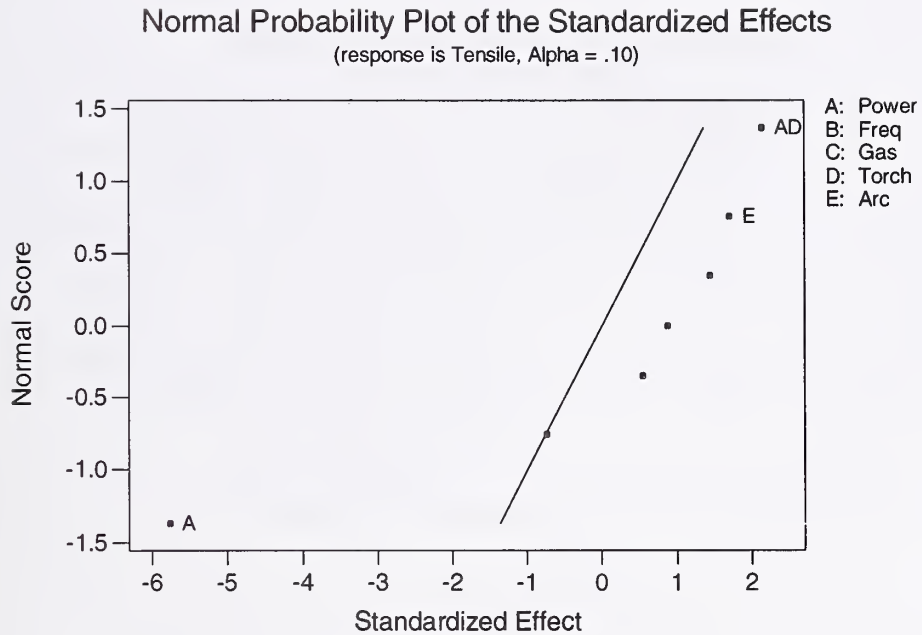
Figure 9. Normal probability plot for tensile load

Normal Probability Plot of the Standardized Effects
(response is Bending, Alpha = .10)
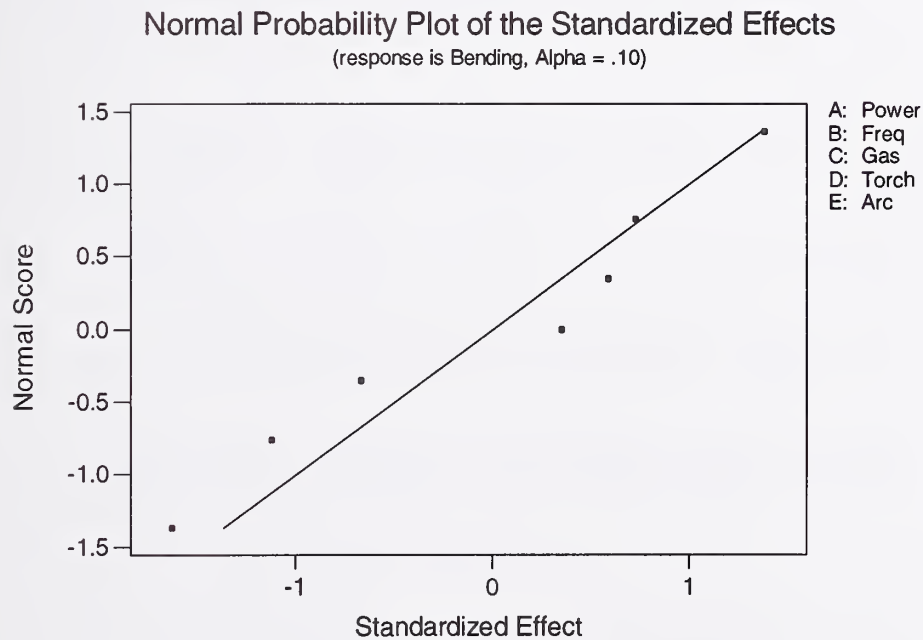
Figure 10. Normal probability plot for bending load
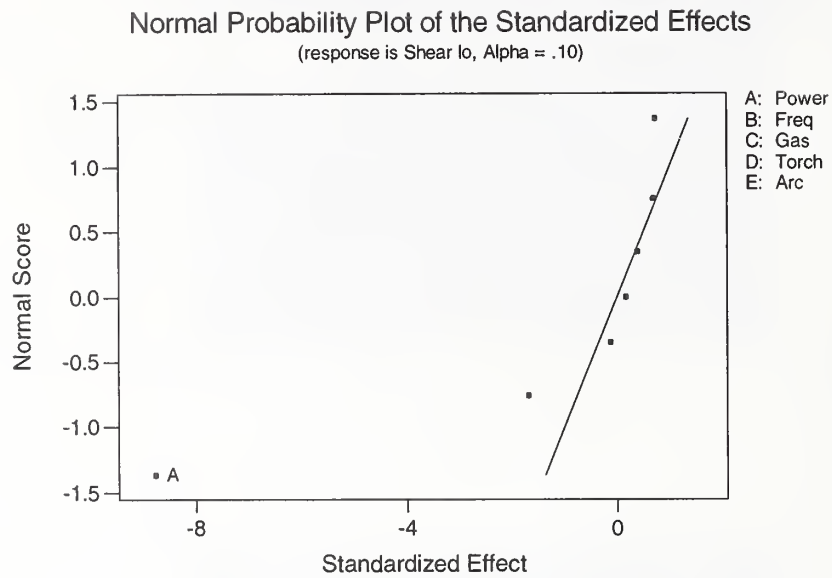
Figure 11. Normal probability plot for shear load
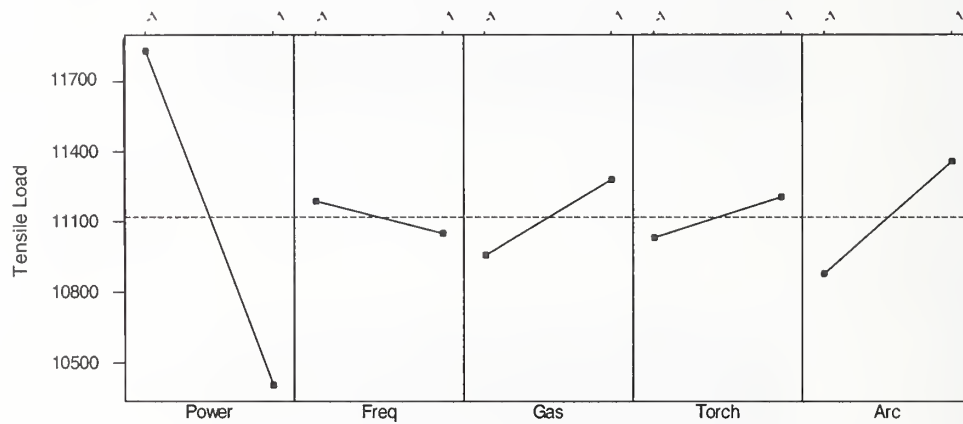
Figure 12. Main effects plot (data means) for tensile load (kN)
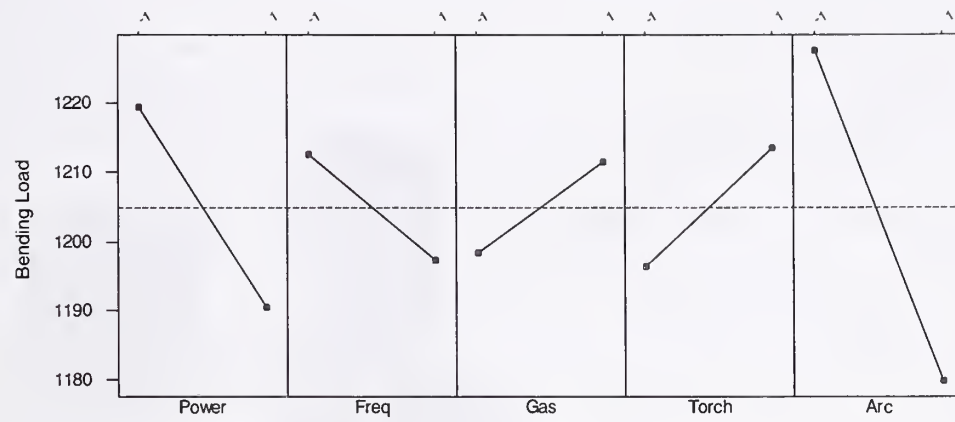
Figure 13. Main effects plot (data means) for bending load
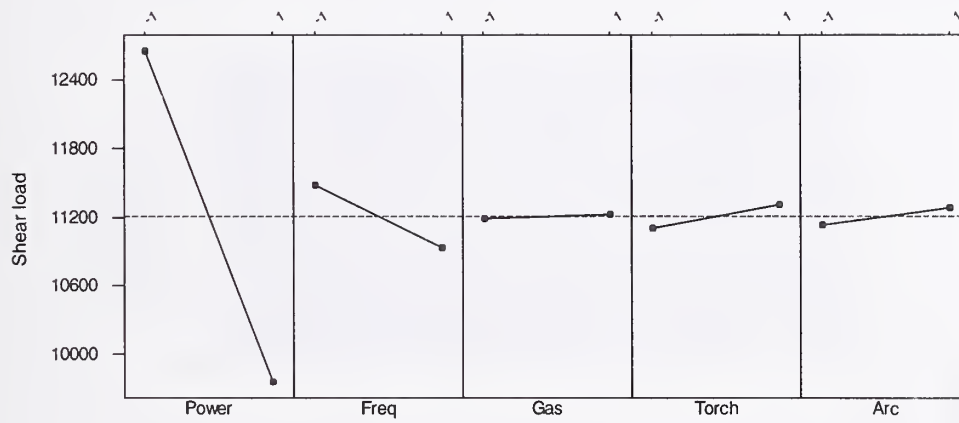
Figure 14. Main effects plot (data means) for shear load

- 4 Welds (A,B,C,D)
- 6 Sections
  - *A₁ – 1 inch from weld A start point*
  - *A₂ – 1 inch from weld A end point*
  - *B₁ – 1 inch from weld B start point*
  - *B₂ – 1 inch from weld B end point*
  - *C – Middle of weld C*
  - *D – Middle of weld D*

T-Node Welds

Weld Sectioning
(Top View)
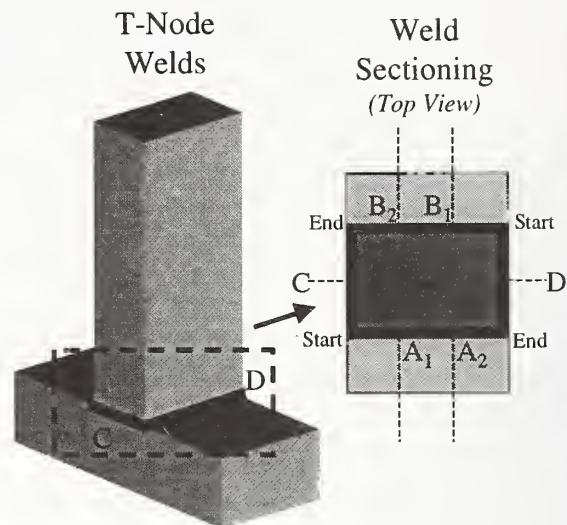
Figure 16. Cutting scheme

Normal Probability Plot of the Standardized Effects
(response is Throat, Alpha = .05)

A: Power
B: Freq
C: Gas
D: Torch
E: Arc
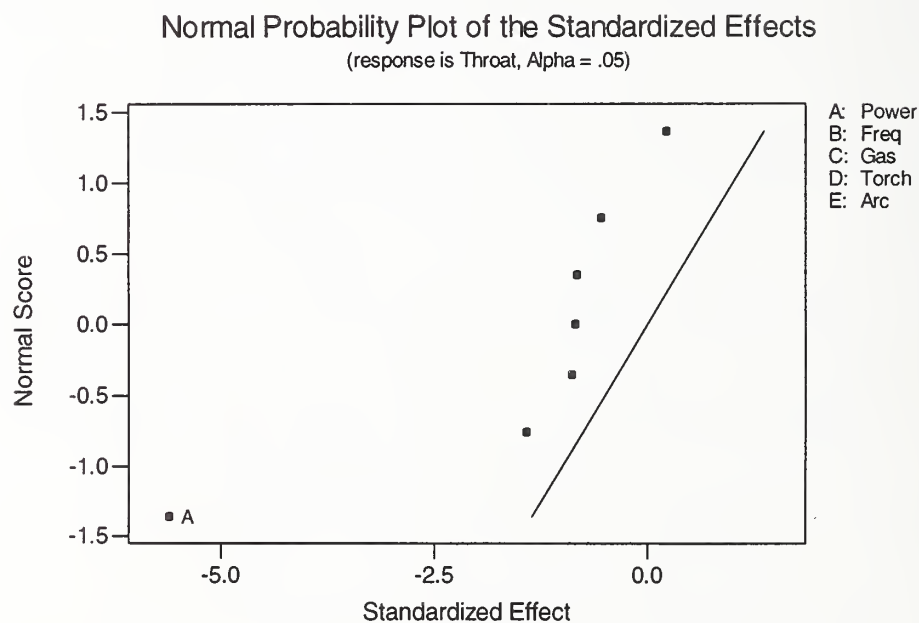
Figure 17. Normal Probability Plot for Throat
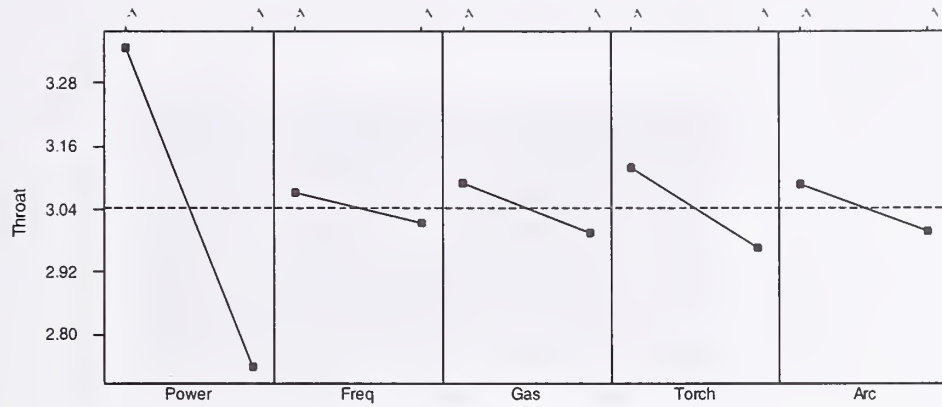
Figure 18. Main Effects Plot for Weld Throat (mm)
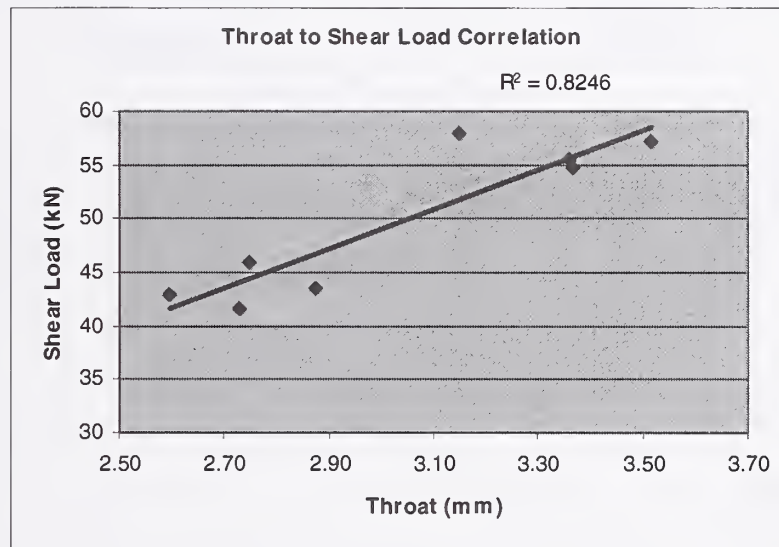
Figure 19. Throat to Shear Load Correlation
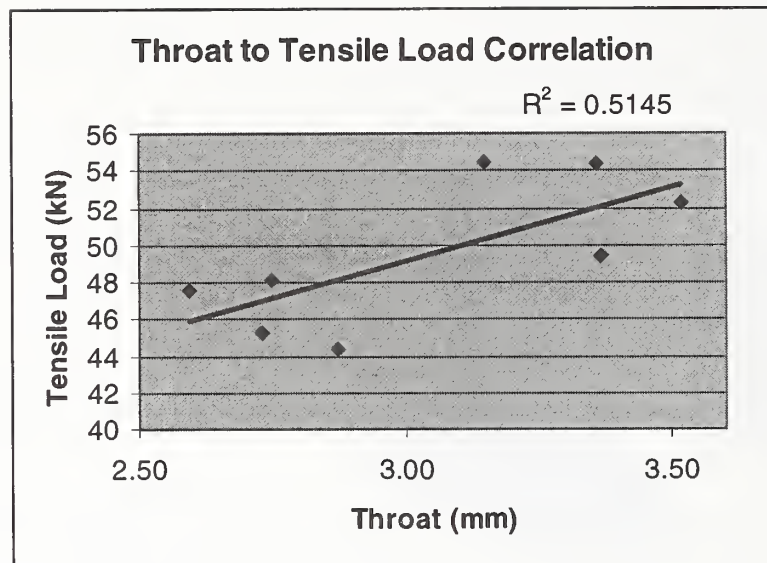
Figure 20. Throat to Tensile Load Correlation
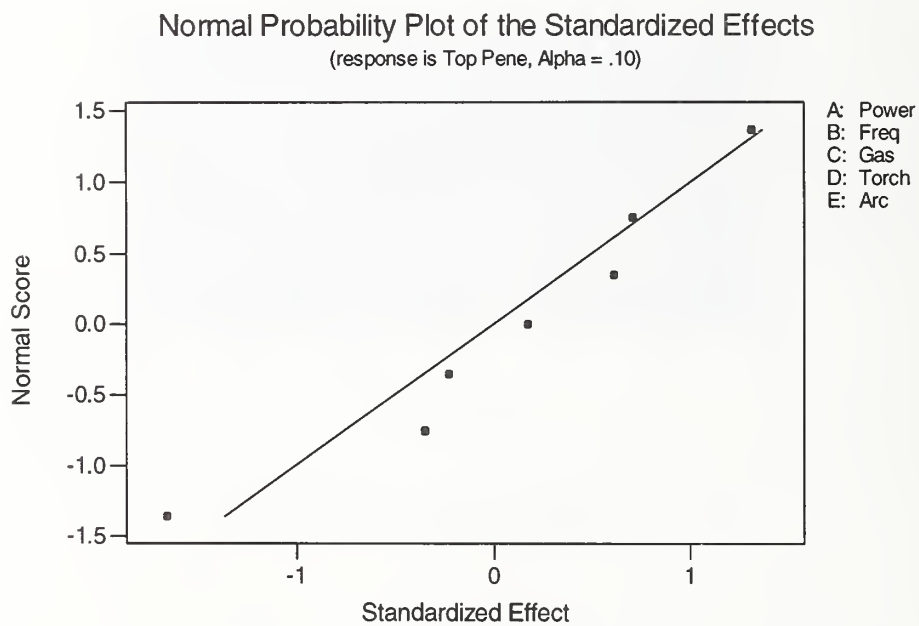
Figure 21. Normal Probability Plot for Top Penetration
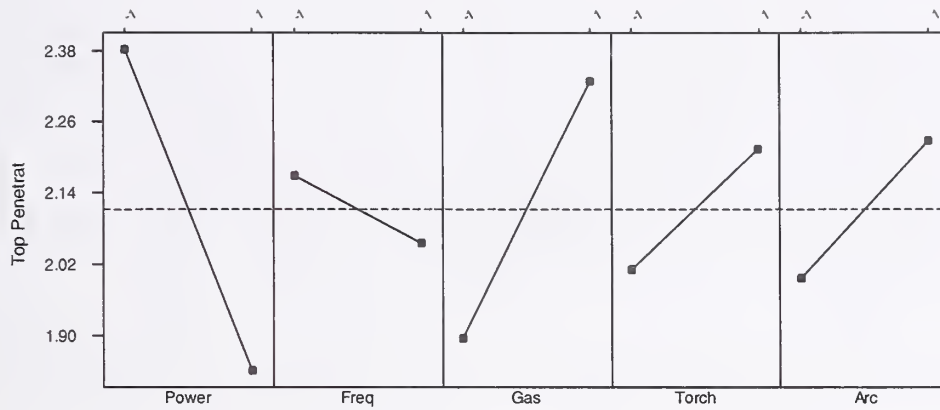
Figure 22. Main Effects Plot (data means) for Top Penetration
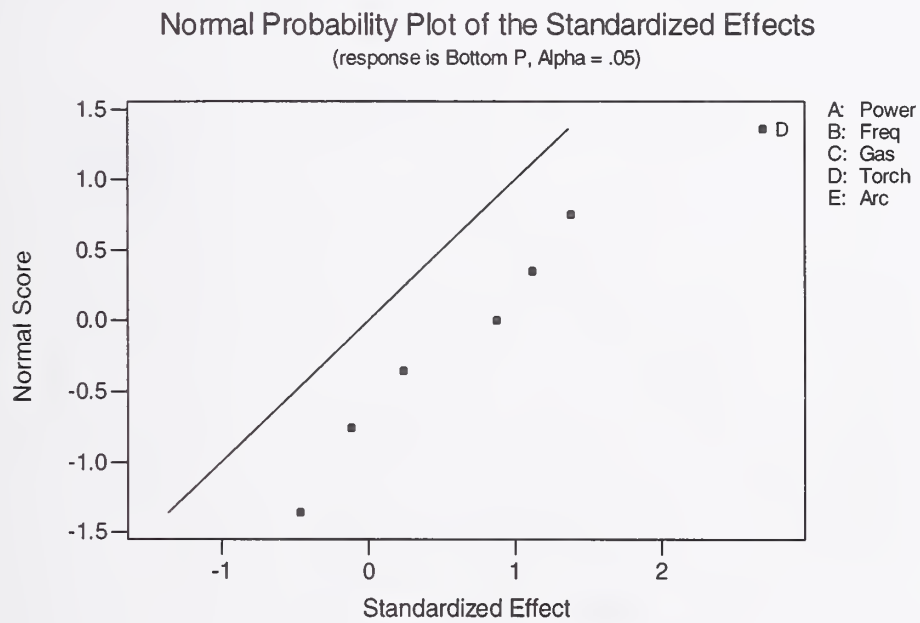
Figure 23. Normal Probability Plot for Bottom Penetration
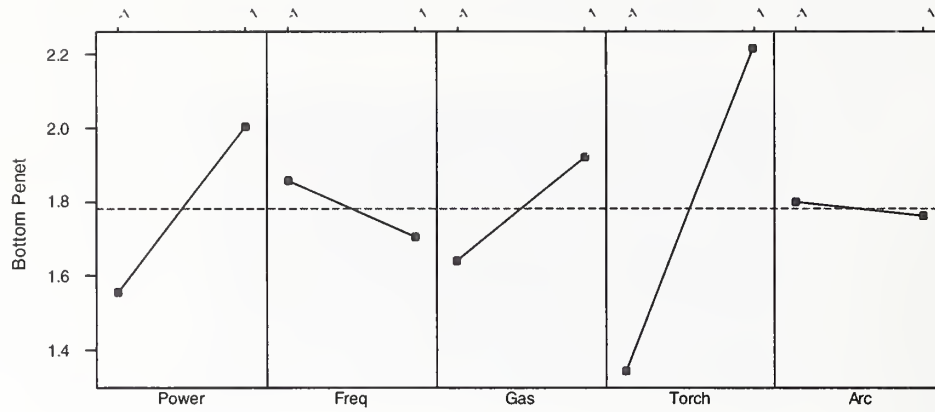
Figure 24. Main Effects Plot (data means) for Bottom Penetration (mm)
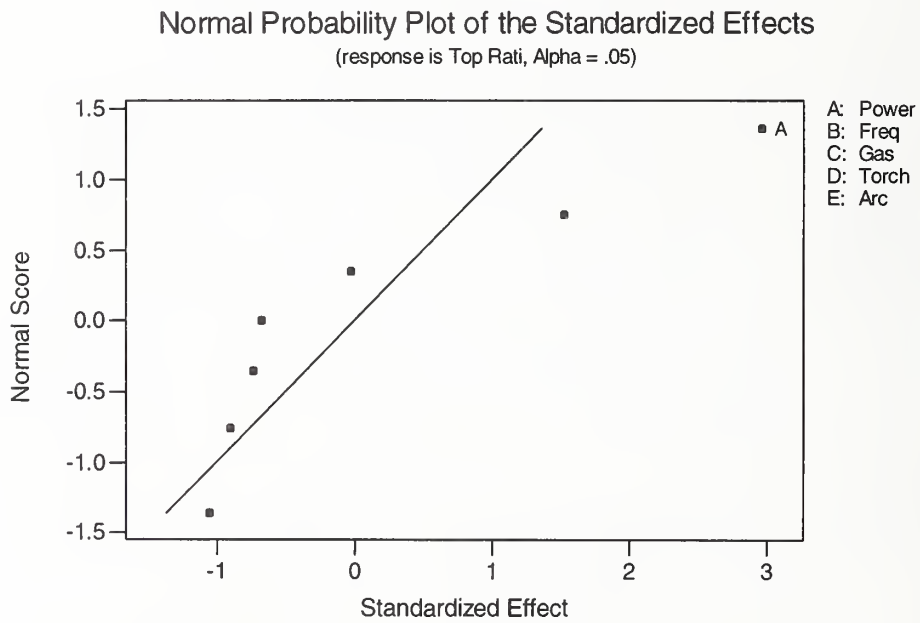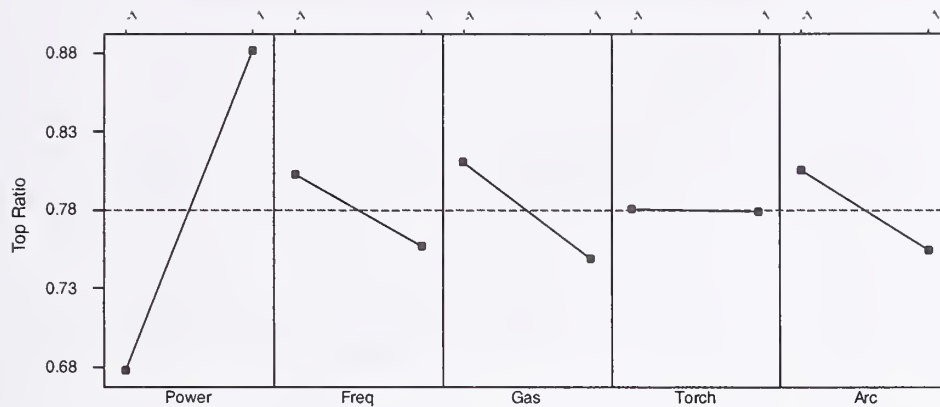

Figure 25. Normal Probability Plot for Top Ratio

Figure 26. Main Effects Plot (data means) for Top Ratio
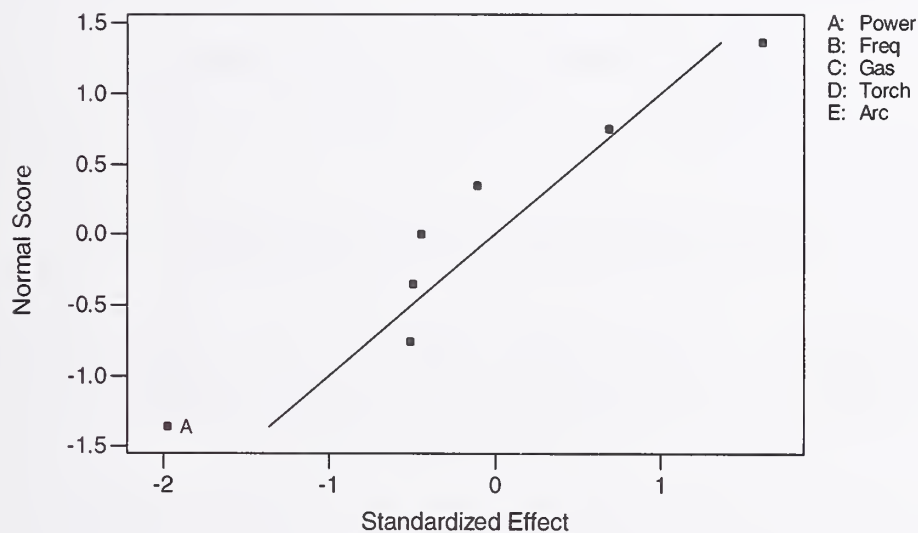
Figure 27. Normal Probability Plot for Bottom Ratio

197

Main Effects Plot (data means) for Bottom Ratio

Figure 28. Main Effects Plot for Bottom Ratio

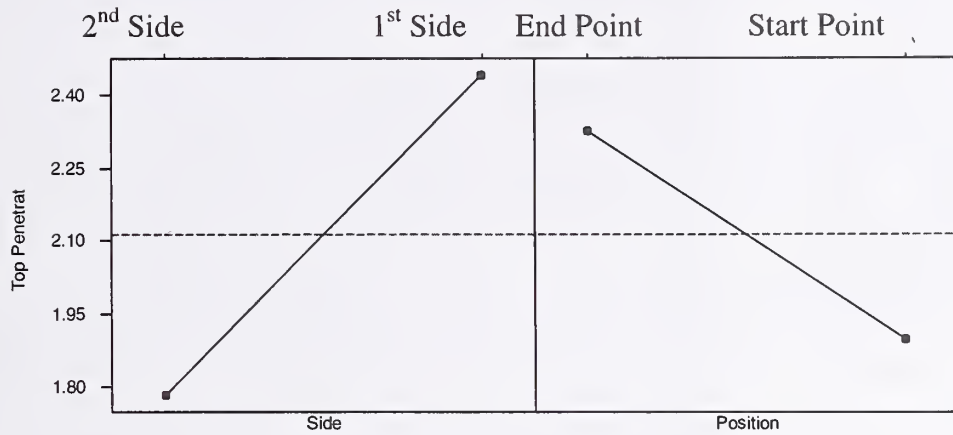Main Effects Plot (data means) for Top Penetrat

Figure 29. Side and Position Effects on Top Penetration
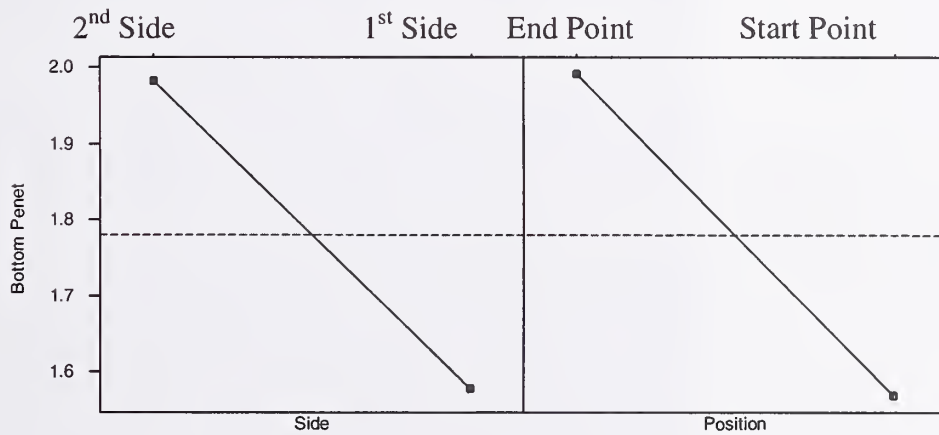
Main Effects Plot (data means) for Bottom Penet

Figure 30. Side and Position Effects on Bottom Penetration

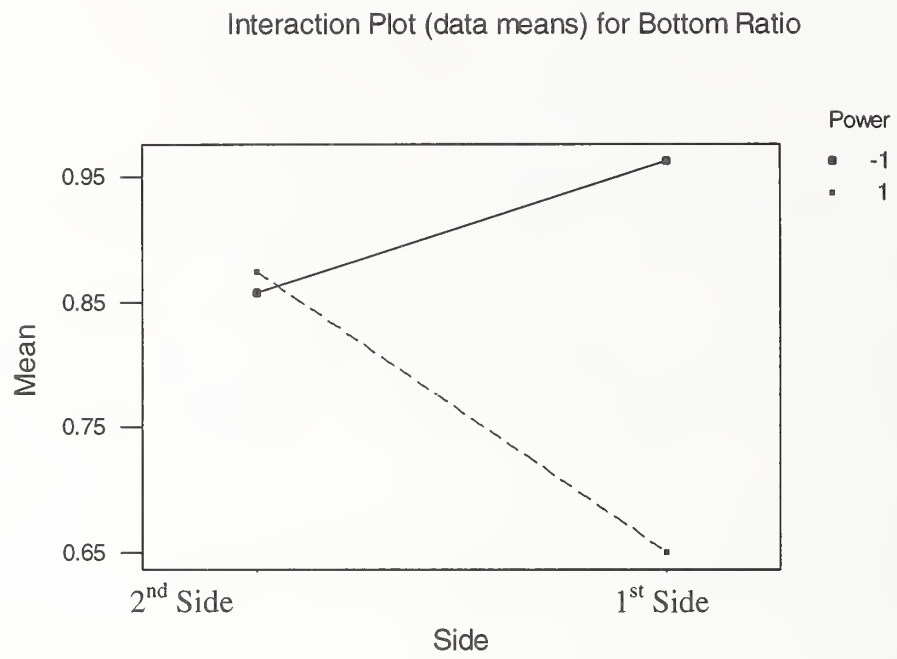Interaction Plot (data means) for Bottom Ratio

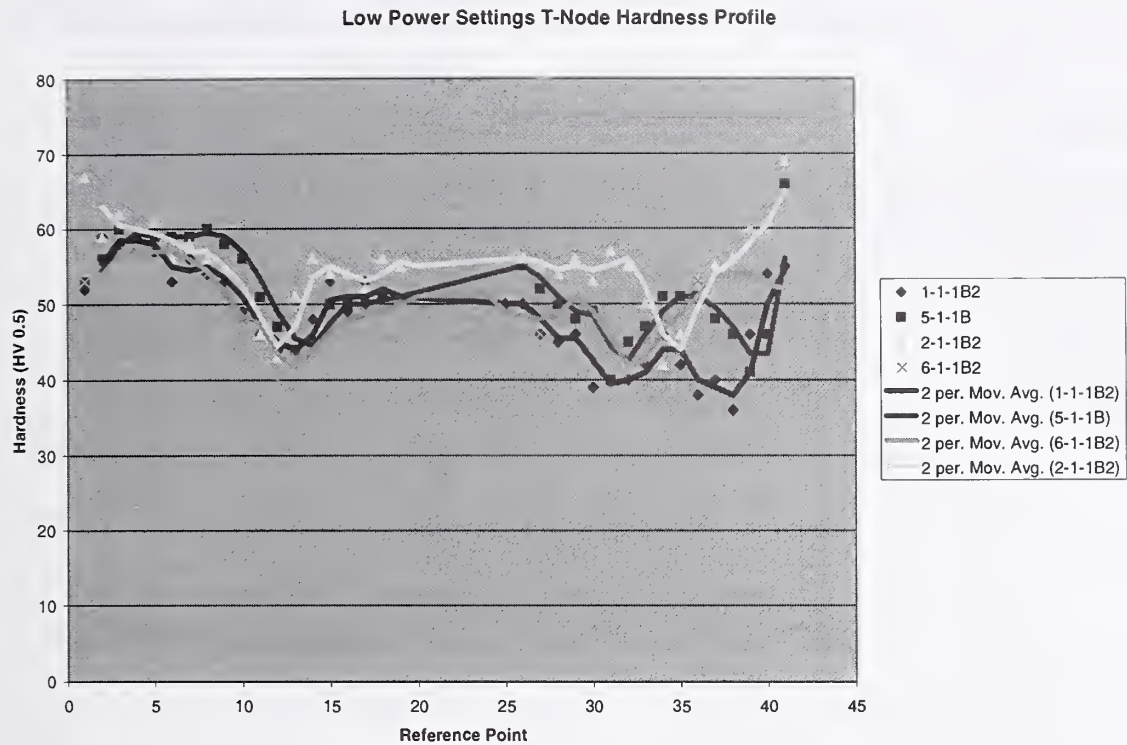Figure 31. Interaction Plot for Bottom Penetration Ratio
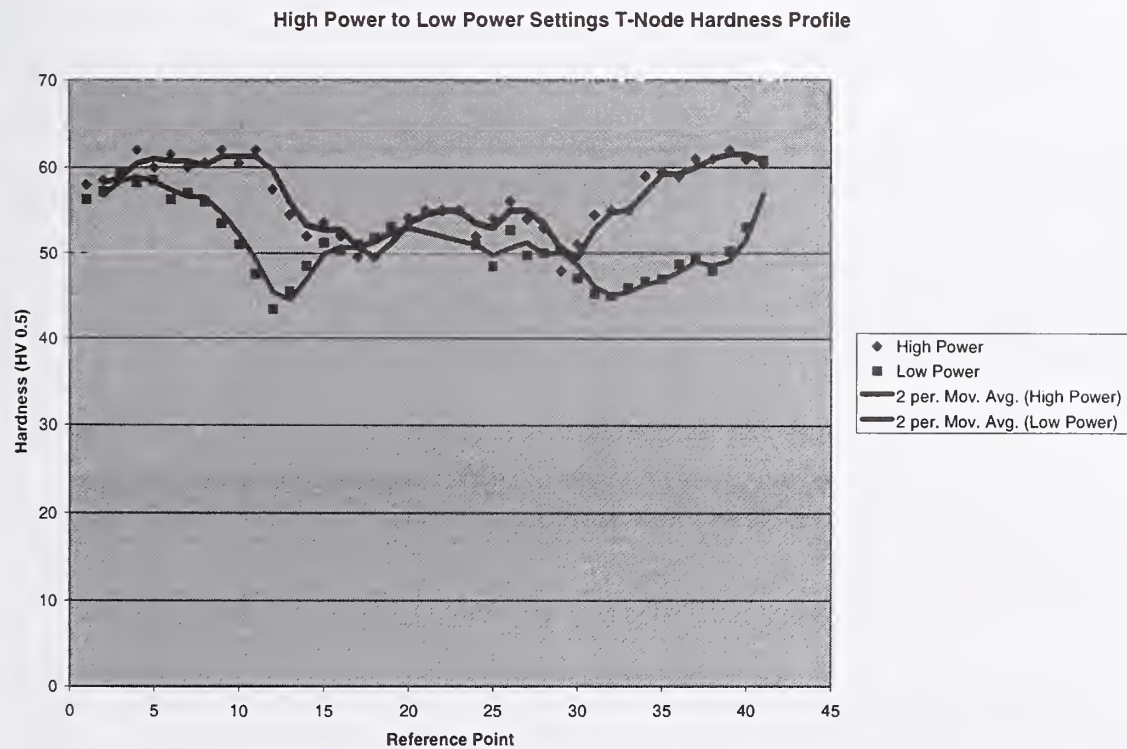
Figure 32. Hardness Profile for Low Power Input Welds

Figure 33. Low Power Input Vs. High Power Input Hardness Profiles

Factor	Low Level	High Level	Unit
Torch Speed	635 (25)	1270 (50)	mm(in)/min
Corresponding Voltage/Current	21.5/150	25.3/220	Volts/Amperes
Pulse Frequency	10	30	Hz
Gas flow rate	0.71 (25)	1.27 (45)	m^3/hr (ft^3/hr)
Torch Angle	45	50	Degrees
Arc Intensity	Normal	Soft	N/A

Table 1. DOE-T1 Process factors matrix

Run	Power Input	Pulse Frequency	Gas Flow Rate	Torch Angle	Arc Intensity
1	-1	-1	-1	-1	-1
2	-1	-1	1	1	1
3	1	1	-1	-1	1
4	1	1	1	1	-1
5	-1	1	-1	1	-1
6	-1	1	1	-1	1
7	1	-1	-1	1	1
8	1	-1	1	-1	-1

Table 2. Experimental matrix

NIST Technical Publications

Periodical

Journal of Research of the National Institute of Standards and Technology—Reports NIST research and development in metrology and related fields of physical science, engineering, applied mathematics, statistics, biotechnology, and information technology. Papers cover a broad range of subjects, with major emphasis on measurement methodology and the basic technology underlying standardization. Also included from time to time are survey articles on topics closely related to the Institute's technical and scientific programs. Issued six times a year.

Nonperiodicals

Monographs—Major contributions to the technical literature on various subjects related to the Institute's scientific and technical activities.

Handbooks—Recommended codes of engineering and industrial practice (including safety codes) developed in cooperation with interested industries, professional organizations, and regulatory bodies.

Special Publications—Include proceedings of conferences sponsored by NIST, NIST annual reports, and other special publications appropriate to this grouping such as wall charts, pocket cards, and bibliographies.

National Standard Reference Data Series—Provides quantitative data on the physical and chemical properties of materials, compiled from the world's literature and critically evaluated. Developed under a worldwide program coordinated by NIST under the authority of the National Standard Data Act (Public Law 90-396). NOTE: The Journal of Physical and Chemical Reference Data (JPCRD) is published bimonthly for NIST by the American Institute of Physics (AIP). Subscription orders and renewals are available from AIP, P.O. Box 503284, St. Louis, MO 63150-3284.

Building Science Series—Disseminates technical information developed at the Institute on building materials, components, systems, and whole structures. The series presents research results, test methods, and performance criteria related to the structural and environmental functions and the durability and safety characteristics of building elements and systems.

Technical Notes—Studies or reports which are complete in themselves but restrictive in their treatment of a subject. Analogous to monographs but not so comprehensive in scope or definitive in treatment of the subject area. Often serve as a vehicle for final reports of work performed at NIST under the sponsorship of other government agencies.

Voluntary Product Standards—Developed under procedures published by the Department of Commerce in Part 10, Title 15, of the Code of Federal Regulations. The standards establish nationally recognized requirements for products, and provide all concerned interests with a basis for common understanding of the characteristics of the products. NIST administers this program in support of the efforts of private-sector standardizing organizations.

Order the **following** *NIST publications—FIPS and NISTIRs—from the National Technical Information Service, Springfield, VA 22161.*

Federal Information Processing Standards Publications (FIPS PUB)—Publications in this series collectively constitute the Federal Information Processing Standards Register. The Register serves as the official source of information in the Federal Government regarding standards issued by NIST pursuant to the Federal Property and Administrative Services Act of 1949 as amended, Public Law 89-306 (79 Stat. 1127), and as implemented by Executive Order 11717 (38 FR 12315, dated May 11, 1973) and Part 6 of Title 15 CFR (Code of Federal Regulations).

NIST Interagency or Internal Reports (NISTIR)—The series includes interim or final reports on work performed by NIST for outside sponsors (both government and nongovernment). In general, initial distribution is handled by the sponsor; public distribution is handled by sales through the National Technical Information Service, Springfield, VA 22161, in hard copy, electronic media, or microfiche form. NISTIR's may also report results of NIST projects of transitory or limited interest, including those that will be published subsequently in more comprehensive form.